Saline seepage in deltaic areas

Preferential groundwater discharge through boils and interactions between thin rainwater lenses and upward saline seepage

Perry de Louw

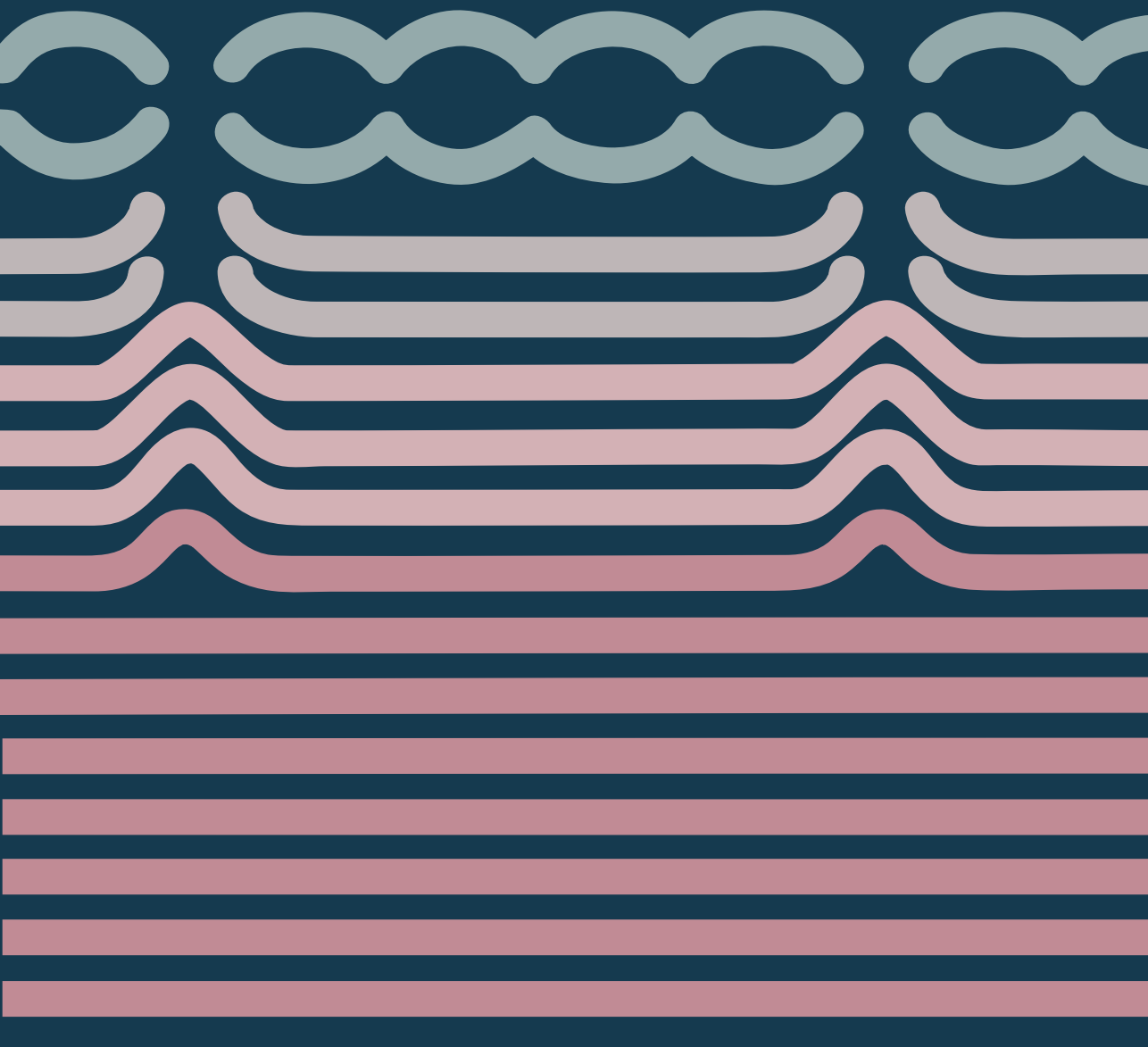

Saline seepage in deltaic areas

Preferential groundwater discharge through boils and interactions between thin rainwater lenses and upward saline seepage

Perry de Louw

Cover design by Su van Doren

Saline seepage in deltaic areas. Preferential groundwater discharge through boils and interactions between thin rainwater lenses and upward saline seepage.
(PhD thesis, Vrije Universiteit Amsterdam)

In Dutch: Zoute kwel in delta's. Preferente kwel via wellen en interacties tussen dunne regenwaterlenzen en zoute kwel.
(Academisch proefschrift, Vrije Universiteit Amsterdam)

Contact: Perry.deLouw@deltares.nl; Tel: +31 (0)6 30548000

This research was funded by Deltares

ISBN/EAN 9789461085429

VRIJE UNIVERSITEIT

Saline seepage in deltaic areas

Preferential groundwater discharge through boils and
interactions between thin rainwater lenses and upward saline seepage

ACADEMISCH PROEFSCHRIFT

ter verkrijging van de graad Doctor aan
de Vrije Universiteit Amsterdam,
op gezag van de rector magnificus
prof.dr. F.A. van der Duyn Schouten,
in het openbaar te verdedigen
ten overstaan van de promotiecommissie
van de Faculteit der Aard- en Levenswetenschappen
op vrijdag 6 december 2013 om 11.45 uur
in de aula van de Universiteit,
De Boelelaan 1105

door

Petrus Gerardus Bernardus de Louw

geboren te Nuenen

promotoren:	prof.dr. P.J. Stuyfzand
	prof.dr. S.E.A.T.M. van der Zee
copromotor:	dr. G.H.P. Oude Essink

Thesis committee:

prof.dr.ir. M.F.P. Bierkens (Utrecht University)
dr. J.K. Groen (VU University Amsterdam)
prof.dr. L. Lebbe (Ghent University, Belgium)
prof.dr.ir. T.N. Olsthoorn (Delft University of Technology)
dr. C.I. Voss (USGS, USA)

Table of contents

Part I: Preferential saline seepage through boils

Part III Synthesis and discussion, summary and conclusions

Chapter 1

1.1 Salinization by saline seepage

The majority of earth's water is saline (97.2%) and freshwater is present in the form of ice (77.4 %), groundwater (22.3%) and surface water (0.3 %) (Fetter, 1994). More than 50% of world's population lives in coastal areas and is largely dependent on fresh groundwater resources for domestic, agricultural and industrial purposes. However, in many coastal areas, groundwater is brackish to saline because of seawater intrusion, marine transgressions and sea spray (e.g. Custodio and Bruggeman, 1987; Stuyfzand and Stuurman, 1994; Post and Abarca, 2010; Werner *et al*., 2013). The salinity of groundwater may pose problems for the sustainable exploitation of fresh groundwater. In the future, the exploitation of fresh groundwater resources will increase due to population and economic growth, intensified agricultural development, and the loss of surface water resources due to contamination (Arnell, 1999; Jelgersma *et al*., 1993; Ranjan *et al*., 2006). In addition, the anticipated sea level rise, climate change (decrease of recharge) and ongoing land subsidence will exacerbate the pressures on coastal groundwater systems (e.g. Green *et al*., 2011; Taylor *et al*., 2012). Coastal aquifers could become more saline at an accelerating rate leading to a loss of fresh groundwater resources.

In low-lying coastal areas that lie below mean sea level (MSL) saline groundwater may reach the surface by upward groundwater flow. This process is referred to as 'saline seepage' and is the main subject of this thesis. The upward moving saline seepage water may (1) discharge directly in lakes, canals, ditches or subsurface drain tiles leading to the salinization of surface waters, (2) mix near the surface with shallow fresh groundwater, or even (3) reach the root zone affecting crop growth and natural vegetation. Future rise in sea level is expected to increase seepage and salt loads to surface waters and reduce the availability of both fresh surface water and groundwater (e.g. Navoy, 1991; Oude Essink, 1996; Van der Meij and Minnema, 1999; Oude Essink, 2001; Vandenbohede *et al*., 2008; Oude Essink *et al*., 2010; Pauw *et al*., 2012). Model simulations show that salt loads from groundwater seepage in several low-lying parts of the coastal zone of the Netherlands will double due to sea level rise by 2100 A.D. (Oude Essink *et al*., 2010).

Predicting effects of future changes and formulating effective water management strategies for a climate proof, sustainable freshwater supply is only meaningful when all relevant processes involving saline seepage are fully understood. Successful implementation of any measure to increase freshwater availability and to mitigate the adverse consequences of future climate change and sea level rise requires knowledge of the spatial variability and dynamic behaviour of saline seepage in deltaic areas. As about one-quarter of the Netherlands lies below MSL, saline seepage leads to the salinization of large areas impacting on agriculture and aquatic ecosystems (Wesseling, 1980; Van Rees Vellinga *et al*., 1981; Van Puijenbroek *et al*., 2004, Van der Eertwegh *et al*., 2006). As such, this makes the Dutch delta as an ideal study area. The research presented in this thesis aims to address the knowledge gap that exists of the understanding and quantification of the dynamic processes involving saline seepage leading to the salinization of surface water, shallow groundwater and soil moisture. The spatial variability and temporal dynamics of saline seepage were studied at different field sites in the coastal area of the Dutch delta. The research spanned both the local scale (ditch, agricultural field) and larger areas like polder catchments and islands. Data collected in the field were complemented with analysis using mathematical models.

1.2 Freshwater supply in Dutch Delta Plan

The flood disaster in 1953 which affected large areas of the south-western delta of the Netherlands and killed 1836 people, was the reason to define a so-called Delta Plan for constructing large flood protection works. Since the subsequent construction of the Delta Works the Netherlands have become the world's best protected delta. However, sea levels are rising, land is subsiding and the summers are expected to become drier and warmer (Haasnoot *et al*., 1999; Van den Hurk *et al*., 2006; IPCC, 2007). To be prepared for these ongoing and future changes a new plan called 'the Delta Program' has been conceived (Delta Program, 2012). This program aims to guarantee that the Netherlands remains safe and attractive. The Delta Program states that 'a major condition for the continued existence of the Netherlands and for a strong economy is a country that is safe from flooding and having a sufficient freshwater supply' (Delta Program, 2012). Policy-makers now realize that, besides the safety issue, there is urgency at a national level to ensure that the Dutch Delta's freshwater supply can withstand future climate change.

A sub-program 'Freshwater supply' is formulated within the Delta Program which aims to develop a long-term strategy for a sustainable and economically effective supply of freshwater. The freshwater sub-program is the responsibility of the Ministry of Infrastructure & the Environment and examines and explores policy in relation to problems and solutions. It is signaled that the current system is approaching its limits and that in dry periods: (1) there could be insufficient freshwater available in rivers, canals and lakes, (2) freshwater inlet points for irrigation purposes can become salinized, and (3) parts of the water system of the south-western delta become salinized without a possibility to supply freshwater. These problems will increase depending on future developments in the supply of and demand for water. Possible solutions include: optimization of water distribution in the main water system, limiting saltwater intrusion in the main rivers in the west, and ensuring alternative freshwater supply systems. Finally, water users are encouraged to adapt to the amount of freshwater that is available and to store freshwater (surface water and rainwater) in the subsoil.

The way the Dutch cope with the present and future threats of sea level rise, land subsidence and salinization, and how they come up with strategies for adaptation and mitigation can be seen as a blueprint for other deltas in the future. The impact on freshwater resources due to future changes could be similar to other deltaic areas worldwide, e.g., the Po (Italy), Mississippi (USA), Nile (Egypt), Mekong (Vietnam), Chinese and Indian deltas and the U.S. Atlantic coast (Navoy, 1991; Sherif and Singh, 1999; Bobba, 1998, 2002; Barlow, 2003; Masterson and Garabedian, 2007; Giambastiani *et al*., 2007; Vandenbohede *et al*., 2008; Post and Abarca, 2010; Custodio, 2010; Barlow and Reichard, 2010). Although the characteristics of these delta areas are obviously different, the general picture is that groundwater management in the coastal zone must face serious impacts from future stresses (Ranjan *et al*., 2009).

The research presented here contributes to the objectives of the Delta Program by providing new quantitative understanding of the salinization mechanisms of saline seepage in the Dutch coastal groundwater system. This provides a scientific basis for formulating monitoring strategies, effective measures and solutions, as well as long-term strategies for a sustainable and economically-effective supply of freshwater.

1.3 Saline seepage in the Netherlands

The groundwater salinity distribution in Dutch coastal aquifers, the hydrogeology, reclamation history and present water management jointly determine the nature, dynamics and spatial variability of present saline seepage systems found in the Netherlands. These characteristics form the basis for the definition of the research questions (section 1.4) and the selection of the study areas. Each will be described in more detail below.

1.3.1 Paleogeography and groundwater salinity

In this thesis, chloride (Cl) concentration is used to represent water salinity because Cl is the major conservative anion found in saline groundwater bodies in the Dutch subsurface which are mixtures of seawater and freshwater. Groundwater salinity is classified based on Cl concentration as fresh (Cl < 0.3 g L^{-1}), brackish (> 0.3 g L^{-1} Cl < 1.0 g L^{-1}) and salt (Cl > 1.0 g L^{-1}).

Fig. 1.1 shows that there is a large spatial variation of the depth of the interface between brackish and saline groundwater. The complexity and wide range of groundwater salinity distributions in Dutch coastal aquifers mainly result from sequential Holocene marine transgressions and regressions (Stuyfzand, 1993; Post, 2004). During the historic episodes of inundation by seawater, salinization of the Dutch coastal aquifer occurred under rapid free convection processes. Post and Kooi (2003) showed that salinization of a 200 m thick Dutch aquifer could have occurred within decades. However, the presence of aquitards within the aquifers may have slowed down or even blocked the infiltration of seawater.

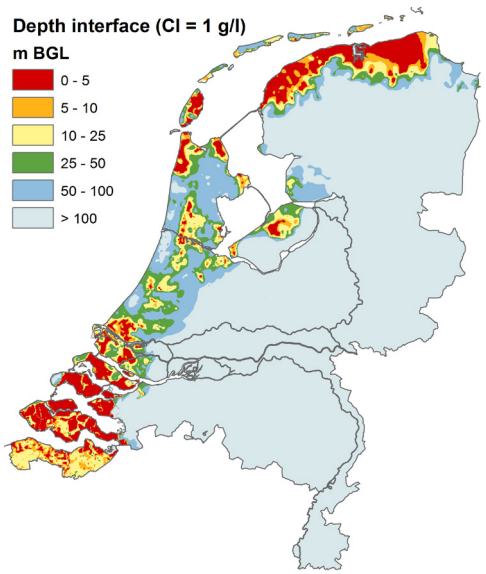

Fig. 1.1. Depth of the brackish-saline interface (Cl = 1 g L^{-1}) of groundwater from Holocene origin (from: http://www2.dinoloket.nl/nl/DINOMap.html).

Fig. 1.2 shows different phases of the paleogeographical development of the Netherlands (Vos and Zeiler, 2008; Vos *et al*., 2011) that importantly impacted on the salinity distribution in the coastal aquifers. Under a continuous and rapid sea level rise since the end of the last ice age (start of the Holocene epoch, ~10 kyr ago) a large part of the Netherlands was progressively getting flooded by the sea. Around 3850 B.C. the extension of the sea was at its maximum (Fig. 1.2a) and the intertidal and submerged area largely coincides with the area where saline groundwater is found within 100 m from the surface (Fig. 1.1). The subsequent development of sand banks and dunes due to a slow down in sea level rise and increase of sediment loads resulted in a partly closure of the coastline around 2750 B.C. (Vos *et al*., 2011; Fig. 1.2b). From that moment until now, the western part of the Netherlands was isolated from the sea and fresh rainwater recharged the upper part of the aquifers, displacing the saline groundwater. This is the reason why a > 20 m thick fresh to

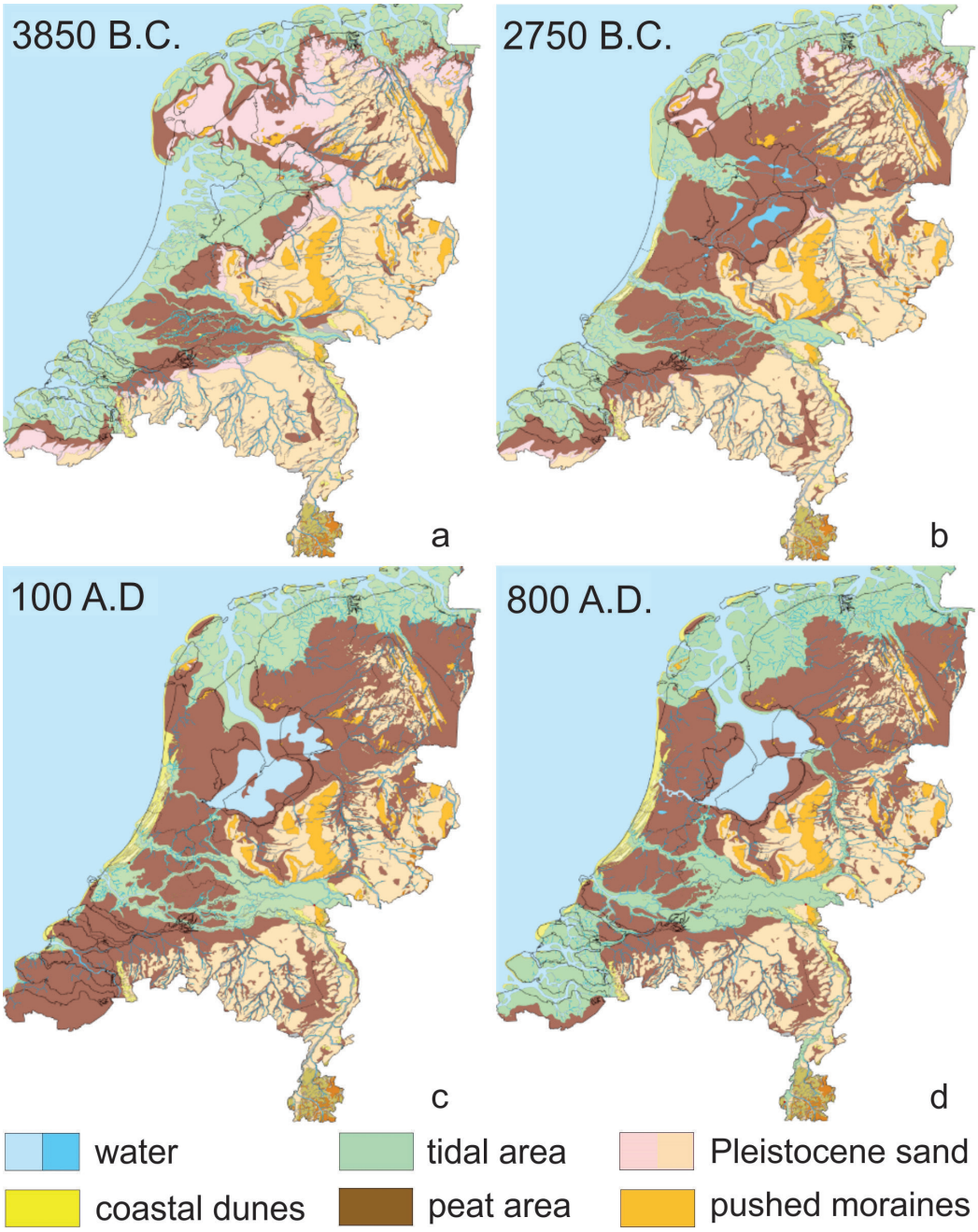

Fig. 1.2. The paleogeographical development of the Netherlands in four phases:
(a) 3850 B.C., (b) 2750 B.C., (c) 100 A.D., (d) 800 A.D. (Vos *et al.*, 2011).

slightly brackish groundwater body on top of saline groundwater is found for most of this area (Fig. 1.1). Further closure of the coastline in the period between 2750 B.C. and 100 A.D. isolated a much larger area from the sea where peat was able to develop under freshwater conditions (Fig. 1.2c). Since Roman times, a combi-

nation of peat mining and drainage of the land by man caused land subsidence and, enhanced by marine erosion, large areas were recaptured by the sea. The south-western part of the Netherlands was again an intertidal, marine salt marsh area from 350 A.D. until 800 A.D. (Fig. 1.2d) which was long enough to salinize the underlying aquifers. A comparison between Fig. 1.1 and 1.2d demonstrates that areas where saline groundwater is found < 5 m depth largely coincide with the intertidal areas during the sub-recent transgression period (~350 A.D. until ~1000 A.D.). These areas are further referred to as the sub-recent transgression areas.

1.3.2 Land reclamation and water management

In the south-western and northern part of the Netherlands, people started around 1000 A.D. to reclaim large areas of land by embankment of the salt marshes (supratidal flats). An embanked land from which the artificially drained excess water needs to be pumped out is called a 'polder' (Van de Ven, 2003). Drainage and peat mining led to further subsidence of these polders, whereas the unembanked land was rising by sedimentation during high tides and storms (Vos and Zeiler, 2008). The present topography in the south-western part of the Netherlands is therefore a result of the age of reclamation and soil type; generally it holds that the older the land, the lower the surface elevation. The lowest polders are now situated at -1.5 to -2.5 m MSL whereas the more recent reclaimed polders have their land surface above MSL. Due to differential subsidence by sediment compaction, the present elevation of former tidal creeks which are composed of sandy sediments is often 0.5 to 1.5 m higher than the surrounding reclaimed salt marshes.

In the western part of the Netherlands, the reclamation of large inland lakes started in the 17th century. This resulted in deep polders with their present surface elevations between 4 and 7 m below MSL (Fig. 1.3a). Some examples of large deep polders are the Haarlemmermeer Polder (1852 A.D.), Zuidplas Polder (1750-1850 A.D.), Schermer-Beemster complex (1600-1635 A.D.), Wieringermeer Polder (1930 A.D.) and the Flevopolders (1942-1968 A.D.) (Schultz, 1992). The polders are drained by a network of ditches and underground drain tiles and water is pumped out into a higher-lying regional water system called the 'boezem' and subsequently conveyed to the sea. Surface water levels in the deep polders are maintained at an elevation of 5 to 8 m below MSL.

1.3.3 Different saline seepage systems

The area that was subject to the Holocene transgressions is the research area where the different saline seepage systems were examined (Fig. 1.3b) and roughly equals the submerged area during the maximum transgression period around 3850 B.C. (Fig. 1.2a). Its surface area covers ~30% of the Netherlands and ~45% lies below MSL. The general hydrogeology in the area is characterized by an aquitard at the top consisting of Holocene peat, loam and clay deposits with low hydraulic conductivity (Fig. 1.3c), also known as the Holocene confining layer (HCL), which covers the underlying Pleistocene-Holocene sandy aquifer (upper aquifer). Although up to four sequential aquifers divided by aquitards are found in the subsoil (Mulder *et al*., 2003; REGIS, 2005), only the HCL and the upper aquifer are of main importance regarding saline seepage systems in the Holocene transgression area.

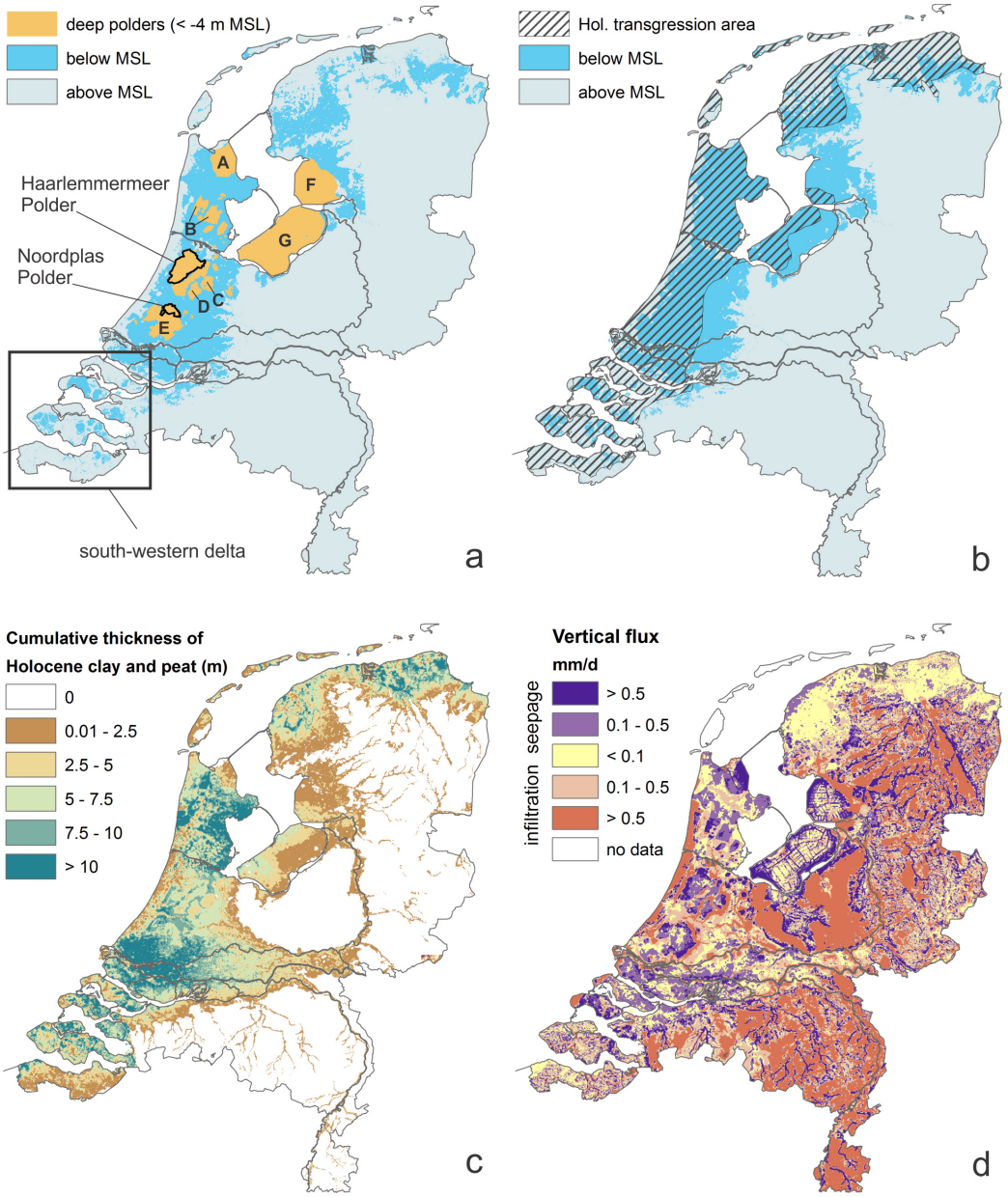

Fig.1.3 (a) The location of the deep polders of the Netherlands and the study areas; A = Wieringermeer Polder, B = Schermer-Beemster complex, C = Polder Mijdrecht, D = Polder Nieuwkoop, E = Zuidplas Polder, F = Noordoost Polder, G = Flevo Polder. (b) Surface below MSL and the Holocene transgression area. (c) The cumulative thickness of the Holocene peat and clay deposits forming the Holocene confining layer (Stafleu *et al*., 2013). (d) The seepage (blue) and infiltration (red) fluxes based on calibrated groundwater model calculations (NHI-2.1, 2011; Van Baaren *et al*., 2013).

The upward groundwater flow from the upper aquifer into the HCL is defined as seepage and occurs when aquifer hydraulic heads exceed phreatic water levels. Seepage water eventually will leave the groundwater system either by groundwater discharge in lakes, ditches or drains or by evapotranspiration. Infiltration indicates the downward flow into the upper aquifer. Fig. 1.3d shows the

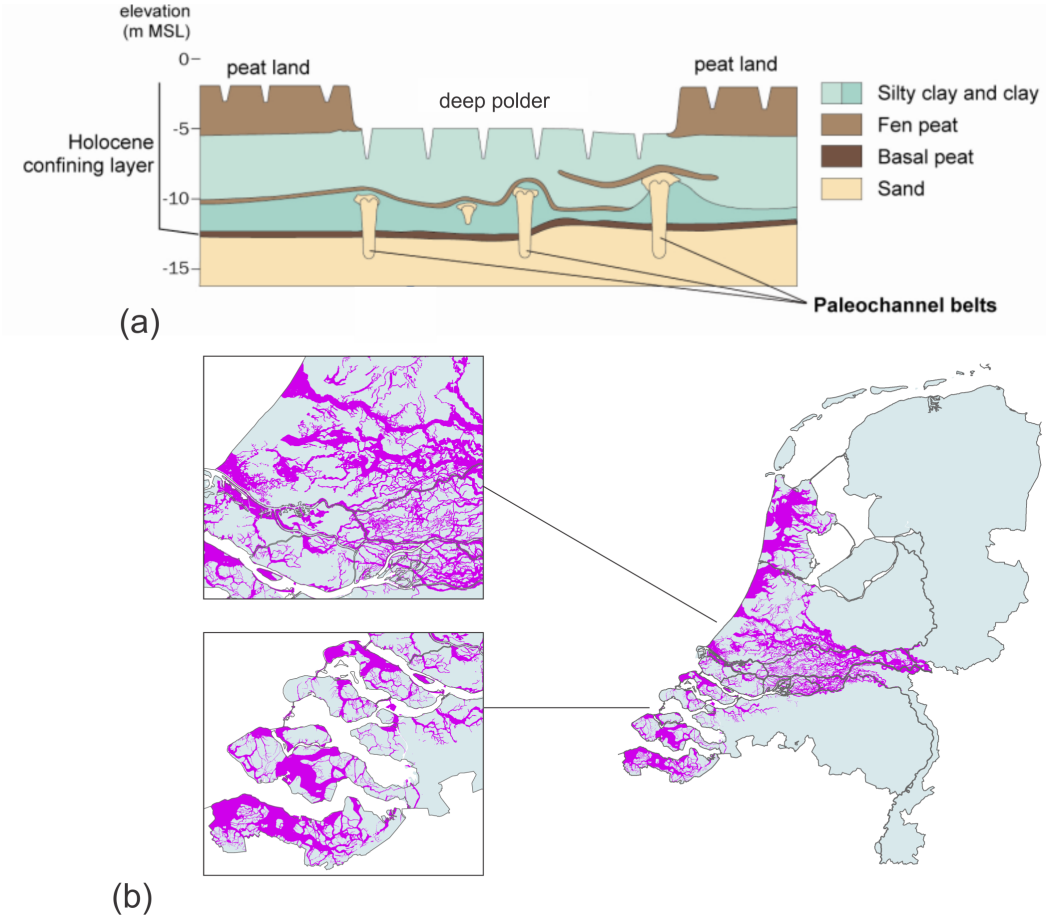

Fig. 1.4 (a) A general picture of the composition of the Holocene confining layer in western Netherlands with sandy paleochannel belts cutting through the lower part of the Holocene confining layer. (b) The location of sandy paleochannels in western Netherlands (Stafleu *et al.*, 2013) and the south-western delta (Stafleu *et al.*, 2011). Maps of paleochannels in the northern coastal area were not yet available.

seepage and infiltration flux for the Netherlands based on results from different, up to date and calibrated groundwater models (NHI-2.2, 2011; Van Baaren *et al.*, 2013). In the western part of the Netherlands, seepage mainly occurs in the deep polders due to their low-lying position creating large vertical hydraulic gradients over the HCL of up to 2.7 m in the Haarlemmermeer Polder. The development of the deep polders since the 17th century largely impacted on the regional groundwater flow systems in the western parts of the Netherlands. Instead of flowing towards the North Sea, groundwater in the aquifers was forced to flow from all directions towards the deep polders. No deep polders exist in the sub-recent transgression areas (south-western delta and northern coastal area) and spatial variations in surface level are more subtle, creating much smaller vertical head differences over the HCL than in the western Netherlands. Beside this, the Holocene clay and peat deposits were subject to marine erosion during the sub-recent transgressions (Vos *et al.*, 2011), resulting in a heterogeneous and spatially variable HCL and a lower hydraulic resistance of the HCL than in the western Netherlands. The seepage and infiltration areas are therefore smaller in the sub-recent

transgression areas operating at a smaller scale compared to the large deep seepage polders in the western Netherlands.

For the purpose of this study, saline seepage in the Holocene transgression area of the Netherlands is divided into two main saline seepage systems occurring in different parts of the Netherlands:

- Saline seepage in deep polders (western Netherlands)
- Saline seepage in sub-recent transgression areas (south-western delta and northern Netherlands)

The division is based on characteristics of both the physics of seepage and the salinity of seepage, the latter of which is determined by the groundwater salinity distribution in the upper aquifer. Their characteristics and differences will be described in the next two paragraphs.

Saline seepage in deep polders

Deep polders are subject to much larger vertical head gradients than the sub-recent transgression areas. This is caused by their low position and a HCL which is generally thick (4 to 15 m) and composed of sediments with low hydraulic conductivity (Weerts, 1996). The lower part of the HCL is the less permeable part which in places consists of a 0.1-0.5 m thick compacted, mineralized peat (basal peat) (Fig. 1.4a). At various locations in the western part of the Netherlands, the compacted peat and overlying loam and clay deposits have been eroded by streams and tidal channels during the Holocene (Van der Valk, 1996; Hijma *et al*., 2009) (Fig. 1.4a-b).These sandy paleochannel belts partly cut through the HCL locally reducing the hydraulic resistance of the HCL (Fig. 1.4a-b).

Another important characteristic of saline seepage in deep polders is the groundwater salinity distribution in the aquifers. This characteristic largely differs from the sub-recent transgression areas. Fig. 1.5 shows an example of a typical salinity depth profile found in aquifers below the deep polders: the groundwater in the upper 5 to 15 m of the sandy aquifer is generally fresh to slightly brackish (Cl concentrations of 0.05 to 1 g L^{-1}), and salinity gradually increases with depth to Cl concentrations of 3 to 8 g L^{-1} at 15 to 40 m below the HCL aquitard. The groundwater salinity directly below the aquitard represents the salinity of the seepage water flowing upward, and hence it is fresh to slightly brackish.

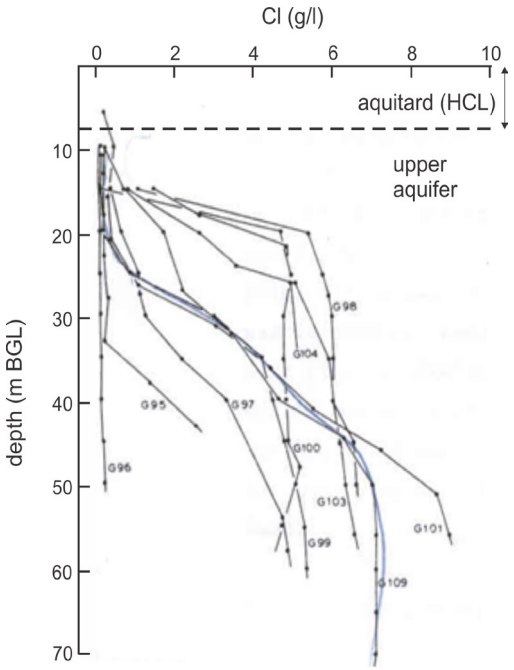

Fig. 1.5. Examples of typical salinity distributions in the upper aquifer found below deep polders in the western Netherlands (Haarlemmermeer Polder, ICW 1976).

Since the early 1960s many attempts have been undertaken to estimate salt loads from seepage into deep polders (e.g. ICW, 1976 and 1982; Wit, 1974; Van Rees Vellinga *et al*., 1981; Griffioen *et al*. 2002; NHI-2.1, 2011). The salt load was obtained by multiplying the estimated seepage flux by the average Cl concentrations of groundwater at the top of the upper aquifer (-10 to -15 m MSL) which

is in general rather fresh as shown in Fig. 1.5. This resulted in large underestimations compared to the observed Cl loads pumped out of the polders showing that the saline seepage systems were not well understood and conceptualized into the models. Furthermore, a localized form of preferential groundwater discharge, called boils, has been observed in deep polders (Vink, 1954; Rijnland, 1967, 1975, 1981, De Louw *et al*., 2001). Boils occur as conduits in the upper aquitard (HCL), connecting the underlying aquifer to the surface and allowing groundwater to discharge at high velocities. When the pressure of water in the aquifer is greater than the pressure exerted by the weight of the overlying stratum, heaving and cracking can occur, creating flow pathways that lead to the development of boils (Holzer and Clark, 1993; Li *et al*., 1996; TACFD, 1999). Up until the start of this PhD research, boils in deep polders had been given little attention and they were not considered in salt load calculations.

The saline seepage in deep polders leads to the salinization of the surface water and subsequently the salinization of the regional water system. As this regional water system is meant to supply large agricultural areas and wetlands with freshwater, salinities must be kept low to meet the standards for crops and ecosystems. For example, the maximum tolerable Cl concentration for potatoes is 200 mg L^{-1} and for flower bulbs even 50 mg L^{-1}, (Roest *et al*., 2003; Van Bakel and Stuyt, 2011). Surface water quality issues typically play a role during the drier and warmer growing season, when the demand for freshwater increases but its availability is limited. As the saline seepage systems of deep polders are not well understood yet, this research addresses this knowledge gap by studying the processes involving saline seepage in two deep polders: Noordplas Polder and Haarlemmermeer Polder (Fig. 1.3).

Saline seepage in sub-recent transgression areas

The most important feature in the sub-recent transgression areas concerning saline seepage is the shallow occurrence (< 5 m BGL) of very saline groundwater (50 to 100 % seawater) (Fig. 1.1; Goes *et al*., 2009). Here, surface water salinization by saline seepage is obvious and makes the water too saline for any use. In absence of fresh surface water, the freshwater availability for agricultural purposes in these saline seepage areas is limited to rainwater lenses which develop below agricultural fields. However, upward moving saline groundwater limits the penetration depth of rainwater, and thus the volume of the rainwater lens (Fig. 1.6). During dry periods, saline groundwater may even reach the root zone via capillary rise, affecting crop growth (Katerji *et al*., 2003; Rozema and Flowers, 2008). The size and dynamic behaviour of these shallow rainwater lenses are of great importance from an agricultural perspective. Their limited size and vicinity to the land surface likely make them vulnerable to climate change (i.e. changing precipitation and evapotranspiration patterns) and sea level rise (i.e. enhancing saline seepage). Thin rainwater lenses in areas with saline seepage are further referred to as RW-lenses.

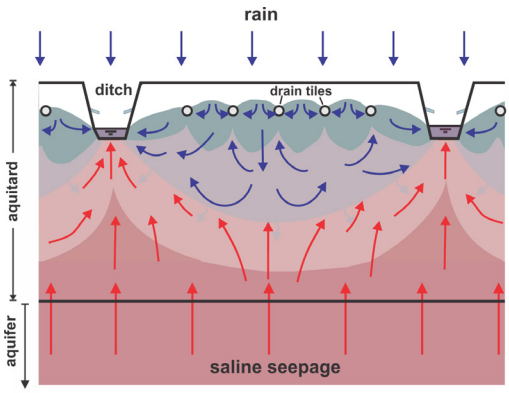

Fig. 1.6. Schematic visualization of a thin rainwater lens in an area with upward seepage of saline groundwater (RW-lens).

So far, research on fresh rainwater lenses in saline groundwater has mainly been focused on so-called Badon Ghijben-Herzberg (BGH) freshwater lenses in elevated areas like sandy dunes along the coast and on small islands that lack an upward groundwater flow component (e.g. Drabbe and Badon Ghijben, 1889; Herzberg, 1901; Fetter, 1972; Van Dam and Sikkema, 1982; Meinardi, 1983; Underwood *et al*., 1992; Stuyfzand, 1993; Collins and Easley, 1999; Bakker, 2000; Sulzbacher *et al*., 2012). BGH-lenses are generally thick and the depth of the fresh-saline interface (Z_{fs}) is mainly controlled by the relative density difference *(β)* and the phreatic water level *(h)* according to the Badon Ghijben Herzberg relation: $Z_{fs} = h / \beta$. However, the characteristics and dynamic behaviour of shallow RW-lenses and the interaction between infiltrating rainwater and saline seepage are not well known. Therefore, the characteristics, spatial variability and dynamics of RW-lenses and the mechanisms controlling them were studied in the south-western delta of the Netherlands (Fig. 1.3).

1.4 Thesis objectives and research questions

The general objective of this PhD-thesis was to gain understanding of the spatial variability and temporal dynamics of saline seepage, quantify the hydrologic processes and extrapolate the findings to larger areas. This research aims to address the knowledge gaps associated with the two main saline seepage systems formulated in the previous section. To study the saline seepage processes leading to salinization of the Dutch delta, the research was divided into two parts: Preferential saline seepage through boils (Part I), and Rainwater lenses in areas with saline seepage (Part II). The specific research questions of this PhD thesis have been addressed in the different chapters and are formulated as follows:

Part I: Preferential saline seepage through boils

For the deep polders, the hypothesis was that seepage is not uniform and preferential saline seepage through boils plays an important role in the surface water salinization.

- What is the nature and spatial variability of saline seepage in a deep polder, and how important is preferential saline seepage through boils? (Chapter 2)
- What is the contribution of different salt sources, and in particular saline boils, to the diurnal variability of salt concentration of surface water and salt loads in a deep polder, and how can it be quatified regarding large uncertainties of inflow quantity and quality? (Chapter 3)
- Is saltwater upconing by preferential seepage through boils the mechanism leading to elevated boil water salinities and what are the controlling factors? (Chapter 4)

Part II: Rainwater lenses in areas with saline seepage

For the sub-recent transgression areas the hypothesis was that the interaction between infiltrating rainwater and saline seepage determines the characteristics and dynamic behaviour of rainwater lenses, and that it plays an important role in the salinization of shallow groundwater and soil water.

- What are the characteristics and spatial variability of thin rainwater lenses in areas with saline seepage and what are the mechanisms and factors that determine their occurrence and size? (Chapter 5)
- What are the temporal dynamics of thin rainwater lenses and mixing processes between infiltrating rainwater and upward saline seepage? (Chapter 6)

1.5 Research approach

The saline seepage processes in deep polders, and in particular the preferential saline seepage through boils (Part I), were studied in two deep polders in the western Netherlands 'Noordplas Polder' and 'Haarlemmermeer Polder'. The research was mainly based on a extensive multi-scale field study which involved the collection of spatial data of surface water and groundwater quality, vertical head gradients, boil discharge and salinity, the collection of temporal data of the polder water discharge and chloride concentration for a period of 2 years, and detailed measurements of local boil systems. Different analytical and numerical methods were used to analyze the field data and quantify the processes.

The characteristics and dynamics of thin rainwater lenses in areas with saline seepage (Part II) were studied in the south-western delta of the Netherlands (Province of Zeeland). Different geophysical and hydro(geo)logical techniques were used to map the characteristics and spatial variability of RW-lenses. The following techniques were applied to obtain detailed salinity-depth profiles at point scale: electrical soil conductivity measurements using the TEC-probe, groundwater sampling at small depth intervals, and electrical cone penetration tests (ECPT). The point measurements were carried out at 49 different locations distributed over the entire Province of Zeeland and which differed in characteristics such as surface level elevation, soil type and groundwater salinity. Non-invasive continuous vertical electrical soundings (CVES) and surface electromagnetic measurements (EM31) were used to map the spatial variation of RW-lenses within an agricultural field. A helicopter-borne frequency-domain electromagnetic (HEM) survey was performed to map the thickness of rainwater lenses for a large area (56 km^2) on the island of Schouwen-Duivenland. Based on all measurements, two tile-drained agricultural fields were selected to study the RW-lens dynamics. To this end, we collected for a period of 2 years monthly data on ground and soil water salinity in combination with daily observations of water table elevation, drain tile discharge and drain water salinity. Numerical modeling was applied to analyze the processes controlling the size and characteristics of RW-lenses and their dynamic behaviour.

1.6 Thesis outline

The five research questions are addressed in the subsequent chapters. Each chapter is based on a paper that has been published in an international peer-reviewed journal.

Part I: Preferential saline seepage through boils

Chapter 2 describes the spatial variability and characteristics of saline seepage in a typical deep Dutch polder (Noordplas Polder) based on observations and analysis of the geological structure of the HCL, head differences, groundwater composition, surface water salinity, polder water discharge and salt load, temperature profiles, and boil observations. Three different forms of seepage were distinguished based on their flux and salinity, and the importance of preferential saline seepage via boils regarding the salinization of the surface waters was demonstrated.

Chapter 3 presents a probabilistic dynamic water and salt balance model to simulate the daily varying surface water salt concentration and salt loads in a deep polder taking into account large uncertainties of inflow quantity and

quality. The model was used to simulate 2 years of daily to weekly observations of discharge, salt loads and salt concentration of water pumped out of the Noordplas Polder. Subsequently, the contributions of different sources, including the three forms of seepage defined in chapter 2, to the surface water salinization were quantified. The water and salt balance calculations confirmed the dominant role of boils to the surface water salinization in deep polders.

Chapter 4 describes the natural saltwater upconing by preferential seepage via boils, identified in chapter 2 and 3 as a key process in the salinization of Dutch deep polders. The hypothesis was that saltwater upconing is the mechanism leading to elevated boil water salinities. Detailed field measurements of two local boil systems in the Noordplas Polder and the Haarlemmermeer Polder were described to demonstrate natural saltwater upconing and to determine the impact of boils on the local groundwater system. Numerical modeling and sensitivity analyses were applied to assess the main factors controlling saltwater upconing and boil water salinity.

Part II: Rainwater lenses in areas with saline seepage

Chapter 5 describes the characteristics and spatial variability of rainwater lenses in areas with saline seepage (RW-lenses) based on different types of field measurements applied at different scales in the south-western delta of the Netherlands. The applied techniques were combined in order to extrapolate measurements at point scale (groundwater sampling, TEC-probe measurements, ECPT) to field scale (CVES, EM31), and even to regional scale using helicopter-borne electromagnetic measurements (HEM). Numerical models were used to analyze the RW-lens developing mechanisms and to determine the main factors controlling the size and characteristics of RW-lenses.

Chapter 6 presents a conceptual model of RW-lens dynamics and the mixing behaviour between rainwater and saline seepage based on field measurements at two tile-drained agricultural fields in the south-western part of the Netherlands and numerical simulations for one of the sites. For the first time, field-based evidence of RW-lens dynamics was systematically collected by monthly ground- and soil water sampling, in combination with daily observations of water table elevation, drain tile discharge and drain water salinity. These observations were reproduced by the numerical model and the model was used to simulate the key RW-lens characteristics and the dynamic processes in the RW-lens.

Part III: Synthesis and discussion, summary and conclusions

The final chapter 7 gives answers to the research questions, and summarizes, integrates and discusses the results of the PhD-research and outlines how this research has furthered the knowledge of saline seepage processes. Based on the findings of this PhD-research, the vulnerability of the Dutch saline seepage systems to climate change and sea level rise is discussed. Subsequently, implications of the findings to the freshwater supply sustainability and strategies are described as well as the effectiveness of some possible adaptation and mitigation measures. A review is given of different field techniques for the mapping and the quantification of saline seepage. The synthesis ends with suggestions for further research.

Part I

Preferential saline seepage through boils

Chapter 2

Upward groundwater flow in boils as the dominant mechanism of salinization in deep polders, the Netherlands

Perry de Louw, Gualbert Oude Essink, Pieter Stuyfzand, Sjoerd van der Zee
Published in Journal of Hydrology 394, 494-506, 2010

Abstract

As upward seepage of saline groundwater from the upper aquifer is leading to surface water salinization of deep polders in the Netherlands, we monitored the processes involved in the Noordplas Polder, a typical deep polder. Our results show three types of seepage: (1) diffuse seepage through the Holocene confining layer, (2) seepage through paleochannel belts in the Holocene layer, and (3) intense seepage via localized boils. They differ with regard to seepage flux, chloride concentration, and their location in the polder; thus, their contributions to surface water salinization also differ. Permeable, sandy paleochannel belts cut through the lower part of the Holocene layer, resulting in higher seepage fluxes than the diffuse seepage through the Holocene layer where there are no paleochannels. The average chloride concentration of paleochannel seepage is about 600 mg L^{-1}, which is six-fold higher than the average concentration of diffuse seepage. The highest seepage fluxes and chloride concentrations are found at boils, which are small vents in the Holocene layer through which groundwater preferentially discharges at high velocities. This results in upconing of deeper and more saline groundwater, which produces an average chloride concentration of 1100 mg L^{-1}. Despite the fact that seepage fluxes are difficult to measure, we were able to calculate that boils contribute more than 50% of the total chloride load entering the Noordplas Polder and they therefore form the dominant salinization pathway.

2.1 Introduction

In many coastal areas, groundwater is saline because of sea water intrusion, marine transgressions and sea spray (Stuyfzand and Stuurman, 1994). The salinity of groundwater may pose problems for the sustainable exploitation of fresh groundwater for drinking water, irrigation or industrial purposes. Land subsidence, climate change and sea level rise accelerate salinization by enhancing the intrusion rate (Oude Essink, 2008), which means that low-lying deltaic areas, such as the deltas of the Mekong, Ganges, Mississippi, and Po rivers, are highly vulnerable (Meisler *et al*., 1984; Bobba, 2002; Ranjan *et al*., 2006; Giambastiani *et al*., 2007; Barlow and Reichard, 2010; Custodio, 2010). In the Netherlands, which has about 25% of its surface below sea level (Fig. 2.1), the upward seepage of saline and nutrient-rich groundwater into deep polders that have been reclaimed from lakes, leads to salinization and eutrophication of the regional surface water (Wesseling, 1980; Van Rees Vellinga *et al*., 1981; De Louw *et al*., 2000, Van Puijenbroek *et al*., 2004, Van der Eertwegh *et al*., 2006). This seepage makes the surface water unfit for irrigation and adversely affects aquatic ecosystems.

Since salinization by groundwater seepage has been a major water quality problem for a long time, there have been several studies on the water and chloride balances of deep polders in the coastal area of the Netherlands (ICW, 1976; Wit, 1974; Van Rees Vellinga *et al*., 1981; Pomper

and Wesseling 1978; Griffioen *et al*., 2002). These earlier studies considered seepage through the confining top layer of clay and peat, with its low permeability, to be spatially uniform. However, this made it impossible to explain the high levels of salt load which were observed (e.g. ICW, 1976; Van Rees Vellinga *et al*., 1981). The earlier assumption of uniform upward seepage was obviously incorrect and indeed, many studies showed that groundwater seepage could occur through preferential pathways (e.g. Becker *et al*., 2004; Kishel and Gerla, 2002; LaSage *et al*., 2008; Kalbus *et al*., 2009). Preferential groundwater seepage may also have important implications for the chemical loading to surface waters (Keery *et al*., 2007; Tesoriero *et al*., 2009). The hydrochemical composition of preferential seepage can be used to distinguish this form of upward groundwater flow from other types. Geological mapping of the lowlands of the Netherlands shows that permeable, sandy paleochannel belts partly cut through the confining top layer (Weerts, 1996; Berendsen, 1998; Berendsen and Stouthamer, 2000; Hijma et. al., 2009) and thus act as preferential pathways for upward groundwater flow. An even more localized form of preferential groundwater flow, called boils, has been observed in deep polders (Vink, 1954; Rijnland, 1967, 1975, 1981; De Louw *et al*., 2004). Boils are vents that connect the underlying aquifer and the surface water or ground level through the confining top layer. They may develop when the pressure of upwelling water is greater than the pressure exerted by the weight of the overlying stratum. This produces heaving and cracking and the occurrence of pin boils, which may enlarge and become sand boils if the erosive forces increase (Holzer and Clark, 1993; Li *et al*., 1996; TACFD, 1999). Pin boils are small springs or upwellings of water, whereas sand boils are larger vents that discharge both water and sediments (Li *et al*., 1996). Permanent, large hydraulic gradients on the edges of deep polders in the Netherlands stimulate the development of such boils. Two types of boils have been described in the literature: flood-induced boils along artificial levees (Turnbull and Mansur, 1961; Kolb, 1976; Sellmeijer and Koenders, 1991; Holzer and Clark, 1993; Li *et al*., 1996; TACFD, 1999; Ozkan, 2003; Ojha *et al*., 2003), and earthquake-induced liquefaction boils (sand blows) (Seed and Idriss, 1967; Holzer and Clark, 1993; Obermeijer, 1995; Li *et al*., 1996, 2004). However, because boils are a fairly common feature of polder areas, and perhaps in other areas with relatively large, vertical pressure gradients, they have been given little attention in the deep polders. The contribution of boils and seepage through paleochannel belts to the salinization of deep polders is therefore unknown.

Here we present evidence for different types of upward groundwater seepage in a deep polder and, from independent physical and chemical observations, we deduce how much boils contribute to chloride loads in the surface water of the polder.

2.2 Material and methods

2.2.1 Study area

The study area is a typical deep polder in the west of the Netherlands called the Noordplas Polder (Fig. 2.1). It covers 37 km^2, of which 86% is used for agriculture (arable farming 62%; pasture 24%) and 14% is urban area. This former lake was reclaimed in different stages between 1750 and 1850 A.D. (Schultz, 1992). Its average soil surface level is -5 m below mean sea level (MSL) which is 2.5 m lower than the surrounding peat lands (Fig. 2.2). The polder is drained by an artificial network of ditches and underground drains. The drained water is pumped out of the

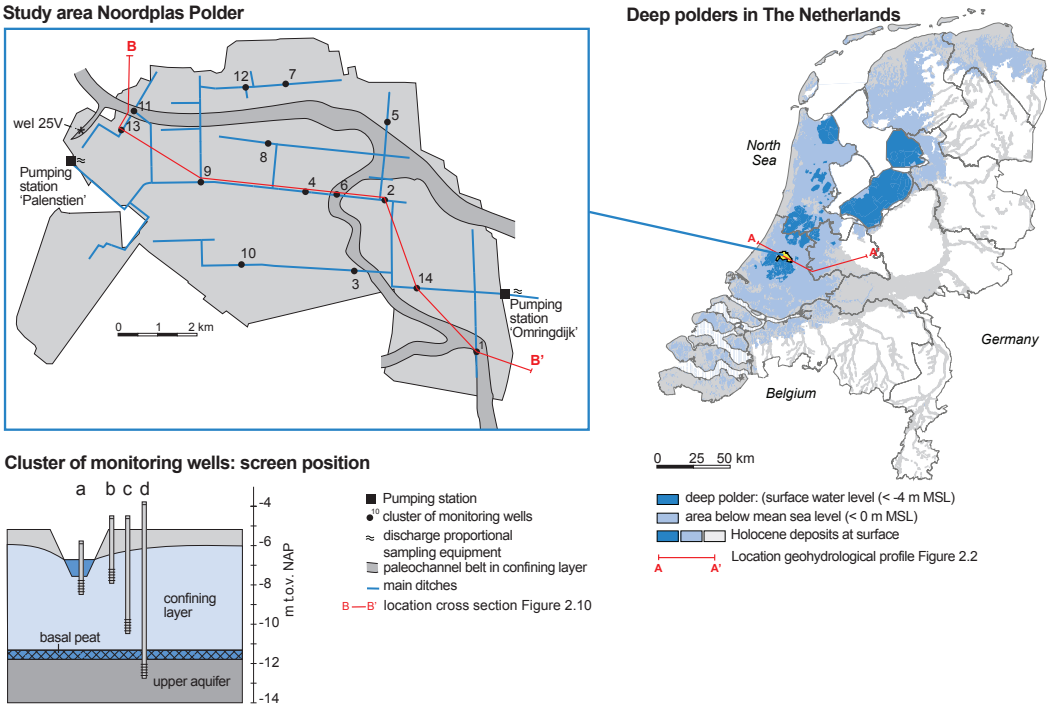

Fig. 2.1. Location of deep polders (reclaimed lake areas) in the Netherlands and of Noordplas Polder (study area), showing monitoring points, main ditches and the paleochannel belts in the Holocene confining layer.

polder into a higher-lying canal (called the 'boezem') at two pumping stations and then conveyed to the sea. During dry periods, fresh water from the regional surface water network is admitted to the polder via inlets (inlet water) to maintain the proper level of surface water and to decrease the chloride concentrations in the surface water by flushing (Van de Ven, 2003). During these dry periods, both the inflow of water via inlets and the outflow via pumps occur simultaneously. The surface water levels in the polder ditches are kept at a nearly constant level of about -6.2 m MSL.

The hydrogeological situation is characterized by two (semi-) confined aquifers of Pleistocene sands, as shown in Fig. 2.2. The upper aquifer is covered by a 6-9 m thick, confining layer of Holocene peat, loam and clay of low permeability (Mulder *et al.*, 2003). The hydraulic conductivity of these sediments varies between 10^{-4} m d^{-1} and 10^{-1} m d^{-1} (Weerts, 1996). The lower part of this Holocene layer is the less permeable part which consists of a 10-50 cm thick compacted, mineralized peat (basal peat). At various locations, the compacted peat and overlying loam and clay deposits have been eroded by streams and tidal channels during the Holocene (Van der Valk, 1996; Hijma *et al.*, 2009). We mapped the locations of these sandy paleochannel belts in the Noordplas Polder (Fig. 2.1) by using the lithological borehole descriptions of the Holocene confining layer derived from the Geological Survey of the Netherlands' database (www.dinoloket.nl). We found that the paleochannels are about 200-300 m wide, at a depth of 3-5 m below the surface. They are in direct contact with the upper aquifer and act as preferential pathways in the Holocene confining layer because of their higher permeability (Fig. 2.2). Weerts (1996) found hydraulic conductivities in the range of 1.0-10.0 m d^{-1} for these sandy paleochannel deposits.

The groundwater in the Pleistocene aquifers is brackish to saline and shows an

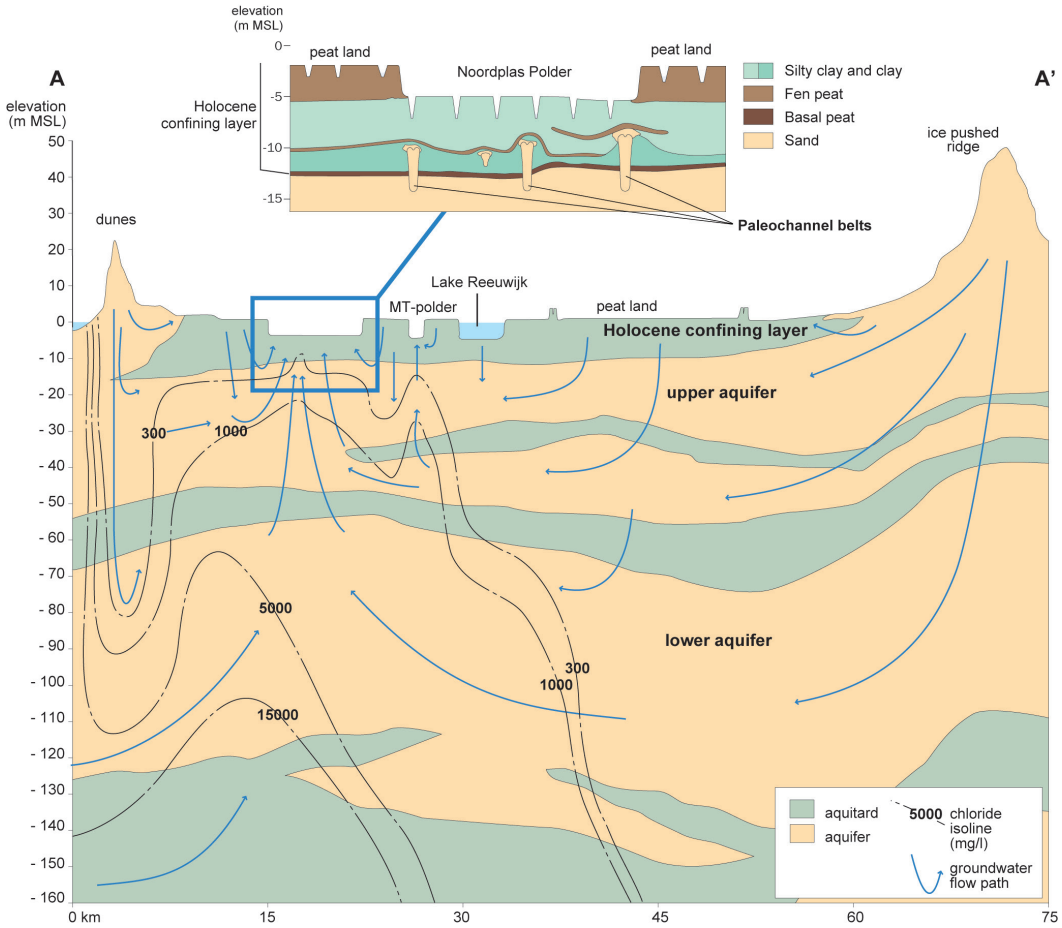

Fig. 2.2. Regional hydrogeological profile across the study area, perpendicular to the North Sea. The position of the aquifers and aquitards is based on descriptions from boreholes at a density of 0.25/km2 (REGIS II, 2005). The chloride distribution is derived from the Dutch national database (www.dinoloket.nl). Position of profile A-A' is indicated in Fig. 2.1

increasing trend of chloride concentrations with depth (Fig. 2.2) (Van Rees Vellinga *et al.*, 1981, Oude Essink, 1996). The origin of salt in this groundwater is mainly linked to the Holocene transgressions (Volker, 1961; Pomper and Wesseling, 1978; Stuyfzand, 1993; Post, 2004; Stuyfzand and Stuurman, 2008). Hydraulic heads in the upper aquifer exceed surface water levels in the polder, resulting in upward seepage of brackish–to-saline groundwater from the upper aquifer into the overlying Holocene layer (Van Rees Vellinga *et al.*, 1981, De Louw *et al.*, 2000). This seepage water finally discharges into the surface water system.

2.2.2 Monitoring program

The groundwater and surface water monitoring program in the Noordplas Polder aimed to identify and quantify water fluxes and chloride loads into the surface water. To determine the daily polder water discharge, the pumping time was recorded automatically at the two pumping stations (Fig. 2.1). Multiplying the total daily pumping time by the pumping rate gave the daily volume

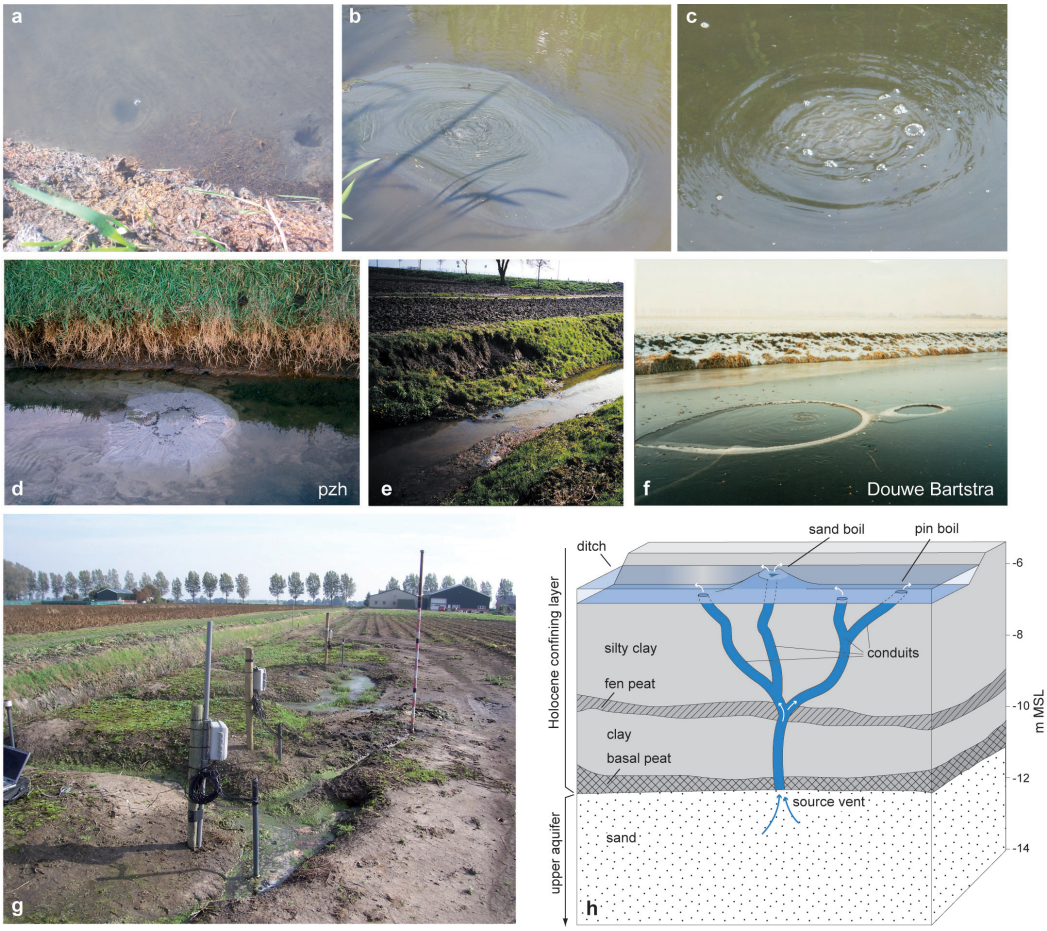

Fig. 2.3. Boils in deep polders: a) pin boil, b) sand boil, c) a boil emitting methane, d) sand volcano, e) collapsed ditch bank, f) hole in ice caused by warmer water welling up from boil, g) sand boils on land, h) schematic diagram of boils with several conduits.

of polder water discharge. The pumping water was sampled automatically with a frequency proportional to the discharge, to determine the chloride loads that leave the polder. The samples were mixed automatically into one bulk sample and collected every 3-7 days; they were analyzed in the laboratory for their chloride content. Multiplying the chloride concentration by the volume of polder water discharged gave the total chloride load being pumped out of the polder. We sampled the inlet water at 5 major inlets and analyzed it for chloride on a monthly basis. Precipitation was measured at two locations in the polder with a tipping bucket rain gauge. The chloride concentration of precipitation was measured once. Daily sums of the potential reference crop evapotranspiration (Makkink, 1957) were obtained from two nearby meteorological stations (Valkenburg and Schiphol) of the Royal Netherlands Meteorological Institute (KNMI).

We installed 14 clusters of groundwater monitoring wells to quantify the water levels and to analyze water composition. The numbered monitoring clusters are shown in Fig. 2.1. We installed 3 clusters (1, 6 and 11) in areas with paleochannel belts in the Holocene confining layer and 11 clusters outside these areas. Each cluster contained 4 monitoring wells with screens at different depths to measure the

change of heads and groundwater composition with depth (Fig. 2.1). The 0.5-m-long screens of the monitoring wells are located just below the ditch bottom (a), in the Holocene confining layer at 2-3 m (b), and at 4-5 m depth (c), and in the upper aquifer at 6-8 m depth (d). Heads were measured every two weeks and 30 monitoring wells were automatically logged every hour. The heads were corrected for density differences by conversion into fresh water heads (Post *et al*., 2007). At every monitoring cluster, we installed a gauge in the ditch for surface water level observations. We sampled and analyzed the surface water and groundwater from screens a, c and d of each cluster twice (April 1999 and September 1999). Before taking groundwater samples, we extracted water from the monitoring wells until pH and EC became stable and the extracted volume was at least three times the volume of the monitoring wells. In the field, we measured pH, temperature (T), electrical conductivity (EC), dissolved oxygen (DO) and bicarbonate (HCO_3). Samples for cation analysis were filtered over 0.45 μm and preserved with 1% concentrated suprapure HNO_3. In the laboratory, we measured major ions (Na, K, Ca, Mg, Cl, and SO_4), nutrients (NH_4, NO_3, NO_2, N-kjel, ortho-P, tot-P) and iron (Fe). We used Stuyfzand's method (1989) to classify the groundwater into chemical types.

We mapped the chloride concentration of the surface water in the main ditches of the polder to determine the spatial variation of saline seepage. To obtain large contrasts in the surface water salinity, the survey was carried out in a dry period (August 1999) when dilution of the seepage water by rainfall was minimal. We took samples from the surface water at 250 m intervals and analyzed them for chloride in the laboratory.

A first attempt to map the boils and to determine their chloride concentration in the Noordplas Polder was done by the Rijnland District Water Control Board in 1967 (Rijnland, 1967). In our field work, we updated their map on the basis of the boils' visible properties and took samples of the boil water for chloride analysis. Boils are evident as small vents in ditches (Fig. 2.3a), where water flows out or where "boiling" of quicksand occurs, as small sand volcanoes (Fig. 2.3b, d), or as collapsed ditch banks (Fig. 2.3e). We observed methane gas escaping through boils (Fig. 2.3c). Boils may be supported by several interconnected conduits in the Holocene confining layer originating from one source vent in the upper aquifer (Fig. 2.3a, g, h). For 15 of the mapped boils, we measured their upward seepage flux and estimated the upward flow velocity. Upward seepage fluxes were determined by collecting the outflowing boil water in a measuring cup during a certain time span. Where the outflow occurred underwater, instead of on land or in ditch banks, we isolated the outflowing boil water from ditch water by using a tube and then measured its flux. Upward flow velocities were estimated by dividing the measured seepage flux by the cross-sectional area of the outflow vent.

We studied one boil in greater detail (boil 25V in Fig. 2.1). We installed 6 monitoring wells at 0, 5, 10, 25, 30, 75 m from this boil, with their screens located in the upper aquifer (7 m depth). Water samples were taken from these wells, from surface water and from the boil water, and analyzed for chloride content. We measured the soil temperature in and around the boil to trace lateral variations in upward groundwater flow and to evaluate its flow pattern (Cartwright, 1974; Van Wirdum, 1991; Taniguchi *et al*., 2003; Becker *et al*., 2004; Bense and Kooi, 2004). The soil temperature was measured with a temperature probe in and around the boil, at up to a depth of 4 m and at intervals of 0.1 m.

2.3 Results

2.3.1 Heads

In Fig. 2.4 we show the observed heads for groundwater monitoring wells in cluster 3. Hydraulic heads in the upper aquifer (screen d) exceed both the surface water levels as well as the heads in the Holocene confining layer (screens a, b and c), indicating a permanent upward groundwater flow from the upper aquifer. Averaged over all the monitoring clusters, the head difference between the upper aquifer and Holocene layer was as much as 1.0 m. These head differences, and consequently seepage fluxes, do not fluctuate much throughout the year. The maximum yearly amplitude of the head differences was less than 20 cm. These observations for cluster 3 are in full agreement with those for all 13 monitoring clusters.

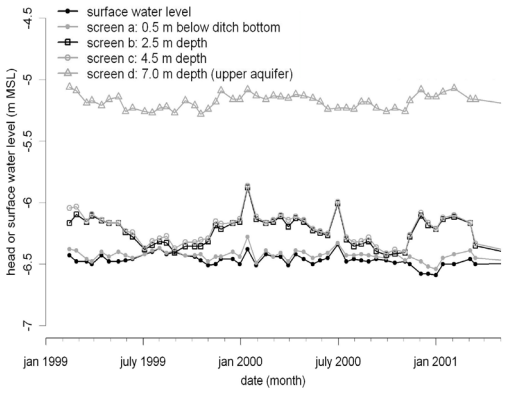

Fig. 2.4. Measured surface water level and hydraulic heads in Holocene confining layer (screens a, b, c) and upper aquifer (screen d) for monitoring wells in cluster 3.

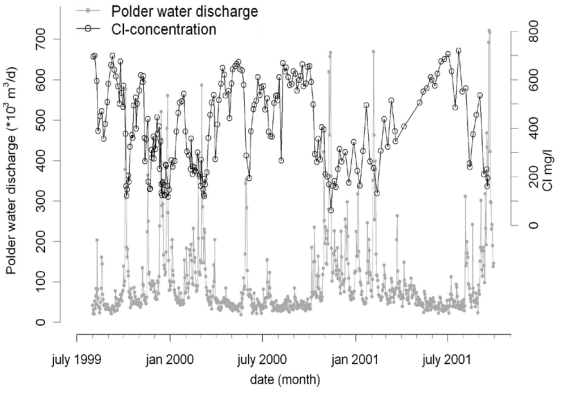

Fig. 2.5. Daily discharge volume and chloride concentration of water pumped out of the polder over period July 1999 – September 2001.

2.3.2 Polder water discharge and chloride concentration

The daily discharge and chloride concentration of the water pumped out of the polder is shown in Fig. 2.5. The total polder water discharge was equal to 33.8 M m^3 y^{-1}, whereas the measured precipitation surplus is only 19.5 M m^3 y^{-1}. The large difference between the polder water discharge and the precipitation surplus indicates that other sources must contribute significantly to the water input, i.e. upward groundwater seepage from the upper aquifer and the admission of inlet water, The total measured chloride load pumped out of the polder equals 11.6 M kg y^{-1}. Periods of higher discharge are typically characterized by low chloride concentrations because of rainwater dilution. These low concentrations (< 350 mg L^{-1}) occur in winter and during wet periods in summer. During dry periods, the relative contribution of saline seepage increases and chloride concentrations reached up to 720 mg L^{-1}. The yearly average chloride concentration of the polder water discharge is about 400 mg L^{-1}.

The surface water chloride concentration in August 1999 varied spatially between 50 mg L^{-1} and 2200 mg L^{-1} (Fig. 2.6). We found elevated chloride concentrations (> 600 mg L^{-1}) near paleochannel belts and at boils.

Table 2.1. Average concentrations of the main chemical constituents (in mg L^{-1}), electrical conductivity (EC, mS cm^{-1}) and pH (-) of surface water and groundwater at different depths (screens a, c, d) for areas with and without paleochannel belts in the Holocene confining layer (HCL).

	Cl	NH_4	NO_3	HCO_3	SO_4	o-P	t-P	K	Mg	Na	Ca	Fe	EC	pH
No paleochannel belts in HCL (N=11, Freq=2)														
Surface water	267	2.8	1.8	528	312	0.1	0.4	15	35	146	251	4.0	n.d.	n.d.
Below ditch bottom (a)	186	17.6	1.0	719	419	1.0	2.0	24	54	139	287	4.2	2.0	6.58
Confining layer, 5 m (c)	117	35.8	0.2	1046	250	4.3	5.2	27	82	132	202	2.1	2.0	6.57
Upper aquifer (d)	117	37.3	0.2	1024	12	1.3	2.9	25	67	119	114	13.8	1.7	6.46
Paleochannel belts in HCL (N=3, Freq=2)														
Surface water	608	5.6	1.0	580	270	<0.05	0.2	15	47	283	283	5.1	n.d.	n.d.
Below ditch bottom (a)	1245	18.7	<0.05	1050	8	<0.05	0.4	19	77	718	236	12.8	4.7	6.49
Confining layer, 5 m (c)	376	28.5	<0.05	976	17	1.9	2.6	21	69	247	185	18.8	2.4	6.43
Upper aquifer (d)	592	27.5	<0.05	1127	9	<0.05	1.1	23	73	369	194	26.8	3.1	6.45

N = number of locations, Freq = number of measurements per location, n.d. = not determined

2.3.3 Groundwater composition

In Table 2.1 we show the average concentrations of the main constituents of the surface water and groundwater at different depths, for the 3 monitoring clusters in areas with paleochannel belts in the confining layer, and the 11 clusters in areas without paleochannel belts. The differences in concentrations between the analyzed groundwater in April 1999 and September 1999 are small (< 5%). However, the chloride concentration of groundwater measured in the upper aquifer directly below the Holocene confining layer (screen d) is spatially quite variable, ranging from 33 mg L^{-1} to 675 mg L^{-1} (Fig. 2.6). The average chloride concentration in the upper aquifer for areas with paleochannel belts was 592 mg L^{-1}. In the 11 sites without paleochannel belts, the average chloride concentration was much lower at 117 mg L^{-1} (Table 2.1). Another remarkable difference are the high SO_4^{2-} concentrations in the Holocene layer (screens a and c) for the areas without paleochannel belts, whereas concentrations of SO_4^{2} are consistently and significantly smaller in areas with paleochannel belts (Table 2.1).

2.3.4 Boils

At 54 locations in the Noordplas Polder we observed intense upward groundwater flow in boils (Fig. 2.6); 17 of these were mapped in 1967 (Rijnland, 1967). We found that 85% of the boils occur in ditches or ditch banks, and only 15% occur on land. As expected, most visible boils occur at the edges of the polder, in ditches and on top of paleochannel belts (Fig. 2.6). At the edges of the polder, the heads in the upper aquifer are largest, increasing the probability of boil development. Underneath ditches and at locations with paleochannel belts, the weight of the Holocene layer is markedly reduced, which also significantly increases the risk of boil development. For 49 of the observed boils it was possible to determine their chloride concentration, from which the average chloride concentration of the boils was found to be as much as 1100 mg L^{-1}, with a median of 1300 mg L^{-1}. The larger boils tended to have even higher concentrations, with a recorded

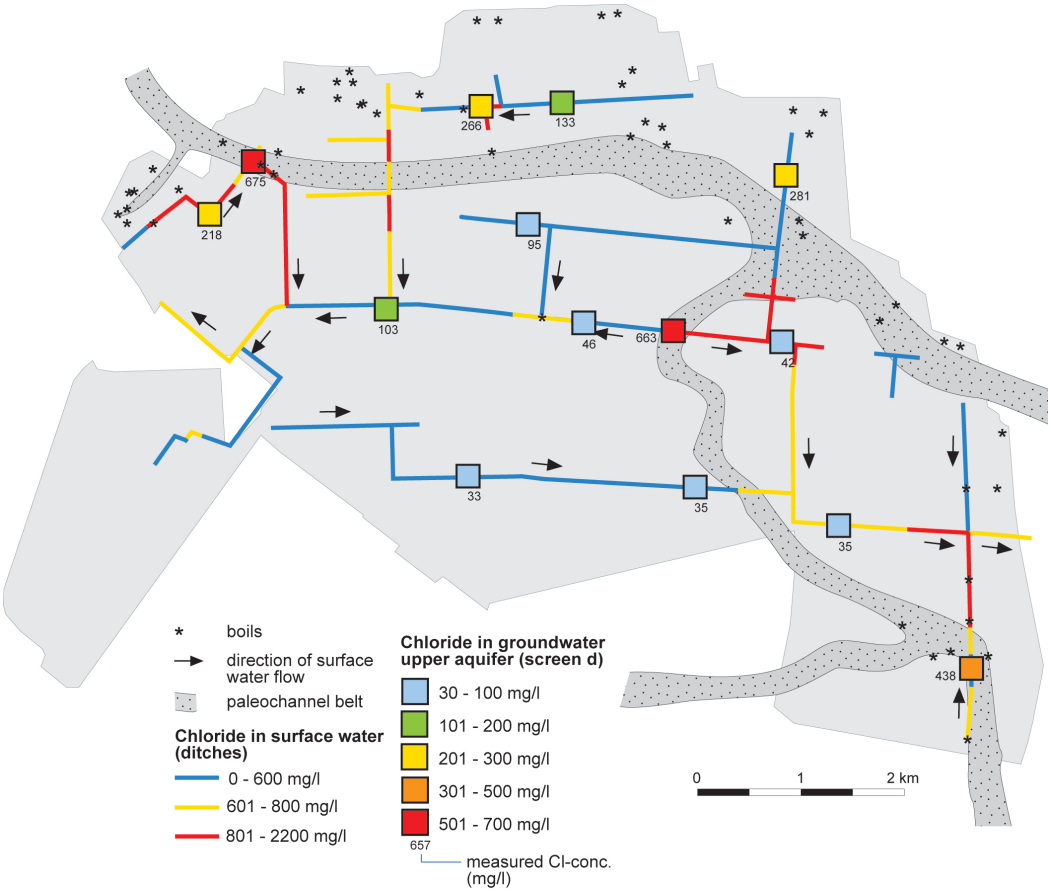

Fig. 2.6. Chloride monitoring results (mg/l) for the Noordplas Polder: surface water in August 1999 (sampling interval 250 m) and groundwater at the top of the upper aquifer, screen d (average of April and September 1999). The mapped boils and location of the paleochannel belts in the Holocene confining layer are indicated.

maximum of 2850 mg L^{-1} (Table 2.2). Fluxes measured at 15 individual boils ranged from 0.5 to 100 $m^3 d^{-1}$ and estimated flow velocities attained as much as 800 m d^{-1}. It must be noted that it was not possible to map all the boils, because they are not visible in the main water courses, which are too wide, too deep and too turbid due to eutrophication. Therefore, it was also not possible to upscale the measured boil fluxes to a total boil flux for the whole polder.

Fig. 2.7 shows the results of detailed soil temperature–depth measurements in and around boil 25V at the end of the summer period (1999). The soil temperature in the boil was relative constant with depth (about 11°C), whereas outside the boil the soil temperature was much higher and decreased from about 17°C at surface level to about 13°C at 3 m depth. Detailed measurements around the same boil showed that the chloride concentration of boil water was nearly twice as high as that of groundwater in the upper aquifer at 7 m depth (Fig. 2.8). The chloride concentration of the surface water downstream of the boil was about twice as high as upstream of the boil.

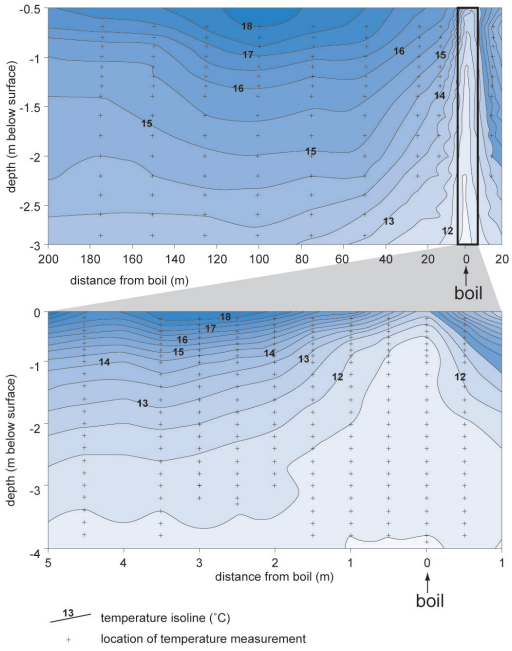

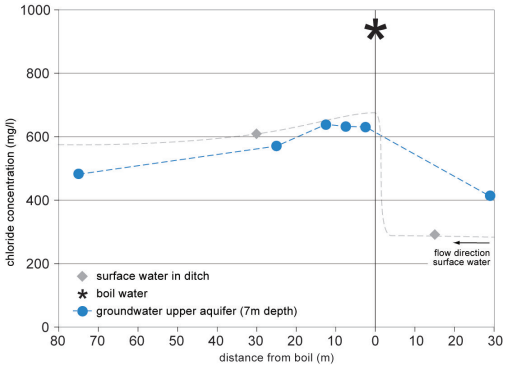

Fig. 2.8. Chloride concentrations of surface water in ditch upstream and downstream from boil 25V, and of groundwater at the top of the upper aquifer at various distances from the boil.

< Fig. 2.7. Temperature–depth profiles in and around sand boil 25V in the Noordplas Polder (see Fig. 2.1 for location). Crosses indicate the depth of temperature measurements (on 15 September 2006).

Table 2.2. Chloride concentrations (mg L^{-1}) of diffuse seepage, paleochannel seepage, boils, polder water discharge, inlet water and precipitation in the Noordplas Polder for monitoring period 01-08-1999 up to 01-08-2001.

	Mean	Median	Sdev	Min	Max	N	Freq
Diffuse seepage	117	95	96	33	281	11	2
Paleochannel seepage	592	663	134	438	675	3	2
Boils	1100	1300	638	337	2850	49	1
Polder water discharge	404	392	177	61	720	2	172
Inlet water	223	135	147	115	455	5	12
Precipitation	12	12	-	12	12	1	1

Sdev = standard deviation, N = number of locations, Freq = number of measurements per location

2.4 Discussion

2.4.1 Types of seepage

The observed head losses in the upward direction were persistent in space and time (Fig. 2.4) and show that there is permanent upward groundwater seepage from the upper aquifer into the overlying Holocene confining layer for the entire area that was monitored. The large spatial variation of chloride concentration of the surface water (Fig. 2.6) implies that upward saline seepage is not uniform in the polder. The elevated chloride concentrations (> 600 mg L^{-1}) of the surface water at boils and near areas with paleochannel belts in the Holocene layer indicate that upward saline seepage occurs preferentially at these locations. These paleochannel belts may well form a conduit for upward groundwater flow because they consist of permeable

sands and cut through the lower part of the Holocene layer, which is less permeable. The locations of these paleochannel belts could be mapped relatively accurately using borehole descriptions of the Holocene layer (about 10 borehole records per km^2, www.dinoloket.nl).

Based on these findings, we have been able to distinguish three types of upward groundwater seepage: (1) diffuse seepage, (2) paleochannel seepage, and (3) intense seepage via localized boils (Fig. 2.9). Diffuse seepage is seen over the majority of the polder (31 km^2), with groundwater flowing upward through the Holocene sediments (peat, loam, clay) of low permeability. Paleochannel seepage is associated with the much more permeable, sandy, paleochannel belt deposits in the Holocene layer and is seen only in the area with these belts (6 km^2). Upward groundwater flow fluxes through these permeable, sandy paleochannel belts are higher than the diffuse seepage fluxes because of the hydraulic conductivity differences. Boils are small, localized vents in the Holocene layer through which groundwater is discharged at high velocities.

2.4.2 Seepage fluxes

Besides the observations of intense outflow of water and the high flow velocities recorded at the boils, there is another quite different indicator that strongly supports the preferentiality of flow and transport in boils. Temperature profiles

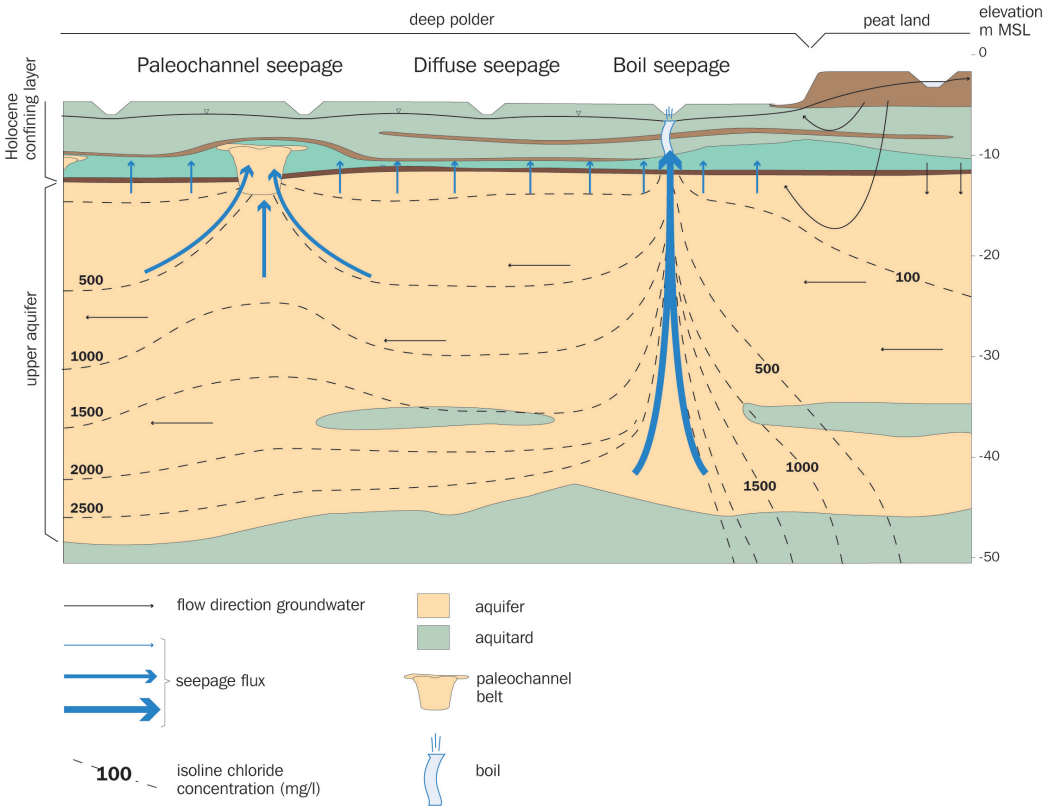

Fig. 2.9. Diagram showing upconing mechanism for the three seepage types with different fluxes and chloride concentrations: diffuse seepage, paleochannel seepage and boil seepage.

around boil 25V clearly showed a flow pattern with very localized, rapid, vertical upward flow (Fig. 2.7). In the Netherlands, seasonal variations in atmospheric temperature normally penetrate into the soil to a depth of 15 m at most (Bense and Kooi, 2004). The year-round soil temperature at this depth is 10.5°C to 11°C. At boils, the penetration of atmospheric temperatures into the soil is counteracted by the rapid upward flow of groundwater with a constant temperature of about 11°C (since it comes from deeper strata). This results in shallow, constant temperature profiles, in contrast with the rest of the area (Fig. 2.7).

Although fluxes at boils can be measured, there is a general consensus that it is extremely difficult to quantify the fluxes of paleochannel and diffuse seepage (e.g. Murdoch and Kelly, 2003; Kishel and Gerla, 2002; Surridge *et al*., 2005; Keery *et al*., 2007). Some of the underlying reasons are that they can be estimated using Darcy's equation but the vertical hydraulic conductivity of the Holocene layer is very uncertain (Weerts, 1996), as well as being highly variable in space. However, our chemical groundwater data demonstrate that seepage fluxes must be much higher in the areas with paleochannel belts cutting into the Holocene layer. To illustrate this, the classified chemical groundwater types (screens a, c and d) were put on a cross-section together with geological data, hydraulic heads and deduced flow paths (Fig. 2.10). The dominant anion in the Holocene layer for the areas without paleochannel belts is SO_4^{2-}, whereas the dominant anion is Cl^- and concentrations of SO_4^{2-} are low in the areas with paleochannel belts and in the upper aquifer (see also Table 2.1). The elevated concentrations in the Holocene layer without paleochannel belts, as compared to the low concentrations in the upper aquifer, indicate that SO_4^{2-} must be enriched in the Holocene layer. The sources of the sulphates are thought to be pyrite (FeS_2), which is abundant in the Holocene organic clays, and peat layers, which release SO_4^{2-} upon oxidation (Ritsema and Groenenberg, 1993; Dellwig *et al*., 2001; Table 2.3). For this to occur, oxic- or nitrate-containing groundwater derived from the surface has to locally penetrate the confining layers down to 5 m depth before flowing upwards again to the surface (Fig. 2.10). Along these flow paths, acid produced during pyrite oxidation will dissolve calcium carbonates (Table 2.3) that are also abundant in the Holocene layer which contains sediments of marine origin (Ritsema and Groenenberg, 1993). Therefore, f-$CaSO_4$ groundwater types are found throughout the Holocene confining layer except in areas with paleochannel belts (Fig. 2.10). In view of the permanent upward flow from the upper aquifer into the Holocene layer, these lenses of locally infiltrated groundwater can only reach depths of 4-5 m depth when upward groundwater fluxes from the upper aquifer are small. Our head measurements confirmed this. The largest head losses (on average 1.0 m) were found between the upper aquifer at 6 to 7 m depth and the Holocene layer at 4 to 5 m depth (Fig. 2.4). This suggests that the lowest permeability is found at the base of the Holocene layer, which is probably caused by the presence of basal peat. We would argue that the lower part of the Holocene layer is locally quasi-impermeable, so that no groundwater from the upper aquifer can flow up into it in some areas. The paleochannel belts with their high hydraulic conductivities cut through this lower, less permeable part of the Holocene layer, and allow for greater upward groundwater fluxes (Fig. 2.10). This relatively strong upward flow prevents shallow groundwater containing oxidants from reaching depths of 4-5 m. Groundwater of the same type (b-NaCl), originating from the upper aquifer, is therefore found in the entire Holocene layer above the paleochannel belts (Fig. 2.10).

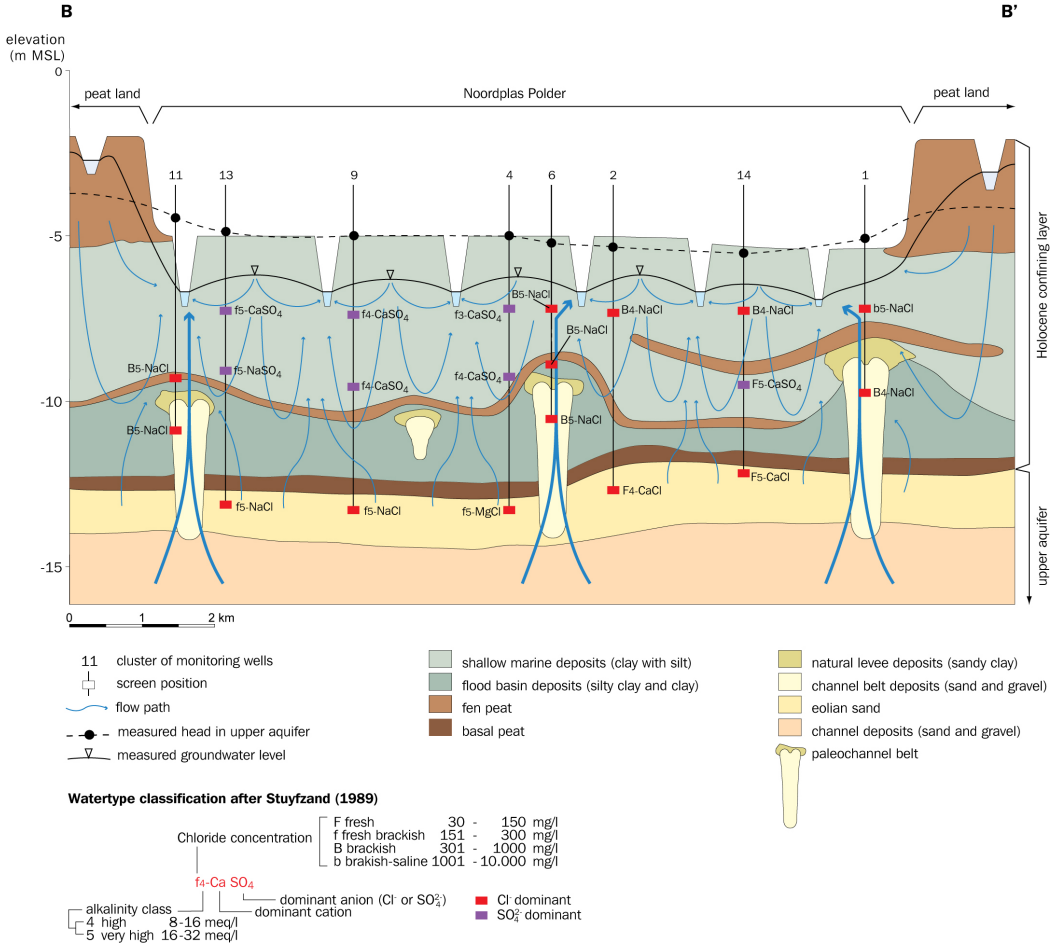

Fig. 2.10. Cross-section across Noordplas Polder with groundwater flow patterns in the Holocene confining layer based on different water types, measured hydraulic heads, and the sedimentary structure of the Holocene confining layer. Position of cross section B-B' is indicated in Fig. 2.1.

Table 2.3. Possible chemical reactions along flow path of local groundwater in the Holocene confining layer

Description	Chemical reaction equation
Oxidation of pyrite by oxygen:	$FeS_2 + 7/2\ O_2 + H_2O \rightarrow Fe^{2+} + 2SO_4^{2-} + 2H^+$
Further oxidation of Fe^{2+} by oxygen:	$Fe^{2+} + ¼\ O_2 + 5/2\ H_2O \rightarrow Fe(OH)_3 + 2H$
Oxidation of pyrite by nitrate:	$FeS_2 + 14/5\ NO_3^- + 4/5\ H^+ \rightarrow Fe^{2+} + 2\ SO_4^{2-} + 7/5\ N_2 + 2/5\ H_2O$
Further oxidation of Fe^{2+} by nitrate:	$Fe^{2+} + 1/5\ NO_3^- + 12/5\ H_2O \rightarrow Fe(OH)_3 + 1/10\ N_2 + 9/5\ H^+$
Dissolution of calcium carbonates:	$CaCO_3 + H^+ \rightarrow Ca^{2+} + HCO_3^-$

2.4.3 Salt water upconing

Diffuse-, paleochannel-, and boil seepage all originate from the upper aquifer (Fig. 2.9). The composition of the groundwater in the upper aquifer directly under the Holocene confining layer therefore determines that of the seepage water. There is a remarkable and consistent difference between the chloride concentrations of the three seepage types. For diffuse seepage, we found low concentrations of about 100 mg L^{-1} and for paleochannel seepage, we found higher chloride concentrations of about 600 mg L^{-1} (Table 2.2). Boils show both significantly and consistently higher chloride concentrations (average about 1100 mg L^{-1}) than the diffuse and paleochannel seepage waters. Hence, relatively high chloride concentrations in the upper aquifer occur consistently at those places where preferential flow occurs. This leads us to believe that the higher fluxes at these preferential conduits are the reason for higher chloride concentrations, as higher fluxes lead to upconing of deeper and more saline water. It has been well established that chloride concentrations of groundwater in the aquifers below Dutch polders increase with depth, as shown in Fig. 2.2 (ICW, 1976; Pomper and Wesseling 1978; Van Rees Vellinga *et al*., 1981; Griffioen *et al*., 2002; Post, 2004). The upconing mechanism of the three seepage types with their different upward groundwater fluxes leading to different chloride concentrations is shown in Fig. 2.9. The mechanism is analogous to salt water upconing in response to pumping of groundwater, which has been described by e.g. Reilly and Goodman (1987), Ma *et al*. (1997) and Bower *et al*. (1999). They show that the salinity and depth of the pumped groundwater increase with pumping rate. Tellam *et al*. (1986) showed regional upconing of saline groundwater in response to low heads at springs in the Mersey Valley, UK, similar to the upconing mechanism in the Noordplas Polder.

Direct evidence of such salt water upconing by preferential seepage is provided by our chloride measurements around boil 25V (Fig. 2.8). As all seepage originates from the upper aquifer, the large differences in concentration over such a short distance can only be explained by local upconing of deeper and therefore more saline groundwater as a result of high upward flow velocities.

2.4.4 Chloride loads from boils

Groundwater flowing up from the upper aquifer, either via the Holocene confining layer, through paleochannel belts or through boils, discharges into the ditches. After mixing with both inlet water and rainwater, it is pumped out of the polder. The daily discharge and chloride concentration of the water pumped out, as shown in Fig. 2.5, is therefore a mix of all these water sources. Their contribution to the total water flux and chloride load varies as a function of time. In the largest part of the polder, the chloride concentration of the seepage water (diffuse seepage) is much lower than the chloride concentration of the polder water (Table 2.2), which implies there must be a large contribution from a saline source with higher chloride concentration.

In a simplified water and chloride balance, we demonstrate that the chloride loads observed in the Noordplas Polder can only be explained by assigning a large contribution to boil seepage. Water and chloride enter the polder via precipitation (P), diffuse seepage (q_d), paleochannel seepage (q_p), boil seepage (q_b), and the inlet of external surface water (q_i). Water leaves via pumping (q_{pump}) and evapotranspiration (ET) while chloride leaves only via pumping. The water balance is expressed as:

$$P - ET + q_i + q_d + q_p + q_b = q_{pump} \quad \text{(in M m}^3\text{ y}^{-1}\text{)} \quad (2.1)$$

Chloride loads are calculated by multiplying the water flux by the corresponding chloride concentration c. The chloride balance is then expressed as:

$$P \cdot c_p + q_i \cdot c_i + q_d \cdot c_d + q_p \cdot c_p + q_b \cdot c_b = q_{pump} \cdot c_{pump} \quad \text{(in M kg y}^{-1}\text{)} \quad (2.2)$$

Filling in the values we measured (see section 3) of P (41.2 M m^3 y^{-1}), ET (21.7 M m^3 y^{-1}), q_{pump} (33.8 M m^3 y^{-1}), $q_{pump} \cdot c_{pump}$ (11.6 M kg y^{-1}) and the chloride concentration c of the different water balance terms (see Table 2.2) into Eq. (2.1) and Eq. (2.2) leads to the following:

$$q_i + q_d + q_p + q_b = 14.3 \quad \text{(M m}^3\text{ y}^{-1}\text{)} \quad (2.3)$$

$$0.5 + q_i \cdot 0.223 + q_d \cdot 0.117 + q_p \cdot 0.592 + q_b \cdot 1.10 = 11.6 \quad \text{(M kg y}^{-1}\text{)} \quad (2.4)$$

To solve these two equations with their four unknowns, we varied water balance terms q_i, q_d, q_p and q_b randomly in all possible combinations, in such a way that their sum was equal to 14.3 M m^3 y^{-1}, which meant that the water balance Eq. (2.3) was correct. The four water balance terms were varied in the range 0–14.3 M m^3 y^{-1}, because their water flux for the whole polder was not known exactly and to explore all possible solutions. For each combination for which Eq. (2.3) was correct, the total chloride load was calculated with the left-hand side of Eq. (2.4). Our results are shown in Fig. 2.11, where the calculated chloride load via boils is plotted against the calculated total chloride load. The points in Fig. 2.11 that show a total chloride load of 11.6 M kg y^{-1} represent the correct solutions to Eq. (2.3) and Eq. (2.4). From the graph we can derive that the observed total chloride load of 11.6 M kg y^{-1} can only be explained with a minimum chloride load via boils of 5.8 M m^3 y^{-1} which is 50% of the total chloride load in the polder.

In earlier studies (ICW, 1976; Wit, 1974; Pomper and Wesseling, 1978, Griffioen *et al.*, 2002), the seepage chloride load was obtained by multiplying the estimated seepage flux by the average chloride concentrations of groundwater at the top of the upper aquifer (-10 to -15 m MSL). This resulted in large underestimations of the total chloride load, and the discrepancy was removed by using the higher chloride concentrations of groundwater at -25 to -35 m MSL, but no justification was given. We have shown that the common assumption by the earlier studies, that upward saline seepage could be considered as a spatially uniform, diffuse process, is incorrect. We consider their choice to use higher chloride concentrations in the water and salt balances is roughly the same as our idea that more saline groundwater of deeper origin contributes to the polder discharge via boils.

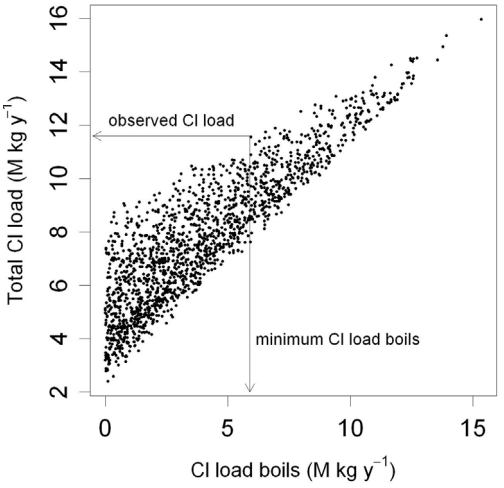

Fig. 2.11 Scatter diagram of calculated chloride load via boils versus calculated total chloride load in the Noordplas Polder.

2.5 Conclusions

From our observations and analysis of the geological structure of the Holocene confining layer, head differences, groundwater composition, surface water salinity, polder water discharge and chloride load, temperature profiles, and boil observations, in a typical deep Dutch polder (Noordplas Polder), we conclude that saline seepage is not a uniform process. We distinguished three types of seepage: (1) diffuse seepage through the Holocene layer, (2) seepage through paleochannel belts that cut through the Holocene layer, and (3) intense seepage via localized boils. These differ with regard to flux, chloride concentration, and the location in the polder where they occur. Their contribution to surface water salinization therefore also differs. The magnitude of the seepage flux reflects the depth from which the groundwater originates, with higher fluxes resulting in upconing of deeper, more saline groundwater (since the salinity of groundwater increases with depth in the Noordplas Polder).

The largest seepage fluxes and highest chloride concentrations were found in boils; these are small, localized vents in the Holocene confining layer through which groundwater discharges at high velocities. Boils were observed in ditches, near the edge of the polder, or in areas with paleochannel belts. Temperature and chloride concentration profiles demonstrated high flow velocities and strong upconing of deeper and more saline groundwater at boils, producing an average chloride concentration of 1100 mg L^{-1}. Permeable, sandy, paleochannel belts cut through the less permeable, lower part of the Holocene confining layer. This results in higher seepage fluxes through the paleochannel belts and upconing of more saline groundwater than found in the diffuse seepage occurring through the Holocene layer. Therefore, the average chloride concentration of paleochannel seepage (600 mg L^{-1}) is much higher than of diffuse seepage (100 mg L^{-1}).

The annual average chloride concentration of the polder water discharge is about 400 mg L^{-1} and may reach 720 mg L^{-1} in dry periods. Given that polder water discharge is a mixture of groundwater seepage, precipitation and inlet water, and that the latter two have a diluting effect, we set out to demonstrate that boils must be responsible for the high chloride concentrations. By integrating our field data and balance calculations, we show that boils are indeed the dominant salinization mechanism and that they contribute more than 50% of the total chloride load to the Noordplas Polder surface water.

In attempts to abate surface water salinization in deep polders, it is worth focusing attention on boils because of their dominant role in the chemical load and their local nature. Both of these features will facilitate the countermeasures needed. Since groundwater discharged via boils has a constant temperature of 11°C, airborne thermal infrared mapping can help to localize them. Although the hydrogeological situation of the Dutch polders is quite specific, our work may have broad implications for other geographical regions. Boils occur where there are significant head gradients, such as areas with e.g. dikes (Li *et al*., 1996; Holzer and Clark, 1993) and dammed reservoirs, but also in brook valleys or river plains. Since boils affect the surface water quality, our approach for quantifying their impact may be adopted if adequate tracers (salt or other chemical tracers, temperature) can be identified to distinguish between the different sources of water.

Chapter 3

Quantifying water and salt fluxes in a lowland polder catchment dominated by boil seepage: a probabilistic end-member mixing approach

Perry de Louw, Ype van de Velde, Sjoerd van der Zee
Published in Hydrology and Earth System Sciences 15, 2101-2117, 2011

Abstract

Upward saline groundwater seepage is leading to surface water salinization of deep lying polders in the Netherlands. Identifying measures to reduce the salt content requires a thorough understanding and quantification of the dominant sources of water and salt on a daily basis. However, as in most balance studies, there are large uncertainties in the contribution from groundwater seepage. Taking these into account, we applied a probabilistic (GLUE) end-member mixing approach to simulate two years of daily to weekly observations of discharge, salt loads and salt concentration of water pumped out of an artificially drained polder catchment area. We were then able to assess the contribution from the different sources to the water and salt balance of the polder and uncertainties in their quantification. Our modeling approach demonstrates the need to distinguish preferential from diffuse seepage. Preferential seepage via boils contributes, on average, 66% to the total salt load and only about 15% to the total water flux into the polder and therefore forms the main salinization pathway. With the model we were able to calculate the effect of future changes on surface water salinity and to assess the uncertainty in our predictions. Furthermore, we analyzed the parameter sensitivity and uncertainty to determine for which parameter the quality of field measurements should be improved to reduce model input and output uncertainty. High frequency measurements of polder water discharge and weighted concentration at the outlet of the catchment area appear to be essential for obtaining reliable simulations of water and salt fluxes and for allotting these to the different sources.

3.1 Introduction

Salinization of surface waters and aquifers is common in coastal areas (Custodio and Bruggeman, 1987; Post and Abarca, 2010) and deltas; in particular; are vulnerable to processes that may enhance salinization, such as land subsidence, climate change and sea-level rise (Oude Essink, 2008). As one-quarter of the Netherlands lies below mean sea level, upward seepage of saline and nutrient-rich groundwater causes salinization and eutrophication of its surface waters (Van Rees Vellinga *et al*., 1981; Van Puijenbroek *et al*., 2004; Van der Eertwegh *et al*., 2006). This seepage makes the surface water unfit for irrigation and adversely affects aquatic ecosystems. Both surface water quality issues typically play a role during the dryer and warmer growing season, when the demand for fresh water increases but its availability is limited. Future rises in sea level and climate change are expected to increase the seepage and decrease the availability of fresh water (e.g. Sherif and Singh, 1999; Ranjan *et al*., 2006; Vandenbohede *et al*., 2008), especially in the deep polders (Oude Essink *et al*., 2010). To determine effective measures for reducing the salt loads in the deep polders

we need to identify and quantify the main sources of water and salt. In this paper we will set up daily water and salt balances to help understand the dynamics observed in salt concentrations (De Louw *et al*., 2010) and to signal problems with salinization during the growing season.

A polder is an artificially drained catchment in which the surface water level in the ditch network is regulated by pumping. Water pumped out of a polder is a mixture of seepage water from the upper aquifer, precipitation and water admitted from a '*boezem*', which is a higher lying surface water canal used for buffering polder water (Fig. 3.1). De Louw *et al*. (2010) distinguished three types of groundwater seepage in a deep polder which differ in flux and salt concentration: (1) diffuse, background seepage through the Holocene confining layer, (2) preferential seepage through permeable, sandy paleochannel belts in the Holocene confining layer, and (3) intense preferential seepage via boils (Fig. 3.1). Boils are small vents in the Holocene confining layer through which water discharges at high rates and which lead to strong upconing of deeper and more

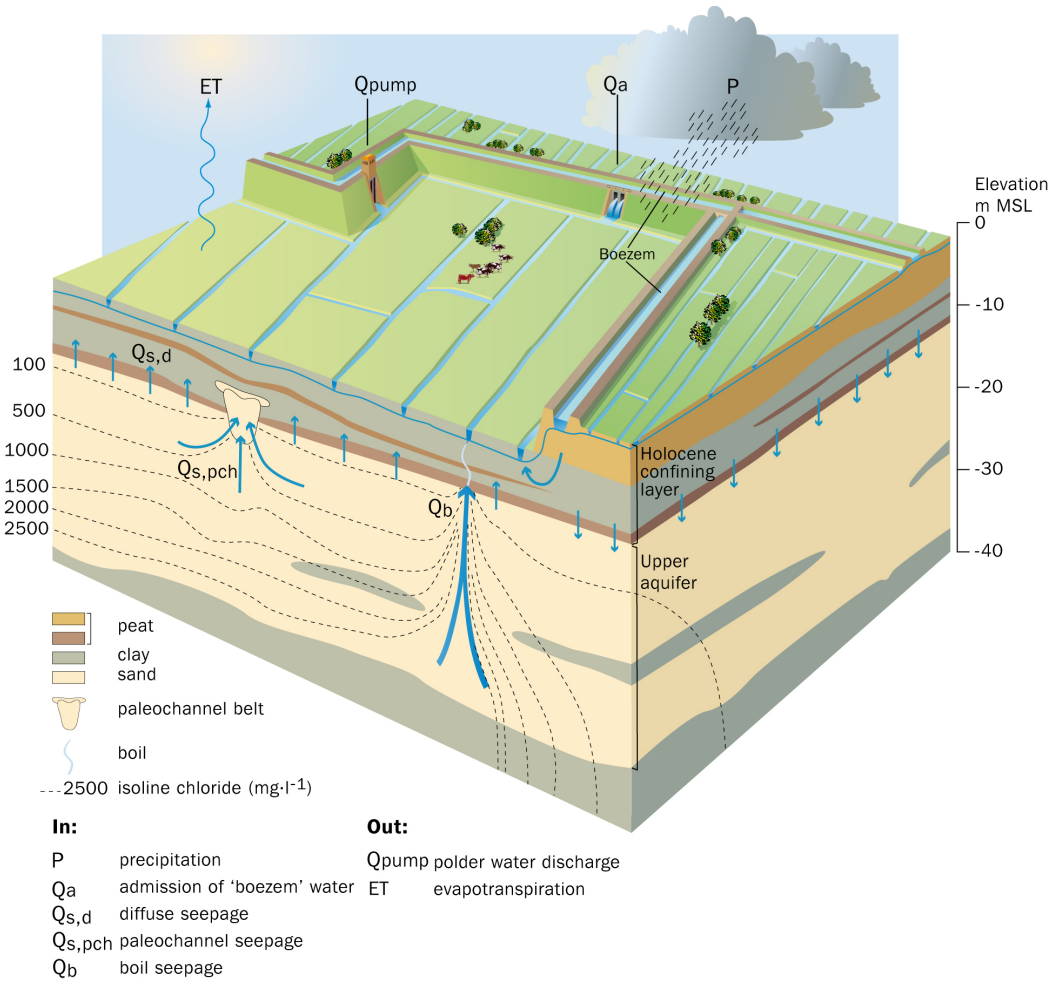

Fig. 3.1. The hydrogeology and water and salt fluxes in a lowland polder catchment area. Upward groundwater seepage from the upper aquifer can be divided into three different types according to De Louw *et al*. (2010): diffuse-, paleochannel-, and boil seepage.

saline groundwater (Fig. 3.1). De Louw *et al*. (2010) presented evidence that preferential seepage via boils is the main salt source of surface waters in deep polders. In general, the contribution of groundwater seepage to stream discharge and quality is difficult to infer directly from field data for several reasons. First, seepage fluxes are highly variable in space and are difficult to measure directly (e.g. Kishel and Gerla, 2002; Murdoch and Kelly, 2003; Surridge *et al*., 2005; Keery *et al*., 2007; Kalbus *et al*., 2009). Second, the composition of groundwater seepage varies spatially and deriving a representative average composition would require a large number of measurements. And third, mapping of preferential groundwater flow routes such as boils for large catchments is an enormous task (Becker, *et al*., 2004; Van Schaik, 2009, De Louw, *et al*., 2010).

Alternatively, an end-member mixing approach (EMMA, Hooper *et al*., 1990) can be applied to estimate seepage fluxes of water and salt indirectly from discharge and concentration measurements at the catchment outlet. EMMA assumes that solute concentrations in a stream result from the mixing of two or more flow routes with a known concentration ('end-members') and it is often used for hydrograph separation into contributions of individual flow routes (e.g. Soulsby *et al*., 2003; Tiemeyer *et al*., 2008; Velde *et al*., 2010). Given the uncertainty of fluxes and concentration of the different sources only a combination of EMMA with an uncertainty and sensitivity assessment will yield meaningful estimations of individual flow routes. A method to determine the uncertainty of model predictions and model parameters –generalized likelihood uncertainty estimation (GLUE, Beven and Binley, 1992)– is broadly used due to its conceptual simplicity, ease of implementation and versatility at handling different models without major modifications to the method itself (Freer *et al*., 1996; Kuczera and Parent, 1998; Blasone *et al*., 2008a,b; Benke *et al*., 2008; Tiemeyer *et al*., 2008). The problem of equifinality, where different parameter sets result in the same model performance, is directly addressed by GLUE procedures (Beven, 1993, 2006).

Our aim is to quantify the main salt sources in a lowland polder catchment area, and particularly the contribution of preferential seepage via boils. We used a probabilistic transient water and salt balance model based on end-member mixing principles to simulate two years of chloride concentration and discharge measurements at the polder catchment outlet. By applying the GLUE framework, we were able to obtain an estimate of the uncertainty in source contribution caused by the model equifinality and the uncertainty in the data. Using this model we calculated the effects of different scenarios involving climate change and adaptive strategies on the salt concentrations in the polder's surface waters.

3.2 Material and methods

3.2.1 Noordplas Polder study area

The study area is a typical lowland catchment area in a deep polder in the west of the Netherlands: Noordplas Polder (latitude 52°04'N, longitude 04°34'E) (Fig. 3.2). It covers 37 km^2, of which 86% is agricultural land (arable farming 62%; pasture 24%) and 14% is urban area. This former lake was reclaimed in different phases in the period 1750-1850 A.D. (Schultz, 1992). Its present mean soil surface level is about -5 m MSL (mean sea level).

Geohydrologically, a 6 m to 9 m thick top-aquitard of Holocene peat, loam and clay deposits with low hydraulic conductivity (Holocene confining layer) lies above a sandy aquifer of Pleistocene aeolian and

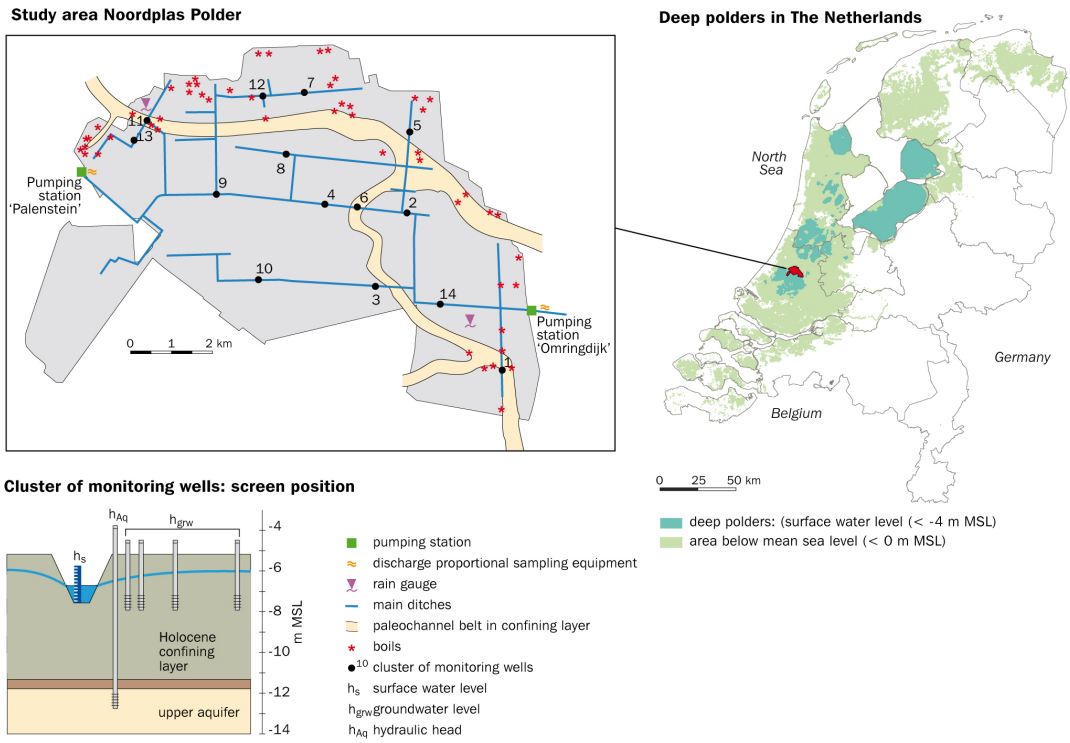

Fig. 3.2. Set up of the monitoring network of the Noordplas Polder and the location of the sandy paleochannel belts and boils (adapted from De Louw *et al.*, 2010).

fluvial sediments with high hydraulic conductivity (Fig. 3.1). The hydraulic head difference between this upper aquifer and the surface water (approximately 1.5 m) causes permanent upward groundwater seepage in the entire polder area. The Holocene confining layer is partly intersected by a network of sandy paleochannel belts caused by erosion by tidal channels during the Holocene (Van der Valk, 1996; Berendsen and Stouthamer, 2000; Hijma *et al.*, 2009). These are in direct contact with the upper aquifer and reduce the thickness of the Holocene confining layer. They act as preferential pathways for water flow and salt transport (Fig. 3.1). Besides these forms of seepage, groundwater from the upper aquifer also enters the surface water via boils (Fig. 3.1). The location of the sandy paleochannel belts and the known boils in the Noordplas Polder are shown in Fig. 3.2.

The polder is enclosed by dikes for protection against flooding. The surface water level in the Noordplas Polder is maintained at a nearly constant level of about -6.2 m MSL because of the agricultural requirements. Excess water is pumped out into the 'boezem' (Fig. 3.1), which is a regional surface water system at a higher elevation (-0.6 m MSL) through which excess polder water is transported to the sea (Van de Ven, 2003). During dry periods, relatively fresh water from the 'boezem' is admitted to the polder at inlets (Fig. 3.1) in order to maintain surface water levels and decrease the surface water salinity in the polder by flushing. However, since this 'boezem' water is a mix of fresh water from the River Rhine and water pumped from other deep polders, its salinity may also be elevated during dry periods. Five major inlet locations of 'boezem' water are managed by the Rijnland District Water Control Board, whereas many small inlets are controlled by farmers.

The major flow routes of water and salt

entering or leaving the polder are shown in Fig. 3.1. Water enters the polder via precipitation, three types of groundwater seepage and the inlet of 'boezem' water, and it leaves the polder via evapotranspiration and the pumping stations. The major part of the precipitation surplus and seepage is temporarily stored in the subsoil as soil water or groundwater before it is discharged. Groundwater is drained by subsurface drains and surface drainage in open ditches. Ditches collect the water from subsurface tile drainage and the excess water is transported through small canals to the pumping stations. The spacing of the tile drainage network is 10-20 m and the most common drainage depth is 1.2 m below soil surface. The long-term mean annual precipitation and potential evapotranspiration (Makkink, 1957) are 916 mm and 615 mm, respectively. The total mean annual volume of water that is pumped out of the polder is as much as 925 mm. The large difference between precipitation surplus and polder water discharge indicates the significant contribution from seepage and admitted 'boezem' water to the polder discharge.

3.2.2 Monitoring water and salt fluxes

The groundwater and surface water monitoring program in Noordplas Polder aimed to quantify daily water and salt fluxes into and out of the polder. The monitoring network is shown in Fig. 3.2 and a summary of the monitoring activities is given in Table 3.1. The most dynamic fluxes in Noordplas Polder are precipitation and evapotranspiration and the water and salt fluxes pumped out of the polder (De Louw *et al*., 2010). These fluxes could be measured relatively accurately on a daily to weekly basis. Multiplying the total daily pumping time with the pumping capacity gives the daily discharge volume of the polder water. The pumping water was sampled automatically with a discharge-proportional frequency to obtain discharge weighted chloride concentrations and to determine the chloride loads out of the polder. The samples were mixed automatically to one bulk sample, stored in a refrigerator in the field and collected every 3 to 7 days, and analyzed in the laboratory for chloride. Multiplying the analyzed discharge weighted chloride concentration by the discharged volume of polder water resulted in the total chloride load pumped out of the polder for every 3 to 7 days. Daily precipitation was measured at two locations with a tipping bucket rain gauge. Daily sums of the potential reference crop evapotranspiration (ET_{mak}) were calculated according to Makkink (1957) from data of the Royal Netherlands Meteorological Institute (KNMI), i.e., the KNMI stations at Valkenburg and Schiphol. Daily ET_{mak}-values were multiplied by a crop factor (Feddes, 1987) and weighted by land use.

Water and salt fluxes into the polder via seepage and the admission of 'boezem' water are much more uncertain than the above mentioned balance terms. The five main inlets controlled by the water board were only measured incidentally and the volume of admitted 'boezem' water at the small inlets controlled by the farmers is unknown. From the management practices of the inlets it is clear that much more 'boezem' water is admitted in summer than in winter. Upward groundwater flow from the upper aquifer in the form of diffuse and paleochannel seepage cannot be measured directly (see Kishel and Gerla, 2002; Murdoch and Kelly, 2003; Surridge *et al*., 2005; Keery *et al*., 2007; Cirkel *et al*., 2010). However, the driving force of these seepage fluxes, the head difference between the upper aquifer and phreatic water levels, was accurately measured bi-weekly at 14 clusters of monitoring wells (see Fig. 3.2). Each cluster consisted of one monitoring well in the upper aquifer, 2 to 4 groundwater wells (in total 48) and a gauge in the ditch for surface water level observations. Water table fluctuations were measured

Table 3.1. Summary of monitoring data of Noordplas Polder for period 1 Aug. 1999 - 1 Aug. 2001.

	Frequency	No. of loc.	Unit	Average	Median	Std.	Min.	Max.	Nr. of obs. per location
Quantitative									
Precipitation	daily	2	mm d^{-1}	2.93	0.76	4.19	0	40.28	731
Evapotranspiration	daily	1	mm d^{-1}	1.54	1.09	1.34	0	5.42	731
Polder water discharge	daily	2	mm d^{-1}	2.53	1.66	2.51	0.51	18.30	731
Main inlets	incidental	5	mm d^{-1}	-	-	-	-	-	-
Small inlets	none	150	-	-	-	-	-	-	-
Head upper aquifer	bi-weekly	14	m+h_s	1.54	1.51	0.38	0.99	2.16	48
Groundwater level	bi-weekly	48	m+h_s	0.42	0.38	0.40	-0.69	1.84	48
Surface water level (h_s)	bi-weekly	14	m MSL	-6.37	-6.42	0.41	-7.65	-5.46	48
Chloride concentration									
Precipitation	once	1	mg L^{-1}	12	-	-	-	-	1
Weighted Cl-conc. polder water discharge	every 3-7 days	2	mg L^{-1}	446	464	179	110	741	172
Total salt load	every 3-7 days	2	t d^{-1}	31.8	27.5	14.5	14.9	140	172
Inlet water in winter	monthly	4	mg L^{-1}	125	130	85	70	250	12
Inlet water in summer	monthly	4	mg L^{-1}	245	220	160	100	500	12
Boils	once	49	mg L^{-1}	1100	1300	638	337	2850	1
Paleochannel seepage	twice	3	mg L^{-1}	592	-	-	438	675	2
Diffuse seepage	twice	11	mg L^{-1}	117	95	96	33	281	2

bi-weekly in the 48 groundwater wells to quantify the process of groundwater storage and drainage. A reliable estimate of total boil fluxes could not be made because the total number of boils is not known. Although 54 boils were found during field inventories (De Louw *et al*., 2010), we are sure that this is only a small part of the total number of boils in the polder. As boils are rather small, concentrated and mainly underwater phenomena, they are hard to find, especially in the larger and deeper canals. At 15 boils we were able to measure the boil flux, which varied between 0.5 and 100 m^3/d (De Louw *et al*., 2010). Although this gave us a better picture about individual boil fluxes and the variation between boils, the total number of boils is unknown and therefore the total boil flux in the polder. Chloride concentrations of the different seepage types were taken from De Louw *et al*. (2010). The chloride concentration of the upper aquifer in areas with and without paleochannel belts in the confining layer was taken as representative for the paleochannel and diffuse seepage, respectively (Table 3.1). The chloride concentration was measured in the upper aquifer monitoring well at the 14 monitoring clusters from which 3 were located in areas with and 11 in areas without paleochannel belts (Fig. 3.2). The average chloride concentration in the upper aquifer for areas with paleochannel belts was 592 mg L^{-1} but only based on 3 locations (Table 3.1). In the 11 sites without paleochannel belts, the average chloride concentration was much lower at 117 mg L^{-1} (Table 3.1). The chloride concentration of boils was determined at 49 boils which showed a large variation between 337 and 2850 mg L^{-1} and an average of 1100 mg L^{-1} (Table 3.1). The larger boils intended to have higher concentrations (De Louw *et al*., 2010). As the three forms of groundwater seepage come from below the aquitard (deeper than 7 m) its composition will not change significantly due to seasonal variation in precipitation and evapotranspiration. This is confirmed

by our monitoring data described in our previous work (De Louw *et al*., 2010). We analyzed the groundwater composition of the upper aquifer at two moments in the year (April and November) and the differences were less than 5%.

3.2.3 Modeling water and salt fluxes

We combined a simple, fast End Member Mixing Approach (EMMA) model with an uncertainty estimation approach, the Generalized Linear Uncertainty Estimation GLUE (Beven and Binley, 1992), to quantify the daily water and salt fluxes and their uncertainties. This model links all the sources to the polder water discharge, concentrations and salt loads and incorporates the uncertainty in the sources. The different water and salt sources considered in the model are shown in Fig. 3.1. Since the three types of groundwater seepage, diffuse-, paleochannel-, and boil seepage, differ with regard to seepage flux and chloride concentrations, they are considered as different end-members.

Water balance

The balance of the surface water network of the polder is given by:

$$Q_{pump}(t) = Q_b + Q_a(t) + Q_{grw,i}(t) \qquad (3.1)$$

Q_{pump} ($L^3\ T^{-1}$) is the pumped volume from the polder into the 'boezem', Q_b ($L^3\ T^{-1}$) is the seepage through boils directly into the surface water network, Q_a ($L^3\ T^{-1}$) is the admission of 'boezem' water into the polder, and $Q_{grw,i}$ ($L^3\ T^{-1}$) is the groundwater flow into the surface water network. Because the pumps maintain a constant surface water level, we disregarded surface water storage changes. Since the majority of boils occur in ditches (De Louw *et al*., 2010) boil seepage, Q_b is assigned directly to the surface water network. Its flux was assumed to be constant because its driving force, the head difference between the upper aquifer and the surface water level, remains relatively constant (De Louw *et al*., 2010). We distinguished different constant water admission fluxes from the 'boezem' during the winter, $Q_{a,w}$ ($L^3\ T^{-1}$), and the summer, $Q_{a,s}$ ($L^3\ T^{-1}$). Infiltration (or leakage) from the higher situated 'boezem' into the polder is not considered as a separate balance term because it has no significant contribution to the total water balance (<< 1%) due to the small area of 'boezem' where such infiltration takes place. To account for the effects of paleochannel belts on the seepage water and salt flux we calculated the groundwater flux into the surface water network ($Q_{grw,i}$) separately for the area with paleochannel belts in the Holocene confining layer ($i = pch$) and for the rest of the polder ($i = d$).

In lowland catchments with free drainage, the transport of solutes is governed by the active extent of the drainage system (Carluer en Marsily, 2004; Wriedt *et al*., 2007; Tiemeyer *et al*., 2007; Molenat *et al*., 2008; Velde *et al*., 2009). In polders, however, the water table and discharge are controlled by a totally artificial drainage network, and surface water levels are regulated by pumps and the admission of 'boezem' water. Therefore, the active drainage system of a polder remains constant and its discharge storage relationship for a single field can be set as representative for the entire catchment. The groundwater flux towards the surface water network $Q_{grw,i}$ ($L^3\ T^{-1}$), is derived by a separate water balance of the groundwater reservoir. Seepage and precipitation are temporarily stored in the subsoil causing the water table to rise. The water table declines due to the drainage of groundwater and evapotranspiration. The water balance of the groundwater reservoir is given by:

$$n_{dr}\frac{\mathrm{d}h_{grw,i}(t)}{\mathrm{d}t} = \frac{\mathrm{d}s_{grw,i}(t)}{\mathrm{d}t} = P(t) - ET(t) + q_{s,i}(t) - q_{ditch,i}(t) - q_{dr,i}(t) \qquad (3.2)$$

With n_{dr} (-) the drainable porosity (or specific yield), h_{grw} (L) the average water table elevation, s_{grw} (L) the total groundwater storage in the saturated and unsaturated zone, P (L T^{-1}) the precipitation rate, ET (L T^{-1}) the evapotranspiration rate, $q_{s,i}$ (L T^{-1}) the seepage flux rate, and q_{ditch} (L T^{-1}) and q_{dr} (L T^{-1}) the groundwater flow rate towards ditches and drains tiles, respectively. The seepage flux rates, $q_{s,i}$ (L T^{-1}), (diffuse seepage, $i = d$, and paleochannel seepage, $i = pch$) are derived by Darcy's law:

$$q_{s,i}(t) = \frac{H_{Aq} - h_{grw,i}(t)}{r_i} \tag{3.3}$$

With H_{Aq} (L) the constant hydraulic head in the upper aquifer. Note that differences in seepage fluxes between locations with and without paleochannels, are only caused by a different hydraulic resistance of the Holocene confining layer, r (T). As the confining layer consists of different lithological layers n with thickness d_n (L) and vertical saturated hydraulic conductivity $k_{v,n}$ (L T^{-1}) the hydraulic resistance of the Holocene confining layer, r (T) is defined as:

$$r_i = \sum_n \frac{d_n}{k_{v,n}} \tag{3.4}$$

The groundwater flow rate towards ditches, q_{ditch} (L T^{-1}), and drain tiles, q_{dr} (L T^{-1}), are derived using the drainage formula of Hooghoudt (1940). We assumed there was no infiltration from surface water during dry periods, since these infiltration fluxes can be neglected compared to the total groundwater drainage flux because of the limited period in which such infiltration takes place, the large ditch distances (> 100 m) and the small area of surface water (< 2%). There is no surface water infiltration via subsurface drains because the drain tiles are always situated above the ditch water level.

$$q_{ditch,i}(t) = (h_{grw,i}(t) - h_s)\frac{4\,kD}{l_s^2} \quad \text{for } h_{grw,i} > h_s$$
$$q_{ditch,i}(t) = 0 \quad \text{for } h_{grw,i} < h_s \tag{3.5}$$

$$q_{dr,i}(t) = (h_{grwi,i}(t) - h_{dr})\frac{4kD}{l_{dr}^2} \quad \text{for } h_{grw,i} > h_{dr}$$
$$q_{dr,i}(t) = 0 \quad \text{for } h_{grw,i} < h_{dr} \tag{3.6}$$

With saturated hydraulic conductivity k (L T^{-1}), layer thickness, D (L), surface water level in ditch h_s (L), drainage level h_{dr} (L + h_s) and spacing between parallel subsurface drains, l_{dr} (L), and ditches l_s (L). Because the upper 5 m of the confining layers with and without paleochannel belts do not differ significantly from each other (De Louw *et al.*, 2010), we used one kD value for both hydrogeological situations.

Finally, the total groundwater flux towards the surface water network is calculated by:

$$Q_{grw,i}(t) = A_i(q_{ditch,i}(t) + q_{dr,i}(t)) \quad (3.7)$$

With A_i the surface area of locations with (i= *pch*) and without (i = *d*) paleochannel belts.

Salt balance

The salt balance equation is obtained by multiplying the fluxes of the water balance equation Eq. (3.1) with the concentration corresponding to the fluxes. The solute balance of the surface water is given by:

$$Q_{pump}(t) \cdot c_{pump}(t) = Q_b \cdot c_b + Q_{a,w} \cdot c_{a,w} + Q_{a,s} \cdot c_{a,s} + Q_{grw,d}(t) \cdot c_{grw,d}(t) + Q_{grw,pch}(t) \cdot c_{grw,pch}(t) \quad (3.8)$$

With c_{pump} (M L^{-3}) the concentration of the water pumped from the polder. The boils have a constant concentration denoted by c_b (M L^{-3}). The concentration of admission water from the 'boezem', c_a (M L^{-3}), is assumed to have different constant values for the winter, $c_{a,w}$ (M L^{-3}), and the summer, $c_{a,s}$ (M L^{-3}).

The concentration of the groundwater flux, c_{grw} (M L^{-3}), is derived from the mass balance of the groundwater reservoir for the area with (i=*pch*) and without (i=*d*) paleochannel belts, Eq. (3.9). We assumed that chloride is completely mixed in the top soil (Rinaldo *et al*., 2006) resulting in an average concentration for the groundwater reservoir. It is expressed by:

$$c_{grw,i}(t) = \frac{m_i(t)}{s_{grw,i}(t)} \quad (3.9)$$

With m_i (M L^{-2}) the total salt mass density, which can be derived from the salt mass balance of the groundwater reservoir:

$$\frac{dm_i(t)}{dt} = P(t) \cdot c_p + q_{s,i}(t) \cdot c_{s,i} - (q_{ditch,i}(t) + q_{dr,i}(t)) \cdot c_{grw,i}(t) \quad (3.10)$$

We assumed that rainfall has a constant concentration, c_p, and that also the diffuse and paleochannel seepage fluxes have constant concentrations: $c_{s,d}$ and $c_{s,pch}$ (De Louw *et al*., 2010).

Table 3.2. Applied ranges of prior uniform distribution of sampled model input parameters for the different GLUE-analyses (GA).

	Parameter	Name	Unit	Parameter ranges for: Modeling water and salt fluxes (GA-A)	Parameter ranges for: Parameter sensitivity and uncertainty analysis (GA-B, GA-C)
Parameters that control incoming fluxes	Q_b	Boil seepage flux	mm d^{-1}	0 – 1.1	0 – 1.1
	$Q_{a,s}$	Admission flux of 'boezem' water in summer	mm d^{-1}	0.1 – 1.0	0 – 2.2
	$Q_{a,w}$	Admission flux of 'boezem' water in winter	mm d^{-1}	0 – 0.3	0 – 2.2
	r_{pch} [1)]	Hydraulic resistance of confining layer with paleochannel belt	d	500-1000	1 – 1500
	r_d [1)]	Hydraulic resistance of confining layer without paleochannel belt	d	3000-6000	1 – 10000
	H_{Aq}	Hydraulic head in upper aquifer	m + h$_s$	1.0 – 2.0	0 – 2.5
	A_{pch}	Area with paleochannel channel belts in confining layer	%	0.12 – 0.22	0.07 – 0.27
Chloride concentration of incoming fluxes	c_b	Cl-conc. of boil seepage	mg L^{-1}	500-2500	1 – 4000
	$c_{a,s}$	Cl-conc of admitted 'boezem' water in summer	mg L^{-1}	100 - 500	1 – 500
	$c_{a,w}$	Cl-conc of admitted 'boezem' water in winter	mg L^{-1}	50 - 200	1 – 500
	$c_{s,pch}$	Cl-conc. of paleochannel seepage	mg L^{-1}	400-800	1 – 1500
	$c_{s,d}$	Cl-conc. of diffuse seepage	mg L^{-1}	50-250	1 – 500
Parameters that control gw-sw interaction	kD [1)]	Transmissivity of confining layer	m^2 d^{-1}	0.1 – 10.0	0.01 – 20.0
	h_{dr}	Level of subsurface drains	m + h$_s$	0 – 0.6	0 – 1.0
	l_{dr}	Spacing between parallel subsurface drains	m	10-30	1 – 50
	l_{ditch}	Spacing between parallel ditches	m	100-200	1 – 300
	n_{dr}	Drainable porosity	-	0.05 – 0.15	0.01 – 0.30

Ranges are based on data from a monitoring campaign (Table 3.1) and collected field data except for [1)] see Weerts (1996).

GLUE application

The calculation speed of our model allowed us to use the GLUE method (Beven and Binley, 1992) to find parameter sets that yielded good agreement with the measurements. This method is based on the idea that the model does not have one optimal parameter set but a collection of parameter sets, each of which perform equally well in reproducing the observations (Freer *et al.*, 1996; Pappenberger *et al.*, 2005; Roux and Dartus, 2006). These parameter sets are derived by Monte Carlo simulation of the model equations, randomly sampling parameters from prior distributions. A calculated "goodness-of-fit criterion" (likelihood) based on predicted and observed responses, evaluates how well a particular parameter combination simulates the system. Cut-off criteria divide the parameter space into 'behavioural' and 'non-behavioural' sets. Behavioural parameter sets are those which perform acceptable on

the basis of available data and knowledge. For each time step, the modeled output is characterized by the distribution produced by the behavioural runs. As is common practice in GLUE applications, the median represents the output estimate (Blasone *et al.*, 2008a) and the uncertainty ranges can be defined by the standard deviation, percentiles or minimum and maximum values of the distribution.

To reproduce enough behavioural runs to reconstruct complete and smooth behavioural parameter distributions we carried out 5.10^8 Monte Carlo simulations, sampling from uniform prior distributions of 17 model input parameters (Table 3.2). The Monte Carlo simulations were carried out with two different prior distribution ranges (Table 3.2). To minimize the uncertainty of the simulated water and salt fluxes we used ranges that were as small as possible (indicated by GA-A in Table 3.2), which were mainly based on our measurements (summarized in Table 3.1). The size of the ranges is a direct representation of the uncertainty of the measurements, which is influenced by factors such as type of parameter, type of measurement, number of locations or observations, and variation of the data. We applied broader ranges for the sensitivity analysis to determine the sensitivity of the parameters within the full range of plausible values for the water system under consideration (indicated by GA-B in Table 3.2). The use of 2 different prior parameter ranges gave also the opportunity the compare the model output uncertainty for a situation with (small ranges) and without (broad ranges) the availability of measurements. We did not include uncertainty in precipitation and evaporation since they could be measured relatively accurately.

Table 3.3. 'Goodness-of-fit' criteria (likelihoods) and cut-off criteria. Model runs are only assigned as behavioural when they satisfy all the individual goodness-of-fit criteria.

Likelihood	Cut-off criterion: behavioural when	Likelihood	Cut-off criterion: behavioural when
NSC Q_{pump}(dyn)	>0.55	NSC Q_{pump} (season)	>0.90
NSC c_{pump} (dyn)	>0.55	NSC c_{pump} (season)	>0.80
NSC L_{pump} (dyn)	>0.25	NSC L_{pump} (season)	>0.85
h_{grw}(dyn)	> 10-percentile AND < 90-percentile	Є(tot)-Q_{pump}, Є(tot)-c_{pump}, Є(tot)-L_{pump}	<5%

dyn = measurement time scale (days for Q_{pump}, 3 to 7 days for c_{pump} and L_{pump}, bi-weekly for h_{grw}), season = quarterly seasonally, tot = entire simulation period.

The model was applied for a period of 791 days of polder water discharge, salt loads and concentration observations (1 Aug. 1999–30 Nov. 2001) of the Noordplas Polder. For each day the model calculates the total discharge by pumps, Q_{pump}, the concentration of the pumped water, c_{pump}, the total pumped chloride loads L_{pump} and the average water table elevation h_{grw}. We compared these model responses with our measurements by calculating likelihoods (Table 3.3) for different time scales; daily to weekly (*dyn*), quarterly seasonally (*season*) and for the entire simulation period (*tot*). The Nash-Sutcliffe coefficient (*NSC*) (Nash and Sutcliffe, 1970) was used to evaluate the modeled Q_{pump}, c_{pump} and L_{pump} on daily to seasonal time scales:

$$NSC = 1 - \frac{\sum_{i=1}^{n} (o_i - p_i)^2}{\sum_{i=1}^{n} (o_i - \bar{o})^2} \qquad (3.11)$$

With o_i the observed and p_i the predicted output value for time step i and $\bar{o}$ the average observed value. We evaluated the total summed water and salt budgets, and average salt concentra-

tions of the discharge water, for the entire simulation period (ϵ(tot)). The calculated water table time series were behavioural when they fitted within the 10 and 90 percentiles of the 48 measured time series. The cut-off criteria for the different likelihoods are listed in Table 3.3. We analyzed the individual NSC's and determined the cut-off criteria which produced an equal number of behavioural runs to assign equal weight to the different NSC-likelihoods. Furthermore, we set the cut-off criteria by trial and error to fit most of our observations between the modeled uncertainty ranges and to keep these ranges as small as possible. The choices of the cut-off criteria are rather subjective and can be seen as the major shortcoming of such Monte Carlo based model evaluation method (Beven, 2006, Blasone *et al*., 2008a). A strong characteristic of the applied GLUE method is the use of likelihoods that evaluate different elements of the water system (discharge, solute concentration and -load and water table elevation) at different time scales. Model runs are only assigned as behavioural when they satisfy all the individual likelihood criteria.

Parameter sensitivity and uncertainty analysis

Apart from aiming at a correct simulation of the observed water and salt fluxes at the polder catchment outlet, we were interested in the sensitivity of the different parameters to the model results. As almost all model parameters are related to measurable parameters, a sensitivity analysis also provides important information for future field data acquisition to reduce measurement uncertainty and improve the model's reliability. Generally, two kind of sensitivity analysis can be distinguished: a global sensitivity and a local sensitivity analysis (Spear and Hornberger, 1980; Tiemeijer, 2007). With local techniques parameter interdependencies are ignored and were found to be unreliable for non-linear relationships between parameters and outputs which are typical for hydrological outputs (Muleta and Nicklow, 2005; Tiemeyer, 2007). Therefore, we used the above described GLUE method for a global sensitivity analysis where all parameters are varied at the same time. The global sensitivity of the parameters for the model output was determined in two ways. First, the global sensitivity of parameters for the total model behaviour was determined. We applied the GLUE method using the same cut-off criteria (Table 3.3) but with wider prior parameter ranges (indicated as GA-B, Table 3.2). In contrast with non-sensitive parameters which show uniform posterior distributions close to their prior distributions, the sensitive parameters show large deviations. The Kolmogorov D statistics for testing of differences in distributions was used as measure of the parameter sensitivity (Roux and Dartus, 2006; Van Huissteden *et al*., 2009). The interdependencies of the model parameters were quantified by the determination of correlation between all behavioural parameter combinations (expressed in R^2). Strong interdependencies (indicated by a large R^2) also revealed which parameters were sensitive to the total model response. Second, we tested the global sensitivity of the model parameters for the individual model output. We calculated R^2 between parameter values and model output errors for total water volume, total salt load, and mean salt concentration for the entire simulation period (ϵ(tot)). In addition, R^2 was calculated between parameter values and model errors on measurement time scale (ϵ(dyn)). To focus on this short time scale, for this analysis we used only behavioural parameter sets with absolute errors in the total water and salt balance and mean concentrations which were smaller than 5%. This GLUE analysis is indicated as GA-C.

3.2.4 Scenario analysis

The model was used to calculate the effects of future changes on surface water salinization. We applied all the behavioural parameter sets retrieved by the GLUE analysis to incorporate parameter and model uncertainty into the predictions. We then worked out three scenarios in detail. Scenario 1 illustrates the effect of the so-called W+ climate scenario for the year 2100, formulated by the Royal Netherlands Meteorological Institute KNMI (Van den Hurk *et al*., 2006). This is the driest of four climate scenarios which are frequently used for analyses in the Netherlands. Compared to the present situation, it is characterized by greater precipitation in winter, and less precipitation and higher evaporation in the summer due to higher temperatures. It is expected that sea-level rise and changes in precipitation surplus will also reduce fresh water availability for admission into the deep polders. Admission water originates from one of the major Dutch rivers (here the River Rhine), and this may become unsuitable if future sea-level rise and decrease of river discharge cause sea water intrusion further upstream on the river. In scenario 2 we calculated the effect of a 50% reduction of admitted 'boezem' water in the summer. To compensate or even reduce the future increase of surface water salinity, it is worth investigating the effectiveness of mitigation measures. Because preferential seepage via boils is the dominant mechanism of salinization in deep Dutch polders (De Louw, *et al*., 2010), measures which reduce the contribution of boils should be effective in dealing with salinization. In scenario 3, we demonstrate the effect of reducing the boil seepage flux by 30% and do not consider the practical implications of this measure.

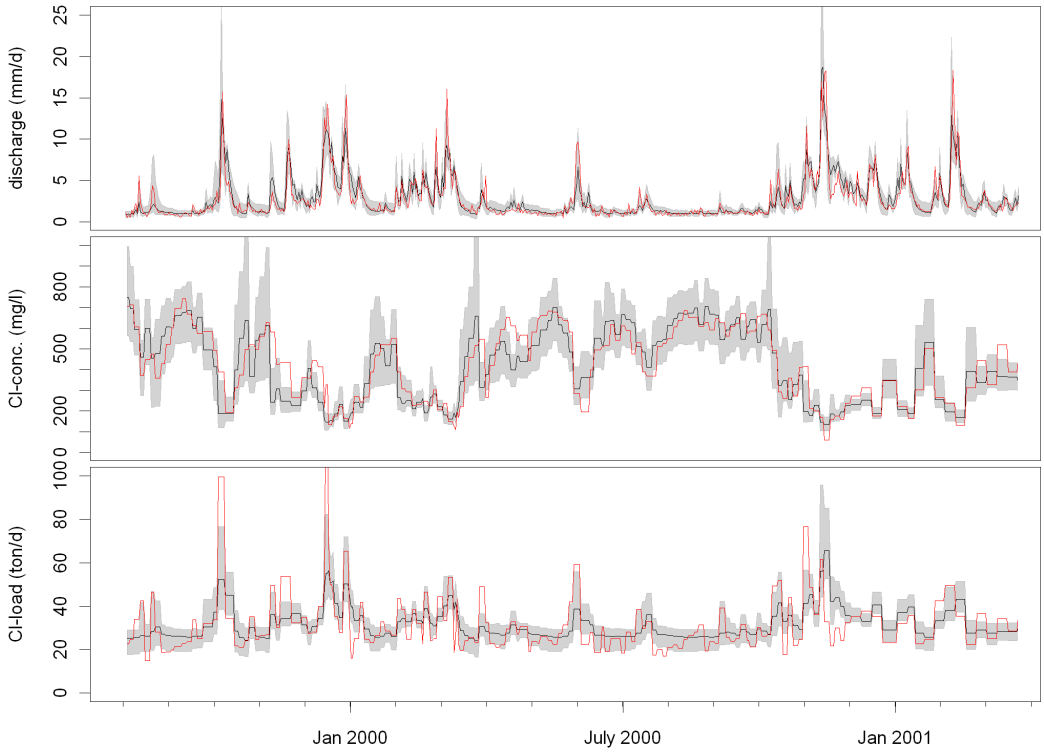

Fig. 3.3. Observed (red) and modeled (median, black) polder water discharge, chloride concentration of discharge water and total chloride loads. Grey area indicates the uncertainty of the model output estimate characterized by the minimum and maximum of the entire ensemble of 59,630 behavioural simulations (GLUE analysis GA-A).

3.3 Results and discussion

3.3.1 Discharge, chloride concentrations and chloride loads

The 5.10^8 Monte Carlo simulations sampling from the prior parameter ranges (Table 3.2) and applying the cut-off criteria from Table 3.3 resulted in 59,630 behavioural simulations (GA-A). The entire ensemble of the behavioural model output of polder water discharge, salt concentration and salt loads are shown in Fig. 3.3, together with the observed time series. The daily observed polder water discharge, both peak and base flow, was simulated well with small uncertainty ranges. However, some of the observed discharge peaks during the summer period are underestimated. This may be due to ignoring the unsaturated zone in our model concept (e.g. development of cracks, unsaturated overland flow). Although the range of the modeled chloride concentrations was larger than the range of the modeled discharge, the observed dynamics were well represented by the calculated median chloride concentration. Note that the blocked shape of the measured chloride concentration and load is caused by the collection of discharge weighted water samples every 3 to 7 days. For comparison, the modeled chloride concentration and load were also converted to average values. Both polder water discharge and salt concentration are highly variable in time and show opposite responses. Low concentrations were found in periods of high discharge due to dilution by the discharge of shallow groundwater and rainfall. Concentrations gradually increased during dry periods when the contribution of drained shallow groundwater decreases and the input of salt sources becomes more dominant.

Compared with polder water discharge and chloride concentrations, the observed chloride loads showed an attenuated variation as a function of time. For 90% of the time, the measured chloride loads were between 20 and 50 t d^{-1}. Chloride loads never dropped to less than 15 t d^{-1}, which indicates a significant saline source throughout the year, even in dry periods with low discharges. Remarkably, major peaks of chloride loads coincided with relatively low chloride concentrations, as they occurred during peak flows (Fig. 3.3). Heavy rainfall events probably mobilized "older" water containing chloride. This chloride originates from seepage which is mixed with infiltrated rainwater and temporarily stored in the groundwater reservoir. The simulations of chloride load dynamics showed less satisfactory results than those of discharge and chloride concentration. This is what we expected, because chloride loads are derived by the multiplication of water discharges and their chloride concentrations, hence errors in both quantities will be expressed in the simulated chloride loads. The modeled peaks of chloride loads were underestimated and during base flow the modeled chloride loads were slightly larger than observed. Considering that total chloride loads are simulated well by applying the cut-off criterion Є(tot)-L that allows a total salt balance error of 5%, we think the underestimated simulated dynamics of chloride loads can be explained by shortcomings in the model concepts that control the storage and discharge of chloride. First, we neglected storage of chloride in the surface water. During dry periods, surface water chloride concentrations increase but transport velocities to the pumps are small due to small discharges. Consequently, new rain showers will accelerate the transport of stored chloride, resulting in elevated chloride loads. Second, the assumption that boils directly discharge into the surface water may have noticeable consequences, since this chloride is therefore not stored in the mixing reservoir like chloride from diffuse and paleochannel seepages, but is instantly released into the surface water without any temporal variation.

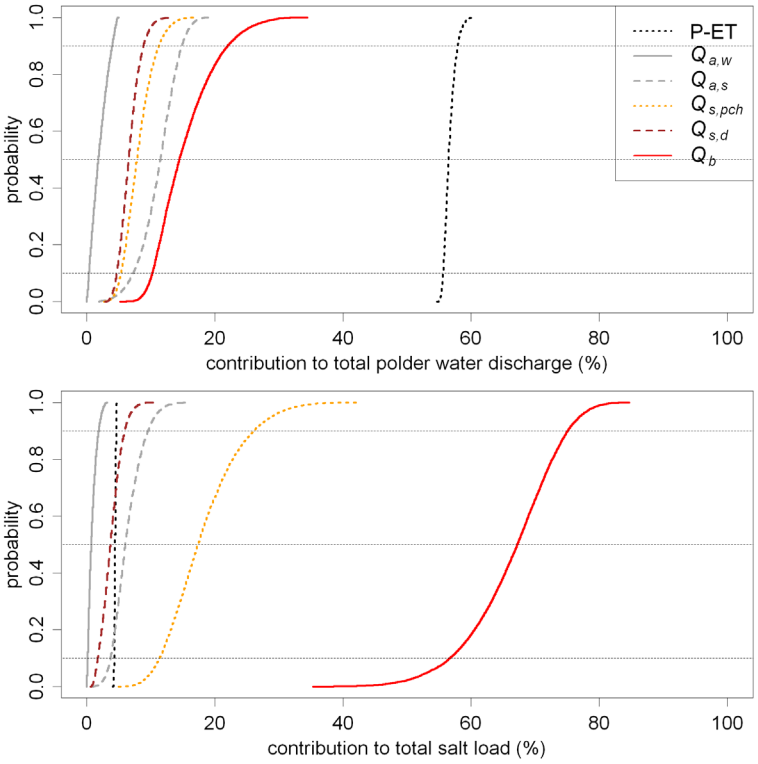

Fig. 3.4. Cumulative probability distribution function for the contribution of different sources to the total polder water discharge and total salt load of the polder (in %) (GLUE analysis GA-A).

3.3.2 Quantification of salt sources

In Fig. 3.4, the cumulative probability distribution function for each source derived from all the behavioural simulations is shown. The dominant water source is precipitation. Precipitation surplus (P-ET) contributes more than 55% to the total polder water discharge. Since we did not vary the precipitation and evapotranspiration fluxes, the range found for this contribution is exclusively the result of the applied cut-off criterion Є(tot)-Q of Table 3.2 that allows a water balance error of 5%. Despite its domination of water input, the contribution of precipitation to the total salt load is small due to its low concentration. The contribution of admitted 'boezem' water to the total salt load is less than 1% in the winter and about 6% (standard deviation ±2.3%) in the summer. Salt loads derived from paleochannel seepage are much larger (18% ±5.7%) than those derived from diffuse seepage (4% ±1.6%), due to the elevated chloride concentration of paleochannel seepage. However, the model results show that the most important salt source is upward groundwater flow through boils, with an average contribution of 66% (± 7.2%) to the total salt load, despite the fact that they contribute only 15% (± 4.7%) to the polder water discharge. In 95% of the behavioural simulations, boils contributed more than 50% to the total salt load of the polder.

Upward groundwater flow from the upper aquifer via boils and via sandy paleochannel belts in the Holocene confining layer are both forms of preferential seepage. The area where they occur is small compared to the total polder area, as is apparent from Fig. 3.2. Our model results show that these forms of preferential seepage together contribute about 84% (± 7.2%) to the total salt load of the polder, and this is primarily the consequence of the high chloride concentrations of water discharged in this way. The average calcu-

lated behavioural value is about 1400 mg L^{-1} (± 320 mg L^{-1}) for boils, which is more than two times that of paleochannel seepage (700 mg L^{-1}) and much higher than that of diffuse seepage (170 mg L^{-1}) or the average concentration of inlet water (150 mg L^{-1}). The concentration difference between the three seepage types can be explained by the upconing mechanism proposed by De Louw *et al*. (2010). Higher seepage fluxes result in upconing of deeper groundwater. Since the salinity of groundwater increases with increasing depth in the Noordplas Polder, higher seepage fluxes are associated with higher chloride concentrations (Fig. 3.1).

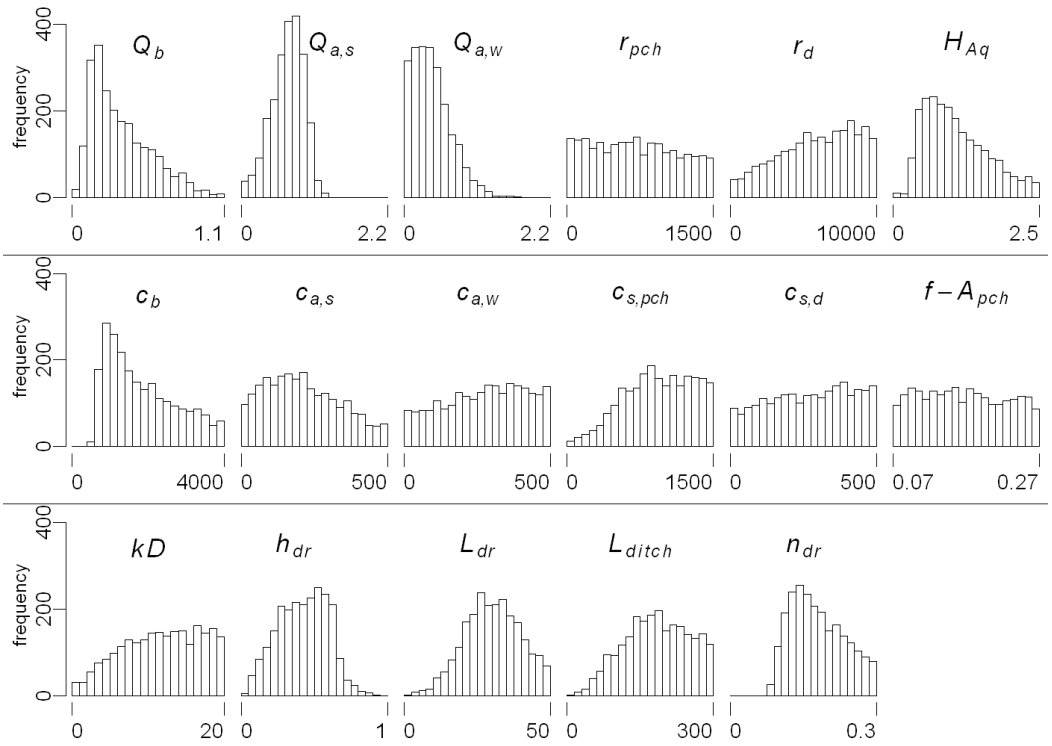

Fig. 3.5. Posterior behavioural parameter distributions for GLUE analysis GA-B. Units of parameter values are listed in Table 3.2.

3.3.3 Parameter uncertainty and sensitivity

The posterior parameter distributions of GLUE analysis GA-B with wider prior parameter ranges than GA-A are shown in Fig. 3.5. The large variation in behavioural parameter value indicates that there is strong equifinality. This equifinality can be reduced by narrowing the ranges of the prior parameter distribution based on measurements or the literature. Table 3.4 shows that smaller prior ranges (GA-A) also lead to smaller uncertainty ranges in the model output. This illustrates that both model input- as well as model output uncertainty can be reduced by incorporating field measurements. Table 3.4 also shows that daily to weekly measurements of polder water discharge, weighted concentration and water table elevation are essential for deriving an adequate set of behavioural parameters to yield a correct simulation of salt and water fluxes. Ignoring the dynamics of the system responses leads to an enormous increase in uncertainty of the model output and source distribution (GA-C). Note that despite the large uncer-

tainty in the model output due to leaving out the daily to weekly measurements, the total water and salt balance errors are still less than 5%.

Table 3.4. Uncertainty ranges for three GLUE analyses with different prior parameter distributions ranges and cut-off criteria. The uncertainty ranges are represented by the statistics of the entire ensemble of daily simulated discharge *Q*, concentration *Cl* and salt load *L* and by the quantified source contribution to total polder water discharge and salt load in %.

GLUE analysis		GA-A				GA-B				GA-C			
Use		Water and salt fluxes, source contribution				Parameter sensitivity and uncertainty analysis				Parameter sensitivity and uncertainty analysis			
Prior parameter ranges		Small ranges based on measurements (Table 3.2)				Wide ranges (Table 3.2)				Wide ranges (Table 3.2)			
Cut-off criteria		Table 3.3				Table 3.3				ϵ(tot)-Q_{pump}, ϵ(tot)-c_{pump}, ϵ(tot)-L_{pump} < 5%			
No. of behaviourals		59,630				2,300				265,641			
		min	mean	stdev	max	min	mean	stdev	max	min	mean	stdev	max
Q	mm d^{-1}	1.8	2.8	0.4	3.8	1.5	2.7	0.4	4.0	0.2	2.7	1.4	53.1
Cl	mg L^{-1}	330	434	37	555	299	429	48	605	120	424	92	1619
L	t d^{-1}	25.6	31.8	2.0	38.5	23.6	32.0	2.8	41.7	3.2	32.2	9.1	227.0
P-ET	%	54.7	56.6	0.9	60.7	53.1	57.1	1.4	65.5	13.8	56.3	2.1	67.5
$Q_{a,w}$	%	0.0	2.0	1.3	5.0	0.0	6.7	4.6	28.8	0.0	10.1	7.7	38.8
$Q_{a,s}$	%	1.9	11.2	2.9	18.9	0.1	13.2	4.5	25.3	0.0	16.3	8.7	40.9
$Q_{s,pch}$	%	2.7	8.1	2.3	17.2	0.0	6.0	4.6	32.2	0.0	3.2	5.6	35.3
$Q_{s,d}$	%	2.9	6.7	1.6	13.8	0.0	4.5	3.1	19.7	0.0	2.6	4.8	62.4
Q_b	%	5.2	15.4	4.7	34.4	0.3	12.5	7.6	38.8	0.0	11.3	7.5	39.2
L_{P-ET}	%	4.1	4.4	0.1	4.7	3.9	4.5	0.3	9.6	1.0	4.5	0.5	15.4
$L_{a,w}$	%	0.0	0.9	0.7	3.2	0.0	6.4	6.2	49.2	0.0	10.1	11.0	77.5
$L_{a,s}$	%	0.7	6.4	2.3	16.3	0.0	9.5	7.0	46.5	0.0	15.2	12.6	100.0
$L_{s,pch}$	%	5.0	18.1	5.7	42.7	0.0	16.8	13.0	88.8	0.0	9.5	18.9	88.2
$L_{s,d}$	%	0.6	3.8	1.6	10.8	0.0	4.0	3.8	25.7	0.0	2.3	5.3	59.1
L_b	%	35.3	66.4	7.2	84.7	0.7	58.8	16.1	100.0	0.0	58.4	20.7	100.0

To improve the reliability of the modeled water and salt fluxes and concentrations, field data can be best collected for those parameters to which the results are sensitive. A strong difference between the posterior behavioural distribution and the prior uniform distribution reveals which parameters can be considered sensitive (Fig. 3.5), and this is indicated by large D-statistics (Table 3.5). Largest D-statistics were calculated for boil seepage Q_b, admission of 'boezem' water in the summer $Q_{a,s}$ and winter $Q_{a,w}$. They have a maximum value above which no behavioural runs were found (Fig. 3.5). It is not surprising that these water balance terms also show a large correlation with the total water balance error (Table 3.5). Table 3.5 shows that total chloride load and mean concentration of the polder water are dominantly determined by boil seepage (Q_b) and its concentration (c_b) as indicated by a large calculated R^2. Behavioural values of c_b show a clear minimum (Fig. 3.5), indicating that boils must have higher chloride concentrations. Furthermore, the large

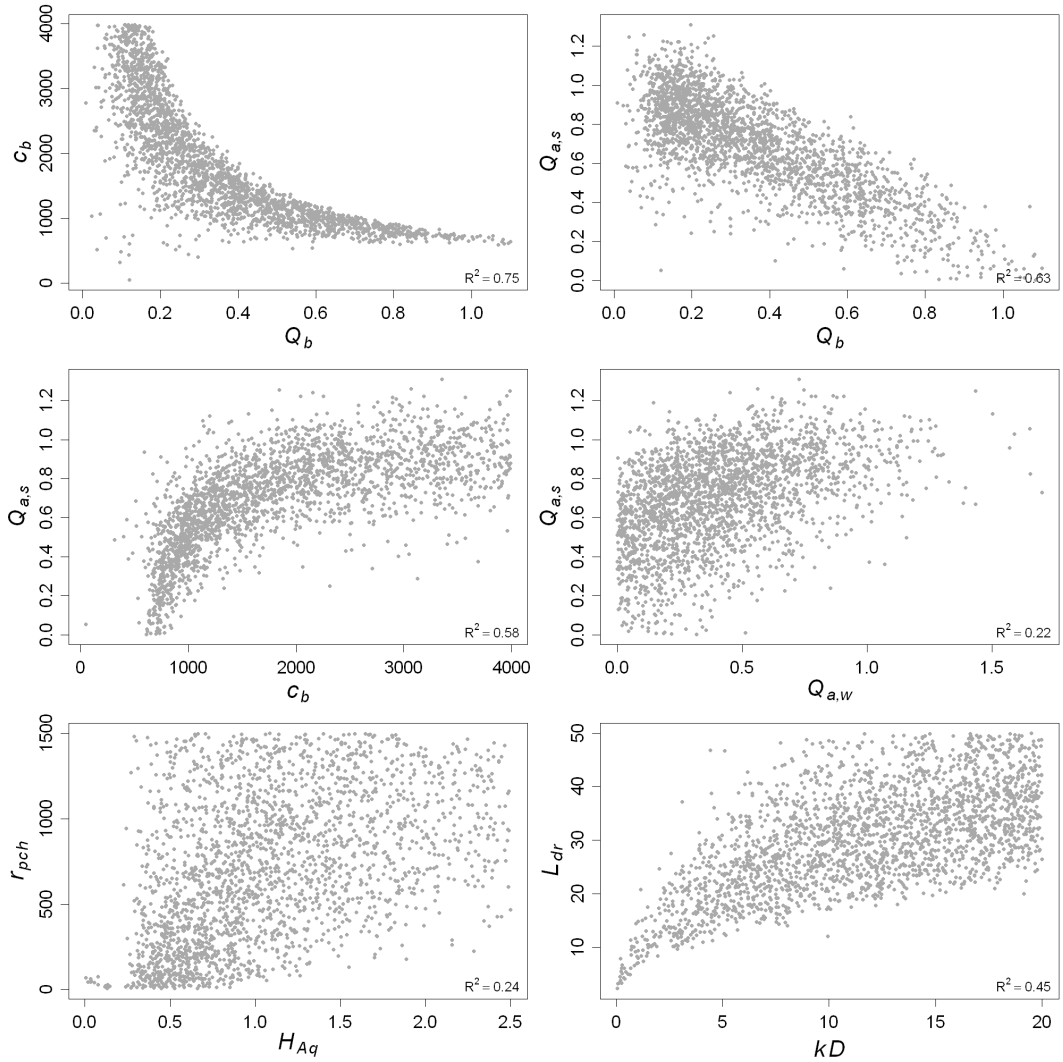

Fig. 3.6. Scatter diagrams for the six most strongly correlated behavioural parameter combinations (GLUE analysis GA-B).

sensitivity of Q_b and c_b is shown by their strong interdependency (Fig. 3.6). The fact that some sensitive parameters are correlated with each other can be used to reduce model input- and output uncertainty. Considering that the total boil flux Q_b is the parameter that is the most difficult to measure, its uncertainty can be reduced by increasing the reliability of the parameters most strongly correlated to it, c_b and $Q_{a,s}$, which can be measured more easily (Fig. 3.6).

The dynamics of the model output are mainly determined by the parameters that control the interaction between groundwater storage and drainage. Some of these parameters show large D-statistics, indicating a large sensitivity for the total system behaviour, but they do not have an impact on the total modeled water and salt volumes. Tile drainage spacing l_{dr} has the largest impact on the polder water discharge dynamics, whereas drainage level h_{dr} and ditch spacing l_{ditch} control the water table and its fluctuations. Fluctuations in chloride concentration are mainly determined by drainable porosity n_{dr}.

Table 3.5. Global sensitivity analysis results. The R^2 for correlations between model input parameter values and model output error $\in$ (tot = entire simulation period, dyn = dynamic, measurement time scale) and the Kolmogorov D statistics for each behavioural parameter distribution from GA-B. Not significant (n.s.) when $R^2 < 0.025$.

	$\in$(tot)-Q_{pump}	$\in$(tot)-L_{pump}	$\in$(tot)-c_{pump}	$\in$(dyn)-Q_{pump}	$\in$(dyn)-L_{pump}	$\in$(dyn)-c_{pump}	$\in$(dyn)-h_{grw}	D
c_b	n.s.	0.320	0.490	n.s.	n.s.	n.s.	n.s.	0.18
Q_b	0.143	0.322	0.201	n.s.	0.049	n.s.	n.s.	0.38
H_{aq}	0.172	0.043	n.s.	n.s.	0.034	n.s.	0.032	0.23
$Q_{a,w}$	0.149	n.s.	n.s.	0.070	0.034	n.s.	n.s.	0.55
$Q_{a,s}$	0.138	n.s.	0.067	n.s.	0.090	n.s.	n.s.	0.48
r_d	0.087	n.s.	n.s.	n.s.	n.s.	n.s.	n.s.	0.10
r_{pch}	0.066	0.043	n.s.	n.s.	n.s.	n.s.	n.s.	0.10
l_{dr}	0.029	n.s.	n.s.	0.220	0.036	0.028	n.s.	0.21
h_{dr}	n.s.	n.s.	n.s.	0.050	n.s.	n.s.	0.337	0.25
l_{ditch}	n.s.	n.s.	n.s.	n.s.	n.s.	n.s.	0.182	0.17
kD	n.s.	n.s.	n.s.	0.095	0.036	n.s.	0.136	0.09
$c_{a,s}$	n.s.	n.s.	0.027	n.s.	0.097	0.039	n.s.	0.19
n_{dr}	n.s.	n.s.	n.s.	0.085	0.051	0.077	0.049	0.24
$c_{s,p}$	n.s.	n.s.	n.s.	n.s.	0.026	n.s.	n.s.	0.16
A_{pch}	n.s.	n.s.	n.s.	n.s.	n.s.	n.s.	n.s.	0.09
$c_{s,d}$	n.s.	n.s.	n.s.	n.s.	n.s.	n.s.	n.s.	0.05
$c_{a,w}$	n.s.	n.s.	n.s.	n.s.	n.s.	n.s.	n.s.	0.05

3.3.4 Scenario analysis

The model was used to calculate the effect and corresponding uncertainty of three different scenarios. We have discussed only the calculated chloride concentrations of the polder water since these reflect water quality rather than loads. For each scenario, the 59,630 behavioural parameter sets resulted in an equally large ensemble of day-to-day time series of chloride concentrations of polder discharge. These ensembles can be characterized by the time series of mean and standard deviation of chloride concentration as shown in Fig. 3.7. As a result of the dryer W+ climate scenario (used for scenario 1), the chloride concentrations of the surface water are slightly higher in summers compared to the present situation. However, after the summer period, the chloride concentration for the dry W+ scenario in the months October and November is significantly larger than that for the present situation. During these months the cumulative precipitation deficit between the present and future climate is at its maximum. The model results show that a reduction in the quantity of 'boezem' water admitted to the polder (scenario 2) will have a large impact on surface water salinity. During dry periods in the summers, when there is no dilution of the saline seepage water, the average chloride concentration increases from 650 to 840 mg L^{-1}. This is also the period when the demand for fresh water irrigation is the largest. Note that the uncertainty of the predictions increases with increasing salinity during dry periods.

It is possible to take different measures to compensate for the effects of future climate change and sea-level rise. Because

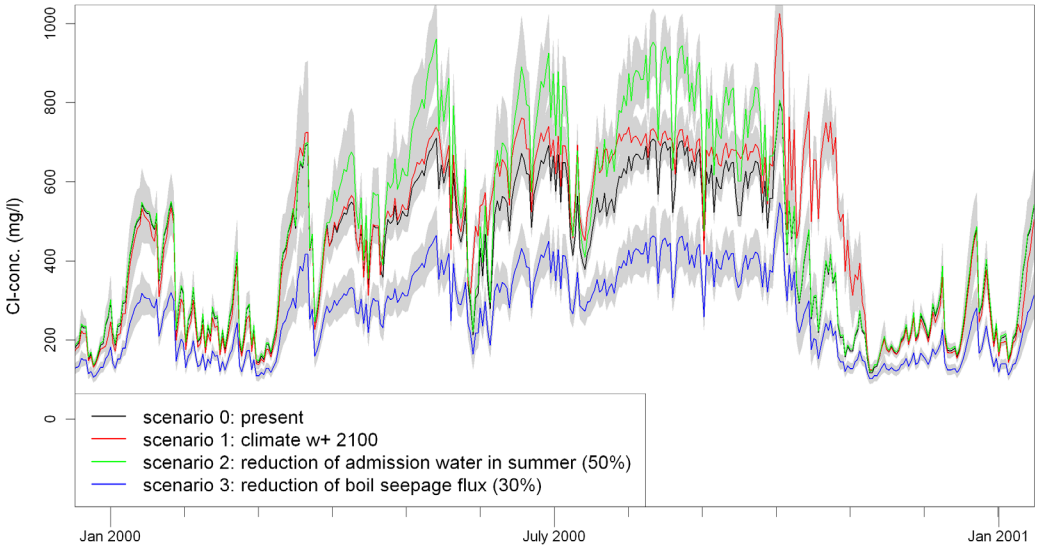

Fig. 3.7. Calculated chloride concentration of the polder water discharge for different scenarios. The coloured lines give the mean value and the grey areas present the uncertainty range (mean ± standard deviation) derived from 59,630 simulations with behavioural parameter sets of GLUE analysis GA-A.

boil seepage is the most dominant source of salt, we demonstrated the effect of reducing the contribution from boils by 30% (scenario 3). This leads to a significant decrease in chloride concentrations, from 650 to 410 mg L^{-1}, during the dry periods in summer and the chloride concentrations never exceeds 460 mg L^{-1} (Fig. 3.7). Note that reducing boil fluxes will probably lead to an increase in the hydraulic head, which will cause an increase of diffuse and paleochannel seepage fluxes. However, since these forms of seepage have a lower salinity, the overall net effect will be positive with respect to the salinization of the surface water.

3.4 Conclusions

In this paper, we have presented a probabilistic (GLUE) end-member mixing approach to modeling daily discharge, salt loads and the salt concentration of water pumped out of an artificially drained polder catchment area. To incorporate the uncertainty of model input parameters, their values were sampled randomly from uniform parameter distributions. The model was conditioned on measurements of daily to weekly polder water discharge, salt concentrations and salt loads leaving the polder and of water table elevation to produce sets of input parameters which simulate the system equally well. With these sets of behavioural parameters, we quantified the contribution and uncertainty of different sources to the water and salt balance of the polder catchment area and the effects of different scenarios. However, the large variation in behavioural parameter values indicates that there is strong equifinality. This is caused by the presence of the many sources that contribute to the water and salt balance of the polder and by the uncertainty of the model input parameters.

Despite the large equifinality and the uncertainty of many of the model parameters, the dominant salt sources could be quantified within an acceptable reliability. Our modeling approach to assessing source contribution demonstrates the need to distinguish preferential from diffuse

seepage. These preferential flow paths are discrete and cover just a small part of the polder. However, their localized nature and intense flow at high velocities leads to upconing of deeper groundwater (De Louw *et al*., 2010). Since salinity increases with increasing depth in the Noordplas Polder, this upconing leads to higher salinities of groundwater being discharged via preferential flow paths than via diffuse seepage. Preferential seepage, which includes upward flow via boils and paleochannel belts, is responsible for about 84% of the surface water salinization in the polder. The observed polder water discharge, salt concentrations and salt loads could only be explained by assigning a large contribution of the total salt load to boils. Boils contribute, on average, 66% to the total salt load and only about 15% to the total water flux into the polder and they therefore form the dominant salinization pathway.

As in most balance studies, discharge rates of water and salt at the polder catchment outlet could be measured relatively accurately as opposed to the incoming fluxes. In particular, uncertainties in the contribution from groundwater seepage are usually large. The model results showed that the equifinality and model input- and output uncertainty can be reduced by narrowing the ranges of the prior parameter distribution. Since our model approach is mainly based on physical and measurable parameters, this can be done by improving the quality of field measurements. Monitoring activities should therefore be concentrated on parameters which are sensitive to the modeled water and salt fluxes. In our case, the most sensitive parameters are boil flux and concentration, and the admission of 'boezem' water, which all show significant interdependencies. This implies that focusing monitoring efforts on increasing the accuracy of a single parameter will automatically lead to a greater accuracy of correlated parameters. The estimation of the total boil flux, which is one of the most uncertain and most important parameters, can therefore be improved by collecting accurate data about the admission of 'boezem' water or boil water salinity. Our results have established the need for frequent measurements of polder water discharge and weighted concentration at the outlet of the catchment in order to obtain reliable simulations of water and salt fluxes and to be able to allot them to the different sources.

Our findings will help to determine salt reduction measures, as we have now established that such measures should focus on preferential flow paths and, in particular, on boils. Scenario calculations show that if the boil flux can be reduced by 30%, the chloride concentrations will decrease significantly, from 650 to 415 mg L^{-1} during dry periods in the summers when the demand for fresh water is highest.

Chapter 4

Natural saltwater upconing by preferential groundwater discharge through boils

Perry de Louw, Alexander Vandenbohede, Adrian Werner, Gualbert Oude Essink
Published in Journal of Hydrology 490, 74-87, 2013

Abstract

Natural saltwater upconing caused by the preferential groundwater discharge of boils is a key process in the salinization of Dutch deep polders. The factors controlling upconing by boil discharge and boil water salinities are poorly constrained and have not been previously documented. We addressed this knowledge gap by investigating upconing mechanisms using field measurements and numerical simulations of simplified situations. Boils occur as conduits in the upper aquitard connecting the underlying aquifer to the surface and allowing groundwater to discharge at rates up to 100 $m^3 d^{-1}$ with Cl concentrations up to 5 g L^{-1}. Boils are found as isolated features or clustered in small areas of 20-100 m^2. Field observations show that preferential flow through boils creates localized and narrow saltwater upconing spikes, causing the elevated boil water salinities. Modeling results indicate that boil water in Dutch polders comprises mixtures of groundwater from a wide range of depths and salinities with larger contributions from shallower and less saline groundwater than from the deeper and more saline water. Similar to previous numerical studies of pumping-induced upconing, the numerical results show that the most important factors controlling the boil salinity in Dutch polders are boil discharge, the horizontal hydraulic conductivity of the aquifer, the depth of the transition zone and the salinity (or density) contrast within the aquifer. When boils are clustered, natural saltwater upconing is a function of the total discharge of a boil cluster, whereas the boil-to-boil salinity variations within a cluster are determined by the discharge of individual boils and their position relative to neighbouring boils. Regional lateral flow significantly modifies flow patterns by dividing the groundwater flow system into a local boil system overlying the regional flow system. Despite this, regional flow has only a minor effect on the relative contributions of saline and fresh groundwater to boil discharge and thus on boil salinity as well.

4.1 Introduction

In many deltaic areas, groundwater is saline because of the combined effects of seawater intrusion and marine transgressions (e.g. Custodio and Bruggeman, 1987; Post and Abarca, 2010). Saline groundwater in the Netherlands originates from Holocene transgressions producing a wide range of salinity distributions (Oude Essink, 1996; Post, 2004; Vos and Zeiler, 2008). Saline groundwater may reach the surface by upward groundwater flow (referred to here as seepage) in areas that lie below mean sea level (MSL). As one-quarter of the Netherlands lies below MSL, saline seepage leads to salinization of surface waters for large areas, impacting on agriculture and aquatic ecosystems (e.g. Van Rees Vellinga *et al.*, 1981; Van der Eertwegh *et al.*, 2006; Oude Essink *et al.*, 2010). The largest seepage fluxes in the Netherlands are found in deep polders, which are reclaimed lakes.

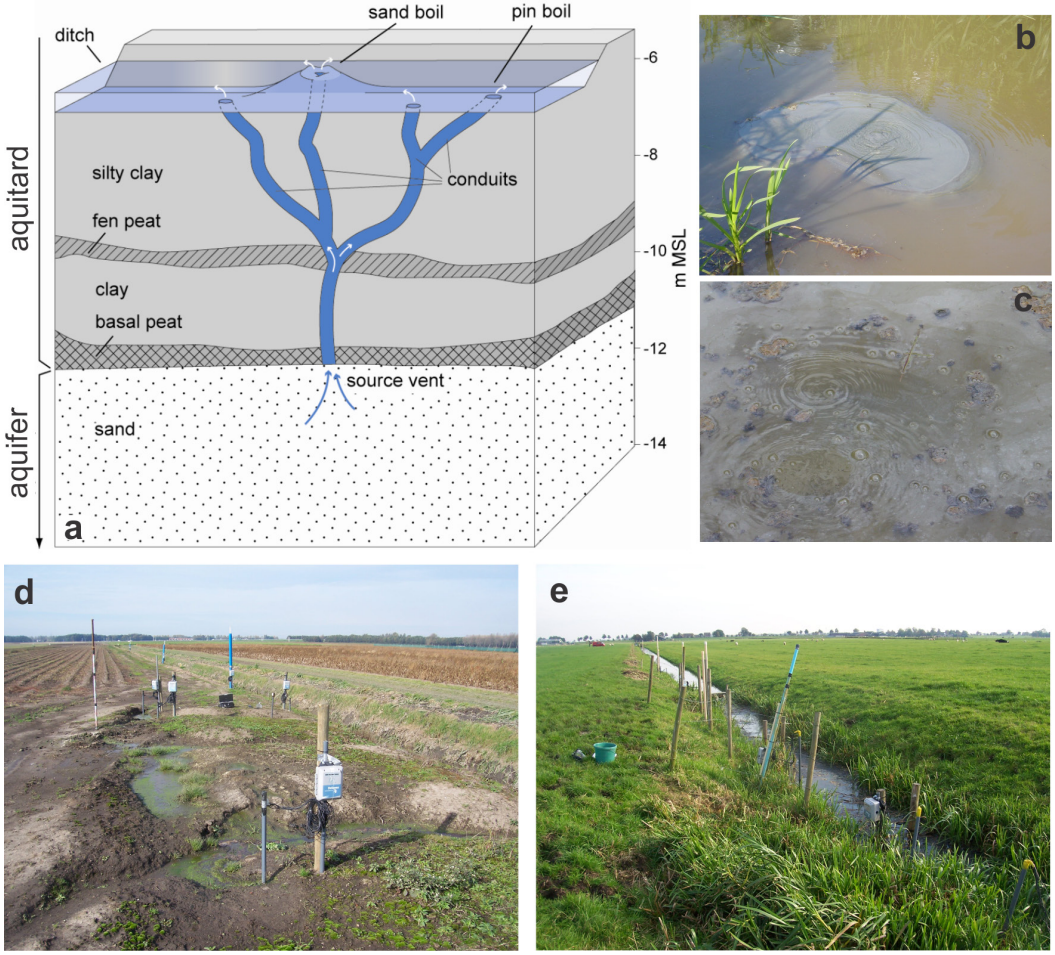

Fig. 4.1. Boils in deep polders: (a) diagram of boils with several conduits in aquitard (adapted from De Louw *et al*., 2010), (b) sand boil, (c) a boil emitting methane, (d) study site A: boils on land and monitoring network, (e) study site B: boils in ditch and monitoring network.

Surface waters in these systems are maintained at levels as low as 4 to 7 m below MSL, causing large upward and lateral hydraulic gradients in the underlying aquifers (e.g. Van Rees Vellinga *et al*., 1981; Oude Essink *et al*., 2010).

De Louw *et al*. (2010) showed that preferential seepage through boils is the dominant salinization source in deep polders in the Netherlands. In these systems, boils occur as conduits in the upper aquitard of peat and clay that connect the underlying aquifer to the surface, allowing groundwater to discharge at high velocities (Fig. 4.1). When the pressure of water in the aquifer is greater than the pressure exerted by the weight of the overlying stratum, heaving and cracking can occur, creating flow pathways that lead to the development of boils (Holzer and Clark, 1993; Li *et al*., 1996; TACFD, 1999). About 85% of the boils mapped by De Louw *et al*. (2010) occurred in ditches and only 15% were found on dry land. Boils occurred either as single boils or as clusters of multiple boils within small boil areas (<100 m^2). Individual boil fluxes ranged from 0.5 to 100 $m^3\ d^{-1}$. Field measurements by De Louw *et al*. (2010) showed that the salinities of boil discharge are much higher than that of diffuse seepage. Diffuse seepage is seen over the majority of the polder, whereby groundwater flows slowly upwards through the soil matrix of the upper aqui-

tard's low-permeability sediments. For example, the median chloride (Cl) concentration of 49 boils in the deep Noordplas Polder was 1.3 g L^{-1}, whereas the median Cl concentration of diffuse seepage was 0.095 g L^{-1} (De Louw *et al*., 2010). Larger boils with higher discharge rates tended to have higher Cl concentrations, i.e. up to 2.9 g L^{-1}. Over 200 boils were observed in the Haarlemmermeer Polder with variable salinities up to 5 g L^{-1} of Cl (Goudriaan *et al*., 2011).

Based on field measurements, De Louw *et al*. (2010) concluded that natural upconing of deep, saline groundwater induced by local, high-velocity flows through boils is the mechanism that leads to high boil salinities. As a result, boils impart high salt loads to deep polder systems. This was demonstrated by De Louw *et al*. (2011a) for the Noordplas Polder, where boils contribute about 66% of the total salt load from only 15% of the total water flux. Despite that the importance of boils in the surface water salinization of deep polders has been clearly demonstrated, the associated saltwater upconing mechanisms remained largely unevaluated. Therefore, saltwater upconing mechanisms controlling boil salinities is the main focus of the present study.

Natural saltwater upconing caused by preferential discharge through boils is expected to involve groundwater flow in the aquifer towards the source vent of the boil, which occurs as a localized point at the bottom of the aquitard (Fig. 4.1a). It is therefore comparable to saltwater upconing induced by the extraction of fresh groundwater overlying saltwater using partially penetrating wells, which has been described extensively in the literature (e.g. Dagan and Bear, 1968; Reilly and Goodman, 1987; Werner *et al*., 2012). Upconing from pumping can create a saltwater cone that is stable under certain conditions, notwithstanding that eventually, some saltwater is expected to reach the well due to dispersion effects (Reilly and Goodman, 1987; Werner *et al*., 2012). Stable upconing plumes are convex in shape and only low-salinity groundwater enters the well (i.e. subcritical conditions), whereas unstable upconing plumes become concave and intercept the well, which subsequently discharges a significant proportion of saltwater (i.e. under critical or supercritical conditions) (Werner *et al*., 2012). Only a few studies have focused on the behaviour of salt plumes that intercept the point of extraction, such as the well screen (e.g. Reilly and Goodman, 1987), possibly because it is the objective of most management strategies to avoid this condition (Werner *et al*., 2009). Most of the boils observed by De Louw *et al*. (2010) discharge considerable salt loads, and hence natural saltwater upconing caused by boils most likely occurs under unstable, supercritical conditions.

Generally, two methods are employed in solving the saltwater upconing problem (Bower *et al*., 1999): the sharp-interface approach and the dispersive solute transport approach. The sharp-interface approach assumes that saltwater and freshwater are immiscible, i.e. separated by an abrupt interface. Mixing is allowed in the dispersive solute transport approach and a dispersive mixing zone between the two fluids is considered. This method represents a more realistic situation, although it is more complex to solve and requires the application of numerical methods (e.g. Diersch *et al*., 1984; Reilly and Goodman, 1987; Zhou *et al*., 2005), whereas the sharp-interface approach has been solved using both numerical and analytical methods (e.g. Dagan and Bear, 1968; Zhang *et al*., 1997; Bower *et al*., 1999). Saltwater upconing has also been studied using laboratory experiments (e.g. Johannsen *et al*., 2002; Werner *et al*., 2009). However, real-world field data pertaining to saltwater upconing are scarce because of the challenges of undertaking field-based measurements of dynamic salt transport near pumping wells (Jakovovic *et al*., 2011).

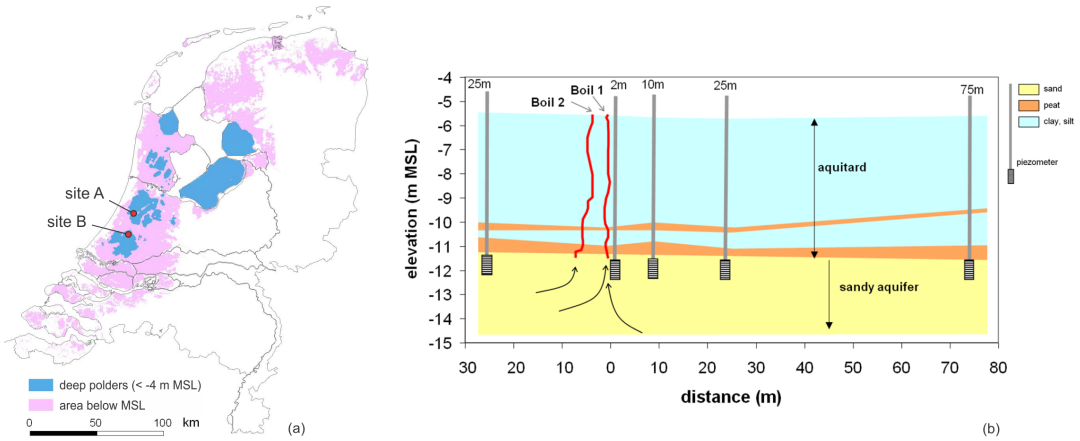

Fig. 4.2. (a) Location of study site A (Haarlemmermeer Polder) and site B (Noordplas Polder), (b) General set up of the monitoring network around the boils of site A.

The intent of this study was to examine key features of natural upconing mechanisms associated with boil discharge in Dutch polders. The following aspects were assessed: (i) sources (depths) of boil water and relationships between boil salinity and boil source depths, (ii) the influence of the regional aquifer salinity distribution on upconing, (iii) interactions between boils in boil clusters, and (iv) the effect of regional lateral flow on upconing processes. A combination of field observations and conceptual model testing using numerical simulations was adopted. Two field situations involving saline boils were investigated to provide observations of natural saltwater upconing, and to constrain numerical models in aspects relating to geometry, salinity, boil discharge, aquifer hydraulic heads and hydraulic properties. Numerical modeling and sensitivity analyses were used to explore the influence of different parameters on upconing processes.

4.2 Study area

Field measurements were carried out in two deep polders in the west of the Netherlands: the Haarlemmermeer Polder and the Noordplas Polder (Fig. 4.2a). These polders were reclaimed from lakes in different stages between 1750 and 1850. Field site A is in the southwest of the Haarlemmermeer Polder and site B is in the north of the Noordplas Polder (Fig. 4.2a). The ground levels at sites A and B are 5.5 m and 4.7 m below MSL, respectively. The hydrogeology of both sites is similar, and is comparable with many other Dutch deep polders. The upper 6-7 m of the subsurface is an aquitard that consists of clay and peat, in which the boils have developed, and overlying a 30-50 m thick sandy aquifer (Fig. 4.1). The aquifer hydraulic heads are permanently above ground level at both sites (De Louw *et al.*, 2010; Oude Essink *et al.*, 2010). At study site A, two boils, 4 m apart, were evident as small vents at the ground surface (Fig. 4.2b). The boils at site B occurred underwater in a ditch, and their outflow vents were not directly visible due to vegetation and turbid water (Fig. 4.1e). However, at least three outflow vents within an area of 10 m x 2 m could be detected using temperature measurements (De Louw *et al.*, 2010) and by observations of upwelling water and methane (Fig. 4.1c).

The regional groundwater salinity distributions in the aquifer of the two deep polders are mainly the result of the past

Holocene transgressions and the reclamation history (Oude Essink, 1996; Post, 2004; Vos and Zeiler, 2008). Salinization of the aquifer occurred by free convection of seawater mixed with river water during the major transgression between 7500 and 4750 BP. The subsequent development of sand banks and dunes isolated the area from the sea, and fresh rainwater recharged the upper part of the aquifer, displacing the saline groundwater. The construction of the deep polders subsequently changed regional groundwater flow direction and created complex salinity patterns, characterized by large transition zones and a wide range of salinities. The groundwater in the upper 5-10 m of the sandy aquifer of both sites is generally fresh to slightly brackish (Cl concentrations of 0.05-1 g L^{-1}), and salinity gradually increases with depth to Cl concentrations of 3-8 g L^{-1} at 15-40 m below the aquitard (Van Rees Vellinga *et al*., 1981; De Louw *et al*., 2010; Oude Essink *et al*., 2010).

4.3 Methodology

4.3.1 Monitoring network

Fig. 4.2b shows the general set up of the monitoring network around the boil area of site A. Site B had a similar monitoring network configuration. Piezometers with a 0.5 m long screen were installed at 7-8 m below the ground surface and at different distances from the boils (i.e. at 2, 10, 25 and 75 m from boil 1, Fig. 4.2b), such that they penetrated the top of the sandy aquifer just below the aquitard. Aquifer hydraulic heads were measured in the piezometers for a period of 2.5 years (January 2009-July 2011), with a 1-h frequency using automated pressure loggers (CTD-divers from Schlumberger Water Service®). Measured heads were converted to equivalent freshwater heads using the equations presented in Post *et al*. (2007). Groundwater was sampled once (18 July 2009) from the piezometers and analyzed for Cl.

Electrical cone penetration tests (ECPT) were carried out to obtain continuous soil electrical conductivity (EC_{bulk}) profiles to a depth of 25 m, and at similar locations to the piezometers. The ECPT measurements were used to map the groundwater salinity distribution in the aquifer to characterize salinity plumes associated with the natural saltwater upconing caused by boils. During penetration, the cone sleeve and tip friction were also measured to provide insight into the lithological composition. To obtain the electrical conductivity of water (EC), EC_{bulk} must be multiplied by the formation factor, which depends on the lithology (e.g. Archie, 1942; Friedman, 2005). The cone sleeve and tip friction measurements in the aquifer showed a relative homogeneous composition of medium-coarse sand, for which a formation factor of 4 applies (Goes *et al*., 2009). Cl concentrations (g L^{-1}) were calculated from the EC (mS cm^{-1}) using the linear relation derived by De Louw *et al*. (2011b): Cl = 0.36EC – 0.45 (valid for ECs > 1.25 mS cm^{-1}). The discharge and EC of the two boils at site A were measured manually by directly collecting the outflowing boil water in a measuring cup. The discharge and EC were measured weekly for a period of 1.5 years. As the outflow vents of the boils at site B were underwater, the boil fluxes and ECs could not be easily measured. The boil salinity at site B was measured once by isolating the boil using a collection vessel.

The possibility of sealing the boils as a measure to abate salinization was examined. Expanding and persisting fluids were injected in the aquifer near the source vent in an attempt to seal the boil. These subsequently flowed towards the source vent due to the flow created by the boil. While these field experiments are not described

in detail in this article, the observed changes in the groundwater system and boil characteristics due to the sudden drop in or cessation of boil discharge (Q_{boil}) are included in the analysis. The boil sealing attempts were carried out on 27th May 2011 at site A and 17th September 2009 at site B.

4.3.2 Numerical modeling of saltwater upconing

Modeling approach

The objective of the modeling was to provide a framework to better understand the field observations and to undertake sensitivity analyses to evaluate the different parameters influencing upconing. The simulated situation was a homogeneous, anisotropic confined aquifer, with each boil represented by a point extraction at the aquifer top. Consequently, the overlying aquitard (and complex, rapid flows through it) was neglected, and the focus was on groundwater flow and saltwater upconing in the aquifer. The simulation of aquitard flow would require the model to predict preferential flow through boil conduits (Fig. 4.1), which are difficult to accurately represent using existing variable-density transport codes. Estimated flow velocities in boils were as high as 800 m d^{-1} (De Louw *et al*., 2010), and the associated travel times of water flowing through the conduits in the order of minutes. Given that the flow processes and temporal and spatial scales for aquitard flow are in contrast to those associated with upconing, conduit flow through the aquitard was not considered. Instead, the boil source vents were simulated as point sinks in the model, because the focus of the paper was aquifer flow and transport processes induced by boil discharge. The models are highly idealized accounts of typical conditions encountered in Dutch deep polders. We intentionally avoid calibration, partly because aquifer parameter distributions and the long-term temporal behaviour at specific sites are not well constrained, but also to allow us to examine simplified situations and develop general intuition about boil-induced upconing processes.

The variable-density flow and transport code SEAWAT version 4 (Langevin *et al*., 2007) was used. Flow and transport may be considered in an axisymmetric domain when a single boil is considered and regional flow is neglected. The parameters of SEAWAT were modified to represent radial flow and transport, reducing the governing equations by one dimension and improving the efficiency of model computations (Langevin, 2008). Fully 3D models were used to incorporate multiple boils and regional flow effects.

Reference case

A reference case was defined and parameterized based on hydrogeological data of the Netherlands (REGIS II, 2005) and aquifer properties, salinity distributions and boil characteristics for the Noordplas Polder (measured by De Louw *et al*. (2010)) and for sites A and B. The parameter values of the reference case are summarized in Table 4.1. The reference case was intended to develop conceptual intuition of functional relationships for idealized conditions, and hence comprises reduced complexity relative to real-world situations. For example, the axisymmetric flow conditions of the reference case preclude the analysis of multiple boils or regional flow effects, which are encountered in field conditions. Regional flow and multiple boils were examined with the more computationally demanding 3D models.

A single-boil entry vent was simulated as a point sink at the top of a 50-m thick (D) homogeneous, anisotropic confined aquifer, with a porosity (n) of 0.30, a horizontal hydraulic conductivity (K_h) of 20 m d^{-1} and a vertical hydraulic conductivity

(K_v) of 6.67 m d^{-1} (i.e. anisotropy of 3) (Fig. 4.3). A constant extraction rate (Q_{boil}) of 30 m^3 d^{-1} was adopted, which falls within the range of 0.5-100 m^3 d^{-1} for measured single-boil fluxes (De Louw *et al*., 2010). Transient simulations for a period of 100 years were undertaken to explore the evolution of upconing following the creation of a new boil. One stress period of 100 years was subdivided in 10,000 flow time steps of 3.65 days. Each flow time step was automatically divided into a number of transport time steps according to the stability criterion Courant number, which was not allowed to be greater than 1 (Langevin *et al*., 2007).

The initial aquifer salinity distribution applied in the models corresponds to the regional aquifer salinity distribution in the absence of boils, and is shown in Fig. 4.3. The fresh groundwater above the transition zone was assigned a Cl concentration (Cl_f) of 0 g L^{-1} with a density (ρ_f) of 1000 kg m^{-3}. For the saline groundwater below the transition zone, a Cl concentration (Cl_s) of 5 g L^{-1} with a density (ρ_s) of 1006.6 kg m^{-3}, a typical value for the aquifers at sites A and B, was adopted. These correspond with a relative density difference ($\beta = (\rho_s - \rho_f)/\rho_f$) equal to 0.0066. The density varied linearly with the Cl concentration because the saline groundwater bodies in the Dutch subsurface are mixtures of seawater (ρ_s = 1025 kg m^{-3}; Cl_s = 19 g L^{-1}), and freshwater (ρ_f=1000 kg m^{-3}; Cl_f = 0 g L^{-1}). De Louw *et al*. (2011b) showed that freshwater-saltwater transition zones in Dutch aquifers can be well described by the spatial moments method. With this method, the derivative of the salinity profile is described by a normal distribution function, from which the centre of mass (1st moment) indicates the centre of the transition zone C_{if} (Fig. 4.3). The Cl concentration at the initial C_{if} position is $0.5Cl_s$. The location of C_{if} was assumed to occur at the position of $0.5Cl_s$, obtained from modeled salinity distributions. The variance (2nd moment) is a measure of the extent of the transition zone. Five times the standard deviation was used to characterize the initial width of the transition zone (W_{if}), which equals the thickness between salinities of $0.01Cl_s$ and $0.99Cl_s$ (Fig. 4.3). The initial position of C_{if} was set at 15 m depth and the initial W_{if} was 15 m, which corresponds with the average conditions in the aquifers at sites A and B (Fig. 4.3).

The reference case was simulated in both axisymmetric and 3D domains for the purposes of comparison. SEAWAT can be manipulated to simulate an axisymmetric geometry by using a grid of one row, *l* columns and *m* layers, and adjusting the input parameters to account for the increase in flow area with radial distance (*r*) (Langevin, 2008). That is, n, K_h, K_v and specific storage (S_s) were scaled by $2\pi r$. The axisymmetric domain was 1500 m long and was represented by 55 variable-spaced columns, with a cell width of 0.5 m at the boil increasing to 50 m at an *r* of 1000 m (Fig. 4.3). The vertical extent was divided into 50 model layers, using thicknesses of 0.5 m (upper 10 m), 1.0 m (10-20 m depth) and 1.5 m (20-50 m depth). Specified-head boundary conditions representing density-corrected hydrostatic conditions were adopted at a distance of 1500 m from the boil. The specified-head boundaries were assigned a constant salt concentration according to the regional aquifer salinity distribution shown in Fig. 4.3. The top and bottom of the aquifer were no-flow and no-mass flux boundaries.

Table 4.1. Parameter values of the reference case and different upconing cases. The parameter values of the reference case are listed under 'Ref'. An upconing case is defined by a 'Nr' and a character 'a', 'b', 'c' or 'd'. Each upconing case differs from the reference case by only one or two parameters for which the values are listed under 'a', 'b', 'c' or 'd'.

Category	Nr	Parameter	Unit	Type of model	a	b	Ref	c	d
boil discharge	1	Q_{boil}	$m^3 d^{-1}$	Axi	5	15	30	50	100
hydrogeology	2	K_h	$m d^{-1}$	Axi	5	10	20	40	60
		K_v	$m d^{-1}$		1.7	3.3	6.7	13.3	20
		K_h / K_v	-		3	3	3	3	3
	3	K_h	$m d^{-1}$	Axi	5	10	20	40	60
		K_v	$m d^{-1}$		6.7	6.7	6.7	6.7	6.7
		K_h / K_v	-		0.75	1.5	3	9	9
	4	K_h	$m d^{-1}$	Axi	20	20	20	20	20
		K_v	$m d^{-1}$		2.2	3.3	6.7	13.3	26.7
		K_h / K_v	-		9	6	3	1.5	0.75
	5	D	m	Axi	25	35	50	75	100
	6	n	-	Axi	0.20	0.25	0.30	0.35	0.45
dispersivity	7	α_L	m	Axi	0	0.05	0.10	0.50	1
		α_T	m		0	0.005	0.01	0.05	0.1
	8	α_L	m	Axi	0.01	0.05	0.10	0.50	1
		α_T	m		0.01	0.01	0.01	0.01	0.01
	9	α_L	m	Axi	0.10	0.10	0.10	0.10	0.10
		α_T	m		0.10	0.02	0.01	0.002	0.001
aquifer salinity distribution	10	C_{if}	m	Axi	5	10	15	20	30
	11	W_{if}	m	Axi	0	10	15	20	30
	12	Cl_s	$g L^{-1}$	Axi	1	2.5	5	10	19
		β	-		0.0013	0.0033	0.0066	0.0132	0.0250
regional flow	13	$\Delta h/\Delta x$	-	3D	0.0001	0.0002	0.0000	0.0003	0.0005
multiple boils	14	*boil config.*	-	3D	A	B	1 boil	C	

Boil configuration A) 3 boils at 2 m distance from each other, Q_{boil} are 18, 10 and 2 $m^3 d^{-1}$
Boil configuration B) 3 boils at 2 m distance from each other, Q_{boil} are 14, 2 and 14 $m^3 d^{-1}$
Boil configuration C) 2 boils at 7 m distance from each other, Q_{boil} are 15 and 15 $m^3 d^{-1}$

The total domain of the 3D model was cut in half along the symmetry axis to reduce calculation times, leading to a domain size of 3000 m in length by 1500 m in width (Fig. 4.3). The boil was placed at the middle of the symmetry boundary so that the side boundaries were at least 1500 m from the boil. The symmetry boundary was considered as a no-flow boundary. Otherwise, the same boundary conditions were applied as for the axisymmetric model. Applying the same cell sizes for 3D models as adopted in the axisymmetric models resulted in extremely long calculation times (>20 days), and this restricted the cell sizes to larger than that used for the axisymmetric model. The model domain of 3000 m by 1500 m was therefore divided into 57 columns and 29 rows. A minimum cell width in the horizontal plane of 1 m was used near the boil, and this increased by a factor of 1.3 to a maximum cell width of 150 m. A thickness of 1 m was adopted for all 50 model layers.

Upconing cases

In total, 56 upconing cases were assessed in undertaking sensitivity analyses. A range of hydraulic and solute transport parameters, representing idealized conditions, typical of the field sites and Dutch deep polders more generally (Table 4.1), were adopted. Each upconing case differed from the reference case by modification of only one or two parameters. Parameters were modified

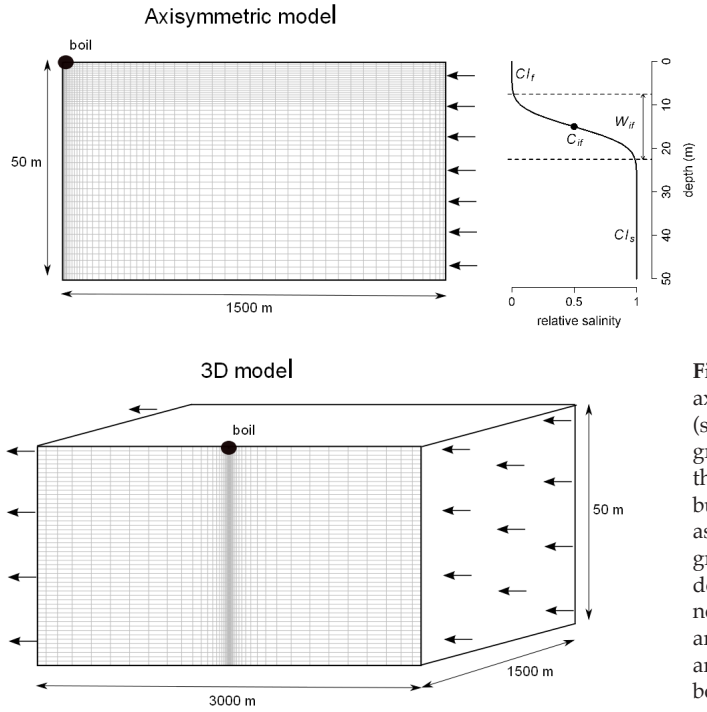

Fig. 4.3. General set up of the axisymmetric and 3D-models (situation with lateral regional groundwater flow is shown) and the aquifer salinity depth distribution adopted into the models as initial condition and applied to groundwater flowing into the model domain. All model boundaries are no-flow and no-mass flux boundaries except those indicated with arrows which are specified-head boundaries.

according to the following categories (Table 4.1): Q_{boil}, hydrogeological properties of the confined aquifer (K_h, K_v, K_h/K_v, D, n), dispersivity (α_L, α_T), aquifer salinity distribution (C_{if}, W_{if}, β), number of boils, and regional flow. Regional flow was introduced in 3D models by modifying the specified-head boundaries normal to the symmetry boundary to control the regional hydraulic gradient and by adopting no-flow conditions to the boundary opposite to the symmetry boundary (Fig. 4.3). Regional hydraulic gradients ranged from 0.0001 to 0.0005 (see Table 4.1). For the multiple boil cases, three different boil configurations (A, B and C, Table 4.1) were simulated. The boils were placed in a line at the symmetry boundary of the 3D model, in a corresponding manner to several field situations where multiple boils occur in or along straight ditches (De Louw *et al*., 2010). The total Q_{boil} in multiple boil simulations was equal to the single Q_{boil} of the reference case.

Model output analysis

The model output analysis involved different aspects of saltwater upconing, including boil salinity, distributions of drawdown and transition zone characteristics (C_{if} and W_{if}), and the sources of boil water. The results of the reference case were compared qualitatively with the field observations of sites A and B to verify that the conceptual model is a reasonable surrogate for typical boil-induced upconing below Dutch polders. Further, the reference case was compared to the results of a simulation without density effects, in which the salt acts as a conservative tracer, to evaluate the mixed convective processes associated with upconing mechanisms, and to explore differences in upconing that might otherwise occur in regions where aquifer salinity contrasts are lower or absent (e.g. in the Nieuwkoop Polder and parts of the Noordplas Polder, Haarlemmermeer Polder and Zuidplas Polder; Van Rees Vellinga *et al*., 1981).

Streamlines and travel times were calculated by 50 forward-tracking particles placed at 1400 m from the boil and equally distributed with depth, using the post-processing package MODPATH version 3 (Pollock, 1994). The vertical variation in groundwater flow rates was assessed to identify the respective depth-contribu-

tions to Q_{boil} thereby offering insights into the sources of boil water. For the axisymmetric and 3D models without regional flow, the contributing depths can be determined from the calculated horizontal flow rates away from the boil (>200 m), where vertical flow velocities are small compared to horizontal flow velocities. The contribution of different depths to Q_{boil} is given as CD_i, where CD_i is the fraction of the total discharge occurring across a depth interval i. Since CD_i represents the sources of boil water, the multiplication of CD_i with the regional aquifer salinity distribution (Cl_i) for an aquifer of thickness D should result in the boil salinity, as shown by the following:

$$boil\ salinity = \sum_{i=m}^{i=1} CD_i \,.\, Cl_i \qquad (4.1)$$

With m the number of layers of thickness D/m. Eq. (4.1) assumes steady-state conditions and neglects dispersion effects.

4.4 Results

4.4.1 Monitoring results

Fig. 4.4a and b shows the measured Q_{boil} and Cl concentrations for site A, during the period 20 April 2011-20 June 2012, which included a boil sealing attempt. Prior to the boil sealing attempt, boil 1 produced an average discharge of 16.5 $m^3\,d^{-1}$ and an average Cl concentration of 2.6 g L^{-1}. For the same period, the average discharge of boil 2 was only 0.7 $m^3\,d^{-1}$ and the average Cl concentration was lower, namely 0.9 g L^{-1}.

The in situ groundwater salinity was determined from ECPT measurements at site A. Fig. 4.4c shows the ECPT-based isochlors of Cl concentrations of 0.5 g L^{-1}, 1.0 g L^{-1}, and 2.5 g L^{-1} in cross section, together with the direct measurements of Cl in piezometers and of boil discharge (boil 1). Saltwater upconing towards the boil is clearly visible in the aquifer. At

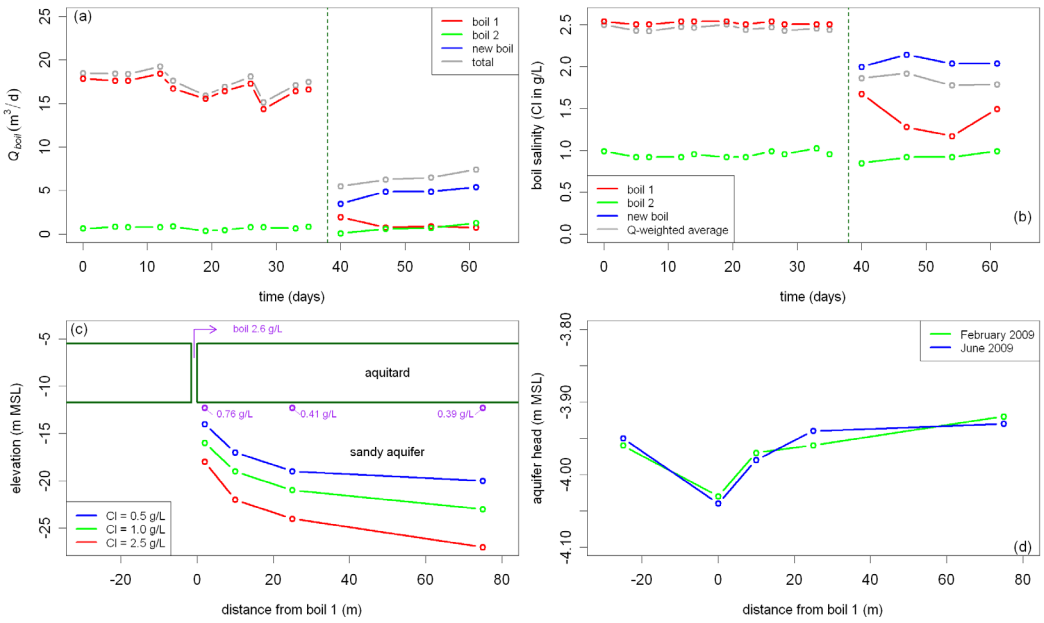

Fig. 4.4. Field measurements of boil site A. (a) Q_{boil} and (b) boil salinity with time; the boil sealing experiment is indicated by the dotted green lines, (c) isochlors of Cl concentration from ECPT measurements and groundwater Cl concentration (in purple), (d) equivalent freshwater aquifer heads.

75 m from the boil, a Cl concentration of 2.5 g L^{-1} is found at 15 m below the aquitard, whereas the same Cl concentration is found 2 m from the boil at 6 m below the aquitard. The 9 m difference in the 2.5 g L^{-1} isochlor is attributed to boil discharge effects. Groundwater Cl concentrations just below the aquitard were 0.39 g L^{-1} at 75 m, 0.41 g L^{-1} at 25 m and 0.76 g L^{-1} at 2 m from boil 1. The boil water Cl concentration was 2.6 g L^{-1}, which is more than three times the Cl concentration of groundwater just below the aquitard at only 2 m from the boil. This illustrates that the boil caused saltwater upconing in the form of steep salinity isochlors (Fig. 4.4c). At site B, the observed upconing was similarly localized and steep. Site B boil water had a Cl concentration of 1.1 g L^{-1}, and the groundwater in the upper aquifer at 2 m from the boil had a Cl concentration of 0.6 g L^{-1}.

Fig. 4.4d illustrates the decreasing trend (towards boil 1) in the equivalent freshwater heads. The head measured at 2 m from boil 1 was about 8 cm lower than at 25 m from the boil, and was about 11 cm lower than at 75 m from the boil. For site B, a similar decreasing trend in the aquifer hydraulic head towards the boil was observed, with a 10 cm lower head at 2 m than at 25 m from the boil. The heads at 25 m and 75 m from the boil were similar (within ± 2 cm). The observed decreasing trends in the aquifer hydraulic heads towards the boil areas of sites A and B are assumed to be the boils' drawdown cone.

Some noteworthy observations were made during the boil sealing experiment. First, the sudden cessation of groundwater discharge caused by sealing the boil 1 vent at site A caused a rapid increase in aquifer hydraulic head of 0.12 m at 2 m from the sealed boil. No

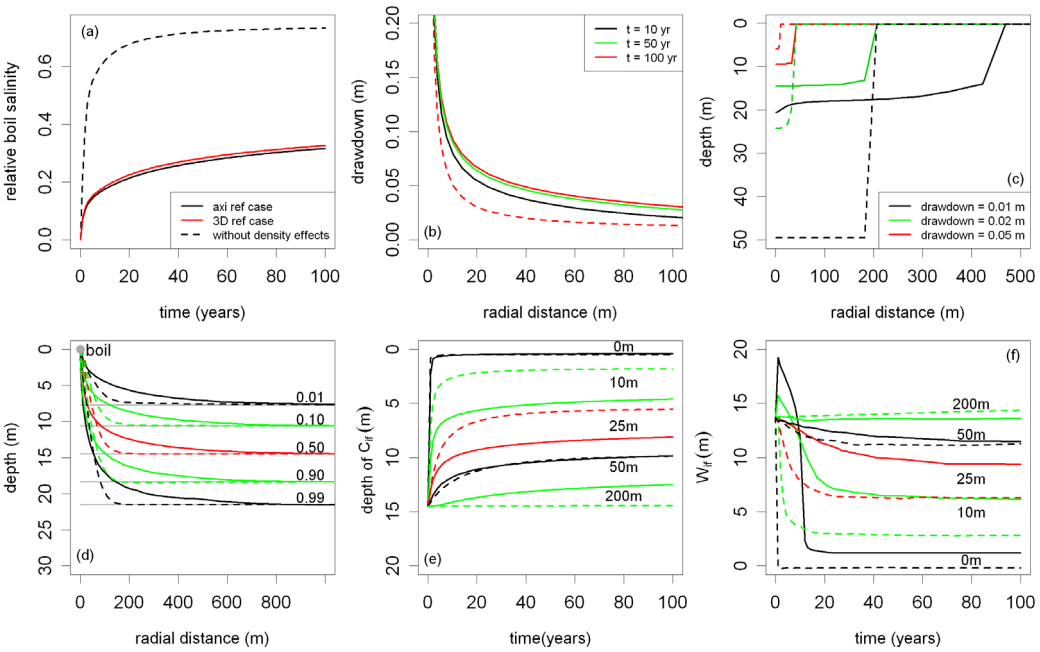

Fig. 4.5. Model results of axisymmetric reference case with density effects (full lines) and without density effects (dotted lines): (a) boil salinity with time, (b) freshwater head drawdown for different simulation times, (c) freshwater head drawdown contours (after 100 yr), (d) upconing of different relative salinity contours (after 100 yr); grey lines indicate the initial position of the salinity contours, (e) change of C_{if} and (f) W_{if} with time at different distance from the boil.

head increase was observed at the other piezometers at larger distances from the boil. Second, the discharge of boil 2 doubled as a result of the boil 1 sealing attempt and the associated increased aquifer hydraulic head. Third, by sealing off both boils 1 and 2, a new boil developed at the surface at 4 m distance from boil 2 with a discharge of about 5 m^3 d^{-1} and a Cl concentration of about 2 g L^{-1} (Fig. 4.4a and b).

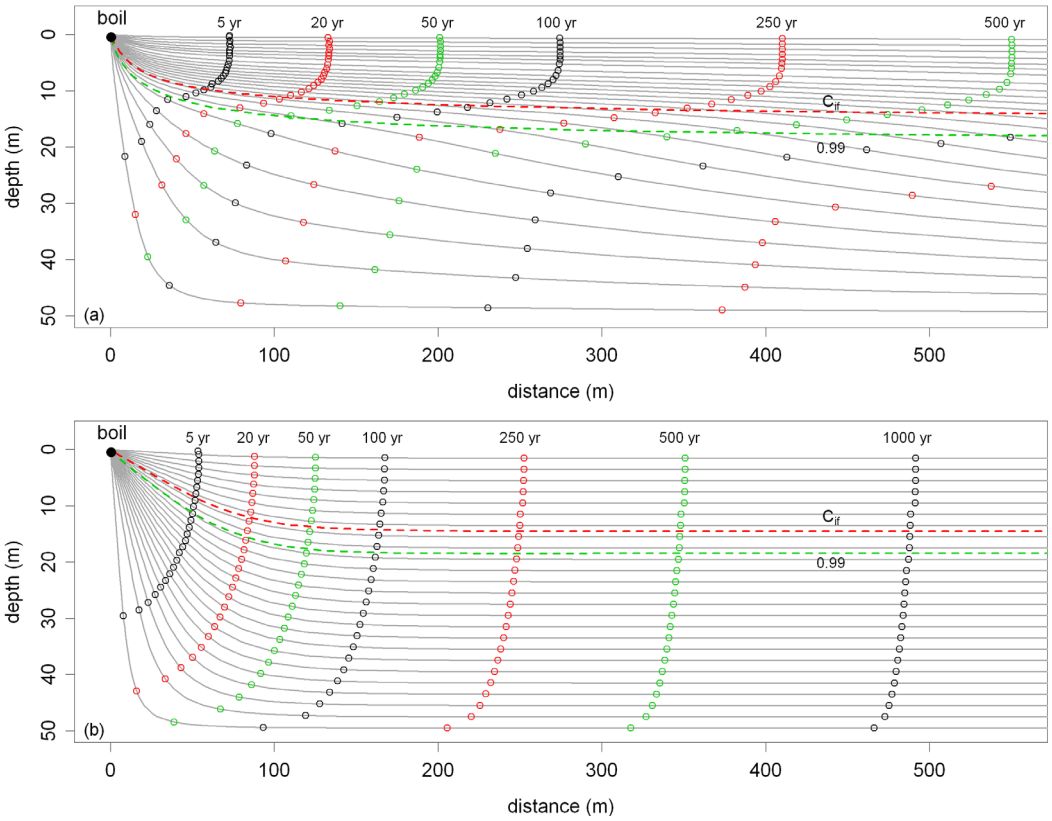

Fig. 4.6. Streamlines towards the boil with travel times to the boil (in yr) for the reference case (a) with density effects and (b) without density effects. The relative salinity contours of 0.50 (C_{if}) and 0.99 (bottom transition zone) are indicated as well. The forward calculated streamlines are based on the flow velocity field after a simulation time of 100 yr. The coloured points at the streamlines indicate the travel time to the boil.

4.4.2 Reference case modeling

The simulation results of the axisymmetric reference case are shown in Fig. 4.5 as solid lines. The boil water salinity increased sharply to $0.20Cl_s$ in the first 15 years, and then increased gradually to $0.32Cl_s$ by 100 years, when it still did not reach a steady-state condition (Fig. 4.5a). Similarly, the aquifer hydraulic head drawdown (Fig. 4.5b) and the groundwater salinity distribution (characterized by C_{if} and W_{if}; Fig. 4.5e and f), did not reach steady state after 100 years. The drawdown at the top of the aquifer rapidly decreased with distance (Fig. 4.5b and c) and with depth (Fig. 4.5c). The drawdown was 0.95 m at the boil vent, 0.20 m at 2 m from the boil and 0.05 m at 39 m from the boil. Fig. 4.5d and f shows that W_{if} decreased towards the boil. This is caused by the convergence of streamlines as shown in Fig. 4.6a. The stream-

line and travel time distributions showed that groundwater flows faster above than below C_{if} (Fig. 4.6a). The contributing depth distribution (given by CD_i) showed an inverse relationship with the aquifer salinity distribution (Fig. 4.7a). That is, the boil extracted more low-salinity groundwater per m aquifer from above C_{if} than high-salinity groundwater from below C_{if}. The fraction of Q_{boil} originating from above C_{if} is referred to here as the shallow contribution (CD_{sh}), which was 0.72 for the reference case.

The differences between the results of the axisymmetric and 3D forms of the reference case model were small. The boil salinity breakthrough curve of the 3D reference model is plotted in Fig. 4.5a, showing slightly higher (i.e. by 3% after 100 years) boil salinity than the axisymmetric reference case. For all other aspects of upconing shown in Fig. 4.5 (drawdown, upconing of salinity contours, C_{if} and W_{if}), the 3D model produced similar (< 1% error) results to the axisymmetric model, and these are therefore not shown in Fig. 4.5b-f.

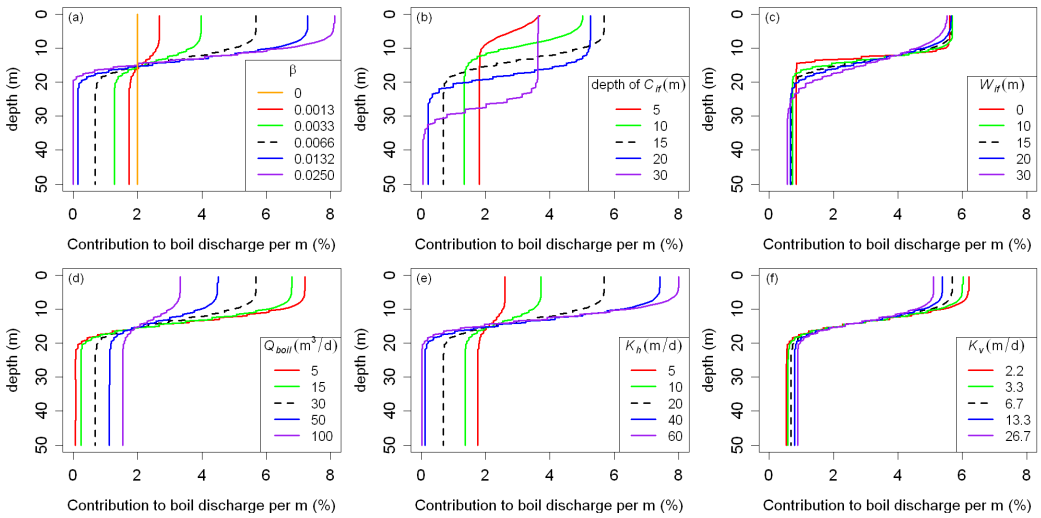

Fig. 4.7. Contributing depth distribution (at T=100 yr) for various upconing cases defined in Table 4.1: (a) β, (b) depth of C_{if}; (c) W_{if}; (d) Q_{boil}; (e) K_h, (f) K_v. The colored lines refer to the different upconing cases listed Table 4.1 and the black dotted lines show the reference case.

4.4.3 Axisymmetric upconing scenarios

Axisymmetric upconing scenarios allowed for the assessment of several factors influencing boil-induced upconing, such as: boil discharge, the regional aquifer salinity (density) distribution (i.e. the specified salinity profile at model boundaries), aquifer properties such as K_h, K_v, D, n and dispersivity. Model results after 100 years are summarized in Tables 4.2, 4.3 and 4.4.

Q_{boil} had a major impact on all aspects of saltwater upconing (Tables 4.2-4). A low discharge rate of 5 m^3 d^{-1} caused a small drawdown cone (drawdown of 0.05 m at 2 m from the boil and at 1.2 m depth; Table 4.2, case 1a). In this case, about 90% of the boil water came from above the C_{if} resulting in a boil salinity of $0.05Cl_s$ (Table 4.4). With a high Q_{boil} of 100 m^3 d^{-1} (case 1d), some 60% of the boil water came from below the C_{if}, leading to a boil salinity of $0.63Cl_s$. Thus, higher discharge rates resulted in more boil water coming from below the C_{if}, and therefore higher boil salinities (Fig. 4.8), as expected (Reilly and Goodman, 1987; Ma *et al.*, 1997).

Table 4.2. Model results of the different upconing cases defined in Table 4.1, showing the distance from the boil and depth below the boil of the 0.05 m drawdown contour after 100 yr of simulation.

			Distance of 0.05 m drawdown (m)					Depth of 0.05 m drawdown (m)				
Category	nr	Parameter	a	b	Ref	c	d	a	b	Ref	c	d
boil discharge	1	Q_{boil}	2	11	39	73	165	1	6	9	12	29
	2	K_h, K_v	177	73	39	12	6	50	14	9	6	3
	3	$K_h, K_v = c$	159	73	39	15	9	50	14	9	6	3
hydrogeology	4	$K_v, K_h = c$	49	45	39	33	28	9	9	9	10	10
	5	D	44	41	39	37	36	10	10	9	9	9
	6	n	41	40	39	38	38	9	9	9	9	9
	7	α_L, α_T	39	39	39	38	38	9	9	9	9	9
dispersivity	8	$\alpha_L, \alpha_T = c$	39	39	39	39	39	9	9	9	9	9
	9	$\alpha_T, \alpha_L = c$	39	38	39	39	39	9	9	9	9	9
Aquifer salinity distribution	10	C_{if}	19	31	39	31	17	6	7	9	11	10
	11	W_{if}	38	39	39	38	36	9	10	9	9	10
	12	β	14	21	39	66	97	7	8	9	10	11
regional flow	13	$\Delta h/\Delta x$	42	40	39	38	35	10	10	9	10	10
multiple boils	14		38	39	39	39		9	9	9	9	

c = constant

Table 4.3. Model results of the different upconing cases defined in Table 4.1, showing the centre depth (C_{if}) and width (W_{if}) of the interface at 25 m from the boil after 100 yr of simulation.

			C_{if} (m below top aquifer)					W_{if} (m)				
Category	nr	Parameter	a	b	Ref	c	d	a	b	Ref	c	d
boil discharge	1	Q_{boil}	13	9	7	6	5	16	16	9	7	7
	2	K_h, K_v	5	7	7	9	10	7	8	9	16	17
	3	$K_h, K_v = c$	7	7	7	8	9	9	8	9	17	18
hydrogeology	4	$K_v, K_h = c$	6	7	7	8	8	8	8	9	9	9
	5	D	8	8	7	7	7	10	9	9	8	8
	6	n	7	7	7	7	7	8	8	9	9	9
	7	α_L, α_T	7	7	7	8	8	7	8	9	15	26
dispersivity	8	$\alpha_L, \alpha_T = c$	7	7	7	7	7	9	9	9	9	9
	9	$\alpha_T, \alpha_L = c$	8	7	7	7	7	25	10	9	7	7
Aquifer salinity distribution	10	C_{if}	2	4	7	12	26	7	8	9	17	24
	11	W_{if}	7	7	7	7	7	5	7	9	11	17
	12	β	5	6	7	9	11	7	7	9	16	17
regional flow	13	$\Delta h/\Delta x$	8	8	7	9	10	12	16	9	19	25
multiple boils	14		8	7	7	7		8	8	9	8	

c = constant

The regional aquifer salinity distribution, characterized by C_{if}, W_{if} and β, had also a major impact on all aspects of upconing (Tables 4.2-4). Upconing was most sensitive to changes in β and C_{if}, whereas W_{if} was of lesser importance

(Fig. 4.8). The significance of the regional aquifer salinity (or density) distribution is clearest in the contributing depth distributions, which show a similar but opposite form to the regional aquifer salinity distribution (Fig. 4.7a-c). As expected, a deeper C_{if} resulted in a larger CD_{sh}, resulting in lower boil salinities (Table 4.4; cases 10a-d). Fig. 4.7a clearly shows that the contributing depth distribution was modified significantly by density effects; a larger β led to a higher CD_{sh} which resulted in lower relative boil salinities (Table 4.4; cases 12a-d). This illustrates the stabilizing effect of the denser saltwater on upconing, as expected (e.g. Dagan and Bear, 1968; Reilly and Goodman, 1987; Jakovovic *et al*., 2011). Neglecting density variations in the aquifer and presuming that salt acts merely as a conservative tracer, resulted in the lowest CD_{sh} (0.30) and the highest relative boil salinity ($0.73Cl_s$) of all simulated cases (except case 10a). In contrast to the density-dependent simulated cases, the density-independent simulation show that travel times were almost equally distributed over depth (Fig. 4.6a) and boil water came from all depths in virtually equal amounts (Fig. 4.7a). Both the drawdown and saltwater cone were steeper and more localized (i.e. smaller lateral extent) without density effects (Fig. 4.5c and d). The density-independent simulation reached steady-state conditions more rapidly, i.e. drawdowns stabilized within 1 year and both boil salinity and the salinity distribution in the aquifer remained constant after 73 years.

K_h had a large impact on all aspects of the natural saltwater upconing mechanism. Larger K_h led to smaller drawdown and saltwater cones, both in height and lateral extent, and lower boil salinities due to larger contributions of shallow, fresher groundwater (Tables 4.2-4). The effect of K_h is clearly visible in the contributing depth distribution (Fig. 4.7e). Effects of K_v were much smaller but opposite to the effect of K_h concerning contributing depths (Fig. 4.7f) and boil salinity (Fig. 4.8). The difference in effects of K_h and K_v consequently means that changing

Table 4.4. Model results of the different upconing cases defined in Table 4.1, showing the relative boil salinity and the shallow contribution *(CD_{sh})* after 100 yr of simulation.

			Relative boil salinity					Shallow contribution, CD_{sh} (fraction)				
Category	nr	Parameter	a	b	Ref	c	d	a	b	Ref	c	d
boil discharge	1	Q_{boil}	0.05	0.12	0.32	0.41	0.63	0.93	0.88	0.73	0.59	0.45
	2	K_h, K_v	0.59	0.51	0.32	0.13	0.10	0.41	0.51	0.73	0.92	0.96
	3	$K_h, K_v = c$	0.66	0.51	0.32	0.13	0.09	0.38	0.51	0.73	0.93	0.97
hydrogeology	4	$K_v, K_h = c$	0.23	0.25	0.32	0.36	0.44	0.79	0.77	0.73	0.70	0.67
	5	D	0.26	0.29	0.32	0.32	0.32	0.77	0.74	0.73	0.71	0.71
	6	n	0.37	0.31	0.32	0.32	0.32	0.74	0.74	0.73	0.73	0.73
	7	α_L, α_T	0.30	0.31	0.32	0.35	0.42	0.75	0.74	0.73	0.70	0.66
dispersivity	8	$\alpha_L, \alpha_T = c$	0.32	0.32	0.32	0.33	0.35	0.73	0.73	0.73	0.73	0.73
	9	$\alpha_T, \alpha_L = c$	0.38	0.36	0.32	0.31	0.31	0.67	0.72	0.73	0.74	0.74
Aquifer salinity distribution	10	C_{if}	0.90	0.66	0.32	0.09	0.02	0.17	0.44	0.73	0.92	0.98
	11	W_{if}	0.29	0.30	0.32	0.37	0.37	0.71	0.74	0.73	0.73	0.71
	12	β	0.67	0.53	0.32	0.13	0.08	0.39	0.54	0.73	0.92	0.98
regional flow	13	$\Delta h/\Delta x$	0.32	0.31	0.33	0.29	0.27	0.72	0.73	0.70	0.73	0.74
multiple boils	14		0.31^{dw}	0.31^{dw}	0.33	0.30^{dw}		0.70	0.70	0.70	0.71	

c = constant; dw = discharge weighted average

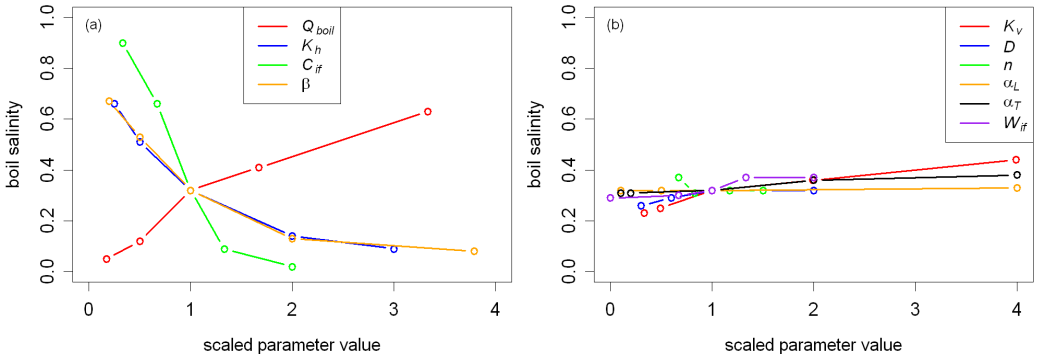

Fig. 4.8. Spider diagrams of relative boil salinity versus scaled parameter value (relative to the parameter value of the reference case) for the different axisymmetric cases listed in Table 4.1. Diagram (a) shows the parameters that had a large impact on boil salinity compared to the parameters shown in diagram (b).

the hydraulic conductivity anisotropy factor, K_h / K_v, of the aquifer did not have a consistent effect on saltwater upconing. Namely, increasing the anisotropy factor by increasing K_h had a much more pronounced effect than by decreasing K_v. The difference in effect between K_h and K_v on pumping water salinity was also found through numerical simulations by Ma *et al*. (1997). D had a relatively minor effect on upconing processes. That is, boil salinities were virtually the same ($0.32Cl_s$) for D values of 50, 75 and 100 m, but noticeably lower for D values smaller than the reference case, i.e. $0.29Cl_s$ for $D = 35$ m and $0.26Cl_s$ for $D = 25$ m (Fig. 4.8).

The longitudinal (α_L) and transverse dispersivity (α_T) did not have a significant effect on drawdown (Table 4.2). In agreement with others (e.g. Reilly and Goodman, 1987; Zhou *et al*., 2005), α_T affected W_{if}, whereas the impact of α_L was negligible (Table 4.3). Larger values of α_T than those used for the reference case resulted in thicker W_{if}, smaller CD_{sh}, and higher boil salinities (Tables 4.3 and 4.4).

4.4.4 3D upconing scenarios

Fig. 4.9 shows results of the 3D simulations of multiple boil cases for three different boil configurations. The calculated salinities of neighbouring boils in a boil cluster varied over a wide range for configuration A and B (Fig. 4.9). For example, the boil salinities after 100 years of the three boils of configuration A were $0.03Cl_s$, $0.23Cl_s$ and $0.37Cl_s$ (Fig. 4.9). Interestingly, the highest boil salinity ($0.49Cl_s$ after 100 years) was simulated for the boil with the smallest discharge (2 m^3 d^{-1}) (i.e. configuration B in Fig. 4.9). This boil was positioned between two high-flow boils, which enhanced saltwater upconing to the middle, low-flow boil because the inflow of shallower and fresher groundwater was impeded. The results also showed that extracting the same amount of groundwater but over a larger area led to slightly wider saltwater cones being formed below the boils (Fig. 4.9). Despite the large differences in boil salinities within a boil configuration, the total salt load was similar for all cases. The largest total Cl load of 49 kg d^{-1} was calculated for the single-boil case, and the smallest Cl load of 45 kg d^{-1} was obtained for configuration C (Fig. 4.9).

Applying a regional groundwater flow component had a large impact on the groundwater flow pattern (Fig. 4.10). The streamlines illustrated in Fig. 4.10 show

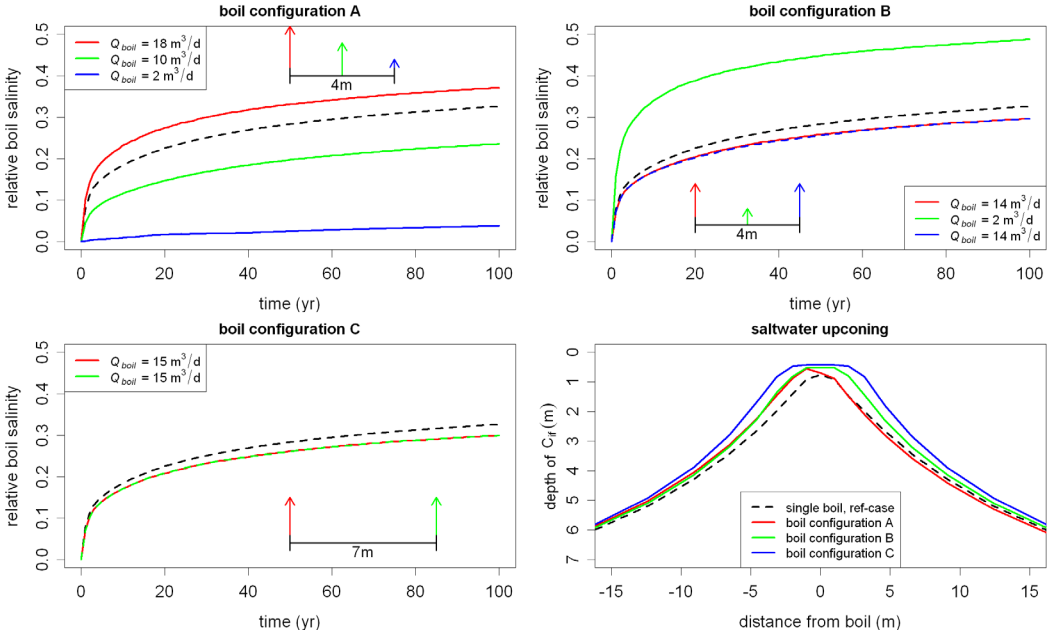

Fig. 4.9. Boil salinity with time and the saltwater upconing for different boil configurations (A-C). Each boil configuration consists of 2 or 3 boils with different discharges with a total discharge equal to the reference case (Q_{boil} = 30 m^3 d^{-1}). The configuration is indicated with colored arrows. The results of the reference case are indicated by a black dotted line.

that sources of boil water are considerably shallower in the presence of a regional gradient typical for Dutch polders. For example, for the case with the smallest regional hydraulic gradient (0.0001; case 13a), the deepest streamline that ended in the boil came from 39 m depth (Fig. 4.10a and b), whereas for cases without regional flow, the whole aquifer (50 m) contributed to Q_{boil} (Figs. 4.6-7). This streamline divided groundwater flow into a local system with groundwater flow towards the boil and a regional system with groundwater flow bypassing the boil, and is referred to hereafter as the dividing streamline. The dividing streamlines of all four regional flow cases are shown in Fig. 4.10c, which shows that a larger regional flow component resulted in a shallower position of the dividing streamline. Surprisingly, regional flow had only small impacts on boil salinity, despite significant changes in the groundwater flow patterns. The largest increase in regional flow (gradient change from 0 to 0.0005) caused a slight decrease in boil salinity from 0.32Cl_s to 0.27Cl_s (Table 4.4, cases 13a-d).

4.5 Discussion

4.5.1 Comparison of field and modeling results

Several aspects of the field situation were simplified or neglected in the numerical model. For example, characteristics such as the salinity distribution across the entire aquifer thickness, the time since boil development, and regional flow rates were largely unknown for the field situation. Despite this, simulated saltwater

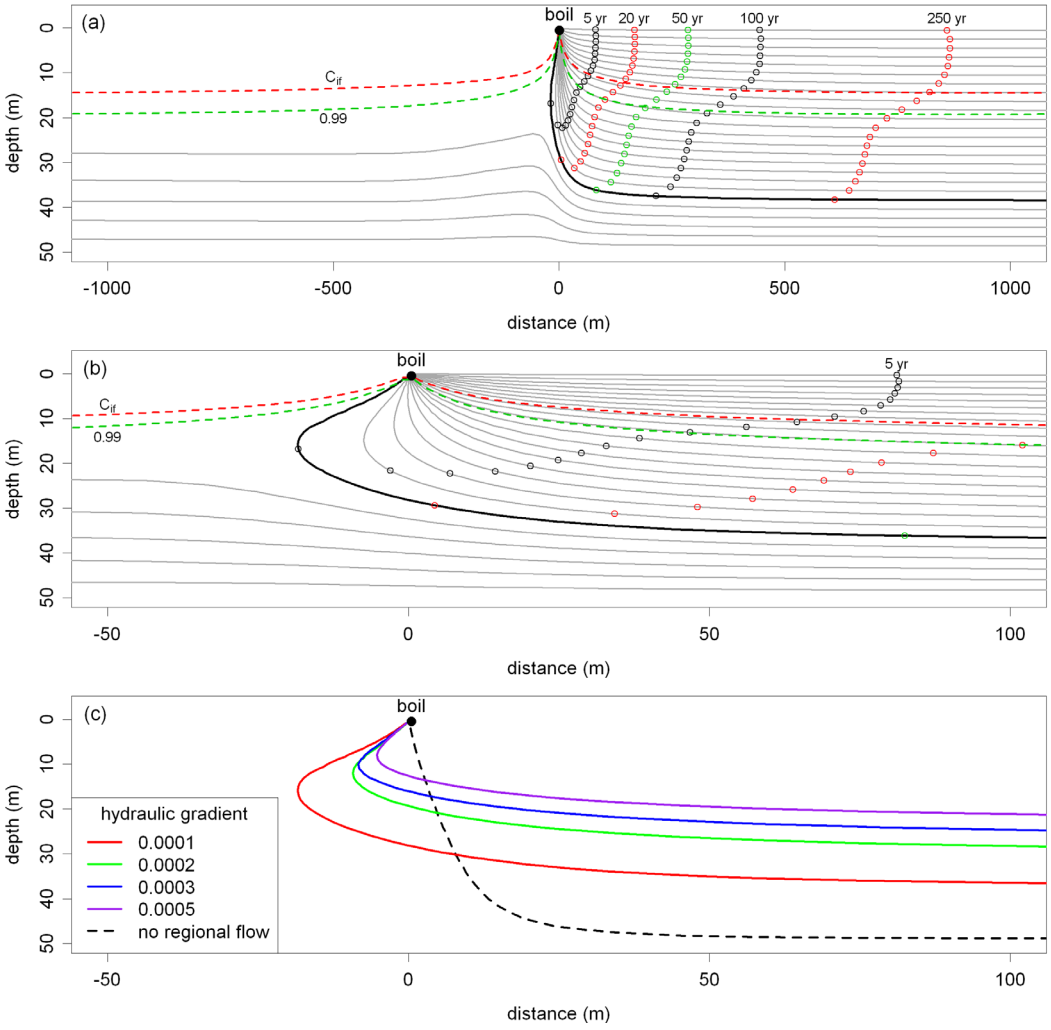

Fig. 4.10. (a) Streamlines towards the boil with travel times to the boil (in yr) for the case with regional flow (hydraulic gradient = 0.0001). The coloured points at the streamlines indicate the travel time to the boil. The relative salinity contours of 0.50 (C_{if}) and 0.99 (bottom transition zone) are indicated as well. (b) Same as Fig. 4.10a but zoomed in. (c) Dividing streamlines for the regional flow cases with different hydraulic gradients and the reference case without regional flow.

upconing and drawdown were largely consistent with the scale of observed values at sites A and B. That is, the model calculated a 9 cm lower head at 2 m than at 75 m from the boil for case 1b (with a Q_{boil} of 15 $m^3\ d^{-1}$; observed Q_{boil} of site A was 17 $m^3\ d^{-1}$), which is of similar magnitude to the observed head difference (11 cm) over the same distance at field site A (Fig. 4.4d). The simulated position of the $0.5Cl_s$ isochlor (8 m deeper at 75 m than at 2 m from the boil) largely corresponds with the field situation (2.5 g L^{-1} isochlor was 9 m deeper at 75 m than at 2 m from the boil; Fig. 4.4c).

The small-scale spatial variations in boil salinity within a small area of clustered boils observed at site A were similar to those obtained from the 3D numerical model. Modeling scenarios showed that salinity variations between clustered boils are determined by the combination of

the discharge and position of individual boils within a boil area. However, the total combined discharge of the boil cluster is the principal factor that controls both saltwater upconing and total salt loads. As such, boil clusters such as those considered here can be reasonably represented as one point sink if the primary concerns are large-scale upconing and boil contributions to surface water salinization.

The differences in observed boil salinities at site A (Fig. 4.4b) indicate that the boils are probably not interconnected within the aquitard in the manner illustrated in Fig. 4.1, but rather, it is more likely that they have their own source vents. The development of new boils when boils 1 and 2 were blocked during the sealing experiment implies that new cracks developed in the aquitard or existing cracks within the aquitard were regenerated. The development of new boils indicates that boil sealing is not a feasible measure to abate salinization at these particular sites.

4.5.2 Sources of boil water

The numerical simulations showed that boil water is a mixture of groundwater from different depths (quantified by CD_i) with different salinities. Mixing is enhanced near the boil where streamlines from different depths and with different salinities converge. To test if CD_i was a valid model output parameter representing the sources (depths) of boil water, the boil salinity after 100 years was calculated with Eq. (4.1) for all axisymmetric upconing cases listed in Table 4.1 and compared with the simulated boil salinity. Fig. 4.11 shows that the boil salinity calculated with Eq. (4.1) correlates well ($R^2 = 0.96$) with the simulated boil salinity and that CD_i is indeed a good representative for the sources of boil water. The slightly overestimation in calculated values is probably caused by boil salinities not reaching steady state after 100 years (Fig. 4.5a).

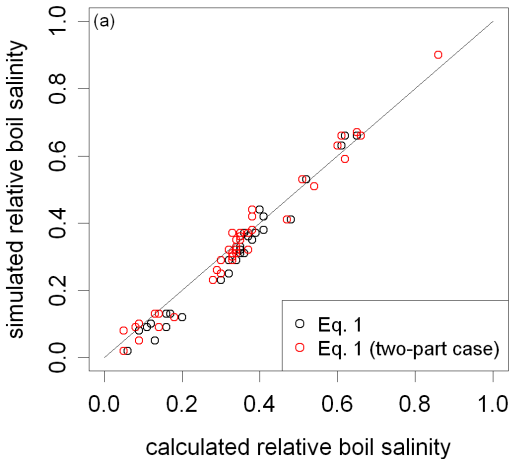

Fig. 4.11. Scatter diagram of the calculated boil salinity using Eq. (4.1) and simplified Eq. (4.1) (two-part case) versus the simulated boil salinity. The data is derived from the model results of all axisymmetric upconing cases listed in Table 4.1.

Boil salinity was also calculated with a simplified form of Eq. (4.1) where $m = 2$, and $i = 1$ and $i = 2$ refer to the part of the aquifer above and below C_{ij}, respectively. Fig. 4.11 shows that the boil salinity calculated using the simplified two-part form of Eq. (4.1) correlated well with both the boil salinity predicted with the numerical model and the calculated boil salinity using Eq. (4.1). This confirms that for aquifer salinity distributions with a symmetric transition zone, CD_i is reasonably simplified to one parameter, which is CD_{sh}. Note that in cases without density effects, CD_i is equally distributed within the aquifer and the boil water solute concentration in steady state is simply the average solute concentration in the aquifer. By doing so for the reference case without density effects, a boil salinity of $0.71Cl_s$ is obtained, which is slightly less than the boil salinity of $0.73Cl_s$ predicted by the numerical model.

4.5.3 Effect of aquifer salinity distribution

There is significant variability in the regional aquifer salinity distributions below Dutch deep polders (Van Rees Vellinga *et al*., 1981; Oude Essink *et al*., 2010) showing ranges of C_{if}, W_{if} and β according to the ranges used for the axisymmetric simulations (Table 4.1). The model results showed that C_{if} and β had a major impact on both CD_{sh} and boil salinity (Fig. 4.8). Hence, the spatial variations in C_{if} and β in Dutch aquifers are probably important factors causing differences in the salinities of boils in Dutch polders. Variations in K_h and Q_{boil} are also likely to cause differences in boil salinities in Dutch polders, with other parameters (K_v, D, n, α_L, α_T, W_{if}) showing reduced sensitivity (Fig. 4.8).

In Dutch aquifers with uniform profiles of density, CD_i and the steady-state boil solute concentration are independent of Q_{boil}, K_h, K_v, D and n, which influence more so travel times and the time required to reach steady state. In contrast, by adding density differences, CD_i and therefore boil salinity depend on many factors (Q_{boil}, K_h, K_v, D, n, α_L, α_T, C_{if}, W_{if} and β). The density distribution in an aquifer determines in what magnitude these factors influence upconing. Even with small density differences (e.g. β = 0.0013, case 12a), density effects cannot be neglected as they still significantly influence CD_{sh} (0.39 for β = 0.0013; 0.30 for β = 0) and boil salinity ($0.67Cl_s$ for β = 0.0013; $0.73Cl_s$ for β = 0). Fig. 4.8 shows that β had more impact on boil salinity in the range of small β, which apply for Dutch aquifers below deep polders, than in the range of large β.

Field measurements from this study and by De Louw *et al*. (2010) and Goudriaan *et al*. (2011) showed that despite the small discharges, almost all boils discharge water with elevated Cl concentrations of up to 5 g L^{-1}. This observation is consistent with the results of numerical simulations and can be explained by the general shallow position of C_{if} (15-40 m below the aquitard) in combination with relatively small β (Cl_s ranges from 15% to 40% seawater) in the study area. These conditions resulted in significant contributions of saline groundwater below C_{if}.

4.5.4 Effect of regional flow

The 3D numerical simulations showed that regional lateral flow divides the aquifer into two flow systems; the local boil system on top of the regional flow system. Consequently, boil water comes from shallower depth (i.e. from above the dividing streamline) compared to the situation without regional flow (i.e. from the entire aquifer). Despite this, CD_{sh} and thus boil salinity were barely influenced by the regional flow component. This follows from the fact that regional flow reduces the effective aquifer thickness for the local flow to the boil, bordered by the dividing streamline. And in addition, the axisymmetric results showed that CD_{sh} are barely influenced by aquifer thickness as long as the entire transition zone is completely within the aquifer (Table 4.4, cases 5a-d). The results imply that boil salinity is not influenced by the position of the boil in the deep polder with respect to the magnitude of regional flow. Regional flow is therefore not an important factor that explains the spatial variability of boil salinities found in the Dutch deep polders.

In most coastal aquifers, regional flow is present to some extent and this is not taken into account in most detailed saltwater upconing models (e.g. Reilly and Goodman, 1987; Ma *et al*., 1997; Zhou *et al*., 2005), probably due to large calculation times. Bear *et al*. (2001) incorporated regional flow in their numerical upconing model but only mentioned the asymmetry of the saltwater cone as an effect of regional

flow. Regional flow will significantly affect pumping water salinity when a part of the transition zone or the entire transition zone is found below the dividing streamline. Regarding this positive effect that regional flow could potentially have on saltwater upconing and therefore on pumping well salinities as well, leaving out the regional flow component can be seen as a worst case scenario.

4.6 Conclusions

In this study, natural saltwater upconing by the preferential groundwater discharge through boils, identified previously as a key process in the salinization of Dutch deep polders, was investigated using field measurements and numerical simulations of simplified situations. For the first time, groundwater salinity distributions attributable to specific boils or boil clusters were measured. The field measurements showed local and steep upconing due to the preferential groundwater discharge of boils. Upconing in numerical models, albeit for idealized situations, showed similar characteristics to field situations.

The numerical results indicated that boil water in Dutch polders comprises mixtures of groundwater from a wide range of depths and salinities. All simulated cases showed a depth-contribution to boil discharge that had a form opposite to the salinity distribution in the aquifer, which illustrates the importance that the salinity (and therefore density) distribution has on saltwater upconing mechanisms. A uniform contribution to boil discharge was produced in simulations with uniform vertical salinity profiles. For aquifers with symmetric transition zones, the contributing depth distribution was well characterized by a two-part model involving only the shallow and deep contribution to boil discharge, defined as the portions of boil water coming from above and from below the centre depth of the transition zone, respectively. Regional lateral flow below Dutch polders impacted the flow patterns significantly by dividing the groundwater flow system into a local boil system overlying the regional flow system. Despite this, regional flow had only a minor effect on the shallow and deep contributions and thus on boil salinity as well.

The most important factors controlling the shallow and deep contribution and therefore boil salinities in Dutch deep polders are boil discharge, the horizontal hydraulic conductivity of the aquifer, the depth of the transition zone and the density difference between groundwater above and below the transition zone. The fact that boils in Dutch polders discharge saline groundwater under relatively low discharge conditions can be explained by the shallow position of the transition zone in combination with relatively small density differences within the aquifer. These conditions result in significant contributions of saline groundwater, from below the transition zone, to boil discharge. The observed spatial variation in boil salinities is probably the result of a combination of variations in boil discharge and the spatial variation of aquifer salinity distributions and the horizontal hydraulic conductivity of the aquifer. Additionally, within a small area of clustered boils, boil salinity varies between individual boils and is determined by the combination of its discharge and its position within the boil area (i.e. relative to neighbouring boils), whereas the total discharge of boil clusters is the principal factor that controls natural saltwater upconing and total salt loads. The width of the transition zone, aquifer thickness, porosity, dispersivity and the vertical hydraulic conductivity did not have major effects on the natural saltwater upconing mechanism by boils.

Part II

Rainwater lenses in areas with saline seepage

Chapter 5

Shallow rainwater lenses in deltaic areas with saline seepage

Perry de Louw, Sara Eeman, Bernard Siemon, Bernard Voortman, Jan Gunnink, Esther van Baaren, Gualbert Oude Essink

Published in Hydrology and Earth System Sciences 15, 3659-3678, 2011

Abstract

In deltaic areas with saline seepage, freshwater availability is often limited to shallow rainwater lenses lying on top of saline groundwater. Here we describe the characteristics and spatial variability of such lenses in areas with saline seepage and the mechanisms that control their occurrence and size. Our findings are based on different types of field measurements and detailed numerical groundwater models applied in the south-western delta of the Netherlands. By combining the applied techniques we could extrapolate measurements at point scale (groundwater sampling, temperature and electrical soil conductivity (TEC)-probe measurements, electrical cone penetration tests (ECPT) to field scale (continuous vertical electrical soundings (CVES), electromagnetic survey with EM31), and even to regional scale using helicopter-borne electromagnetic measurements (HEM). The measurements show a gradual mixing zone between infiltrating fresh rainwater and upward flowing saline groundwater. The mixing zone is best characterized by the depth of the centre of the mixing zone D_{mix}, where the salinity is half that of seepage water, and the bottom of the mixing zone B_{mix}, with a salinity equal to that of the seepage water (Cl-conc. 10 to 16 g L^{-1}). D_{mix} is found at very shallow depth in the confining top layer, on average at 1.7 m below ground level (BGL), while B_{mix} lies about 2.5 m BGL The model results show that the constantly alternating upward and downward flow at low velocities in the confining layer is the main mechanism of mixing between rainwater and saline seepage and determines the position and extent of the mixing zone (D_{mix} and B_{mix}). Recharge, seepage flux, and drainage depth are the controlling factors.

5.1 Introduction

In many deltaic areas, the groundwater is saline because of seawater intrusion and marine transgressions (Custodio and Bruggeman, 1987; Stuyfzand and Stuurman, 1994; Weert *et al*., 2009, Post and Abarca, 2010). In areas that lie below mean sea level (MSL) saline groundwater may reach the surface by upward groundwater flow, which we define here as seepage. This leads to salinization of surface waters and shallow fresh groundwater bodies and makes the water unfit for irrigation, drinking water supply or industrial purposes (e.g. Van Rees Veilinga *et al*., 1981; Van den Eertwegh *et al*., 2006; Giambastiani *et al*., 2007; De Louw *et al*., 2010, 2011). A future rise in sea level is expected to increase the seepage and salt loads to surface waters and reduce the availability of both fresh surface water and groundwater (e.g. Meisler *et al*., 1984; Navoy, 1991; Oude Essink, 1996; Van der Meij and Minnema, 1999; Vandenbohede *et al*., 2008). Model simulations show that salt loads from groundwater seepage in several low-lying parts of the coastal zone of the Netherlands will be doubled due to sea level rise by 2100 A.D. (Oude Essink *et al*., 2010).

In contrast to the salt loading process to surface waters by saline groundwater seepage, little attention has so far been given to the interaction of upward flowing saline groundwater with infiltrating rainwater in the topsoil, as illustrated in Fig. 5.1. The upward movement of saline groundwater prevents rainwater from infiltrating to greater depths, resulting in shallow rainwater lenses (Fig. 5.1). Under certain conditions the rainwater lens may become so small, or even disappear, that saline groundwater may reach the root zone via capillary rise, affecting crop growth (Katerji *et al*., 2003; Flowers, 2004; Steppuhn *et al*., 2005; Rozema and Flowers, 2008) and natural vegetation (Jolly *et al*., 2008; Antonellini and Mollema, 2009). Shallow rainwater lenses in areas with saline seepage are very vulnerable to climate change (changing precipitation surpluses) and to a rising sea level (enhancing seepage) as shown by Maas (2007).

Here we focus on the occurrence of shallow rainwater lenses in areas with saline seepage and the processes involved. So far, research into fresh rainwater lenses in saline groundwater has mainly been focused on so-called Badon Ghijben-Herzberg (BGH) freshwater lenses in elevated areas like sandy dunes along the coast and on small islands that lack an upward groundwater flow (e.g. Drabbe and Badon Ghijben, 1889; Herzberg, 1901; Fetter, 1972; Van Dam and Sikkema, 1982; Meinardi, 1983; Underwood *et al*., 1992; Collins and Easley, 1999; Bakker, 2000). BGH-lenses are generally thick and the depth of the freshwater-saline interface (H) is mainly controlled by the relative density difference (β) and the water table (h): $H=h/\beta$.

Some analytical and numerical steady-state approaches to modeling rainwater lenses under conditions of upward groundwater seepage have been described (Schot *et al*., 2004; Maas, 2007; Eeman *et*

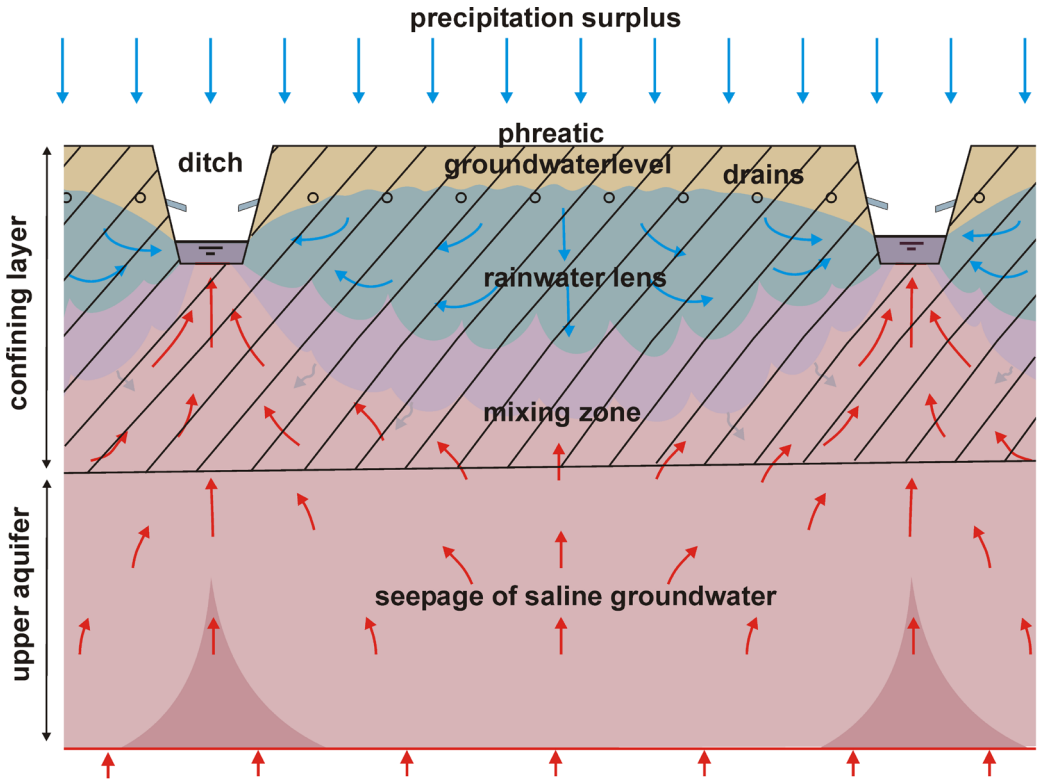

Fig. 5.1. Conceptual visualisation of a shallow rainwater lens on top of saline groundwater seepage.

al., 2011). Eeman *et al*. (2011) investigated the parameter groups that dominate the mixing processes for physically feasible ranges of parameters, using the analytical approach by Maas (2007) and the numerical transport code SUTRA (Voss and Provost, 2008). Schot *et al*. (2004) used a numerical model to simulate the development of rainwater lenses in fens under fresh groundwater seepage conditions. So far, theoretical models for shallow fresh rainwater lenses have not been based on actual observations, since there were no detailed measurements available. In addition, predicting the effects of climate change and sea level rise, and formulating mitigation measures is only meaningful when the current situation of these shallow rainwater lenses on top of seeping saline groundwater is known.

In this article we aim to determine the characteristics and spatial variability of rainwater lenses in areas with saline seepage based on field measurements and numerical density dependent groundwater models. Moreover, we determine the main factors that control the characteristics and occurrence of these shallow rainwater lenses. Our study area was the province of Zeeland, situated in the south-western delta of the Netherlands, where saline groundwater with chloride concentrations exceeding 10 g L^{-1} is found within five meters below ground level (Goes *et al*., 2009). Different field techniques, such as groundwater sampling, TEC (temperature and electrical soil conductivity)-probe measurements, electrical cone penetration tests (ECPT), continuous vertical electrical soundings (CVES), electromagnetic survey with EM31 and helicopter-borne electromagnetic measurements (HEM) were used to map the thickness of these shallow rainwater lenses and the mixing zone from fresh to saline groundwater.

5.2 Paleogeography, geomorphology and hydrogeology of study area

The study area lies in the south-western delta of the Netherlands (Fig. 5.2a). The current landscape, groundwater flow systems and groundwater salinity mainly result from sequential Holocene marine transgressions and regressions, and human activities such as peat mining and land reclamation. Under a continuous sea level rise during the Holocene, Zeeland was submerged from 7500 B.P. (before present) until 5000 B.P. (Van de Plassche, 1982; Vos and Zeiler, 2008) and the infiltration of seawater salinized the underlying Pleistocene aquifers by free convection (Post, 2004). After this period of maximum transgression, sedimentation processes began to dominate and, as a consequence, the land rose above mean sea level. Then peat was formed under freshwater conditions and this covered Zeeland between 3800 B.P. and 2000 B.P. Since Roman times, peat mining and drainage of the land by man has caused subsidence enhanced by marine erosion (Fig. 5.2b). Zeeland was again totally submerged from 350 A.D. until 750 A.D. (Fig. 5.2b). Around 1000 A.D. people started to reclaim large pieces of land by the embankment of the salt marshes (supra-tidal flats) (Fig. 5.2b; Vos and Zeiler, 2008). Such an embanked land which is drained artificially is called a 'polder' (Van de Ven, 2003). Shrinkage of peat and clay by drainage and peat mining led to further subsidence of these polders, whereas the unembanked land was rising from sedimentation during high tides and storms (Vos and Zeiler, 2008).

The present topography is therefore a result of the age of reclamation; the older the land, the lower the surface elevation. The lowest polders are situated at -1.5 to -2.5 m MSL whereas the more recent polders

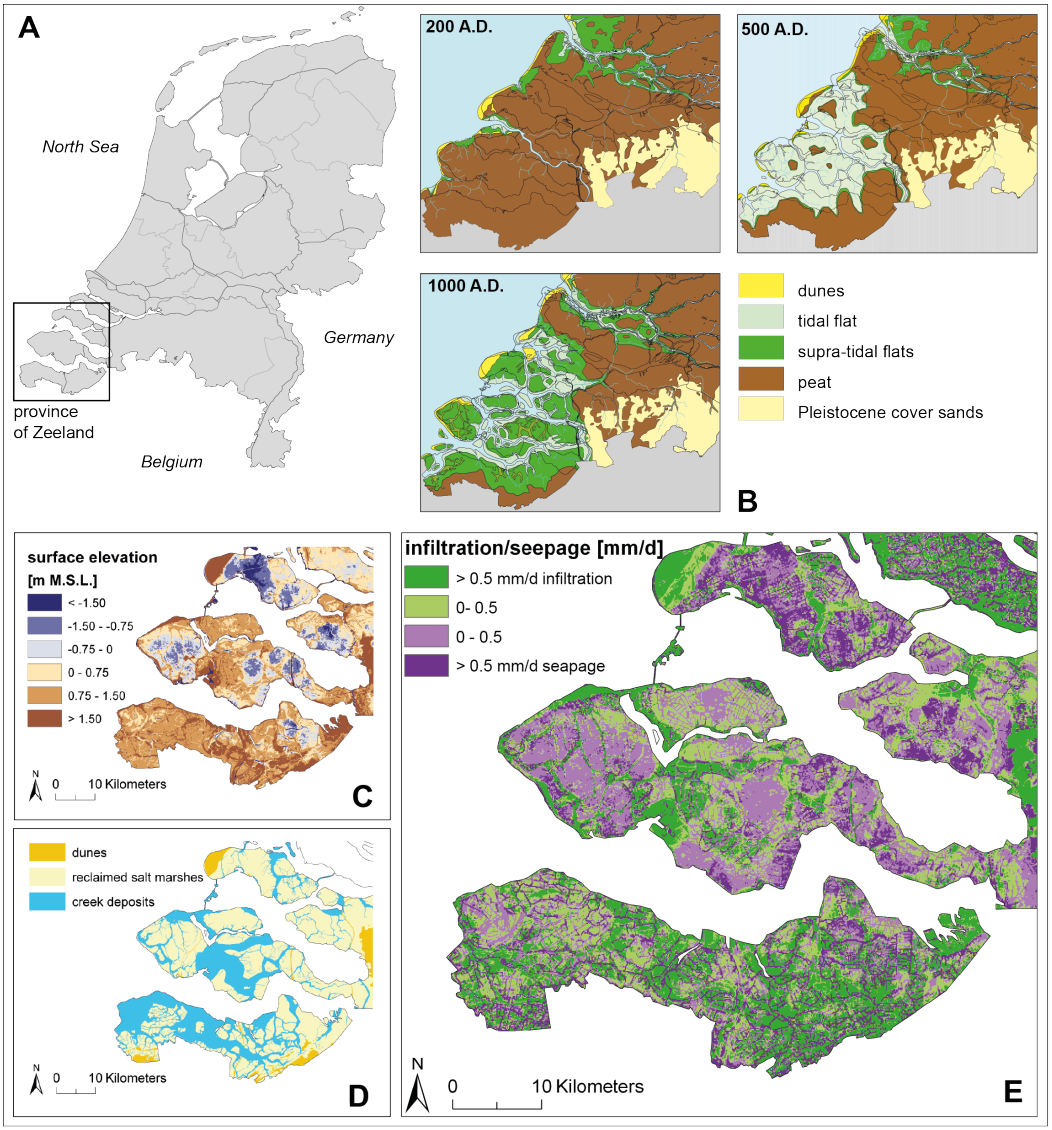

Figuur Louw 11RS 01

Fig. 5.2. (a) Location of study area. (b) Paleogeography of study area in 200 A.D., 500 A.D., 1000 A.D. (Vos and Zeiler, 2008; by courtesy of Vos). (c) Surface elevation. (d) Position of the dunes, reclaimed salt marshes and sandy creek deposits (from: REGIS II, 2005). (e) Infiltration and seepage flux (result of regional groundwater model; Van Baaren *et al.*, 2013).

have their land surface above mean sea level (Fig. 5.2c). As the former tidal creeks consisted of sand, they did not subside like the surrounding clayey and peaty salt marshes. The present land surface at these sandy creek ridges is therefore often 0.5 to 1.5 m higher than the surrounding land (Fig. 5.2c-d). In the western coastal area, sandy dunes were formed during the Holocene that now reach elevations of +30 m MSL. Taking into account that the present elevation has a large impact on the groundwater flow system, the study area can be divided into three major geomorphic units: (a) reclaimed salt marshes, (b) sandy creek ridges and (c) the dunes (Fig. 5.2d). Fresh rainwater infiltrates the dunes and the elevated sandy creek ridges, whereas upward groundwater seepage occurs mainly in the low-lying reclaimed salt marshes (Fig. 5.2e). The salt marshes are intensively drained by a regular system of

ditches and tile drainage to make the land fit for agriculture. Tile drainage usually leads to the rapid discharge of shallow groundwater during rainfall events (e.g. Tiemeijer *et al*., 2007; Van der Velde *et al*., 2009). The ditches lie some 50 to 300 m apart and tile drainage is applied at a depth of about 1 m, with a distance of 10 to 15 m between the drains. Surface water levels are maintained at a nearly constant level by pumping and admission of water from surface water reservoirs at higher elevations, like in most lowland polder catchments, (e.g. De Louw *et al*., 2010).

Besides elevation and drainage characteristics, the composition of the Holocene deposits plays an important role in groundwater flow and the formation of shallow fresh rainwater lenses on top of the present saline groundwater. Due to the dynamic paleogeographical evolution of the study area during the Holocene, the lithology is fairly heterogeneous. An east-west lithological cross-section of the island of Schouwen-Duivenland shows the general build-up of the Holocene sediments on top of late Pleistocene cover-sands (Fig. 5.3). In most of the area, the fining upward sequence of the Holocene deposits resulted in a thin confining layer of clay and peat on top of an aquifer of Pleistocene and Holocene fine to coarse sands (upper aquifer). The confining top layer of clay and peat (top aquitard) is on average 4 m thick. The upper aquifer of Holocene and Pleistocene sands has a thickness of 20 to 60 m and is separated from the lower aquifer by a 5 m thick clay layer that is sometimes absent. The hydrogeological base varies from a depth of 130 m in the northern part to 30 m in the southern part of the study area. For the development of rainwater lenses in saline groundwater, the shallow part of the hydrogeology of the study area, i.e. the upper aquifer and confining top layer, is of main interest. We define seepage as the upward groundwater flow from the upper aquifer into the confining top layer (Fig. 5.1). This seepage water, groundwater coming from the upper aquifer, will eventually exit the groundwater system by either drainage or evapotranspiration.

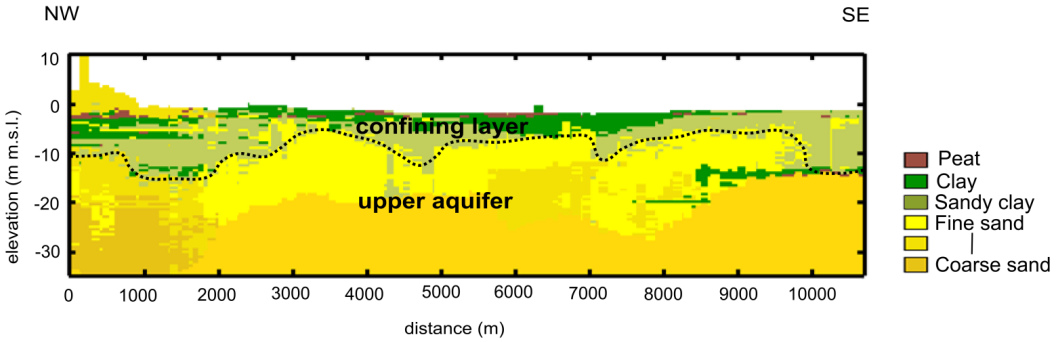

Fig. 5.3. A NW-SE lithological cross-section of the island of Schouwen-Duivenland (see Fig. 5.4 for location of cross-section). The cross-section is derived from a detailed 3D geological model of Zeeland based on 5 drillings per 1 km^2 that were classified into geological units (GeoTOP, Stafleu *et al*., 2011).

5.3 Materials and methods

5.3.1 Mapping rainwater lenses

We used different geophysical and hydrological techniques to map the characteristics of rainwater lenses on top of upward-seeping saline groundwater. We carried out the measurements at different spatial scales, varying from point scale to island scale. As salinity changes rapidly in space and with depth, we needed high-resolution techniques that could record this variability. We applied the following techniques to obtain detailed salinity-depth profiles at point scale: electrical soil conductivity measurements using the TEC-probe, groundwater sampling at small depth intervals, and electrical cone penetration tests (ECPT). We used non-invasive continuous vertical electrical soundings (CVES) and surface electromagnetic measurements (EM31) to map the spatial variation of rainwater lenses within an agricultural field (0.05 km^2). A helicopter-borne frequency-domain electromagnetic (HEM) survey was performed to map the thickness of rainwater lenses for a large area on the island of Schouwen-Duivenland (56 km^2). Fig. 5.4a-d shows the locations of the different measurements in the study area. At site 11, an agricultural field (Fig. 5.4c), we applied all our measurement techniques to compare their results and to improve the inversion models of the geophysical techniques. This site was chosen because of its position at a transition from a low-lying, clayey reclaimed salt marsh at -0.7 m MSL to a higher sandy creek ridge lying at -0.2 m MSL (Fig. 5.4c). The measurement techniques will be described briefly below.

TEC-probe

The TEC-probe is suitable for manual 1D measurements of temperature and the electrical conductivity (EC_{soil}) of soft soils like peat and clayey soils (Van Wirdum, 1991). The electrodes and temperature sensor are located at the far end of the probe. The probe has a diameter of 22 mm and the electrode distance is 50 mm. We carried out TEC-probe measurements once at 27 agricultural sites with differing hydrogeology and geomorphology (Fig. 5.4a). At each site, TEC-probe measurements were done in a ditch and at different distances from the ditch; from the water table downward at 0.1 m intervals until a depth of 4.0 m. Measured EC_{soil}s were automatically corrected to obtain a specific EC_{soil} for a reference temperature of 25^{o}C. To obtain the electrical conductivity of groundwater (EC_w), EC_{soil} must be multiplied by the formation factor (FF), which depends mainly on the lithology (Archie, 1942; Keary and Brooks, 1991; Friedman, 2005). We determined the formation factor (FF) for seven different soil types based on 584 measured EC_w–EC_{soil} pairs (Table 5.1). EC_{soil} was measured with the TEC-probe and EC_w was obtained by groundwater sampling. EC_w-values were transformed to chloride concentrations using a calibration curve based on a linear regression analysis (R^2=0.98) of 79 groundwater samples: $Cl\ (g\ L^{-1}) = EC_w\ (mS\ cm^{-1}) * 0.36 - 0.45$. The 79 groundwater samples were taken from 79 different piezometers at site 11 and site 26 (see next paragraph). Simultaneously with the TEC-probe measurement, we made a detailed soil description to assess the formation factor. The TEC-probe measurements were carried out in the period January – March 2007.

Groundwater sampling

From the 27 TEC-probe sites we selected two sites on the island of Schouwen-Duivenland, site 11 (Fig. 5.4c) and site 26 (Fig. 5.4d), where we installed clusters of piezometers for sampling groundwater to derive chloride-depth profiles. The clusters were installed in ditches and at different distances from the ditches in the fields (Fig. 5.4c-d). The clusters in the fields

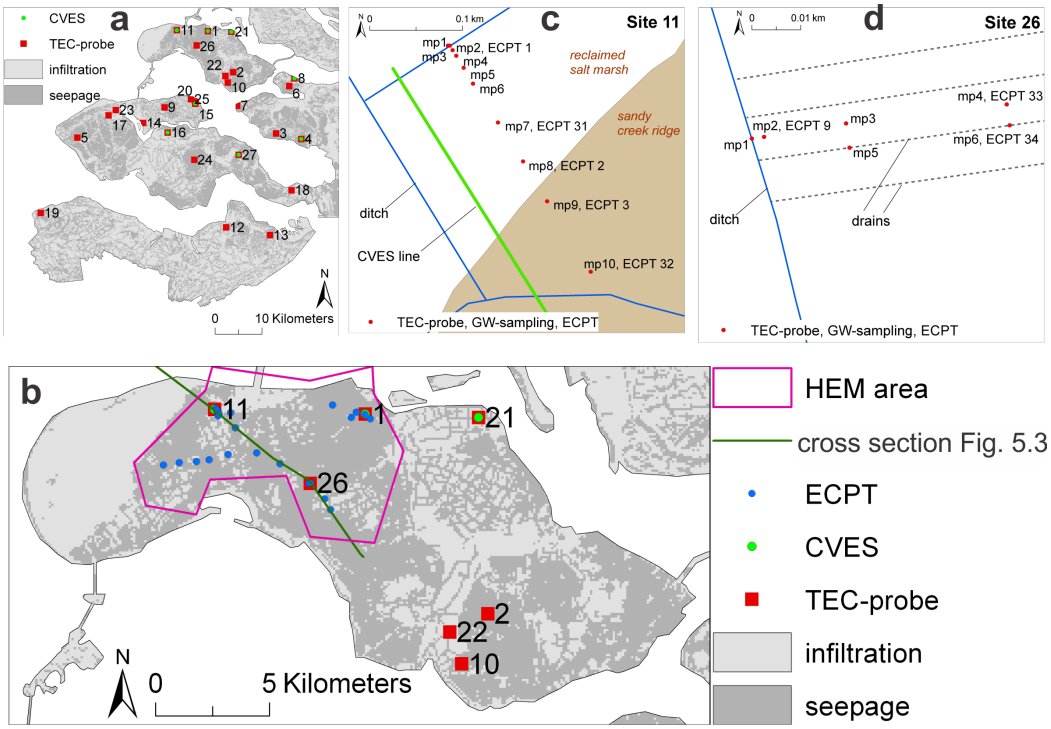

Fig. 5.4. Position of field measurements at different scales. (a) Province of Zeeland. (b) Island of Schouwen-Duivenland. (c) Agricultural field, site 11. (d) Agricultural field, site 26.

Table 5.1. Formation factors (FF) for different lithological units

Lithology	Average FF	Std	No. of samples
Peat	2.1	0.7	41
Clay	2.5	0.6	192
Sandy clay / clayey sand	2.8	0.8	52
(Clayey) fine sand	3.2	0.4	299
Medium coarse sand	4*		
Coarse sand	5*		
Sand with gravel	6-7*		

* FF taken from Goes *et al.* (2009)

were located between two drains, except for the two clusters mp 5 and mp 6 (mp = monitoring point) at site 26. These two clusters were positioned near (< 0.2 m) a drain to measure the effect of tile drainage. Each cluster contained 6 to 7 piezometers with 0.16 m long screens at depths (bottom of screen) of 0.8 m, 1.0 m, 1.3 m, 1.6 m, 2.0 m, 3.0 m and 4.0 m below ground level (BGL). Before taking groundwater samples, we extracted all the water from the piezometers and waited several hours until the piezometers had re-filled with groundwater. The electrical conductivity of the sampled groundwater was measured in the field monthly for a period of 2 years (January 2009 - December 2010) and chloride was analyzed in the laboratory in April 2009. Hydraulic heads were measured as well to determine the head change with depth. The heads were monitored hourly in the period September 2008 until January 2011 using CTD-diver data loggers. Heads were corrected for density differences by conversion to freshwater heads (Post *et al.*, 2007).

Continuous vertical electrical soundings: CVES

We carried out the CVES-measurements in profiles (with a length of 150 to 350 m) perpendicular to the ditches at 8 of the 27 TEC-probe sites (Fig. 5.4a). Some of the results and a detailed set up of the CVES-measurements were described by Goes *et al*. (2009). The CVES measurements were done with an AbemSAS4000 connected to four multi-electrode cables, with electrode spacing of 1 m to obtain a detailed resolution both horizontally and in depth. The measured electrical resistivity data were inverted into real soil resistivities using SensInv2D (Geotomographie, 2004). The CVES-measurements were carried in the period September - October 2007.

Electromagnetic EM31 survey

We carried out an EM31-survey at site 11 in September 2009 to obtain an overview of the spatial variation of groundwater salinity in the shallow subsoil within one agricultural field. The EM31 is an electromagnetic instrument that measures the apparent electrical bulk conductivity of the shallow subsoil (McNeill, 1980). The upper layers contribute more to the bulk conductivity than the lower layers. The average penetration depth of these measurements was about 6 m, which is less than the penetration depth of the CVES-measurements (about 20 m). However, the EM31-measurements allowed us to map a larger area in a horizontal plane (about 0.1 km^2). The EM31-measurements with a spacing of 5 m have been interpolated to a conductivity map, which represents the bulk conductivity of the top 6 m of the subsoil.

Helicopter-borne electromagnetic measurements (HEM)

A helicopter-borne survey was conducted by the airborne geophysics group of the German Federal Institute for Geosciences and Natural Resources (BGR) on August 25-26 2009 (Siemon *et al*., 2011). The survey, covering a large part of the island of Schouwen-Duivenland (Fig. 5.4b) required three survey flights to map an area of about 56 km^2 with 31 WNW-ESE lines and 16 NNE-SSW tie lines at 200 m and 500 m line spacing, respectively, totalling 313 line-km. Electromagnetic, magnetic and radiometric data, as well as position data, were acquired simultaneously. The electromagnetic system we used was a RESOLVE towed "bird" consisting of five horizontal-coplanar (HCP) coil systems and one vertical-coaxial (VCX) coil system, with measuring frequencies ranging from 387 Hz to 133 kHz. The average sensor altitude was 33 m above ground level. About 84,300 resistivity-depth inversion models were derived from the HCP data using a Marquardt-Levenberg smooth multi-layer inversion procedure (Siemon *et al*., 2009). The models consist of 15 layers. All resistivities and the thickness of the top layer are derived by the inversion procedure. The thickness of the other 14 layers remained fixed during the inversion and increased slightly with depth. The degree of model smoothing was optimised in order to avoid oscillation of the model resistivities.

Electrical cone penetration tests (ECPT)

We contracted a geotechnical company (www.bmned.com) to carry out 23 ECPTs on Schouwen-Duivenland to obtain 1D electrical conductivity profiles down to a depth of 25 m (Fig. 5.4b). The technique is comparable with a manual TEC-probe measurement but can also be applied in sandy soils and down to greater depths. Besides measurements of the soil's electrical conductivity (EC_{soil}) during penetration, the cone sleeve and tip friction were also measured to determine the lithological composition (BMNED, 2011). The ECPTs were carried out in the HEM pilot area (Fig. 5.4b) in March 2011, in order to derive conductivity depth profiles, which could be subsequently used to check the calibration of the HEM system and to optimize the inversion of the HEM data.

5.3.2 Numerical modeling of rainwater lenses

We constructed two different types of groundwater models to increase our insight into rainwater lenses on top of saline groundwater: (1) a 3D-model that was able to reproduce the different types of field measurements at site 11, and (2) various smaller-scale 2D conceptual models to focus on the mixing of saline seepage and infiltrating rainwater, and the flow to drains in detail. These models were used to analyze the sensitivity of different parameters.

Set-up of 3D-model

We set up the 3D-model with the numerical transport code MOCDENS3D (Oude Essink, 2001-a) for site 11 and a small area around it (modeled area is 1 km^2) at a transition from a low-lying, clayey reclaimed salt marsh to a higher sandy creek ridge (Fig. 5.4b-c). Different kinds of measurements were available for this site to evaluate the performance of the model. The model area was divided into cells of 5 by 5 m and the subsoil was divided into 41 layers of 0.3 to 5 m, up to a maximum depth of 35 m, to accurately model salt transport. The hydrogeological schematization and parameterization was based on our field measurements and the Dutch Geohydrological Information System (REGIS II, 2005). The molecular diffusion coefficient D_m for porous media was assumed to be $8.6 \cdot 10^{-5}$ m^2 d^{-1}. The longitudinal dispersivity was set equal to 0.1 m and the ratio transversal to longitudinal dispersivity was 0.1. These rather small values are based on numerous case studies of Dutch and Belgian aquifer systems with marine and fluvial deposits (e.g. Stuyfzand, 1993; Lebbe, 1999; Van Meir, 2001; Oude Essink, 2001-b; Vandenbohede and Lebbe, 2007). Fixed heads were applied at the model boundaries and were deduced from the regional groundwater model of the province of Zeeland (Van Baaren *et al.*, 2013). We determined the location and dimensions of ditches and subsurface drains in the field and applied it to the model. The period of 1906-2006 was simulated with stress periods of 10 days. Recharge was calculated from precipitation and evapotranspiration data from two nearby meteorological stations (Kerkwerve and Wilhelminadorp) of the Royal Netherlands Meteorological Institute (KNMI). A 100-year simulation period was long enough for the groundwater chloride distribution at the sandy creek ridges to reach a state of equilibrium with the boundary conditions.

Set-up of 2D-model

From the 3D-model we zoomed into low-lying seepage areas to focus on the mixing of infiltrating fresh rainwater and upward-seeping saline groundwater between two ditches. Based on our findings with the 3D-model and our field measurements, we constructed a conceptual cross-sectional 2D-model between two ditches of a tile-drained agricultural field with upward-seeping saline groundwater (Fig. 5.5). For this modeling exercise we used the numerical transport code SEAWAT version 4 (Langevin *et al.*, 2007). The cell size in a horizontal direction was 1 by 1 m and the layer thickness in the vertical direction was 0.1 m. The total thickness of the reference model was 3.0 m, which equals the thickness of the confining layer. Parameter values for the reference model and sensitivity models are given in Table 5.2 and are based on field data. We assumed that all the incoming fluxes due to recharge and seepage between the ditches discharge into drains and ditches and therefore applied no-flow boundaries at the model sides. We applied a constant upward seepage flux Q_s with chloride concentration Cl_s from the upper aquifer into the Holocene confining layer (Fig. 5.5). Although the confining layer consists of a sequence of different soil types, we considered it to be homogeneous. The effect of soil composition heterogeneity

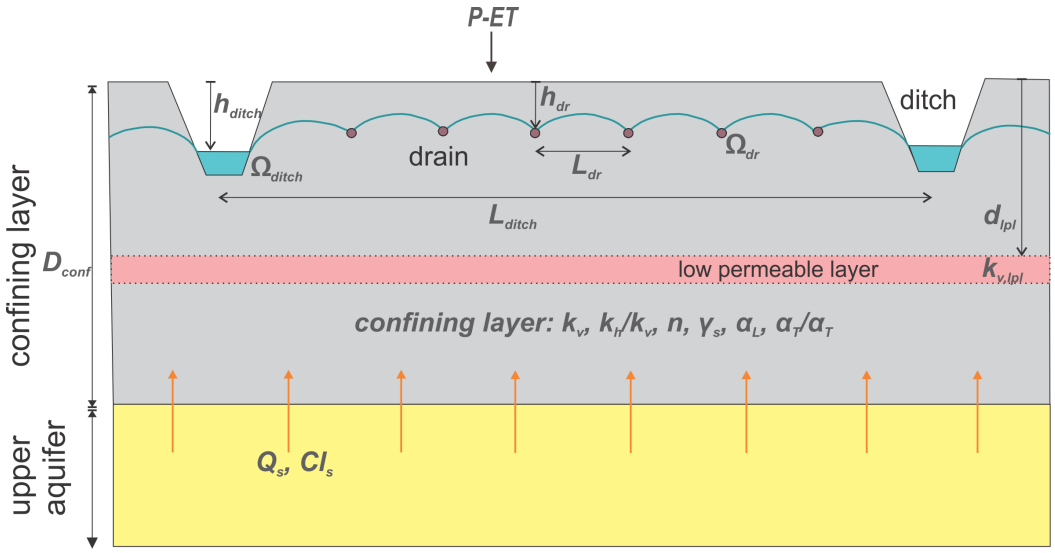

Fig. 5.5. Conceptual schematization of the cross-sectional 2D-models.

Table 5.2. Parameter values of the 2D reference model (Ref) and the sensitivity models (Ref--,Ref-, Ref+, Ref++)

	Para-meter	Description	Unit	Ref --	Ref -	Ref	Ref +	Ref ++
1	Q_s	seepage flux	mm d^{-1}	0.05	0.15	0.25	0.5	1.0
2	*P-ET*	recharge (average)	mm d^{-1}	0.25	0.5	0.75	1.0	1.25
3	Cl_s	Cl-conc seepage	g L^{-1}	0.01	5.0	10.0	15.0	19.0
4	L_{dr}	spacing between 2 subs. drains	m	2.5	5	10	15	20
5	h_{dr}	depth of drains	m	-1.4	-1.2	-1	-0.8	-0.6
6	Ω_{dr}	drainage resistance	d	0.5	1	2.5	5	7.5
7	L_{ditch}	spacing between 2 ditches	m	25	50	100	150	200
8	h_{ditch}	surface water level	m	-1.75	-1.5	-1.25	-1	-0.75
9	Ω_{ditch}	drainage resistance ditch	d	1	2.5	5	10	20
10	D_{conf}	thickness confining layer	m	0	2	3	4.5	6
11	k_v	vert. hydr. conductivity of confining layer	m d^{-1}	$0.1{\cdot}10^{-2}$	$0.5{\cdot}10^{-2}$	$1.0{\cdot}10^{-2}$	$2.5{\cdot}10^{-2}$	$5.0{\cdot}10^{-2}$
12	k_h/k_v	anisotropy factor (k_v=constant)	-	1	2.5	5	7.5	10
13	n	porosity	-	0.06	0.1	0.14	0.18	0.22
14	γ_s	specific yield	-	0.15	0.2	0.25	0.3	0.35
15	d_{lpl}	depth low permeable layer (LPL)	m	- 0.7	- 1.0	none	- 1.5	- 2.5
16	$k_{v\text{-}lpl,1.5}$	k_v of LPL, depth LPL = -1.5m	m d^{-1}	$0.3{\cdot}10^{-3}$	$0.6{\cdot}10^{-3}$	$1.2{\cdot}10^{-3}$	$2.4{\cdot}10^{-3}$	$4.8{\cdot}10^{-3}$
17	$k_{v\text{-}lpl,2.5}$	k_v of LPL, depth LPL = -2.5m	m d^{-1}	$0.3{\cdot}10^{-3}$	$0.6{\cdot}10^{-3}$	$1.2{\cdot}10^{-3}$	$2.4{\cdot}10^{-3}$	$4.8{\cdot}10^{-3}$
18	α_L	longitudinal dispersivity coefficient	m	0.01	0.05	0.1	0.25	0.5
19	α_L/α_T	ratio. α_T = transversal dispersivity coeff.	-	1	5	10	15	20

is addressed in the sensitivity analysis by applying a 0.2 m thick layer with a very low permeability at different depths in the confining layer, as we think this may influence groundwater flow and solute transport in the shallow groundwater system.

The initial groundwater chloride concentration in all model layers was set equal to the chloride concentration of

the upward-seeping groundwater Cl_s. A rainwater lens can develop in this saline groundwater body under a variable recharge with fresh rainwater (Cl = 0.02 g L^{-1}) and a constant seepage flux. Daily values of recharge were determined from daily precipitation P and potential reference crop evapotranspiration ET at the KNMI meteorological stations. We used data from the year 2005 because these were representative for the annual average precipitation surplus (= 0.75 mm d^{-1}), and applied them for every year during the whole simulation period. The total precipitation and evapotranspiration for the winter months (October until March) was 397 mm and 108 mm respectively. The total precipitation and evapotranspiration for the summer months (April until September) was 425 mm and 440 mm respectively. A simulation period of 30 years was long enough for all model simulations to reach a stationary situation, which means that the annual mass balance did not change significantly from year to year. The model output was analyzed for the thirtieth year.

Sensitivity analysis

We carried out a sensitivity analysis with the 2D-model for 19 model parameters, which are mainly physical and geographical parameters (Table 5.2). One parameter at a time was modified while the others remained fixed. The modified parameter values were based on field measurements and surveys, and geographical and geological data; they represent plausible ranges for the study area. We tested the parameter sensitivity for rainwater lens characteristics for a location in the middle between two drains (bdr) and for a location at a drain (dr), both at the largest possible distance from the ditches (Fig. 5.5). Besides the sensitivity analysis, we used results from the 2D-models to study vertical flow processes in more detail at and between the drains with respect to lens characteristics.

5.4 Results and discussion

5.4.1 Characteristics of the mixing zone in seepage areas

The form of the mixing zone between infiltrating rainwater and saline groundwater was obtained accurately with the point measurements by the TEC-probe (Fig. 5.6) and ECPT soundings (Fig. 5.7). At 17 of the 27 TEC-probe sites, we measured a gradual mixing zone between rainwater and saline groundwater; these are shown in Fig. 5.6. At the other 10 locations, we found a constant and fresh groundwater profile with depth. The measured smooth curved mixing zones are well described by the spatial moment method (Eeman *et al*., 2011). With this method the chloride concentration change with depth, i.e. the derivative of the chloride profile, is described by a normal distribution function, from which the centre of mass (1st moment) indicates the centre of the mixing zone D_{mix} (first graph in Fig. 5.6). The variance (2nd moment) is a measure of the extent of the mixing zone. By fitting the normal distribution function through the measurements, we derived five characteristics from it (first graph in Fig. 5.6): the depth of the centre of the mixing zone D_{mix}, the bottom of the mixing zone B_{mix}, the half-width of the mixing zone W_{mix} (= D_{mix} - B_{mix}), and the minimum and maximum chloride concentrations Cl_{min} and Cl_{max}. B_{mix} was defined as the depth where the chloride concentration was Cl_{max}. We used these lens characteristics in the further analysis of our measurements and model results.

The lens characteristics D_{mix}, B_{mix} and W_{mix} derived from the TEC-probe and ECPT measurements are summarized in

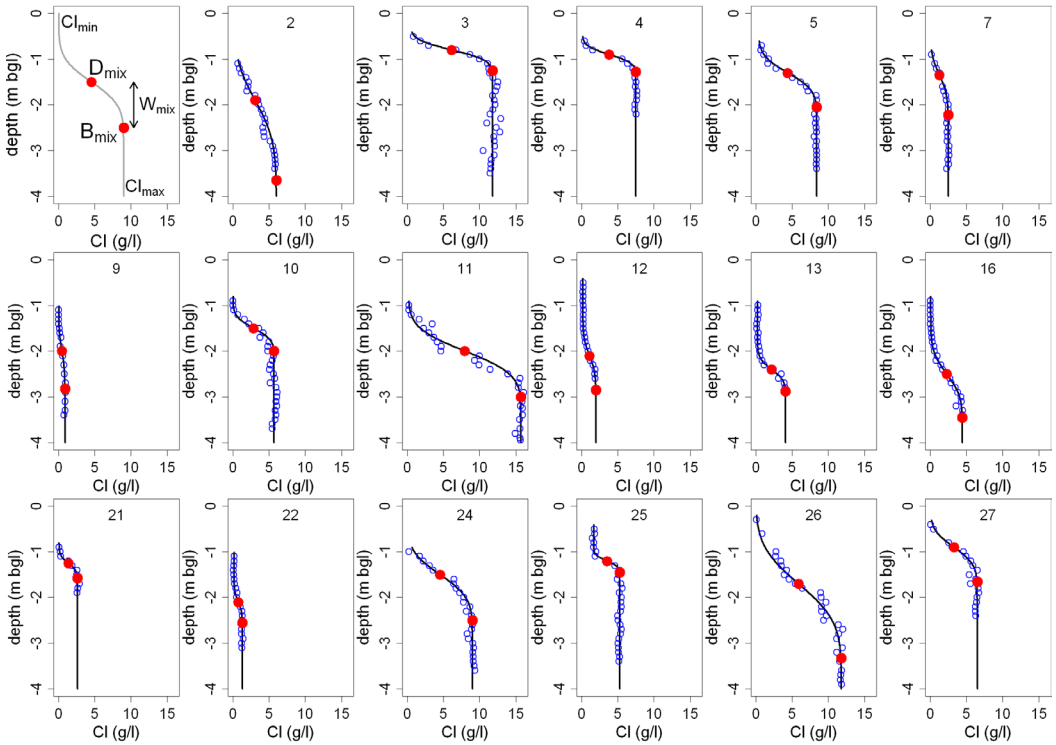

Fig. 5.6. Characteristics of a rainwater lens, D_{mix}, B_{mix}, W_{mix}, Cl_{min}, Cl_{max} (first plot) and 17 measured salinity profiles with the TEC-probe (blue circles) at different seepage locations in the province of Zeeland (see Fig. 5.4a for TEC-probe locations). The measured salinity profiles are characterized by the fitted salinity profiles based on spatial moments (black line).

Table 5.3. In the seepage areas, the depth of the centre of the mixing zone was found to be very shallow with a median depth of D_{mix} of 1.7 m BGL. Mixing occurred no deeper than 5.5 m depth (=B_{mix}) and always in the confining layer. TEC-probe results showed a large variation of Cl_{max}, 0.9-15.7 g L^{-1} (Fig. 5.6). The ECPT conductivity profiles, which go much deeper than TEC-probe profiles, showed that below the mixing zone the salinity remains relatively constant (at value Cl_{max}) until a depth of at least 25 m (Fig. 5.7). However, there was one exception: ECPT-12 was located in a seepage area at about -1.5 m MSL and showed a constant freshwater profile to a depth of 25 m. The contrast with the salinity profile of ECPT-13 (with D_{mix} at 1.5 m BGL, situated only 600 m from ECPT-12 and at the same elevation) is large. However, the explanation was rather simple: the freshwater profile at ECPT-12 was caused by lateral fresh groundwater flow from the elevated dunes (at 1 km to the west) that did not reach ECPT-13. The ECPTs are additionally valuable for the thicker rainwater lenses in the elevated areas, such as the sandy creek ridges (e.g. ECPT-32 and ECPT-4 in Fig. 5.7). Nine ECPTs were made at the sandy creek ridges where D_{mix} varied between 4 and 11 m depth, and B_{mix} varied between 8 and 14 m depth (Table 5.3).

The TEC-probe and ECPT data showed there was no sharp boundary between infiltrating fresh rainwater and saline seepage groundwater, but a gradual mixing zone with a median half-width W_{mix} of 0.9 m. Although this is much smaller than at the sandy creek ridges with a median W_{mix} of 3.0 m (Table 5.3) and what is usually found for BGH-lenses on islands and dunes (e.g. Fetter, 1972; Underwood *et al.*, 1992; Stuyfzand, 1993; Sakr, 1999), the mixing zone in the seepage areas can be labelled as relatively wide compared to its depth. Therefore, the analytical

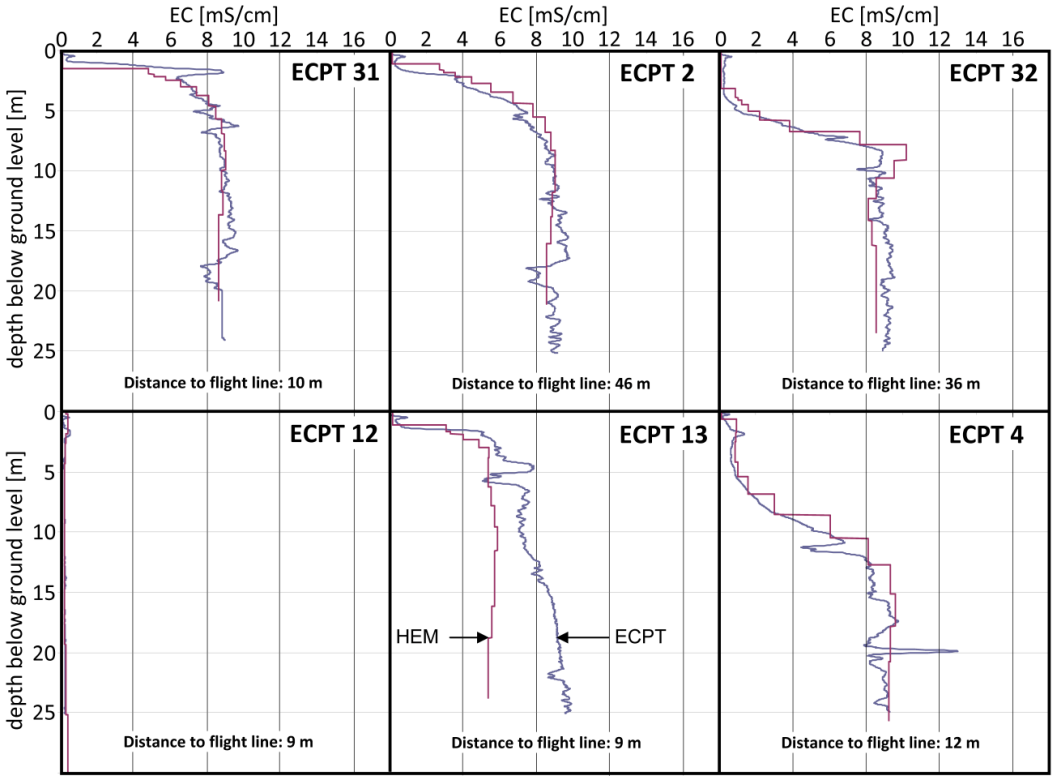

Fig. 5.7. Comparison of six ECPT soundings and smooth 15-layer HEM inversion models (for location see Fig. 5.14).

and numerical approaches that assume a sharp interface and satisfactorily simulate BGH-lenses (e.g. according to Van der Veer, 1977; Van Dam and Sikkema, 1982; Sikkema and Van Dam, 1982; Sakr, 1999; Boekelman, 2001) should not be applied to these shallow rainwater lenses. As the mixing zones occur at shallow depth, their position and width is of great importance for the freshwater availability for crop growth. In most seepage areas, we did not find any fresh groundwater (i.e. Cl <0.3 g L^{-1}). The upper groundwater is already a mix of seepage water and rainwater, which indicates that part of the mixing process very likely occurs in the unsaturated zone.

Table 5.3. Summary of lens characteristics in seepage and infiltration areas derived from TEC-probe and ECPT measurements.

			TEC-probe			ECPT			TEC + ECPT
		Unit	Range	Median	No.	Range	Median	No.	Median
Seepage areas	D_{mix}	m BGL	0.8 – 2.5	1.5	17	1.2 – 3.5	1.7	13	1.7
	B_{mix}	m BGL	1.2 – 3.6	2.5	17	2.0 – 5.5	3.7	13	2.8
	W_{mix}	m	0.2 – 1.7	0.7	17	0.5 – 3.7	1.5	13	0.9
Infiltration areas	D_{mix}	m BGL	> 4.0	> 4.0	10	4.0 – 11.0	6.3	9	
	B_{mix}	m BGL	> 4.0	> 4.0	10	8.0 – 14.0	8.5	9	
	W_{mix}	m	?	?	10	1.0 – 5.5	3.0	9	

Maximum penetration depth of TEC-probe was 4 m BGL, penetration depth of ECPT was 25 m BGL
D_{mix} = centre of mixing zone, B_{mix} = bottom of mixing zone, W_{mix} = half width of mixing zone (= $D_{mix} - B_{mix}$).

5.4.2 Rainwater lens variation within agricultural fields

Monitoring results at agricultural sites 11 and 26

Fig. 5.8 shows the chloride-depth profiles derived from groundwater samples at different locations within the agricultural fields of site 11 and site 26 (for location, see Fig. 5.4c-d). For both sites, we measured a relatively constant chloride depth profile beneath the ditch, with a chloride concentration of 16 g L^{-1} for site 11 and 12 g L^{-1} for site 26. In contrast to the locations in the field, there was no mixing beneath the ditch and upward flowing saline groundwater exfiltrates in the ditches without mixing. At most monitoring locations in both fields, the same salinities as beneath the ditches were found at 3 to 4 m depth, but upwards from here the salinity decreased, indicating the presence of the mixing zone. Although there were no significant differences in mixing zone characteristics for the different distances from the ditch at site 26, the position in relation to the drains did have an impact on the mixing zone. The monitoring locations near drains showed a smaller mixing zone at a shallower depth when compared to the monitoring locations between drains (site 26, Fig. 5.8).

In agricultural site 11 we found a large spatial variation in the salinity profiles (Fig. 5.8). Within about 200 m, the salinity at 2 to 4 m depth increased from fresh (Cl = 0.03-0.05 g L^{-1}) at the sandy creek ridge, mp10, to almost seawater (Cl = 14 to 16 g L^{-1}) in the lower-lying clay area, mp1 to mp7. Location mp8 showed an intermediate salinity profile between these two extremes (Fig. 5.8). This large spatial salinity gradient at site 11 was identified by all the measuring techniques we used (i.e. groundwater sampling, TEC-probe, ECPT, CVES, EM31, HEM). D_{mix} and B_{mix} derived from TEC-probe and ECPT measurements were plotted in a cross-section as well as the measured freshwater heads at 1.5 m and 4 m depth (Fig. 5.9). Although the spatial variation of rainwater lens thickness could be followed nicely with the CVES-measurement, the exact lens characteristics D_{mix} and B_{mix} could not be derived. This is due to the fact that the penetration depth could not be derived exactly from the electrical measurements. As such, we plotted the 3 Ωm isoline of the real inverted soil resistivity in the cross-section to illustrate the strong gradient in groundwater salinity (Fig. 5.9).

As the confining layer is about 2.5 to 3 m thick at site 11, the freshwater head at 4 m depth represents the regional hydraulic head of the upper aquifer. In the seepage area, where D_{mix} was shallower than 2 m, the freshwater head at 4 m depth was higher than the freshwater head at 1.5 m depth indicating upward vertical flow (Fig. 5.9). As freshwater head gradients are larger than the relative density difference that accounts for the buoyancy effect, the vertical flow direction (upward or downward) can be derived directly from the head measurements (Post *et al*., 2007). The average freshwater head difference was about 0.1 m (mp5 to mp8) increasing towards the NW-ditch with a maximum freshwater head difference in the ditch of 0.65 m. This large freshwater head difference at the ditch causes a strong upward seepage flux which hinders the infiltration of surface water which results in a constant salinity profile ($D_{mix} = B_{mix}$). At the elevated sandy creek ridge, the freshwater head at 4 m depth was about 0.1 m lower than at 1.5 m depth, creating a downward flow and a much thicker rainwater lens with D_{mix} at 4 to 7 m depth and B_{mix} at 8 to 10 m depth. The strong upconing of saline groundwater was remarkable at the SE-ditch in the sandy creek ridge at only a few metres distance from the area where rainwater infiltrates to a large depth (Fig. 5.9). Due to the low surface water level maintained in the ditch of -1.95 m MSL (the same as for NW-ditch), the approximately

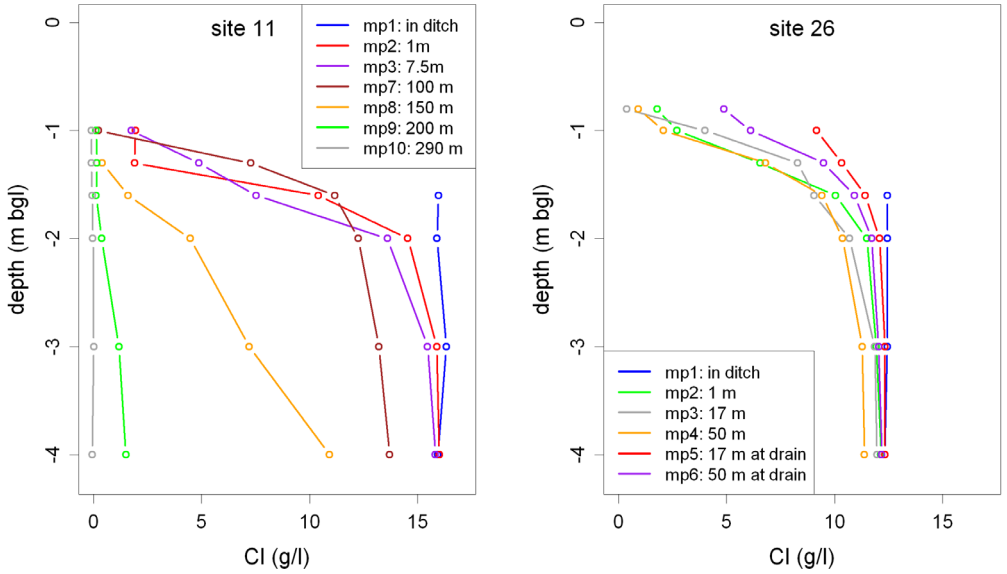

Fig. 5.8. Salinity profiles measured by groundwater sampling for sites 11 and 26 (on 21 January 2010).

0.6 m higher freshwater head in the upper aquifer creates a strong upward flow of saline groundwater. The freshwater head and salinity measurements at site 11 prove that the vertical flow direction (seepage or infiltration) even with small freshwater head differences can cause large differences in rainwater lens thickness.

Comparison of 3D-model and monitoring results at site 11

The techniques applied at agricultural site 11 are complementary to each other, varying from absolute chloride profiles (down to 4 m depth) and ECPT conductivity profiles (down to 25 m depth) at point scale to the surface (CVES, EM31) and airborne (HEM) measurements to follow the spatial variation of the rainwater lenses. This made the site suitable for evaluating the performance of the rainwater lens model in both an infiltration and a seepage situation. Fig. 5.10 shows the comparisons between the field observations and the model results for the 3D-numerical model. We found that the spatial variation of the modeled chloride concentration, averaged for the top 6 m (Fig. 5.10a) showed good agreement with the EM31-measurements (Fig. 5.10b): with low salinities on the sandy creek ridge and high salinities in the seepage area. The calculated bottom of the mixing zone (B_{mix}) at the sandy creek ridge was about 8 m below ground level, which is in agreement with the ECPT and HEM results (ECPT 32 in Figs. 5.7, 5.9 and 5.11). The lateral variation of rainwater lens thickness measured by the 1D techniques (D_{mix} and B_{mix}, see Fig. 5.9) and CVES (see Fig. 5.9 and Fig. 5.10e) is well reproduced by the numerical model (Fig. 5.10d). The measured chloride profiles, both absolute concentrations and the position and width of the mixing zone, showed good agreement with the modeled profiles (Fig. 5.10c). To summarize, the current fresh and saline groundwater system could be simulated well with the 3D numerical model.

Results of 2D-model

The findings of the 3D-model (parameterization and schematization) were used to construct the conceptual 2D-model for the seepage area. Fig. 5.11 shows the results of the 2D reference model. Upconing of saline groundwater at the drains was clearly visible, whereas the rainwater lens reached a greater depth

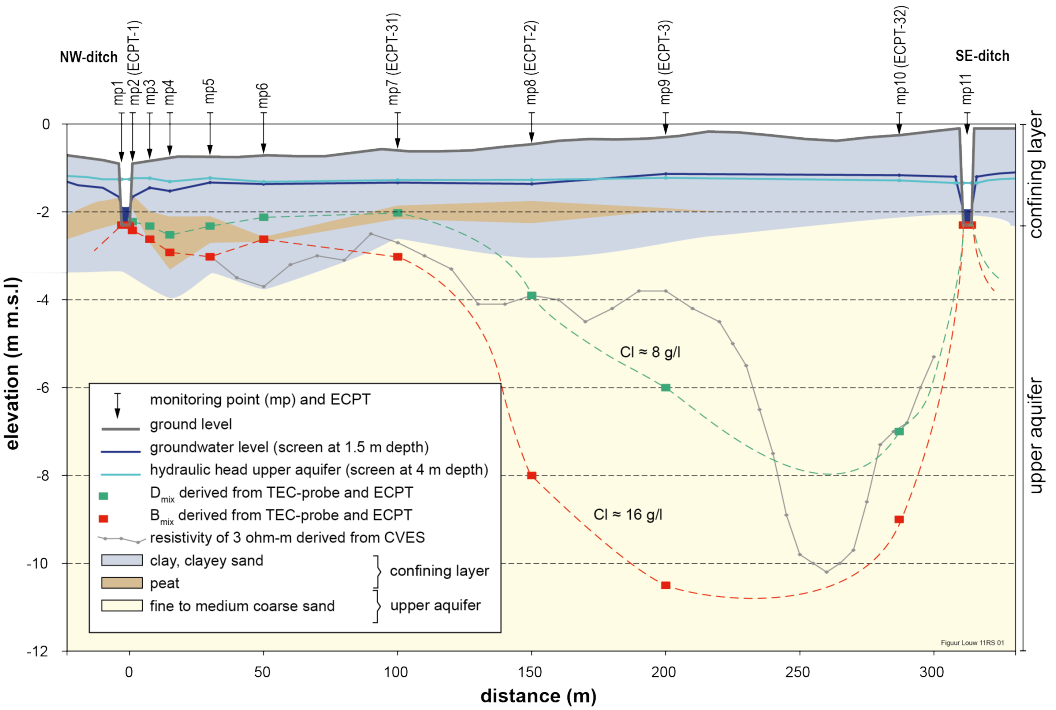

Fig. 5.9. Cross-section of site 11 with the measured hydraulic head at 1.5 m and 4 m depth (on 21 January 2010), D_{mix} and B_{mix} derived from TEC-probe and ECPT, and the real inverted soil resistivity isoline of 3 Ωm derived from CVES measurements. Note that the CVES-line was situated about 60 m from the 1D measurements (Fig. 5.4c) and therefore shows a sharper gradient.

between the drains (Fig. 5.11a and b). This corresponds with the measurements at site 26 (Fig. 5.8). The chloride profile and freshwater head were plotted for a location between two drains, and at a drain (Fig. 5.11b-c). This was done for the time step with the highest freshwater heads (wet period) and for one with the smallest freshwater heads (dry period). The heads between the drains were significantly higher than at the drains for the wet period. In the dry period, when heads dropped below drain level, the heads were equal.

The sensitivity of 19 model input parameters (Table 5.2) was tested for the lens characteristics; the centre depth D_{mix}, the bottom B_{mix} and the half-width W_{mix} of the mixing zone. Fig. 5.12 shows the results for the model parameters with an effect larger than 0.1 m on one of these lens characteristics compared with the reference model. As D_{mix}, B_{mix} and W_{mix} did not fluctuate much through the whole period (annual amplitude about 0.1 m), we presented average values in Fig. 5.12. The effects on D_{mix} and B_{mix} were more evident between the drains than at the drains. The parameters seepage flux Q_s (Fig. 5.12a), precipitation surplus $P\text{-}ET$ (Fig. 5.12b) and drainage depth h_{dr} (Fig. 5.12d) had the largest effect on D_{mix} and B_{mix}. Larger Q_s and smaller $P\text{-}ET$ led to a mixing zone at shallower depth. D_{mix} at the drains was always within 0.1 m of the applied drainage depth h_{dr}. The longitudinal dispersivity α_L was obviously the principal factor for W_{mix} (Fig. 5.12k). The other parameters not presented in Fig. 5.12 (including the chloride concentration of the seepage Cl_s, drainage resistance of the drains Ω_{dr}, drainage resistance of the ditch bottom Ω_{ditch}, and porosity n did not significantly influence the lens (effects were smaller than 0.1 m). The results of the sensitivity analysis will be further discussed in sections 5.4.4, 5.4.5 and 5.4.6.

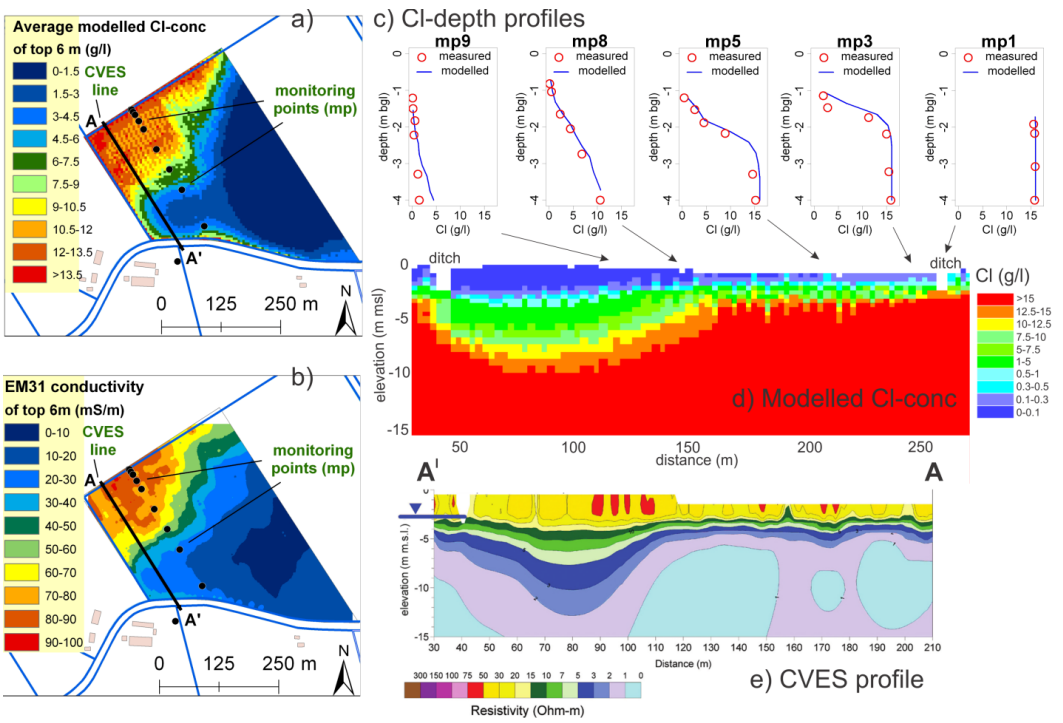

Fig. 5.10. Comparison of model results (3D-model) with field measurements (EM13, Cl-depth profiles, CVES) for site 11.

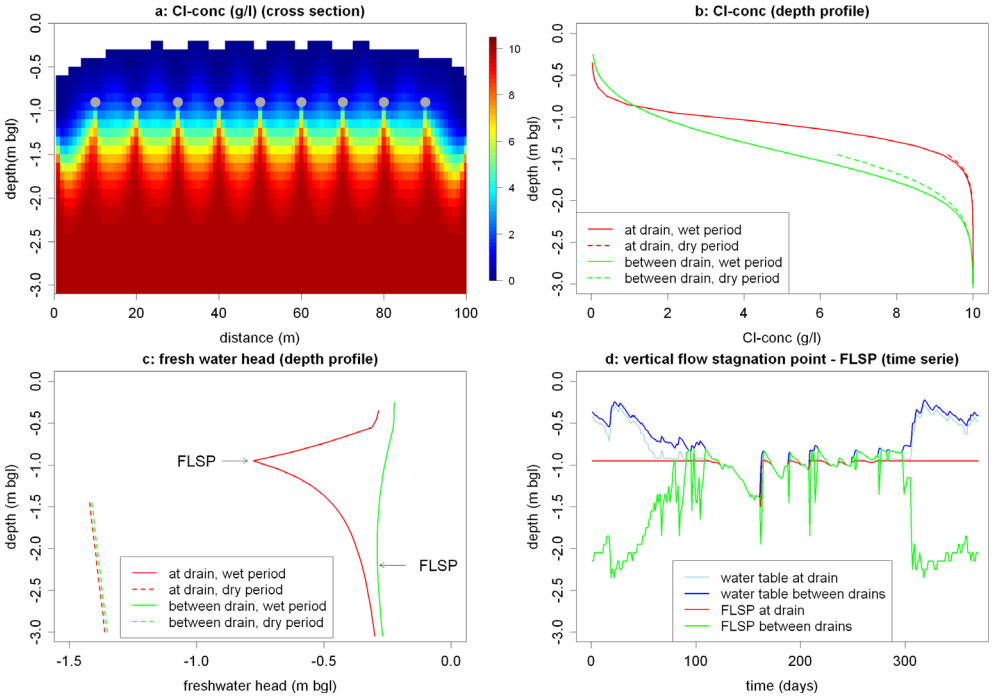

Fig. 5.11. Model results of the reference 2D-model. (a) Cl-concentration in cross-section between two ditches (wet period). (b) Cl-conc. – depth profile for a location at and between drains (wet and dry period). (c) Fresh-water head depth profile for location at and between drains (wet and dry period). (d) Time series of vertical flow stagnation point (FLSP) and the water table elevation for a location at and between drains.

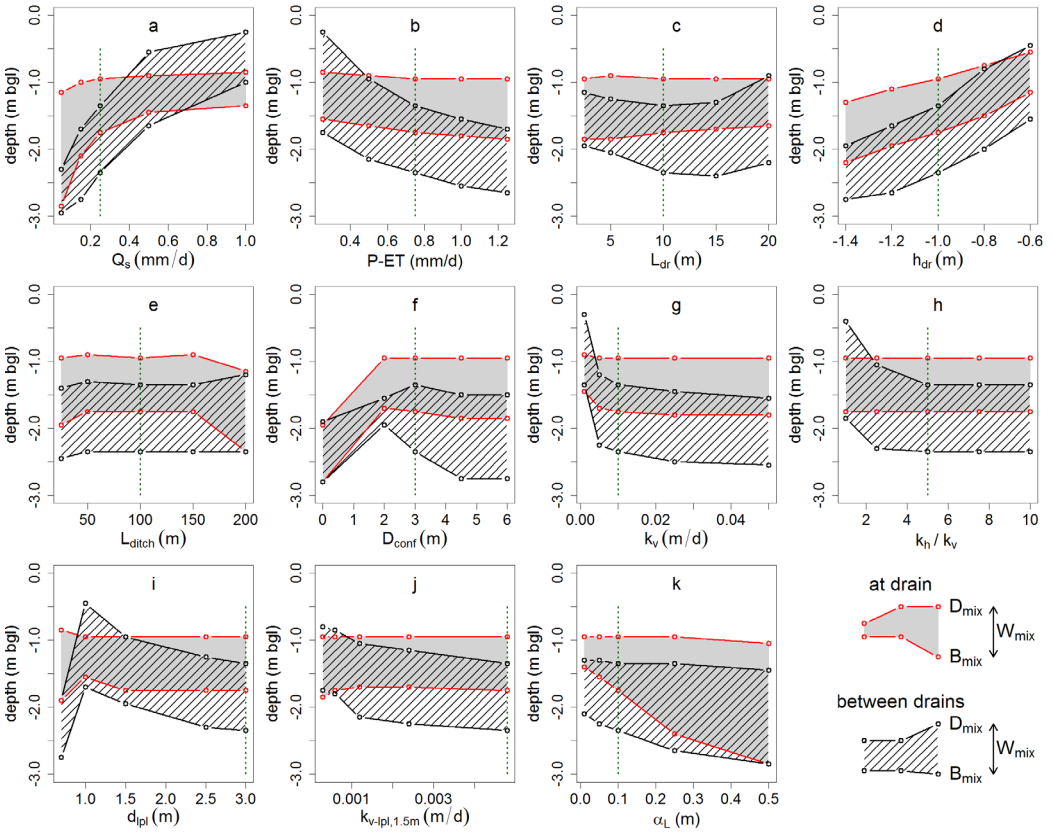

Fig. 5.12. Results of the sensitivity analysis for the 11 most sensitive parameters for lens characteristics D_{mix}, B_{mix} and W_{mix} (effect > 0.1m). The x-axis gives the parameter values of the reference model and the four sensitivity models; the y-axis gives the position of D_{mix} and B_{mix} for the different models, for a location at a drain and between two drains. The green dotted line indicates the position of the reference model.

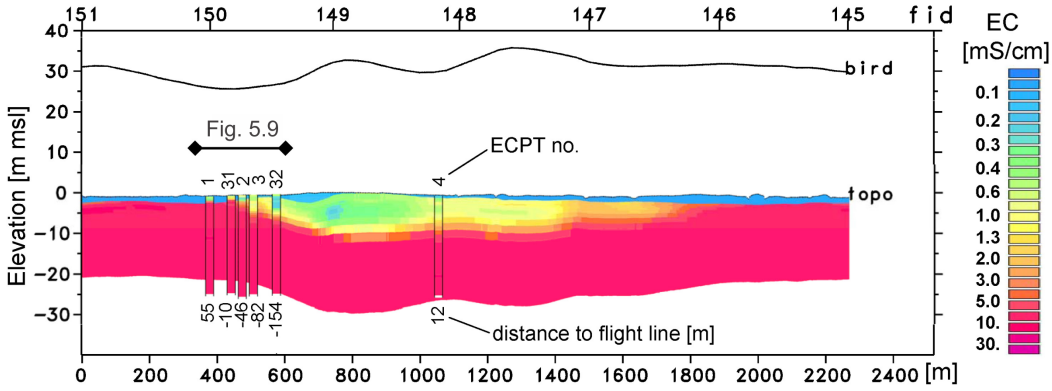

Fig. 5.13. Cross-section showing the electrical conductivity of smooth 15-layer HEM inversion models along a west-east flight line and nearby ECPT measurements (for location see Fig. 5.14).

5.4.3 Spatial variation of rainwater lens thickness: HEM results

The HEM data inverted to layered-earth resistivity-depth models reveal the spatial distribution of the electrical conductivity down to depths of about 20-30 m in the lowlands and of more than 60 m in the dune area. Conductivity contrast of fresh and saline groundwater dominated the inverted HEM models rather than differences in lithology. 2D cross-sections were produced for all survey lines. As an example, part of a west-east flight line is shown in Fig. 5.13 crossing the agricultural field of site 11 and the sandy creek ridge. The results of the smooth multi-layer HEM models agreed very well with nearby ECPT measurements, which are plotted as coloured columns in the cross-section. Only ECPTs having a horizontal distance of less than the maximum footprint size of the HEM measurements (150 m) were projected to the flight-line. Fig. 5.7 shows a comparison of six ECPT soundings and corresponding HEM models at site 11 (ECPT 31, 2, 32, 4) and close to the dune area (ECPT 12 and 13).

The analysis of the mixing zone derived from the detailed TEC-probe and ECPT data showed that the depth of the centre of the mixing zone, D_{mix}, is a consistent and easy to determine parameter to characterize the rainwater lens. We used D_{mix} to indicate the thickness of the rainwater lens which also includes the unsaturated zone. To derive D_{mix} from the HEM data, we determined the depth of the strongest vertical conductivity gradient within a resistivity range of 2-5 Ωm. This was done for the 84,300 1D resistivity-depth inversion models and interpolated to a 50 m grid size map (Fig. 5.14) representing D_{mix} for the entire airborne survey area. In a large part of the survey area (> 50%) the mapped rainwater lens was thinner than 2 m. Thicker rain water lenses occurred in the eastern part of the survey area (D_{mix} = 5-10 m BGL), close to site 11 and the adjacent fossil sandy creek (D_{mix} = 8-20 m BGL) and, of course, in the dune area (D_{mix} > 20 m BGL).

The HEM-survey on the island of Schouwen-Duivenland made it possible to analyze the spatial variation of rainwater lenses by correlating D_{mix} derived from the 84,300 HEM-models, to geographically varying features. The thickness of the rainwater lens, D_{mix}, is clearly related to surface elevation (Fig. 5.15a) and to seepage and infiltration fluxes (Fig. 5.15b). Note that surface elevation and seepage/infiltration flux are strongly correlated; seepage occurs in low-lying polders below sea level and infiltration occurs in dunes, sandy creek ridges and polder areas above sea level (compare Fig. 5.2c with 5.2e). The HEM-results showed that rainwater lenses in low-lying seepage areas were, on average, 2 m thick (i.e. from ground level to D_{mix} including unsaturated zone). The thinnest rainwater lenses were found in areas below -2 m MSL. There was a sharp increase in thickness when vertical flow changed from seepage to infiltration (Fig. 5.15b). This shows that vertical flow (seepage or infiltration and fluxes) is the mechanism that controls the development of rainwater lenses.

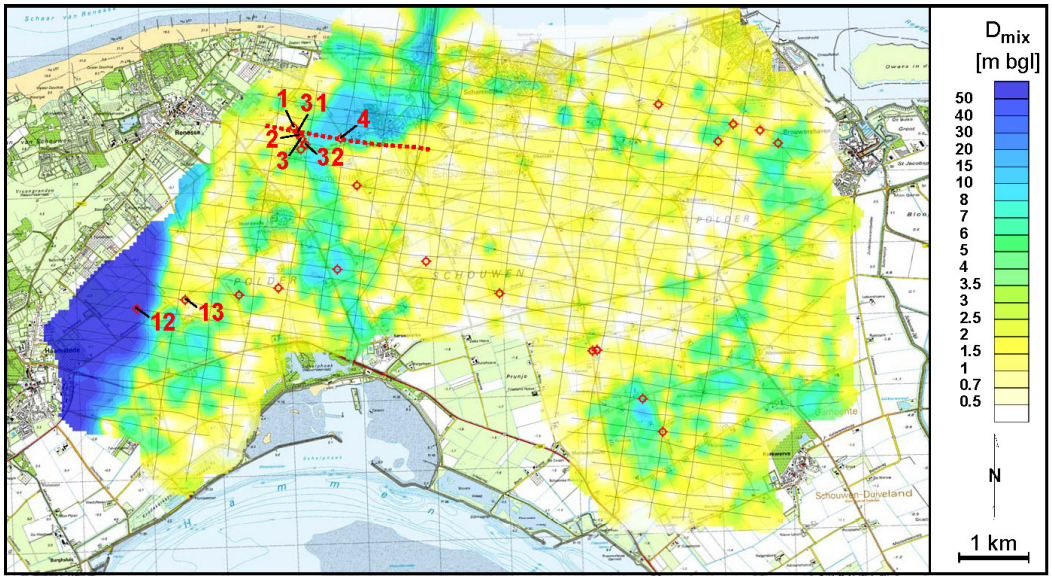

Fig. 5.14. Estimated depth D_{mix} (average position of the mixing zone in m below ground level) derived from HEM inversion models. All flight lines (black lines) and the location of the ECPTs (red circles, those shown in Figs. 5.7 and 5.13 are numbered) are plotted on top of the depth map. The red dots indicate the position of the cross-section shown in Fig. 5.13.

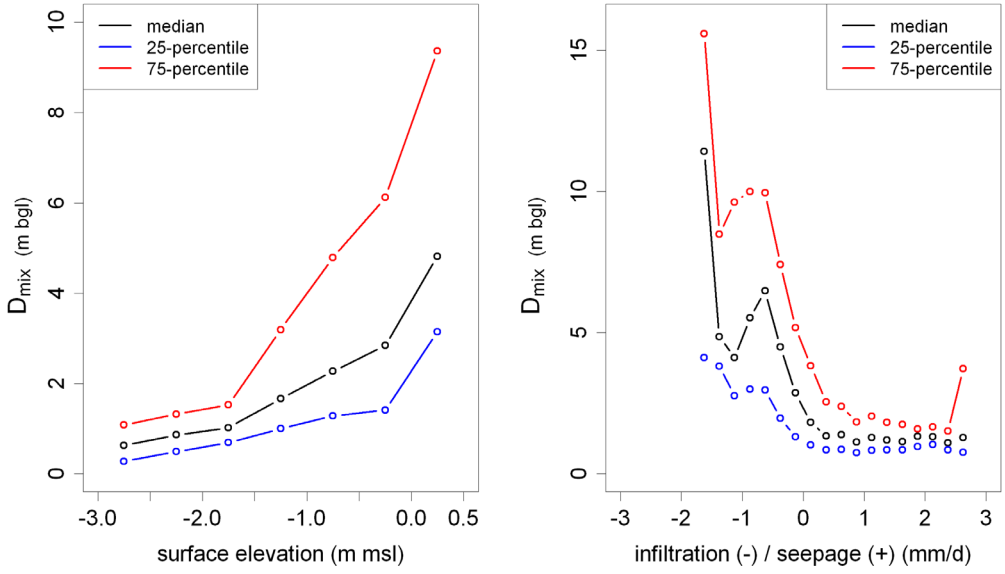

Fig. 5.15. Relation of D_{mix} derived from 84,300 HEM-measurements with (a) Surface elevation (m MSL) and (b) Infiltration and seepage flux (mm/d). The 25-, 50- and 75-percentile of D_{mix} was determined and plotted for different classes of surface elevation and flux (dots represent middle of class).

5.4.4 Vertical flow stagnation point

Both the freshwater head and salinity measurements at site 11 (Fig. 5.9) and the correlation of D_{mix} with seepage/infiltration flux (Fig. 5.15) show that rainwater lens thickness is mainly the result of the vertical head gradient and vertical flow. To extend the understanding of the role of vertical flow on rainwater lens characteristics, we studied the vertical head and flux profiles of the 2D-model results in more detail. Here we introduce the vertical flow stagnation point (FLSP), which is the point below which the flow switches from having a vertical downward to a vertical upward component. This point is best illustrated with a freshwater head depth profile at a drain, see Fig. 5.11c. Drainage of groundwater causes a dip of the hydraulic head at the drains, which results in groundwater flow towards the drain from both above and below. As variable density flow is driven by both head gradients and density differences, we determined FLSP from the calculated vertical fluxes directly rather than deriving it from the calculated freshwater head gradients. Fig. 5.11d shows the daily FLSP for a period of 1 year for the reference model. At the drains, the FLSP was always at drainage level, except in the periods when the water table dropped below the drains. Then the vertical flow component was upwards for the entire saturated profile and the FLSP equalled the water table. The FLSP between the drains was much more variable with time than the FLSP at the drains (Fig. 5.11d). The maximum depth of FLSP between the drains was 2.35 m, which occurred when the water table was at its maximum and causing the largest downward head gradient. When the water table dropped, the FLSP moved to shallower depth and upward flow became more important. During the dry season, when the water table dropped below the drains, there was only upward groundwater flow and the FLSP was equal to the water table. The temporal variation of FLSP was driven by water table fluctuations resulting from the daily variation of precipitation and evapotranspiration and intense drainage of groundwater.

The FLSP time series (one year of daily fluctuating FLSPs) were determined for all 76 sensitivity models, for which the parameters are listed in Table 5.2 as well as the correlation with the lens characteristics D_{mix}, B_{mix} and W_{mix}. For nearly all sensitivity cases, the FLSP at the drains was situated at drainage level during periods when the water table was above drainage level. The depth of the centre of the mixing zone, $D_{mix,}$, at the drain was also situated at drainage level in 90% of the sensitivity cases. Although D_{mix} was fixed at the drains, D_{mix} between the drains was much more variable between the different sensitivity cases (see Fig. 5.12) and other parameters than drainage level (h_{dr}) played an important role. For every sensitivity model, the average depth of the FLSP between the drains was determined from the FLSP-time series and plotted against D_{mix} (Fig. 5.16a). The scatter plot shows that D_{mix} between the drains had a strong linear and positive correlation with the annual average position of the FLSP between the drains (R^2=0.91). It is remarkable that the large variation of FLSP between the drains during the year resulted in a fairly steady depth of D_{mix} (maximum annual amplitude = 0.1 m). This can be explained by the fact that vertical flow velocities were very small (maximum of 1.2 mm d^{-1}) compared to the change in position of the FLSP (annual amplitude = 1.5 m). Note that the upward or downward movement of a water particle is not exactly vertical because its flow path is the result of both the vertical and horizontal flow components. The calculated horizontal flow velocities were on average 1.7 times larger than the vertical flow velocities.

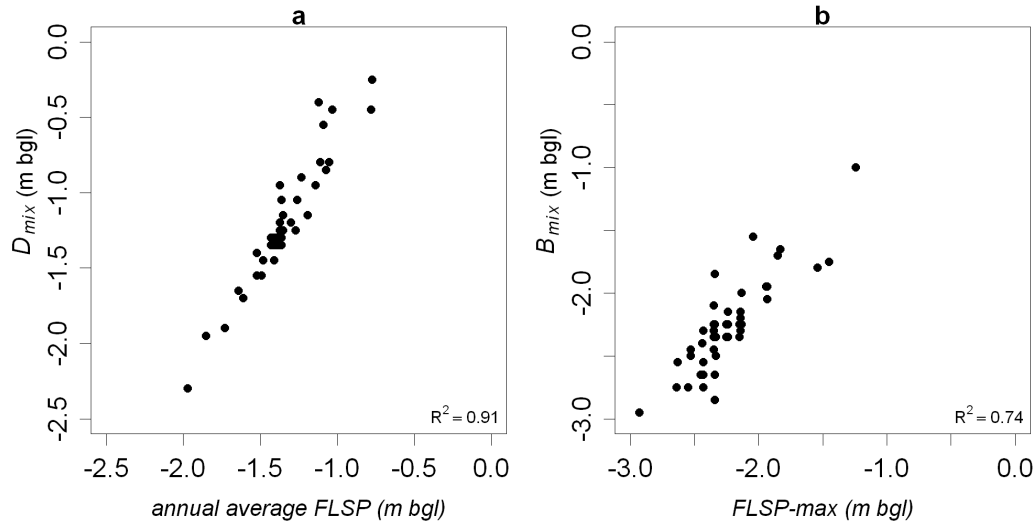

Fig. 5.16 . Scatter diagrams of calculated vertical flow stagnation points (FLSP) and lens characteristics D_{mix} and B_{mix} derived from the results of the different sensitivity models (see Table 5.2). The FLSP, D_{mix}, and B_{mix} are derived for a location between two drains.

The bottom of the mixing zone B_{mix} between the drains corresponded approximately with the maximum depth of FLSP which is the maximum depth where downward flow occurred during a year (Fig. 5.16b). Below FLSP-max the vertical flow direction is always upward and advective mixing is not possible. Mixing below FLSP-max between the drains can therefore only be the result of molecular diffusion. However, at the drains, B_{mix} was always below drainage depth and in most cases even 0.5 to 1.0 m deeper than FLSP-max at the drains. Additionally, B_{mix} at the drains was correlated with B_{mix} between the drains (R^2=0.46), which indicates that mixing below the drains occurred by upward flow of groundwater that was infiltrated between the drains. The results show that the constantly alternating upward and downward flow at low velocities in the confining layer indicated by the varying position of the FLSP is the main mechanism of mixing between rainwater and saline seepage and determines the position and extent of the mixing zone.

5.4.5 Controlling factors: hydrogeology, drainage, seepage flux and recharge

Our measurements show that the mixing of the upward flowing saline groundwater with infiltrating rainwater occurred in the confining top layer. This was caused by the permanently higher freshwater heads in the upper aquifer compared to the lower part of the confining top layer. FLSP-max was therefore always situated within the confining layer and consequently also B_{mix}. Given that lenses in seepage areas develop within the confining layer, the heterogeneity of the confining layer may have an additional effect on the lens characteristics. The sequence of confining sediments with different vertical hydraulic conductivities determines the freshwater head change with depth within the confining layer. When these freshwater head gradients are large enough, they influence the FLSPs and therefore D_{mix} and B_{mix}. The sensitivity analysis showed that a 0.2 m thick low permeable layer (k_v = 10^{-3} m d^{-1}) within the confining layer (k_v = 10^{-2} m d^{-1}) had a significant impact when it

was put in the upper 2 m of the confining layer (Fig. 5.12i, parameter d_{lpl}). When the low permeable layer was situated above the drains, drainage of groundwater was much more difficult, resulting in higher water tables, deeper FLSPs and thicker rainwater lenses between the drains. A low permeable layer situated below the drains hinders the further downward flow between the drains, resulting in shallower FLSPs and thinner rainwater lenses between the drains (Fig. 5.12i).

The large impact of drainage depth on D_{mix} and B_{mix} was shown by our field measurements (Fig. 5.8) and model calculations (Fig 5.11 and Fig. 5.12, h_{dr}). At the drains, upconing of saline groundwater was observed (Fig. 5.8) and calculated (Fig 5.11a) and D_{mix} was fixed at drainage level. Besides the drainage depth, the magnitude of incoming fluxes, both from above (recharge) and below (seepage), had a large impact on lens characteristics (Fig. 5.12a-b, Q_s and *P-ET*). More recharge led to higher water tables and consequently to deeper FLSPs and therefore to thicker rainwater lenses. Thinner lenses are calculated with larger upward-seepage fluxes, which cause the FLSPs to move upwards. The dominant role of recharge and upward-seepage makes the shallow rainwater lenses very vulnerable to climate change and sea level rise. The Royal Netherlands Meteorological Institute (KNMI) formulated four different climate scenarios which are equally likely to occur (Van den Hurk *et al*., 2006). The W+ climate scenario is the driest (2.5% reduction of precipitation and 7.5% increase of evapotranspiration) and has the largest expected sea level rise of 0.85 m by the year 2100. A sea level rise would cause an increase of the hydraulic head in the aquifers, which would result in an increase of seepage flux. However, this effect of sea level rise decreases rapidly with the distance from the Dutch coast as concluded by Oude Essink *et al*. (2010). Both sea level rise and a reduction of the precipitation surplus may lead to thinner rainwater lenses. Since drainage depth is another important factor that determines rainwater lens thickness, adapting the tile drainage systems may effectively reduce the negative consequences of climate change and sea level rise. Thus, a better understanding of rainwater lenses could lead to practical measures for maintaining agriculture water storage systems.

5.4.6 Head-driven versus density-driven flow

The sensitivity analysis showed that the salinity of the upward-seeping groundwater does not have a significant influence on lens characteristics. We varied the salinity of the seepage water between freshwater and seawater (Table 5.2) and effects on D_{mix}, B_{mix} and W_{mix} were smaller than 0.1m. Therefore we suggest that density-driven flow is of minor importance and lens characteristics in the seepage areas are principally controlled by head gradients. Simmons (2005) stated that even small concentration differences may lead to density-driven flow gradients equal to typical field-scale hydraulic gradients. Whether density-driven or head-driven flow is the dominant process is dependent on a complex interplay between fluid and soil properties, and the competing demands of both free and forced convection and dispersion. Our proposition that head-driven flow dominates the rainwater lens development in areas with saline seepage is supported by our different observations. Firstly, in seepage areas the hydraulic head in the upper aquifer was permanently higher than heads in the confining layer. This prevented the water from infiltrating to depths below the bottom of the confining layer. Secondly, large head gradients typically developed in these shallow groundwater systems, strongly influenced by intensive drainage and daily changing

recharge. The vertical freshwater head gradients are generally much larger than the relative density difference that accounts for the buoyancy effect and therefore dominates vertical flow. Besides the large head gradients, the temporal variation of the FLSP played an important role. For depths above B_{mix}, the vertical flow direction changed throughout the year. During downward flow, the density-driven flow strengthened the head-driven flow of saline groundwater whereas during upward flow the density-driven flow opposed the head-driven flow. The net effect of density-driven flow was diminished by this constantly changing vertical flow direction.

In contrast to the quick response of the intensively drained groundwater systems, there are the much slower responding groundwater systems where BGH-lenses develop; these slower systems have large drainage distances and no upward flow of saline water due to elevation like the dunes. The precipitation surplus is not drained but fully used for the recharge of the groundwater system. Under a relatively constant recharge regime, a gradual downward head gradient causes the downward flow of rainwater to much greater depths. In homogeneous aquifers, the vertical downward flow is then only limited by the buoyancy force of the surrounding saline groundwater and its density determines lens thickness. These systems build up much larger lenses than the head-driven flow in the intensively drained seepage areas. This difference in the lens developing mechanisms explains the sudden increase in lens thickness shown in Fig. 5.15b when moving from a seepage situation to one of infiltration.

5.5 Conclusions

We determined the main characteristics and spatial variability of shallow rainwater lenses in areas with saline seepage and the mechanisms controlling them. Our findings are based on different types of field measurements and detailed numerical groundwater models applied in the south-western delta of the Netherlands. We observed a gradual mixing zone between infiltrating fresh rainwater and upward-flowing saline groundwater. Detailed measurements at point scale (groundwater sampling, TEC-probe, ECPT) were needed to determine the precise form of the mixing zone and to fully characterize the rainwater lenses. The smooth curved mixing zone was best characterized by the depth of its centre D_{mix}, and by the bottom of the mixing zone B_{mix}, where the salinity was equal to that of the seepage water. We were able to extrapolate these lens characteristics obtained by our point measurements to agricultural field scale using surface geophysics (CVES, EM31), and even to a larger area (56 km^2) at regional scale using helicopter-borne electromagnetic measurements (HEM). In the seepage areas, the centre of the mixing zone D_{mix} occurred at very shallow depth, on average 1.5 to 2 m below ground level, and the bottom, B_{mix}, occurred no deeper than 5.5 m, always within the confining layer. Below this mixing zone, the salinity stayed relatively constant until at least 25 m depth, with chloride concentrations of 10 to 16 g L^{-1}. Since the mixing zone occurs at shallow depth and most rainwater lenses lack fresh groundwater, its position and width is of great importance for a sufficient supply of freshwater for crop growth. Capillary rise of saline groundwater is very likely to occur in the present situation, possibly causing damage to crops.

Head-driven vertical flow dominates the rainwater lens formation in areas with saline seepage in two ways at different scales. A regionally driven upward groundwater flow from the upper aquifer into the confining layer prevents the rainwater from infiltrating to depths

below the bottom of the confining layer. This explains the limited size of the lenses. Mixing between rainwater and saline seepage water therefore always occurs within the confining layer driven by large vertical head gradients at a local scale. These head gradients in the confining layer constantly change due to the interplay of upward seepage, variable recharge and drainage of groundwater resulting in alternating vertical flow directions. The constantly alternating upward and downward flow at low velocities in the confining layer is the main mechanism of mixing and determines the position and dimensions of the lens. Whether a water particle is flowing upward or downward is indicated by the position of the vertical flow stagnation point (FLSP) which is the depth where the downward flow component meets the upward flow component. The annual average position of the FLSP determines the position of the centre of the mixing zone D_{mix} and the maximum depth of the FLSP determines the bottom of mixing zone B_{mix}. Recharge, seepage flux, and drainage depth are the controlling factors. Unlike rainwater lenses in seepage areas, the vertical downward flow of rainwater in the infiltration areas is only limited by the buoyancy force of the surrounding saline groundwater. This leads to much thicker rainwater lenses, varying from 5 to 15 m thick lenses in the sandy creek ridges to 100 m thick lenses in the dunes.

This study provides information on rainwater lens characteristics and formation mechanism for rain-fed coastal lowlands below sea level with upward saline seepage into a confining top layer and intense drainage of shallow groundwater. In these deltaic areas, freshwater availability is often limited to shallow rainwater lenses which are vulnerable to climate change and sea level rise. Our findings may help to formulate effective measures such as adapting tile drainage systems to compensate the negative consequences of these future threats. As density differences did not influence lens formation in areas with saline seepage, our findings may also be applicable to fresh groundwater systems. Rainwater lenses in brook valleys and wet meadows with upward groundwater seepage may limit the development of groundwater-dependent ecosystems. The great advantage of studying rainwater lens formation in saline seepage areas arises from the large salinity contrast between rainwater and groundwater, which is easy to measure, even by non-invasive geophysical methods.

Chapter 6

Rainwater lens dynamics and mixing between infiltrating rainwater and upward saline groundwater seepage beneath a tile-drained agricultural field

Perry de Louw, Sara Eeman, Esther Vermue, Gualbert Oude Essink, Vincent Post
Published in Journal of Hydrology 501, 133-145, 2013

Abstract

Thin rainwater lenses (RW-lenses) near the land surface are often the only source of freshwater in agricultural areas with regionally-extensive brackish to saline groundwater. The seasonal and inter-annual dynamics of these lenses are poorly known. Here this knowledge gap is addressed by investigating the transient flow and mixing processes in RW-lenses beneath two tile-drained agricultural fields in the Netherlands. Evidence of RW-lens dynamics was systematically collected by monthly ground- and soil water sampling, in combination with daily observations of water table elevation, drain tile discharge and drain water salinity. Based on these data, and numerical modeling of the key lens characteristics, a conceptual model of seasonal lens dynamics is presented. It is found that variations in the position of the mixing zone and mixing zone salinities are small and vary on a seasonal timescale, which is attributed to the slow transient oscillatory flow regime in the deepest part of the lens. The flow and mixing processes are faster near the water table, which responds to recharge and evapotranspiration at a timescale less than a day. Variations of drain tile discharge and drain water salinity are also very dynamic as they respond to individual rain events. Salinities of soil water can become significantly higher than in the groundwater. This is attributed to the combined effect of capillary rise of saline groundwater during dry periods and incomplete flushing by infiltrating freshwater due to preferential flow through cracks in the soil. The results of this study are the key to understanding the potential impact of future climate change and to designing effective mitigating measures such as adapting tile-drainage systems to ensure the future availability of freshwater for agriculture.

6.1 Introduction

In many coastal areas worldwide, groundwater is brackish to saline because of the combined effects of seawater intrusion and marine transgressions (e.g. Post and Abarca, 2010; Werner *et al*., 2013). In such areas, freshwater lenses recharged by rainwater are often the only water resource available for agriculture and drinking water. The best-known type of freshwater lens is the Badon Ghijben-Herzberg (BGH) lens (Drabbe and Badon Ghijben, 1889; Herzberg, 1901), which develops in areas with saline groundwater where recharge creates an elevated water table in areas like dune belts along the coast (e.g. Stuyfzand, 1993; Vandenbohede *et al*., 2008), below islands (e.g. Chidley and Lloyd, 1977; Underwood *et al*., 1992), and even in inland desert areas (e.g. Kwarteng *et al*., 2000).

Another type of a rainwater-fed lens forms in areas where saline groundwater migrates to the surface by upward groundwater flow (referred to here as seepage), such as the coastal area of the Netherlands

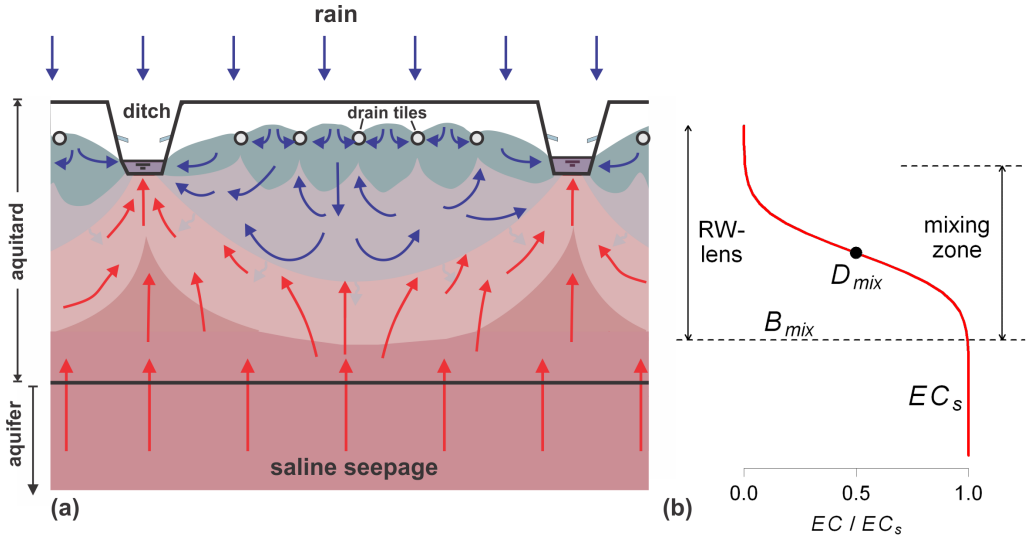

Fig. 6.1. (a) Schematic cross-section visualizing the conceptual model of a RW-lens in an area with upward seepage of saline groundwater. (b) Vertical profile of the electrical conductivity (EC) of groundwater at an arbitrary point in the RW-lens. The vertical extent of the RW-lens at any point is from the base of mixing zone (B_{mix}) to the water table. The depth of the centre of the mixing zone (D_{mix}) is at the point where the EC is 50% of the seepage water salinity (EC_s).

(De Louw *et al*., 2011; Velstra *et al*., 2011) and Belgium (Vandenbohede *et al*., 2010) and the Po-delta, Italy (Antonellini *et al*., 2008). They differ from BGH-lenses in that the upward moving saline groundwater limits the penetration depth of rainwater, and thus the volume of the freshwater lens (De Louw *et al*., 2011; Eeman *et al*., 2011). Field measurements by De Louw *et al*. (2011) in the south-western delta of the Netherlands showed that the transition zone between infiltrated rainwater and upward seeping saline groundwater occurs within 2 meters below ground level (BGL) and that nearly all mapped lenses lacked truly fresh groundwater (chloride concentration < 0.3 g L^{-1}). These lenses are the object of the current study, and are referred to as RW-lenses. For the purpose of this study, the vertical extent of the RW-lens is bounded by the water table and the depth below which no rainwater penetrates (B_{mix}, which is the depth at which the salinity equals the salinity of regional groundwater, Fig. 6.1). With this definition, the RW-lens is not purely a freshwater lens, and salinities within the RW-lens vary both in space and in time.

The dynamic behaviour of salinities within RW-lenses and the soil moisture in the unsaturated zone above them is of great importance from an agricultural perspective. It is expected that lens thickness and mixing zone properties are not steady state and will respond to temporal recharge variations at intra- and inter-annual timescales, as well as to seepage variations on a longer timescale. Due to their limited size and vicinity to the land surface, RW-lenses are vulnerable to changing precipitation and evapotranspiration (which control recharge) patterns. During dry periods, saline groundwater can reach the root zone via capillary rise, affecting crop growth (Katerji *et al*., 2003; Rozema and Flowers, 2008). Besides recharge and seepage, another important factor that controls the size of the RW-lens is tile drainage (De Louw *et al*., 2011; Velstra *et al*., 2011). Adapting drainage systems has been proposed as an effective water management strategy to mitigate the predicted adverse consequences of increased drought and sea level rise (e.g. Poulter *et al*., 2008). The latter may enhance upward seepage rates (Maas, 2007; De

Louw *et al*., 2011; Eeman *et al*., 2011, 2012), thus negatively impacting the freshwater volume stored in RW-lenses.

Successful implementation of any measure to make the RW-lenses more resilient to future climate change requires knowledge of their dynamic behaviour. So far, research into lens dynamics has mainly been focused on BGH-freshwater lenses (e.g. Drabbe and Badon Ghijben 1889; Herzberg, 1901; Meinardi, 1983; Underwood *et al*., 1992; Collins and Easley, 1999; Bakker, 2000; Stoeckl and Houben, 2012). Stoeckl and Houben (2012) examined the development and flow dynamics of freshwater lenses by physical experiments on laboratory scale. Underwood *et al*. (1992) examined the dynamic behavior of the mixing zone of a BGH-lens of a generalized atoll groundwater system and found that mixing is controlled by oscillating vertical flow due to tidal fluctuation, while recharge determines lens thickness. On Jeju Island (Korea), measurements showed small tidally-induced variations, but no long-term seasonal variation of the fresh-salt water interface (Kim *et al*., 2006). In BGH-lenses the response to recharge variations is in the order of decades (e.g. Vaeret *et al*., 2011; Oude Essink, 1996). Rotzoll *et al*. (2010) observed thinning rates of 0.5 to 1.0 m y^{-1} in thick freshwater lenses in Hawaii due to long term groundwater withdrawal and reduced recharge.

In the absence of long-term field data for RW-lenses, their response at intra-annual and inter-annual timescales remains poorly characterized and understood. De Louw *et al*. (2011) reported that, since temporal variations were not measured, they could not conclusively determine if the noted absence of fresh groundwater was a transient or a permanent feature of the RW lens. Velstra *et al*. (2011) used DC resistivity measurements to delineate RW-lenses in the northern coastal area of the Netherlands and found seasonal variations in lens-thickness. However, the use of geophysics to monitor temporal variations of shallow subsurface resistivities is difficult due to the limited resolution, impact of unsaturated zone conditions and non-unique interpretation of the measurement data (Goes *et al*., 2009). Recently, Eeman *et al*. (2012) developed a theoretical relation between lens thickness variations and sinusoidal recharge variations. Their study showed how temporal thickness variations of a RW-lens increased with increasing recharge amplitude and with decreasing recharge frequency including damping and delay in the response of the lens, but the model was not corroborated with measured data. To understand the complex RW-lens field behaviour, direct measurements of groundwater and soil water salinities are much needed.

The intent of the present study was to address the knowledge gap that exists on the temporal dynamics of RW-lenses. To this end, a comprehensive set of data was collected at two tile-drained agricultural fields in the Netherlands. The data consisted of groundwater and soil water salinities, groundwater levels, drain tile discharge and drain water salinity, precipitation and evapotranspiration. The main objectives were (i) to obtain direct, field-based evidence of RW-lens dynamics, and (ii) to quantify the temporal variations of the flow and mixing processes within the RW-lens. The main focus was on the control of recharge and tile drainage. A numerical flow and transport model was used to complement the collected field data and to support the dev elopment of a conceptual model of RW-lens dynamics.

6.2 Study area

Two of the 27 agricultural sites examined by De Louw *et al*. (2011) were selected to monitor the RW-lens dynamics and mixing behaviour between March 2009 and January 2011. These sites were referred to as sites 11 and 26 in De Louw *et al*. (2011) but here as site A and B, respectively. These sites were selected primarily because of their representative hydrogeological conditions and rainwater lens characteristics, which are typical for the saline seepage areas of the south-western part of the Netherlands (De Louw *et al*., 2011). Practical considerations, such as accessibility of the sites and a nearby electricity supply, also played a role. Monitoring sites A (latitude 51°42′04′′N, longitude 03°51′26′′E) and B (latitude 51°43′44′′N, longitude 03°47′57′′E) are both situated on the Schouwen-Duivenland island in the south-western part of the Netherlands (Fig. 6.2a). The mean annual precipitation and potential Makkink (1957) evapotranspiration for the period 1980-2010 are 815 mm and 613 mm, respectively (data from the Royal Netherlands Meteorological Institute KNMI). Groundwater is predominantly saline, and originates from Holocene transgressions during the periods 7500 BP to 5000 BP and 350 AD to 1000 AD (Vos and Zeiler, 2008; Post *et al*., 2003). Upward seepage of saline groundwater occurs where the land surface lies below mean sea level (MSL).

Site A is a 300 m long agricultural field located at the transition from a former salt marsh to a tidal creek paleo-channel (Fig. 6.2c). Due to differential subsidence by sediment compaction, the land surface elevation of the paleo-channel (-0.2 m MSL) is presently above that of the salt marsh sediments (-0.7 m MSL). The field is bordered by ditches with a surface water level which is maintained at an depth of 1.3 m BGL, and the field is tile-drained at a depth of 1.0 m BGL with a horizontal drain separation of 10 m. Fine-grained to medium coarse-grained sand is found between 2.5 m and 30 m BGL, which belongs to a regionally-extensive aquifer. The aquifer is confined by 2.5 m of heterogeneous low-permeability sediments comprised of peat, clay and sandy clay at the former salt marsh and sandy clay to clayey sand at the creek ridge (Fig. 6.2c). As freshwater head gradients between 1.5 m and 4 m depth were considerably larger than the relative density difference that accounts for the buoyancy effect, the vertical flow direction (but not the magnitude) can be inferred directly from the head measurements (Post *et al*., 2007). At the former salt marsh, the measured heads were permanently higher in the sandy aquifer at 4 m depth than at 1.5 m depth in the aquitard, resulting in a continuous upward groundwater flow (De Louw *et al*., 2011, Fig. 6.2c). At the creek ridge, the freshwater head was lower at 4 m depth than at 1.5 m depth, indicating downward flow. Due to these different vertical flow patterns, the RW lenses below the former salt marsh are thin ($1.5 < B_{mix} < 3$ m) compared to the creek ridge ($4 < B_{mix} <$ 10 m) (De Louw *et al*., 2011). Only the data collected in the former salt marsh zone with permanent upward seepage is presented in this paper.

Site B is located in a former salt marsh at an elevation of -2.0 m MSL and is bordered by a ditch with a surface water level maintained at 1.1 m BGL (Fig. 6.2d). Drain tiles with a length of ~80 m are located at a depth of 0.70 m BGL with a horizontal separation of 10 m. The upper 2.5 m of the subsoil consists of silty clay and a 0.10 - 0.15 cm thick peat layer at about 0.5 m depth. Between 3.0 m and 4.5 m BGL a sequence of clayey fine sand and sandy clay occurs. These low-permeability sediments form a semi-confining unit, below which the same regionally-extensive sandy aquifer as at site A is found. Head gradients indicate that permanent upward seepage occurs everywhere below the agricultural field, and the RW-lenses have a thickness between 1.5 and 2 m (de Louw *et al*., 2011). Shrinkage cracks in the clayey top soil were observed during the driest months of the year (May – October).

6.3 Methods

6.3.1 Monitoring network

The monitoring networks of site A and B consisted of measurement points at various distances from the northwestern (site A) and western (site B) ditch, at which time-series data of groundwater salinity, soil water salinity, water table elevation and hydraulic head were collected at different depths (Fig. 6.2c-d). The measurement points were located between two subsurface drain tiles, except for MP4 and MP5 of site B, which were positioned within 0.2 m of a drain tile to assess the effect of tile drainage (Fig. 6.2d).

At each measurement point a cluster of piezometers was installed (Fig. 6.2b). Each cluster consisted of 6 or 7 piezometers with 0.16 m long screens at depths (bottom of screen) of 0.8 m, 1.0 m, 1.3 m, 1.6 m, 2.0 m, 3.0 m and 4.0 m BGL. Piezometers with pre-fabricated bentonite plugs of the same diameter as the auger borehole were used to avoid preferential flow. The electrical conductivity (EC) of groundwater samples was measured in the field every month for a period of 22 months (March 2009 – December 2010). Before taking ground-

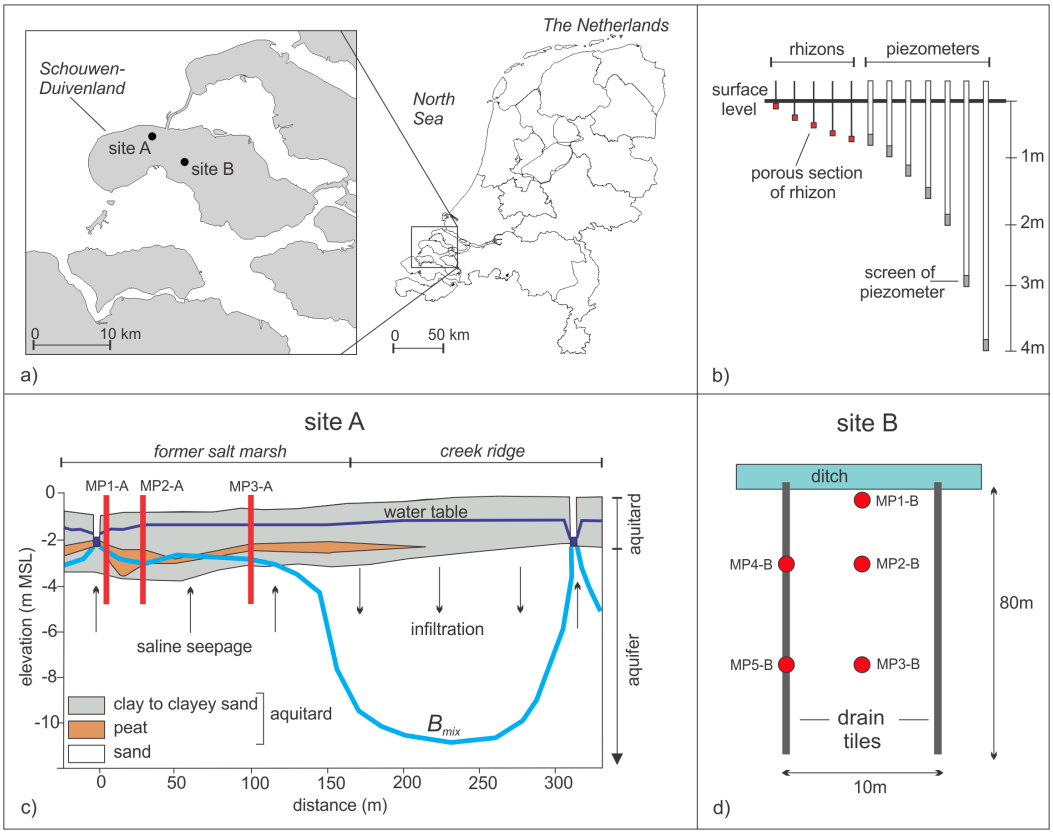

Fig. 6.2. (a) Map showing the location of study sites; (b) Schematic diagram showing the depths below ground surface of the rhizons and piezometers installed at each measurement point. The minimum and maximum distances between installed piezometers and rhizons of a measurement point are respectively 0.5 and 2.5 m; (c) Cross section at site A showing the geology, water table, vertical flow direction, the base of the RW-lens (B_{mix}, De Louw *et al.*, 2011) and the locations of the measurement points (red vertical lines); (d) Plan view of site B showing the location of the measurement points, the ditch and the drain tiles.

water samples for measurement, all the standing water was extracted from the piezometers. The piezometers were then allowed to re-fill with groundwater, which could take up to several hours due to the low permeability of the sediments. Errors in the order of 1-5% were associated with the EC measurements due to calibration difficulties in the field.

At each measurement point a cluster of soil moisture samplers (rhizons from Rhizosphere®) were installed to obtain soil water samples (Fig. 6.2b). The porous section of the rhizons had a diameter of 2.5 mm, a length of 100 mm and an average pore size of 2.5 μm. Each cluster contained 5 rhizons at depths (measured from the bottom of the porous section) of 0.15 m, 0.30 m, 0.45 m, 0.60 m and 0.75 m BGL. Suction was applied for at least 4 hours, after which the soil water was collected and the EC was measured in the field. When the amount of collected water was insufficient for an EC measurement, demineralized water was added and the measured EC was corrected for dilution. Soil water was sampled monthly on the same days as the groundwater was sampled, for a period of 17 months (July 2009 – December 2010).

At all measurement points, the hydraulic head at 4 m depth was recorded between March 2009 and January 2011 with a 1-hour frequency using data-logging pressure transducers (Schlumberger Water Service Divers®). Measured heads were converted to equivalent freshwater heads using the equations presented in Post *et al*. (2007). The water table elevation was inferred by measuring the water level in a piezometer with a 1.0 m long screen installed at a depth between 0.5 m and 1.5 m BGL.

At site B the drain tile discharge (Q_{drain}) and salinity (EC_{drain}) were measured from February 2010 to January 2011. The ends of 2 drain tiles (Fig. 6.2d) were connected and the discharge water was collected in a container (1 m × 0.6 m × 0.6 m). A known volume of water was pumped from the container automatically with a water-level-controlled-pump, and the number of pumping events per hour was recorded automatically. These recordings were multiplied by the pumping volume to obtain Q_{drain}. Water level fluctuations in the container were measured with a pressure transducer to verify the pumped volumes and the inferred Q_{drain}. The EC of the collected drain water was measured hourly in a small compartment installed in the pipe connecting the 2 drain tiles using a CTD-diver from Schlumberger Water Service®.

Precipitation (P) was measured at both sites with a tipping bucket rain gauge which reported rainfall at 1-hour intervals. Daily sums of the potential Makkink (1957) evapotranspiration (ET_p) were obtained from the nearest meteorological station of the KNMI (Wilhelminadorp, at 23 and 19 km from site A and B respectively). The obtained ET_p data is assumed to be representative for both field sites since the data of KNMI show that evapotranspiration patterns in the Netherlands are rather uniform (Sluijter *et al*., 2011). The retention characteristics of the soil were determined based on samples taken from 0.2 and 0.4 m BGL following the method described in Stolte (1997).

6.3.2 Numerical modeling

Spatial and temporal discretization

A RW-lens between two drain tiles under the field conditions of site B was simulated using the variable-density flow and transport code SEAWAT version 4 (Langevin *et al*., 2007). The setup of the model is shown in Fig. 6.3a. A cross-section perpendicular to the drain tiles was modeled, which had a length of 10 m and a thickness of 4.5 m, i.e., the thickness of the aquitard at site B. Drain tiles were implemented at the left and right boundaries at 0.7 m BGL

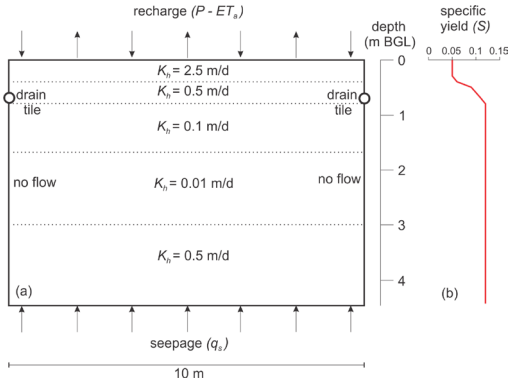

Fig. 6.3. (a) Schematic representation of the setup of the SEAWAT-model of the RW-lens between two drain tiles at site B. (b) The specific yield (S)-depth relation is derived from measured water table fluctuations and precipitation data using Eq. (6.1).

(Fig. 6.3) through the MODFLOW drain package (Harbaugh *et al*., 2000). The side boundaries were no-flow and no-solute flux boundaries. All inflows, i.e. recharge and vertical upward seepage, were applied at the top and bottom model boundaries, respectively. Water could leave the system by tile drainage and evapotranspiration. The mesh consisted of 40 columns of 0.25 m, 1 row of 0.25 m, and 45 layers of 0.1 m.

Simulation time spanned a period of 20 years. The same sequence of daily varying recharge, calculated using the meteorological data of 2009 and 2010 as detailed below, was repeated 10 times. After some initial simulations it was found that subdividing each stress period of 1 day into 20 flow time steps provided adequate simulation of the water table fluctuations. The flow time steps were automatically subdivided into a number of transport time steps according to the Courant number which was not allowed to be greater than 1 (Langevin *et al*., 2007).

Hydraulic parameters

The hydraulic parameters varied with depth based on the lithological strata that were encountered in the auger holes (Fig. 6.3a). The Dutch Geohydrological Information System (REGIS II, 2005) contains an extensive database of hydraulic conductivity measurements of soil materials in the south-western part of the Netherlands, and provides a range of horizontal (K_h) and vertical hydraulic conductivity (K_v) for each material type. The values of K_h and K_v that were adopted after calibration lie within the range of values in REGIS II. The hydraulic conductivity anisotropy factor (K_h / K_v) was set to 5 for the entire model (REGIS II, 2005; De Louw *et al*., 2011).

The moving water table was simulated through MODFLOW's cell wetting and drying option. With this option, model cells are made inactive when the head falls below the bottom of the cell. The cell becomes active again (that is, it rewets) once the head in the underlying cell rises above the cell's bottom (Harbaugh *et al*., 2000). For the highest active cells a specific yield (S) was used to account for storage changes due to a fluctuating water table, whereas a confined storage coefficient was used for all fully-saturated cells below. The use of a specific yield parameter to simulate water table fluctuations is a gross simplification of the conditions in the field, as it does not take into account the dynamic conditions in the unsaturated zone, which vary continuously as a result of rainfall, evapotranspiration and tile drainage. Different strategies have been proposed in the literature to account for this (e.g. Acharya *et al*., 2012), but here the following approach was used in this study to determine S. For selected periods throughout the year, S was quantified based on measured water table fluctuations and rainfall amounts using:

$$S = \frac{\sum_{t=1}^{n} P(t)}{(h(n)-h(1))} \qquad (6.1)$$

where h is the water table depth (m BGL), P is the daily rainfall (m d^{-1}), and n represents the number of days considered for the calculation. 12 periods of continuous increasing water levels ranging in

length between 2 and 5 days were selected. A relation was found between S calculated according to Eq. (6.1) and the water table depth, which was implemented in the model by letting the specific yield vary with depth (Fig. 6.3b). A constant value of S of 0.12 was applied at a depth below 0.7 m BGL. Above this depth, S decreases to 0.05 for the upper 0.3 m. The values of S were not adjusted during calibration.

Seepage

The vertical seepage flux from the aquifer into the aquitard was estimated based on measured data of site B for a period of 343 days (6 February 2010 - 13 January 2011), based on a salt mass balance for the tile drains:

$$\sum_{t=1}^{n} q_s(t) = \frac{\sum_{t=1}^{n} (Q_{drain}(t) \,.\, EC_{drain}(t))}{EC_s \,.\, A} \tag{6.2}$$

where n = 343, q_s is the vertical seepage flux (m d^{-1}), Q_{drain} is the measured drain tile discharge (m^3 d^{-1}), A is the surface area that contributes to Q_{drain} (m^2), and EC_{drain} and EC_s (mS cm^{-1}) denote the drain and seepage water salinity, respectively. This assumes that all dissolved salt that is discharged by the drain tiles originates from seepage and that no storage of salt occurs during the considered period. With these assumptions, the vertical seepage flux calculated according to Eq. (6.2) was q_s = 0.29 mm d^{-1}.

Recharge

To calculate the recharge, daily values of the actual evapotranspiration (ET_a) are required, which, in principle, could be based on reported values of the potential Makkink (1957) evapotranspiration ET_p for the KNMI meteorological station in Wilhelminadorp multiplied by a crop factor f. The value of f is unknown, and it was found that the model outcomes had a high sensitivity to this parameter. Therefore, the daily values of ET_a were determined based on water balance considerations instead. Using the same data as for the estimation of q_s, the total ET_a between day 1 and day 343 was first calculated according to:

$$\sum_{t=1}^{n} P(t) - \sum_{t=1}^{n} ET_a(t) + \sum_{t=1}^{n} q_s(t) = \sum_{t=1}^{n} \frac{Q_{drain}(t)}{A} \tag{6.3}$$

Eq. (6.3) was solved for $\sum_{t=1}^{n} ET_a(t)$ using measured values of P and Q_{drain}, and values of q_s based on Eq. (6.2). Subsequently, a surrogate crop factor f_s for the considered period was calculated by:

$$f_s = \frac{\sum_{t=1}^{n} ET_a(t)}{\sum_{t=1}^{n} ET_p(t)} \tag{6.4}$$

The calculated value of f_s was 0.69, and accounts for all processes that reduce ET_p, such as crop type, growth stage and plant stress due to limited soil moisture availability and the presence of salt in the root zone. Daily values of ET_a were then obtained by the multiplication of f_s with the daily values of ET_p. Finally,

daily recharge fluxes for the model were obtained by subtracting the daily values of ET_a from P. Daily recharge could be either positive or negative with this approach, and was applied to the highest active model cells.

Salt transport

Chloride (Cl) was used to represent salinity in the model and a linear relation between density (ρ) and Cl concentration was assumed. To compare the model-calculated concentrations with the field measurements, modeled Cl concentrations (g L^{-1}) were converted into ECs (mS cm^{-1}) using the linear relation derived from measured Cl - EC pairs of 79 groundwater samples taken at site A and B (De Louw *et al.*, 2011): EC = 2.78Cl + 0.45. Water entering across the bottom model boundary was assigned a Cl concentration of 12 g L^{-1} based on measured data. The same Cl concentration was used as the initial Cl concentration in all model cells, allowing a RW-lens to develop in the saline groundwater body.

The negative recharge that was applied in the model when $ET_a > P$ constitutes a sink for both water and solutes. Conceptually, negative recharge is considered to represent water loss from the saturated zone by capillary rise. In the field, depending on the salinity of groundwater at the water table, variable amounts of solutes are thereby moved into the unsaturated zone and temporarily stored. During recharge events, the solutes residing in the unsaturated zone are flushed. To replicate this behaviour in the model, a Cl concentration of 1.25 g L^{-1} was assigned to the water entering the system as recharge. This value was chosen such that the total salt mass leaving the model by capillary rise equaled the total salt mass entering the model by recharge.

Preliminary model runs showed that in order to reproduce the width of the mixing zone, longitudinal and transversal dispersivity values of 0.1 m and 0.01 m, respectively, were adequate. These values are commensurate with values adopted in numerous case studies in comparable settings (e.g. Stuyfzand, 1993; Lebbe, 1999; Van Meir, 2001; Oude Essink, 2001; Vandenbohede and Lebbe, 2007). The molecular diffusion coefficient for Cl in porous media was assumed to be $8.6 \cdot 10^{-5}$ m^2 d^{-1}.

Model calibration

The model was calibrated manually by optimizing the fit between the simulated and measured (i) salinity-depth profiles at and between the two drain tiles, (ii) daily observations of Q_{drain}, (iii) EC_{drain}, and (iv) water table elevation. The Nash-Sutcliffe coefficient (*NSC*, Nash and Sutcliffe, 1970) was used to quantitatively evaluate the dynamic model performance:

$$NSC = 1 - \frac{\sum_{t=1}^{n} (o_t - s_t)^2}{\sum_{t=1}^{n} (o_t - \bar{o})^2} \qquad (6.5)$$

in which o_t represents the observed and s_t the simulated value for day t, and $\bar{o}$ the mean of the observed values. The model output for the twentieth year (corresponding to the year 2010) was used to compare to the field data.

The outcomes of the calibrated model were used to analyze vertical flow velocities, transient path lines and travel times towards the drain tiles. The path lines and travel times were calculated by forward-tracking particles placed at the centre of every model cell, using the post-processing package MODPATH version 3 (Pollock, 1994).

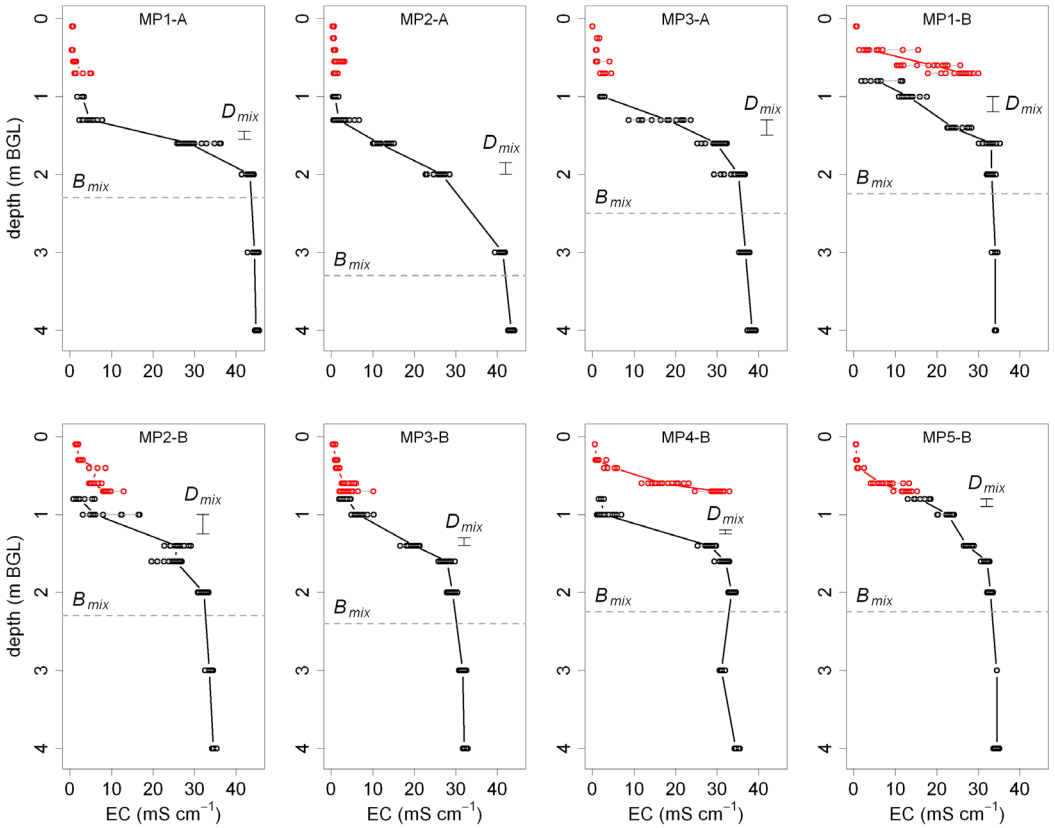

Fig. 6.4. Depth profiles of soil water salinity (in red) and groundwater salinity (in black) for sites A and B, based on monthly measurements during the period March 2009 – December 2010. The individual measurements are indicated by dots and median values are connected by a full line. The amplitude of the displacement of D_{mix} during the monitoring period and the depth of B_{mix} is indicated for each measurement point.

6.4 Field observations

6.4.1 Groundwater salinity and RW-lens thickness

Fig. 6.4 shows the salinity of the water in the saturated and unsaturated zone as a function of depth for all monitoring locations. The data show the existence of a 1 – 1.50 m wide mixing zone at a depth D_{mix} (= centre of mixing zone with a salinity half that of seepage water) of around 1.5 m BGL, and B_{mix} of around 2.2 m BGL. Only location MP2-A had a wider mixing zone (about 2 m), with B_{mix} at about 3.3 m BGL. Below the mixing zone the salinity stayed constant with depth until a depth of at least 25 m BGL (De Louw *et al.*, 2011). The salinity below B_{mix} is therefore considered to be representative of the salinity of the groundwater (EC_s) that constitutes the vertical seepage. At site A the average EC_s for MP1-A and MP2-A was 44 mS cm^{-1} (σ^2 = 0.88) while at site B the average EC_s for all five locations was 34 mS cm^{-1} (σ^2 = 1.12). The EC_s for MP3-A was lower (about 37 mS cm^{-1}) than for the other two locations at site A. This is probably due to the presence of the nearby thick freshwater lens that laterally mixes with the upward flowing saline groundwater in the aquifer (Fig. 6.2c).

The scatter of the data points in Fig. 6.4 shows that the temporal salinity variations are significantly larger around D_{mix} than around and below B_{mix}. The variations

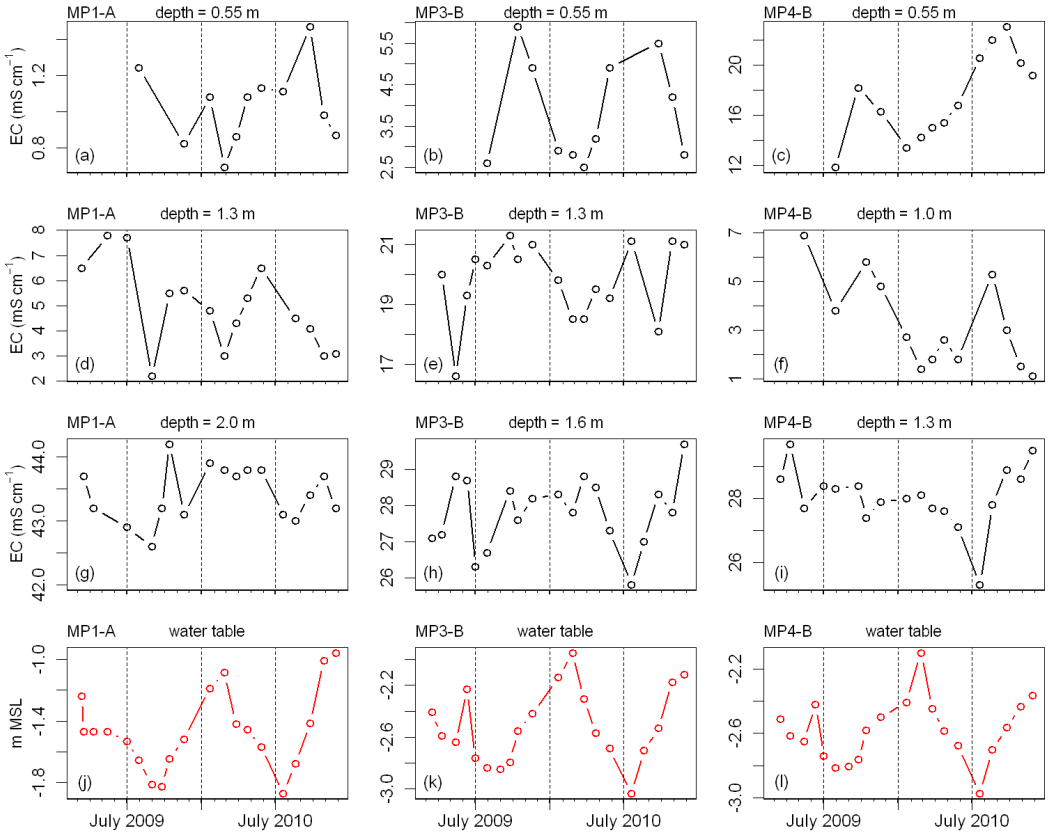

Fig. 6.5. Graphs showing time series for measurement points MP1-A (left panel), MP3-B (middle panel) and MP4-B (right panel) of (a-c) soil water EC at 0.55 m, (d-i) groundwater EC at two different depths and (j-l) water table elevation.

below B_{mix} were smaller than the accuracy of the EC-readings. A seasonal trend of groundwater salinity was found for some of the shallow screens: groundwater salinities decreased when the water table rose and vice-versa for sampling depths of 1.3 m and 1.6 m at MP1-A and MP2-A, 0.8 m, 1.0 m and 1.3 m at MP3-B and 1.0 m at MP4-B (Fig. 6.5d-f). Although salinity variations were less pronounced for larger depths, the data suggest that at sampling depths of 2 m and 3 m at MP1-A and MP2-A, 1.6 m and 2 m at MP3-B, and 1.3 m and 1.6 m at MP4-B, salinities show the opposite trend, i.e., they increased with increasing water level, and decreased with decreasing water level (Fig. 6.5g-i).

Despite the observed temporal salinity variations at each sampling depth, the mixing zone location and width remained almost unchanged (Fig. 6.4). The maximum displacement of D_{mix} of all salinity profiles was between 0.05 m and 0.25 m and B_{mix} stayed virtually at a fixed position throughout the entire 22-month measurement period (Fig. 6.4). Water table fluctuations, on the other hand, were highly dynamic, and changed in response to individual rainfall events as well as on a seasonal timescale (Fig. 6.6). As a result, the RW-lens thickness was highly dynamic as well, and varied by up to 1.2 m per year.

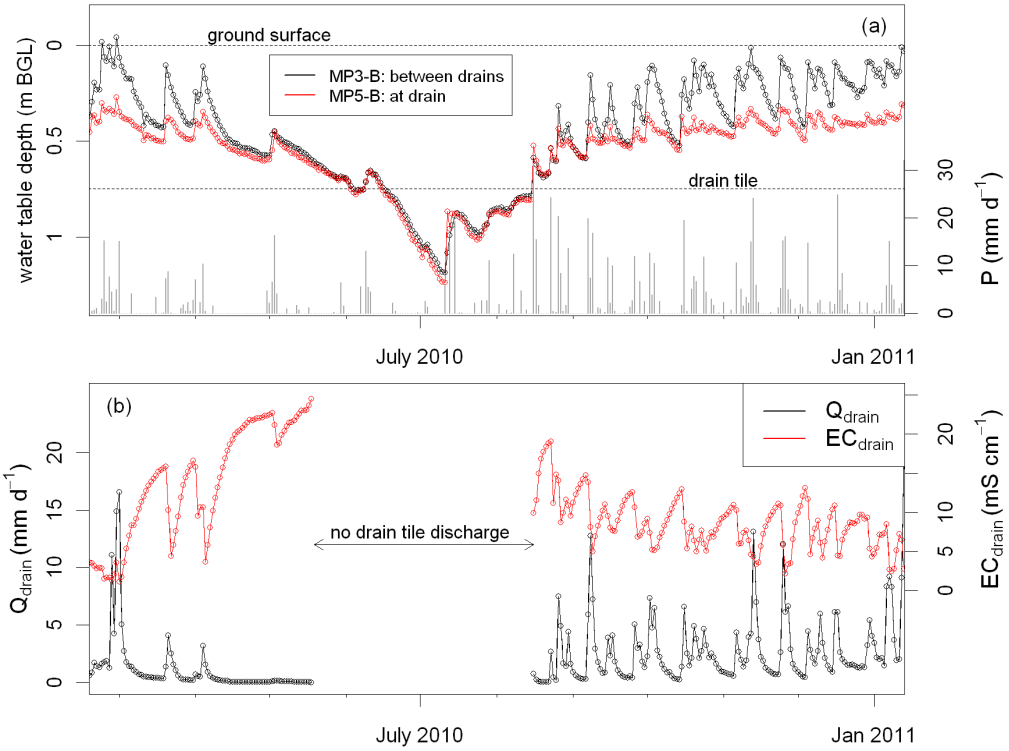

Fig. 6.6. Graphs showing times series at site B of (a) the water table at a drain tile and between two drain tiles and daily precipitation P, and (b) Q_{drain} and EC_{drain}. Water table elevations above the ground surface indicate conditions of surface ponding.

6.4.2 Soil water salinity

In general, soil water salinities increased with depth at both sites, but soil water salinities are notably higher at site B than at site A (Fig. 6.4). At site A, salinities within the root zone (sampling depths 0.15 m, 0.25 m, and 0.4 m) were always below 1.7 mS cm^{-1}, while they reached up to 15 mS cm^{-1} at site B. It should be noted though that extracting soil water was more difficult at site A and therefore data of dryer periods could not be obtained, except for sampling depth 0.55 m of MP1-A. Another conspicuous difference is that for three locations at site B soil water salinities were much higher than in the saturated zone (Fig. 6.4), which was not the case at site A.

For the sampling depths where sufficient samples could be collected throughout the year a clear seasonal trend in soil water salinity was observed. Selected examples of this seasonal behaviour are shown in Fig. 6.5a-c. Higher soil water salinities occurred during periods with low water tables (Fig. 6.5j-l), low P and high ET_a.

6.4.3 Drain tile discharge and drain water salinity

Fig. 6.6 shows the observed Q_{drain} and EC_{drain}, as well as the water table at a drain tile and between two drain tiles. The data cover a period of almost 1 year. Drain tiles carried discharge when the water table was above the drain tile level, and the discharge increased when the water table rose due to precipitation. EC_{drain} varied with Q_{drain}, where an increase of Q_{drain} caused a rapid and pronounced decline in EC_{drain}, followed by an increase of EC_{drain} when the discharge decreased. Fig. 6.7b shows that EC_{drain} was linearly correlated with water table depth, with EC_{drain} decreasing when the water table was rising. EC_{drain} never exceeded 25 mS cm^{-1} or fell below 2 mS cm^{-1}. The largest salt loads (discharge times salt concentration) occurred during peak discharge events (Fig. 6.7d) when drain water salinities were low.

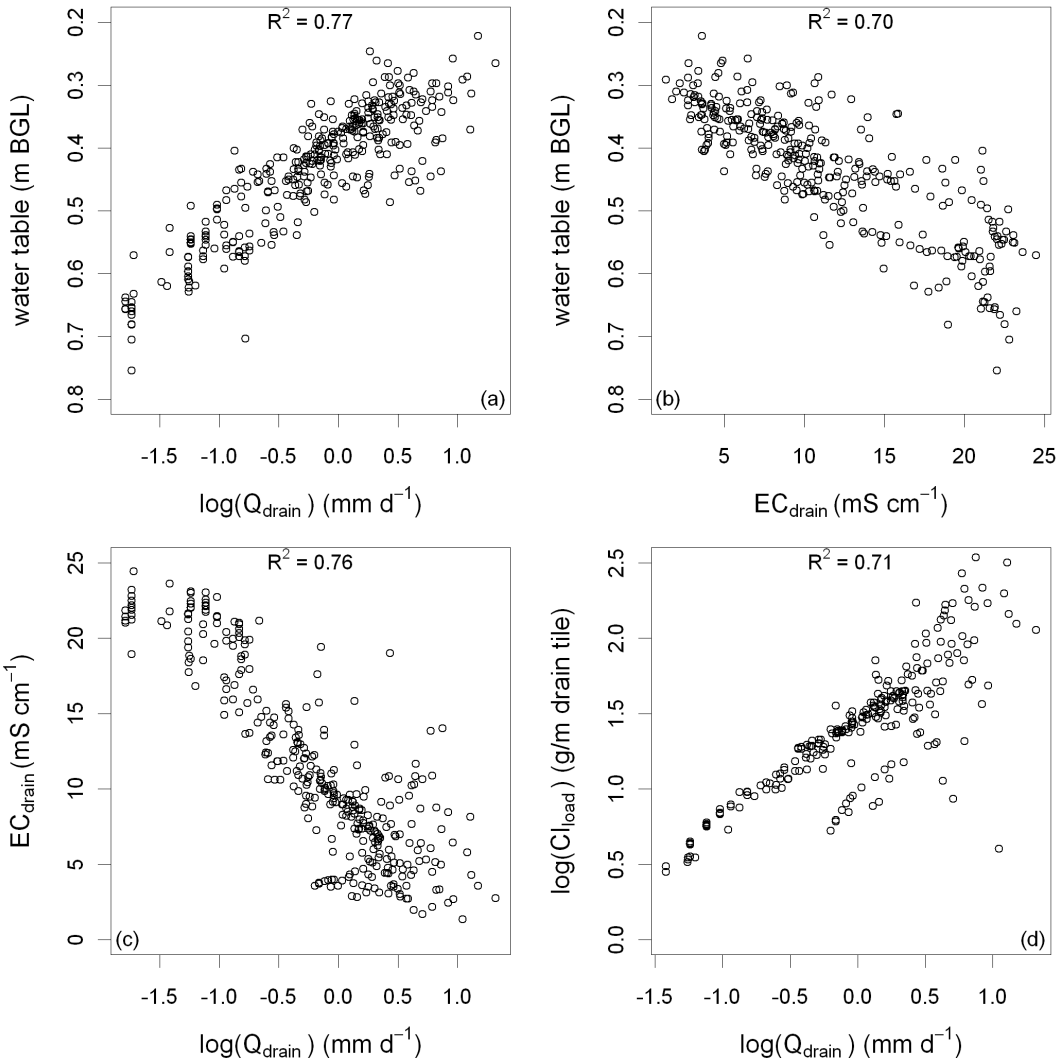

Fig. 6.7. Scatter diagrams showing measurements at site B of (a) the water table elevation at MP5-B versus log(Q_{drain}), (b) the water table elevation at MP5-B versus EC_{drain}, (c) EC_{drain} versus log(Q_{drain}) and (d) log(Cl_{load}) versus log(Q_{drain}). The salt load Cl_{load} is expressed in g Cl discharged per m drain tile.

6.5 Model outcomes

Because the model started with initial Cl concentrations of 12 g L^{-1} a spin-up time was required during which the RW-lens developed. It was found that after 8 years the total solute mass in the model between consecutive 2-year recharge cycles changed < 0.1%, indicating that there was no long-term change in the lens volume. Fig. 6.8 shows the comparison between the observed and model-simulated dynamics of Q_{drain}, EC_{drain}, and the water table elevation between the drain tiles during the measurement period. Also shown are the time-averaged observed and simulated salinity-depth profiles at and between the drain tiles. The simulated dynamics of Q_{drain} correspond well to the observed dynamics (NSC = 0.65) (Fig. 6.8a). In order to achieve this fit, high values of K_h (2.5 m d^{-1}) needed to be assigned to the upper 0.4 m of the subsoil. Cracks were observed at the surface, in particular during summer, and these are believed to be the cause for the relatively-high K_h value for this soil type. The adopted values of S (0.05 – 0.09) were adequate to reproduce the observed response of the water table elevation and Q_{drain} to recharge.

During calibration it was found that with a constant f_s = 0.69, the simulated water table fell too deep in the summer. Simulations with f_s = 0.60 for the summer half of the year (15 April – 14 October) and f_s = 1.0 for the winter half of the year (15 October – 14 April), resulted in a much better fit with the observations whilst leaving the total ET_a for the period unchanged. The justification on physical grounds for this approach is the reduction of ET_a in summer due to limited soil moisture availability and salt stress. In an analogous way, q_s was set to 0.16 mm d^{-1} for the winter half of the year and to 0.42 mm d^{-1} for the summer half of the year, which is commensurate with the observed change in the difference between the head at 4 m depth and the water table. With these adjustments, the observed water table could be satisfactory simulated (NSC = 0.81) (Fig. 6.8c).

The measured depth and width of the mixing zone at and between the drain tiles were well simulated by the model (Fig. 6.8d). Both the field data and the model

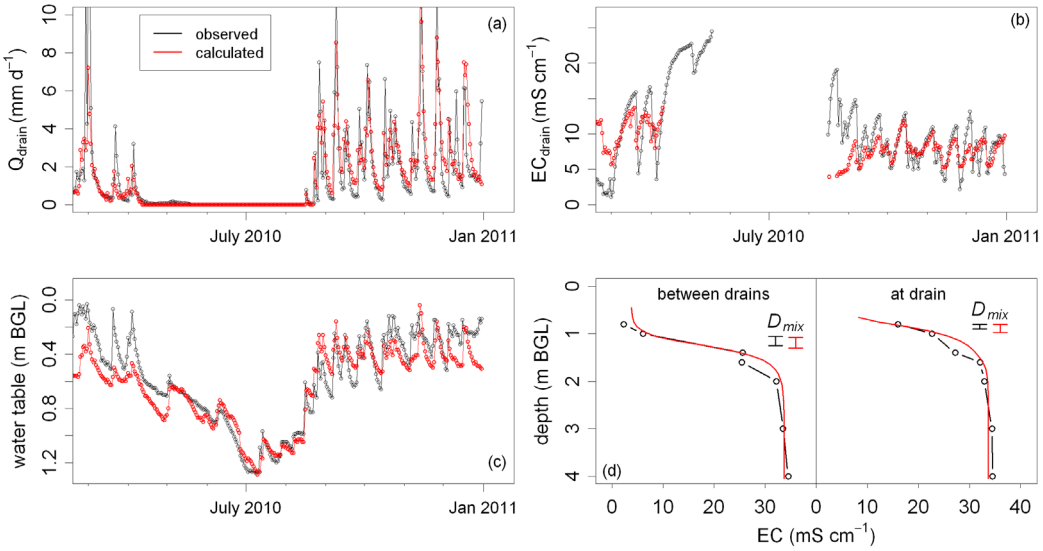

Fig. 6.8. Graphs showing the comparison between observed and calculated (a) Q_{drain}, (b) EC_{drain}, (c) water table between the two drain tiles, and (d) salinity-depth profiles at and between the two drain tiles. The observed and calculated variation of D_{mix} is indicated as well.

results show a thicker RW-lens between the drain tiles than at the drain tile. The small vertical seasonal displacements of D_{mix} and virtually steady position of B_{mix} were also reproduced by the numerical model (Figs. 6.8d and 6.9a).

The observed dynamics of EC_{drain} could only be partially reproduced by the model (NSC = 0.01 for the entire period of available data; 0.42 for the period after 15 September 2010). The largest discrepancies between simulated and observed values occurred directly after the summer period when drain tiles start discharging again and simulated values of EC_{drain} are lower than observed (Fig. 6.8b). This is believed to be attributable to the fact the salinity of the recharge water after a period of drought is higher in the field than the constant Cl concentration of 1.25 g L^{-1} used in the model. Attempts to increase the simulated EC_{drain} after periods of drought and EC_{drain} dynamics throughout the year, such as by adopting higher K_h and lower S-values for the upper soil, different salinities of recharge for summer and winter, smaller cells around the drain tile and lower dispersivity values, resulted in little improvement, or a significant worsening of the fit for the other metrics.

6.6 Discussion

6.6.1 Groundwater dynamics

The time-series data showed that D_{mix} did not vary more than 0.25 m during the measurement period. The temporal depth variation of D_{mix} showed a seasonal trend rather than a response to individual rain events, with a deeper D_{mix} during the winter half of the year when the water table was high (Fig. 6.9a). The small vertical displacement of the mixing zone explains the observed seasonal salinity variations in the RW-lens, which are illustrated in the next example. The salinity gradient around D_{mix} is about 4 mS cm^{-1} and 3 mS cm^{-1} per 0.1 m depth interval for sites A and B, respectively (Fig. 6.4). From this it can be inferred that a vertical displacement of D_{mix} of only 0.05 - 0.25 m results in seasonal salinity variations of 2 - 10 mS cm^{-1} for site A and 1.5 – 7.5 mS cm^{-1} for site B, which is in accordance with the observations (Fig. 6.5) and model results (Fig. 6.9b). The upward and downward movement of D_{mix} and seasonal salinity variations suggest that there exists a seasonally oscillating flow regime.

The effect of the transience of the flow on the dynamics of the salinity distribution was analyzed by using the calibrated model to determine, for every point in the cross-section, the percentage of time during which the flow has a vertical upward component. Fig. 6.10 shows that between 2.5 to 5 m from the drain tile, the flow around D_{mix} was upward half of the time, and downward half of the time. Average absolute vertical and horizontal flow velocities around D_{mix} were in the order of 1-2 mm d^{-1} and 5-10 mm d^{-1}, respectively. These small velocities and the fact that the flow alternates in vertical flow direction result in little vertical displacement, which explains why the seasonal variation of D_{mix} is only small. The numerical experiments of Eeman *et al*. (2012) showed much larger seasonal displacements of D_{mix} (0.5 - 1.0 m per year). This is probably due to the fact that they considered a different hydrogeological setting, i.e., a sandy aquifer without the presence of a low-permeability aquitard on top allowing for much larger vertical flow velocities than in cases RW-lenses develop within an aquitard.

Beyond this, the calibrated model was used to determine the temporal dynamics of the vertical flow stagnation point (FLSP), which is the point below which the flow switches from having a vertical downward to a vertical upward component (De Louw *et al*., 2011). The FLSP at the point between

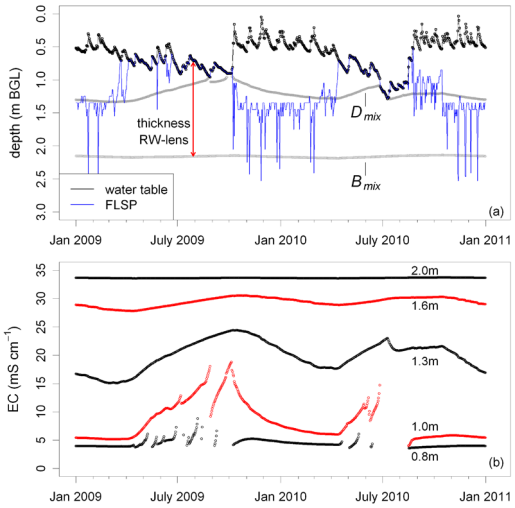

Fig. 6.9. Graphs showing model results between the drain tiles: (a) time series of the water table, D_{mix}, B_{mix} and the vertical flow stagnation point (*FLSP*) for a period of two years (2009-2010), (b) temporal variations of groundwater salinity at different depths. No results are shown for depths of 1.0 m and 0.8 m when model cells were above the calculated water table and hence inactive.

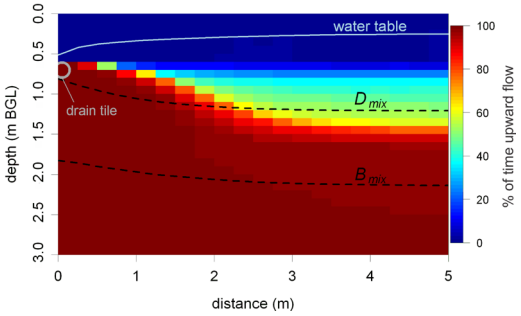

Fig. 6.10. Contour plot that shows for every model cell the percentage of time during which groundwater flow has an upward flow component (determined for a period of two years, 2009 - 2010). The average positions of D_{mix} and B_{mix} for the modeled period 2009-2010 are indicated as dashed lines.

the drain tiles shows a clear correlation with the elevation of the water table (Fig. 6.9a), whereby a rising water table resulted in a deeper FLSP. The FLSP responds rapidly to water table fluctuations. Flow is downward for a large part of the RW-lens when the water table is high, but when the water table falls below the drain tile all flow in the RW-lens is upward (Fig. 6.9a)

The oscillatory flow regime is further believed to be a driver for the mixing of infiltrated rainwater and saline groundwater in a RW-lens (De Louw *et al*., 2011). This is illustrated by the transient path lines within the RW-lens (Fig. 6.11a). Path lines started from different locations within the RW-lens show that certain regions of the subsurface sometimes receive inflow from (i) recharge across the water table, (ii) saline groundwater from seepage, or (iii) a mixture of the two. Path lines originating in the fresh- and saltwater zone cross each other over time, indicating mixing. The bends of the path lines indicate seasonal changes of periods with different recharge; path lines are predominantly horizontally oriented during winter when there is a significant flow towards the drain tile, and nearly vertical flow occurs during summer when the water table dropped below drain tile elevation. The oscillatory regime is most dynamic for the zone 2.5 - 5 m from the drain tile (Fig. 6.10). Closer to the drain tile, flow between B_{mix} and D_{mix} is upward for most of the time (Fig. 6.10). Nonetheless, both observations and simulations highlight the presence of a mixing zone below the drain tile. The calculated path lines show that this mixing zone groundwater results from mixing of rainwater with seepage at larger distance from the drain tile subsequently flowing towards the drain tile. Fig. 6.11b shows that within the RW-lens (i.e., above B_{mix}) the maximum travel time towards the drain tiles is 3.5 years.

6.6.2 Soil water dynamics

Important mixing processes occur in the zone where the water table fluctuates and conditions alternate between saturated to unsaturated. For both sites A and B this zone extends from ground surface to 1.3 m BGL. When the water table falls, water

with variable dissolved salt concentrations is retained as soil water, which will mix and become diluted with infiltrated rainwater when the soil saturates again. The temporary storage of salt in soil water has an important damping effect on groundwater salinity variations when the RW-lens grows by the recharge by rainwater. For example, the average fillable porosity (Acharya *et al*., 2012) of the top soils of site B is ~0.07 (*S* in Fig. 6.3), while the average total porosity (i.e. the volumetric soil moisture content at saturation) is ~0.49. Consequently, infiltration of 1 mm of rainfall leads to the saturation of ~14 mm of soil. Assuming instantaneous mixing when the soil gets saturated, the salinity of this saturated part will then equate to 0.07 / 0.49 = 1/7 times the salinity of the infiltrated water plus 0.42 / 0.49 = 6/7 times the salinity of resident soil water. The salinity of the mixture will thus be close to that of the soil water before saturation since the resident soil water is diluted by only a small amount of infiltrated water. This clearly shows that the salinity of groundwater recharge is controlled by mixing processes in the unsaturated zone, which is believed to be the explanation for the observed absence of truly fresh groundwater at site A and B (Figs. 6.4 and 6.5) and most other locations measured by De Louw *et al*. (2011).

The average salinity of soil water increases gradually with depth from low values near the land surface to the groundwater salinity at the water table, except at the monitoring points MP1-B, MP2-B and MP4-B at site B. At these locations the soil water at 0.55 and 0.70 m BGL were found to have higher salinities than the groundwater at 0.80 and 1.0 m BGL (Fig. 6.4). This is attributed to the co-existence of macro-pores (e.g. cracks) and small pores in the top soil, and the following mechanisms are thought to operate. Infiltration of rainwater occurs preferentially through the macro-pores, whereas capillary rise of water is strongest in the smallest pores. The smallest pores also can retain soil water against increasingly negative soil water potentials during summer. When the water table lowers, the concurrent loss of soil moisture due to drainage and evapotranspiration is, at least partially, compensated by capillary rise. At the same time, the salinity of the groundwater just below the water table becomes more saline as the water table fall 'decapitates' the lens and the vertical separation between the water table and the base of the RW-lens becomes smaller. The salinity of the soil water in the small pores thereby increases with time during summer, as the water that rises by capillary effects becomes ever more saline. This effect is much smaller or even absent in the macro-pores. The high salinities in the small pores can persist during the infiltration events, as infiltration of rainwater occurs preferentially via the macro-pores, by-passing the soil aggregates in which the smaller pores reside. Pulses of relatively freshwater can recharge the RW-lens in this way, while high salinities persist in the unsaturated zone.

6.6.3 Drainage dynamics

Under no conditions during the measurement period did the drain water consist solely of saline seepage water, which can be inferred from the fact that EC_{drain} never reached the EC of the seepage water of about 35 mS cm^{-1} for site B (Fig. 6.6). This can be explained by the presence of a mixing zone below the drain tile (Fig. 6.4; MP4-B and MP5-B) and the path lines in the RW-lens (Fig. 6.11a) which indicate that groundwater flowing towards the drain tiles is mixed groundwater.

The seasonal timescale of variation of groundwater and soil water salinity contrasts starkly with the high-frequency dynamics of EC_{drain}, which responds almost instantaneously to individual rain events (Fig. 6.6). Cracks are thought to play an

important role in this dynamic behaviour, facilitating the rapid infiltration of rainwater and responses of drain tile discharge and salinity to rainfall. Velstra *et al*. (2011) found similar fast responses and also allotted this to the existence of cracks in the clayey top soils. The dynamics of EC_{drain} (Fig. 6.6) indicate a fast mixing of infiltrated rain water and mixing zone groundwater. Particle tracking analysis shows that path lines originating from different depths converge and mix in the drain tile (Fig. 6.11a). This is further illustrated in Fig. 6.11b in which the red dotted line the region delineates (based on particle tracking) that contributes to a rainfall-driven drainage event with duration of 7 days (11 - 17 November 2010). For this event about 80% of the discharged water came from above the drain tile level with a low salinity close to that of rainwater, and about 20% came from below the drain tile level with salinities representative of the mixing zone. The linear relation between the water table and drain water salinity (Fig. 6.7b) implies that a higher water table leads to a larger fraction of infiltrated rainwater and a smaller fraction of mixing zone groundwater in drain water. However, the measurements also showed that despite the lower fraction of saline groundwater in drain water, the absolute amount of saline groundwater drained increases with water table elevation (Fig. 6.7d). From this it is inferred that during a water table rise, an increase of the flow of saline groundwater from the mixing zone towards the drain tile is triggered, which is confirmed by the model results (not shown). Drain water will therefore never consist of solely rainwater which explains why EC_{drain} never fell below 2 mS cm^{-1} (Fig. 6.6).

6.7 Conclusions

In this study, the temporal dynamics of thin RW-lenses and the mixing between rainwater and saline seepage were investigated using field measurements at two tile-drained agricultural fields in the south-western part of the Netherlands and numerical simulations for one of the sites. Upward saline seepage limits the size of the RW-lens and the freshwater availability for agriculture purposes. The base and the centre of the mixing zone were found at a depth of 1.8 – 3.3 m BGL and 0.8 – 1.8 m BGL, respectively. For the first time, field-based evidence of RW-lens dynamics was systematically collected by monthly ground- and soil water sampling, in combination with daily observations of water table elevation, drain tile discharge and drain water salinity. These observations were reproduced by the numerical model. Based on the field data and numerical modeling of the key lens characteristics, a conceptual model of RW-lens dynamics and mixing behaviour was presented of which the most important characteristics are summarized below.

The thickness of the RW-lens varied up to 1.2 m due to water table fluctuations in response to individual recharge events. The position of the centre of the mixing zone D_{mix} showed a much smaller change (< 0.25 m), and fluctuated at a much longer, seasonal time scale. The base of the RW-lens stayed virtually at the same position. The small variations in the position of the mixing zone can be explained by the slow transient oscillatory flow regime in the deepest part of the RW-lens. This oscillatory flow regime also controls the mixing between infiltrated rainwater and seepage water in a RW-lens.

The flow and mixing processes are much faster near the water table, which fluctuates on a daily basis in response to recharge and evapotranspiration, and conditions alternate between saturated to unsaturated. When the water table falls, most of the water with variable dissolved salt concentrations is retained as soil water, which will mix and become diluted with only a small amount of infiltrated rainwater when

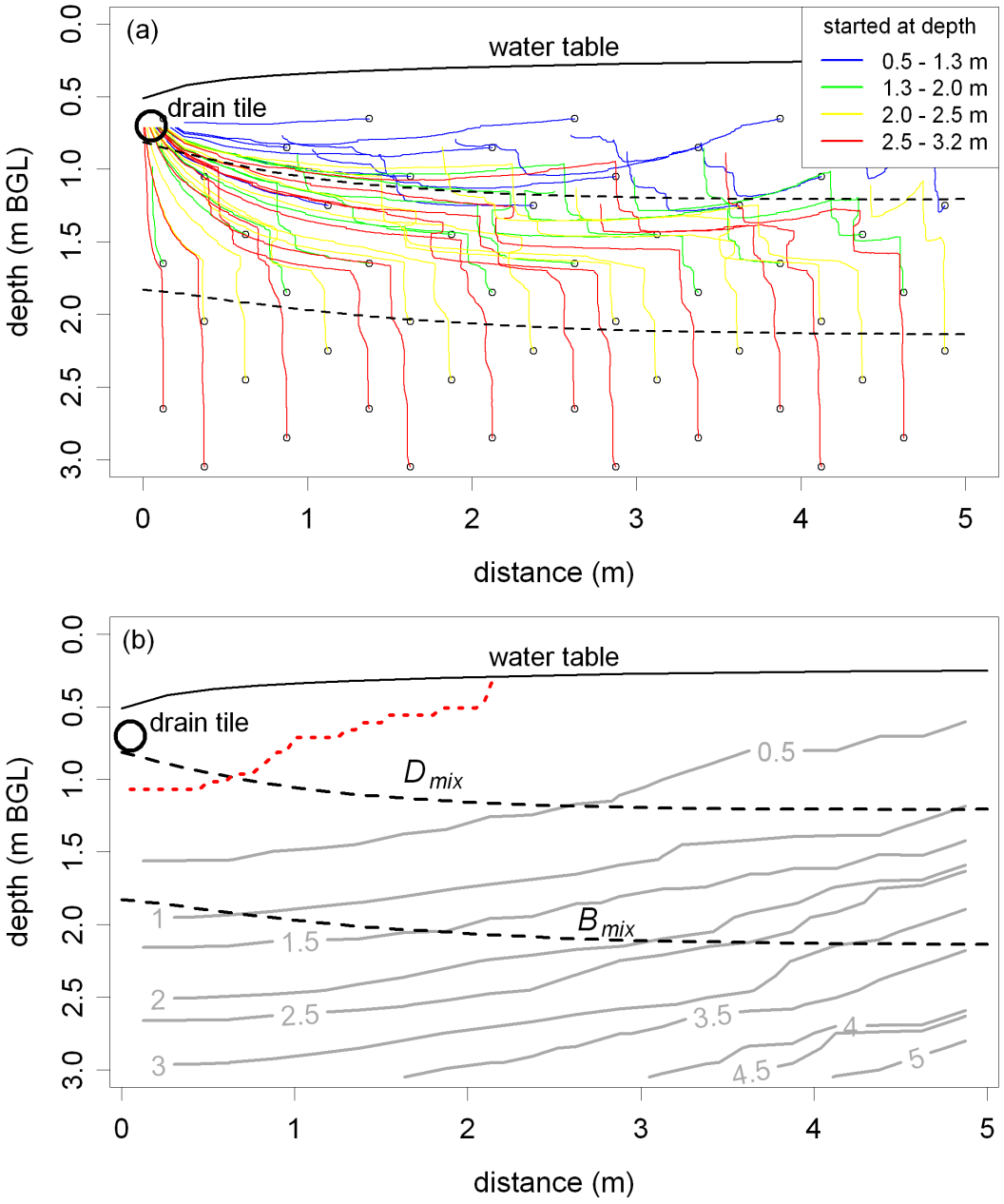

Fig. 6.11. Cross sections showing (a) transient path lines started at 1 January 2009, at different locations in the cross section, (b) travel time to the drain tile (in years). The red dotted line delineates the bottom of the zone around the drain tile that contributed to a rainfall-driven drainage event with duration of 7 days (11 - 17 November 2010). The average positions of D_{mix} and B_{mix} for the modeled period 2009-2010 are indicated as dashed lines.

the soil saturates again. The salinity of the mixture will thus be close to that of the soil water before saturation, which explains the observed absence of very fresh groundwater. Although the mixing processes are fast, the temporary storage of salt in soil water has an important damping effect on groundwater salinity variations when the RW-lens grows due to the recharge by rainwater.

Salt migrates upwards into the root zone by capillary rise of the groundwater at the water table. As the water table falls during the summer, the water rising through the capillaries originates from deeper parts of the RW-lens and is therefore more saline. Salinities of soil water can become significantly higher than in the groundwater due to the unsynchronized effects of capillary rise of saline water during dry periods and the flow of infiltrated rainwater during wet periods being restricted to cracks in the soil.

Preferential flow through cracks is thought to play an important role in the rapid response of the drain tile discharge to individual rain events. Groundwater of variable salinity, originating from different parts of the RW-lens, as well as infiltrated rainwater, contributes to the drain tile discharge in proportions that vary on a timescale of hours to days, and this causes the dynamic behaviour of drain water salinity.

The small dimensions and dynamic behaviour of the RW-lenses, especially the rapid removal of recharge through drain tiles and the loss of freshwater by evapotranspiration, make them vulnerable to climate change. RW-lenses may be expected to shrink due to evapotranspiration during drier summers, which are expected to become more frequent under future climate change (Van den Hurk *et al.*, 2006), but the projected increase in winter precipitation may not compensate for the lens shrinkage because the tile-drainage system efficiently discharges the recharge. Alternative tile-drainage configurations that promote prolonged retention and storage of infiltrated freshwater in RW-lenses could be a way to mitigate the potential adverse effects of future climate change. The optimal design of such configurations will be the subject of future research.


Deltares

Part III

Synthesis and discussion, summary and conclusions

Chapter 7

7.1 Introduction

This thesis describes the research results of the analysis of the spatial variability and temporal dynamics of salinization processes involving saline seepage in the Dutch delta. Two main saline seepage systems were distinguished that operate in different parts of the Holocene transgression area of the Netherlands. They differ in characteristics, such as the physics and salinity of the seepage, their contributions to the salinization of the Dutch delta and their vulnerability to climate change and sea level rise. The two main systems are:

I saline seepage in deep polders (reclaimed lakes) in the western Netherlands, and
II saline seepage in sub-recent transgression areas in the south-western delta and northern Netherlands.

Schematic representations of both systems are shown in Fig. 7.1. In the deep polders, salinization of surface waters occurs predominantly by preferential saline seepage through boils causing saltwater upconing of deeper and more saline groundwater (Fig. 7.1a). This system was analyzed in Part I of this thesis. The sub-recent transgression areas are characterized by the shallow occurrence (< 5 m below ground level, BGL) of very saline groundwater (50-100% sea water) (Fig. 7.1b). Here, saline seepage limits the freshwater availability to thin rainwater lenses below agricultural fields leading to the salinization of shallow groundwater and soil water (occasionally in the root zone). This system was analyzed in Part II of this thesis.

The spatial variability and temporal dynamics of salinization processes involving saline seepage of both systems were analyzed and quantified based on field campaigns supported by numerical and analytical methods. The field campaigns involved field techniques applied at scales varying from local point scale to measurements at polder catchment and island scale. Preferential discharge through boils was examined in two deep polders in the western part of the Netherlands: the Noordplas Polder and the Haarlemmermeer Polder. In each polder, one boil was examined in detail. In the Noordplas Polder, an extensive monitoring campaign was conducted to identify the dominant salt sources and to quantify their temporally varying contribution to surface water salinization. The characteristics and dynamics of thin rainwater lenses were examined in the saline seepage areas of the south-western delta of the Netherlands. A time series of data was collected at two tile-drained agricultural fields at the island of Schouwen-Duivenland.

The next section (section 7.2) summarizes, integrates and discusses the findings of this research by answering the five research questions defined in the Introduction. With the gained knowledge of saline seepage systems, their vulnerability to future climate change and sea level rise is considered in section 7.3, while implications for sustainable fresh water supply are given in section 7.4. To mitigate the adverse consequences of increased droughts and sea level rise, several measures are conceivable from which some have already been tested in the field. Which measures are likely to contribute to an effective water management strategy regarding the mechanisms that control saline seepage and rainwater lens dynamics is discussed in section 7.5 and 7.6. Based on the experiences with different field techniques, a short review of field methods to measure and monitor saline seepage processes is given in section 7.7. The final part of this chapter (section 7.8) gives suggestions for further research.

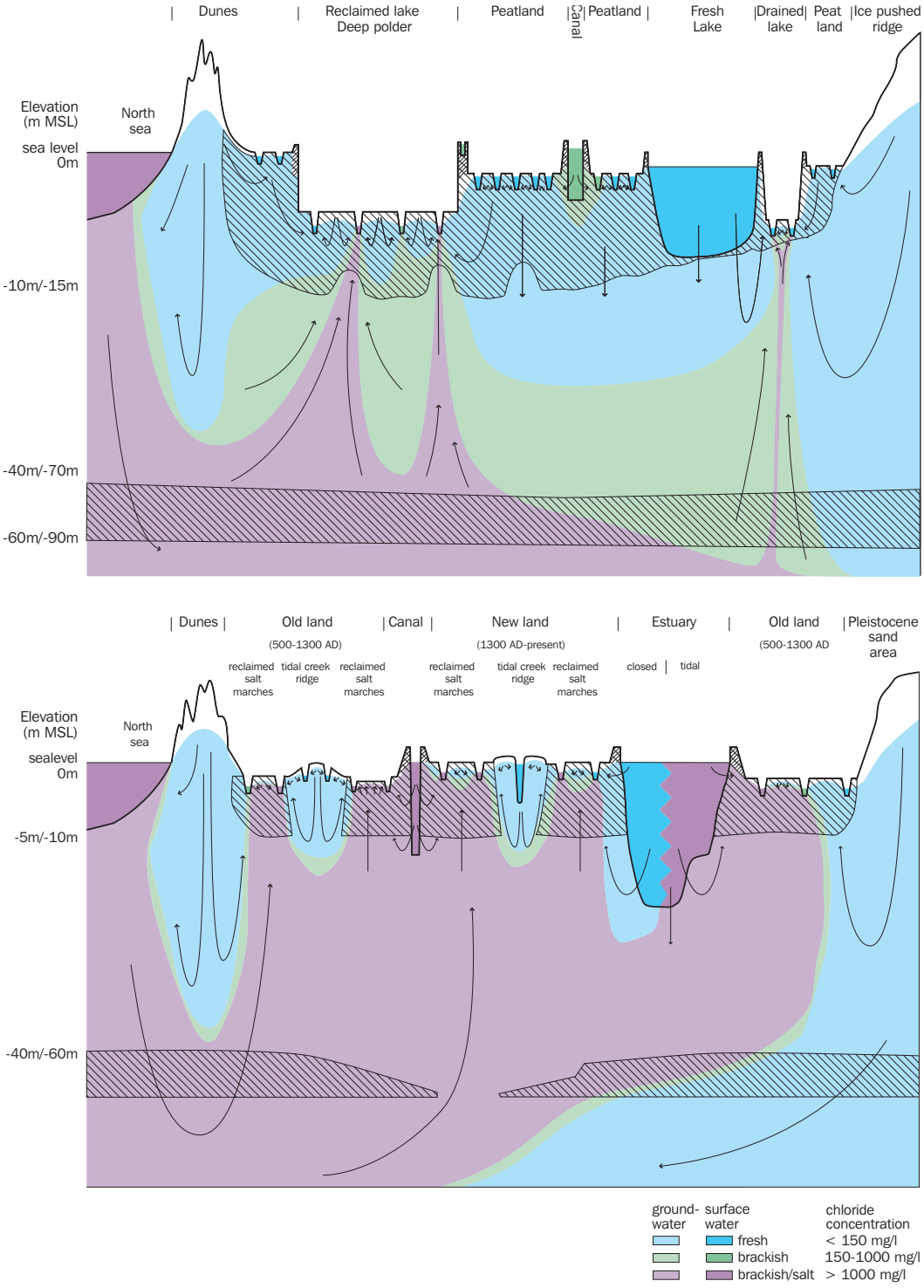

Fig. 7.1. Schematic representations of two important saline seepage systems in the Dutch delta: (a) preferential saline seepage in deep polders via boils causing saltwater upconing of deeper and more saline groundwater, (b) saline seepage in sub-recent transgression areas resulting in thin rainwater lenses.

7.2 Questions and answers

7.2.1 Part I: Preferential saline seepage through boils

Research questions:

- What is the nature and spatial variability of saline seepage in a deep polder, and how important is preferential saline seepage through boils? (Chapter 2)

- What is the contribution of different salt sources, and in particular saline boils, to the diurnal variability of salt concentration of surface water and salt loads in a deep polder, and how can it be quantified regarding large uncertainties of inflow quantity and quality? (Chapter 3)

- Is saltwater upconing by preferential seepage through boils the mechanism leading to elevated boil water salinities and what are the controlling factors? (Chapter 4)

Preferential versus uniform, diffuse seepage

We conclude that saline seepage is not a uniform process. This is based on observations and analysis of the geological structure of the Holocene confining layer (HCL), head differences, groundwater composition, surface water salinity, polder water discharge and salt load, temperature profiles, and boil observations, in a typical deep Dutch polder (Noordplas Polder) described in chapter 2. Three types of seepage were distinguished in a deep polder which differ in flux and salt concentration (Fig. 2.9):

1. diffuse, background seepage through the low permeability sediments (clay, peat) of the HCL;
2. preferential seepage through permeable, sandy paleochannel belts in the HCL;
3. intense preferential seepage via boils.

Boils are small conduits in the upper aquitard (HCL) that connect the aquifer with the surface through which groundwater preferentially discharges at very high velocities in the order of 10^2 to 10^4 m d^{-1}. The largest seepage fluxes and highest chloride concentrations are found in boils producing an average chloride concentration of 1100 mg L^{-1} for the Noordplas Polder, with a recorded maximum of 2900 mg L^{-1}. Permeable, sandy paleochannel belts cut through the less permeable, lower part of the HCL, resulting in higher seepage fluxes through paleochannel belts and a much higher average chloride concentration (~600 mg L^{-1}) than found for the diffuse seepage (average Cl concentration ~100 mg L^{-1}). The differences in salinity for the seepage types are explained by the combination of the typical salinity distribution found below deep polders (gradually increasing with depth in salinity from fresh to salt, see Fig. 1.5) and upconing mechanisms. Concentrated types of seepage at higher rates tend to discharge groundwater from deeper strata with more salty groundwater than diffuse types of seepage at low rates which discharge only fresh groundwater from the aquifer top.

The annual average chloride concentration of the water pumped out of the Noordplas Polder is about 400 mg L^{-1} and may reach 720 mg L^{-1} in dry periods. Given that polder water discharge is a mixture of seepage, precipitation and inlet water, and that the latter two have a diluting effect, we set out to demonstrate that boils must be responsible for the high surface water salinities.

Although the findings are based on data collected in the Noordplas Polder, field observations and boil mapping in other deep polders in the western Netherlands confirm that boils occur in most deep polders and play an important role in

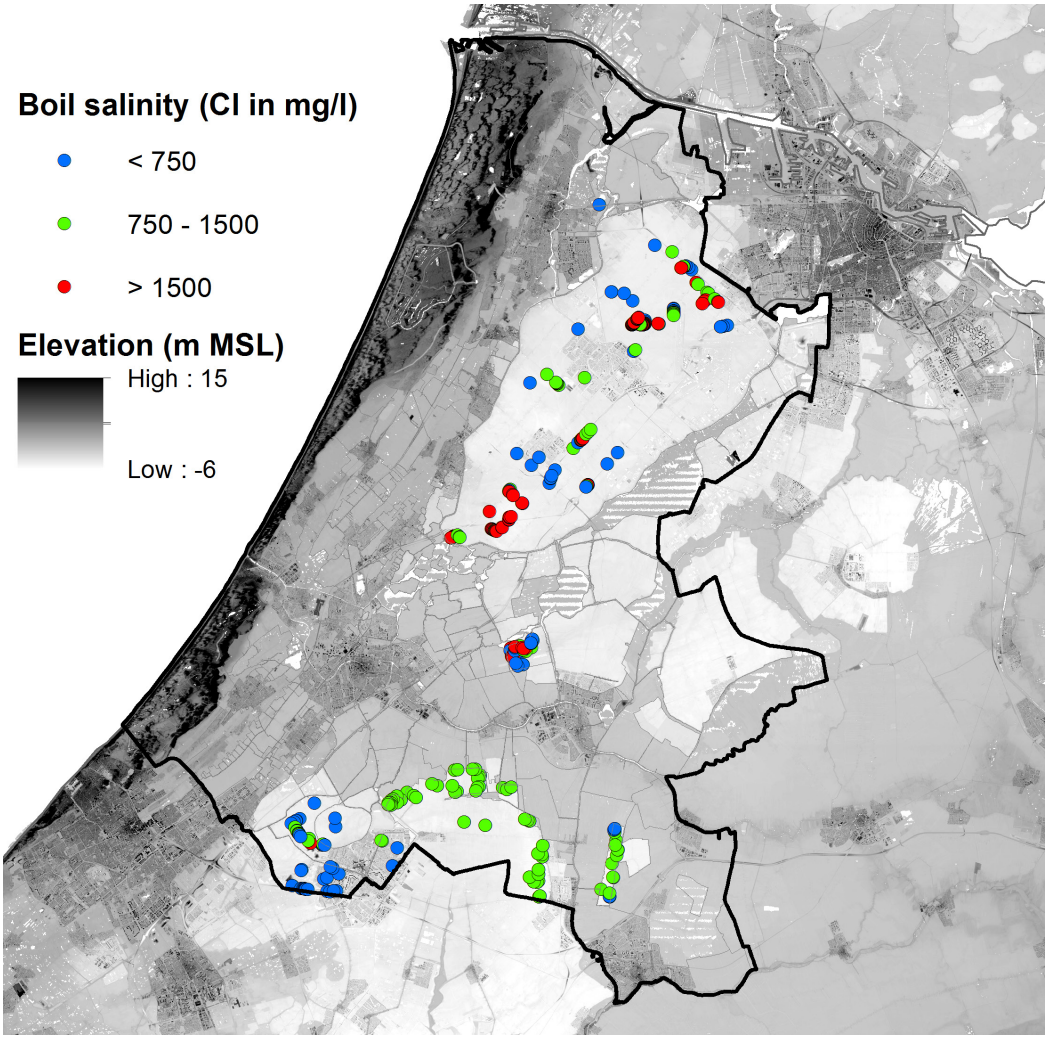

Fig. 7.2. Mapped boils and their measured Cl concentration for six deep polders in the water management area of the Rijnland District Water Control Board (Rijnland, 2013).

surface water salinization. A recent survey in the larger canals of 6 deep polders in the water management area of the Rijnland District Water Control Board shows the omnipresence of saline boils in deep polders (Rijnland, 2013; Fig. 7.2). In total, 369 boils were found with an average Cl concentration of 1200 mg L^{-1}. It must be noted that only the larger navigable canals were mapped which is less than 1% of the total polder area and only 9 % of all canals and ditches in the polder (data of the Haarlemmermeer Polder). The saltiest boils were mapped in the Haarlemmermeer Polder with an average Cl concentration of 1500 mg L^{-1} (n = 195) and a recorded maximum of 5000 mg L^{-1}. Also in other deep polders in the western Netherlands (e.g. Polder Groot Mijdrecht, Schermer, Wieringermeer Polder) saline boils were observed (Zaadnoordijk *et al.*, 2009; personal observations).

Since salinization by groundwater seepage has been a major water quality issue, there have been several studies on the water and chloride balances of deep polders in the coastal area of the Netherlands (Wit, 1974; ICW, 1976; Pomper and

Wesseling 1978; Van Rees Vellinga *et al*., 1981; Griffioen *et al*., 2002; Oude Essink *et al*., 2010; NHI-2.1, 2011). The salt load was obtained by multiplying the estimated seepage flux by the average Cl concentrations of groundwater at the top of the upper aquifer (-10 to -15 m mean sea level, MSL), which is, in general, fresh as shown in Fig. 1.5. This resulted in large underestimations of the salt loads which made it impossible to explain the high levels of observed salt loads. The discrepancy was removed by using the higher Cl concentrations of groundwater at -25 to -35 m MSL (Wit, 1974; ICW, 1976), but no justification was given. We have shown that the common assumption by the earlier studies, that upward saline seepage could be considered as a spatially uniform, diffuse process, is incorrect. Their choice to use higher chloride concentrations in the water and salt balances is conceptually the same as our idea that more saline groundwater of deeper origin contributes to the polder discharge via boils. Furthermore, based on the findings of in this study, boils were inserted into the Dutch hydrological model instrument (NHI-2.1, 2011) significantly improving the calculation of salt loads by seepage with the new model instrument (NHI-2.2, 2011).

Quantification of salt sources in deep polders: boils as dominant salinization mechanism

In chapter 2 we have demonstrated that three different types of seepage occur in deep polders and that boils are an important salinization source of surface water. However, to define effective measures to reduce salt loads and Cl concentrations of surface waters in deep polders and of regional water systems, it is necessary to identify the dominant sources of water and salt and quantify their fluxes on a daily to weekly basis. This small time scale is essential because the salinity of polder water is highly variable in time as it responds to individual rain events, and water quality issues typically play an important role during the warmer and drier growing season. However, as in most balance studies there are large uncertainties in the contribution from groundwater seepage. In the Dutch deep polders, the number of boils and thus the total boil flux is unknown, while the hydraulic resistance of the HCL, which determines diffuse and paleochannel seepage, is uncertain. Additionally, the amount and dynamics of the admission of external water (i.e. inlet of 'boezem' water) into the polder (for surface water level control, salinity control and irrigation) are only known within certain ranges due to the unknown number of uncontrolled inlets and the lack of sufficient monitoring data of the larger inlets controlled by the Water Boards.

To quantify the water and salt fluxes in a deep polder on a daily time scale, and taking into account the uncertainty of parameters, a probabilistic (GLUE) dynamic water and salt balance model on a daily time scale has been set up and successfully applied to the Noordplas Polder. This water and salt balance model is presented in chapter 3. The model requires input parameters such as the salinity and fluxes of the different sources shown in Fig. 3.1, and parameters controlling the dynamic groundwater surface water interaction such as drainage network characteristics (level and spacing) and hydraulic conductivities of the top soil. To incorporate the uncertainty of model input parameters, their values were sampled randomly from uniform parameter distributions within ranges which were defined based on measurements. The model was conditioned on measurements of daily to weekly polder water discharge, salt concentrations and salt loads leaving the Noordplas Polder, and on water table elevation, in order to produce sets of input parameters which simulate the system equally well. With these sets of behavioural parameters, we quantified the contribution and uncertainty of different sources to the water and salt balance of the deep polder and the effects of different scenarios.

The results showed that the far most dominant salinization source in the Noord-

plas Polder is boil seepage with an average contribution of 66% (± 7.2%) to the total salt loads, while contributing only 15% (± 4.7%) to the total water flux. Standard deviations are given between brackets. The observed polder water discharge, salt concentrations and salt loads could only be explained by assigning such a large contribution of the total salt load to boils. The other preferential form of seepage, i.e. paleochannel seepage, contributed 18% (± 5.7%) to the total salt loads. Thus, preferential seepage, which includes both upward groundwater flow via boils and via paleochannel belts, is responsible for > 80% of the surface water salinization in the polder. This is primarily caused by the high chloride concentrations of these preferential forms of seepage compared to diffuse seepage.

Not salt load but surface water salt concentration is the key parameter to look at when evaluating the impact of salinization on agriculture and aquatic ecosystems. The model results showed that, despite the with time virtually constant contribution of boils, the surface water Cl concentration is highly variable in time due to dilution by rainwater and shallow groundwater during rain events. Boils were assigned a constant flux throughout the year. This is based on the findings that most boils (~80%) occur in ditches and canals where the observed head differences between aquifer and surface water are nearly constant, as presented in chapter 2 (Fig. 2.4). This constant head difference is a typical feature of most Dutch deep polders (De Louw and Stuurman, 2005). The temporal variations of the observed surface water Cl concentration were well reproduced by the presented probabilistic water and salt balance model. It makes this model an appropriate assessment tool for the quantification of salt sources in deep polders, and for predicting the effects of climate change and mitigation measures to abate surface water salinization.

The omnipresence of saline boils in Dutch deep polders and the typical salinity distributions found below most deep polders (i.e. fresh above salt groundwater) makes us to believe that boils are the most likely dominant salinization source in most Dutch deep polders. For example, the measured yearly average Cl concentration of polder water pumped out of the Haarlemmermeer Polder is about 500 mg L^{-1} (Rijnland, 2013) and it's observed dynamics are comparable to those found for the Noordplas Polder. Furthermore, rough estimates for Polder Mijdrecht, which is the polder with the highest salt load in the Netherlands, indicate a contribution of boils to the total salt load larger than 80% (Zaadnoordijk *et al*., 2009).

Saltwater upconing as key feature of saline boils

Our field measurements in the Noordplas Polder and the Haarlemmermeer Polder evidenced local and steep upconing of deeper and more saline groundwater due to the preferential groundwater discharge via boils. Based on these field observations and numerical simulations presented in chapter 4, we conclude that saltwater upconing is the key mechanism leading to elevated salinities of boil water.

The numerical simulations showed that boil water is a mixture of groundwater from different depths with different salinities. Mixing is enhanced near the boil where streamlines from different depths and with different salinities converge. The largest increase of boil water salinity occurs in the first 5 to 20 years after boil creation. The contribution of different aquifer depths to boil discharge (further referred to as the contributing depths distribution) showed an inverse relationship with the aquifer salinity distribution. That is, the boil extracted per meter aquifer more low-salinity groundwater from above the centre of the transition zone (shallow contribution) than high-salinity groundwater from below the centre of the transition zone (deep contribution). This is due to the buoyancy force established by density differences which gives an extra upward lift to fresh groundwater

with lower density compared to saline groundwater below the transition zone. In aquifers with uniform density profiles, all depths contribute equal amounts to the boil's discharge. This is independent of boil discharge rate and aquifer properties, such as horizontal and vertical hydraulic conductivity, aquifer thickness and porosity. In contrast, by adding density differences, the contributing depths distribution and therefore boil salinity depend on many factors of which the key factors controlling saltwater upconing mechanisms are: (i) boil discharge rate, (ii) aquifer's horizontal hydraulic conductivity, and (iii) the aquifer salinity (= density) distribution characterized by the position of the centre of the transition zone and density difference between groundwater above and below the transition zone. The density distribution in an aquifer determines to what magnitude these factors influence upconing, i.e. the three controlling factors have more impact when density differences are large. The impact of the width of the transition zone, aquifer thickness, porosity, vertical hydraulic conductivity and regional lateral flow gradients on saltwater upconing and boil water salinity is rather insignificant. It must be noted that regional lateral flow significantly modifies flow patterns in the aquifer by dividing the groundwater flow system into a local boil system overlying the regional flow system. However, despite this, regional flow has only a minor effect on the relative contributions of saline and fresh groundwater to boil discharge and thus on boil salinity when the transition zone is entirely within the local boil system.

The large spatial variation of boil water salinity found in deep polders, as described in chapter 2 and shown by the recently carried out boil survey (Fig. 7.2), is explained by spatial variations of the three factors that control upconing: boil discharge rate, horizontal hydraulic conductivity and salinity-density distribution. In chapter 2, we showed that boil discharge rates are highly variable in space varying from 0.5 up to 100 m^3 d^{-1} for the Noordplas Polder and the Haarlemmermeer Polder, and that larger boils with higher discharge rates tended to have higher Cl concentrations. Even within a boil cluster, a small area of about 25 to 100 m^2 with multiple boils, boils discharge water at various rates. Salinity variations between boils within a boil cluster are determined by the combination of the discharge and position of individual boils within the boil area. However, the total salt load discharged by a boil cluster is a function of the total discharge of a boil cluster. As such, boil clusters can be reasonably represented as a single sink, if the primary concerns are large-scale upconing and boil contributions to surface water salinization. The large spatial variations of the aquifer salinity distribution in the western Netherlands (Fig. 1.1) and within a deep polder (Fig. 1.5) determine to a large extent the spatial variation of boil salinity. In some deep polders (e.g. Polder Nieuwkoop; Rijnland, 2013) boils discharge fresh groundwater which is explained by absence of any saline groundwater in the upper aquifer. Since the spatial variability of the horizontal hydraulic conductivity of the upper aquifer is small (REGIS, 2005), it has only a minor impact on the spatial variation of boil salinity.

7.2.2 Part II: Rainwater lenses in areas with saline seepage

Research questions:

- What are the characteristics and spatial variability of thin rainwater lenses in areas with saline seepage and what are the mechanisms and factors that determine their occurrence and size? (Chapter 5)

- What are the temporal dynamics of thin rainwater lenses and mixing processes between infiltrating rainwater and upward saline seepage? (Chapter 6)

Characteristics of rainwater lenses in areas with saline seepage

The characteristics of rainwater lenses in areas with saline seepage (further referred to as RW-lens) were determined by using different types of field measurements applied at different scales in the south-western delta of the Netherlands. We could extrapolate measurements at point scale (groundwater sampling, temperature and electrical soil conductivity (TEC)-probe measurements, electrical cone penetration tests (ECPT)) to field scale (continuous vertical electrical soundings (CVES), electromagnetic survey with EM31), and even to regional scale using helicopter-borne electromagnetic measurements (HEM). Point measurements were needed to determine the precise form of the mixing zone and to characterize the rainwater lens, and to understand the mixing processes between rainwater and saline seepage. Point measurements below 30 agricultural fields showed a gradual mixing zone between infiltrated rainwater and upward seeping saline groundwater. However, a mixing zone was absent below the ditches where only saline seepage water was found, demonstrating that RW-lens development is limited to the area between the ditches. The centre of the mixing zone D_{mix} was found at a median depth of 1.7 m BGL and almost all mapped RW-lenses lacked truly fresh groundwater. The HEM-measurements in the seepage areas (n = 59.000) showed a median depth of D_{mix} of about 1.5 m BGL. For the purpose of this study, the RW-lens was defined as the entire groundwater body from the base of the mixing zone (B_{mix}, which is the depth at which the salinity equals the salinity of regional groundwater) to the water table. With this definition, the RW-lens is not purely a freshwater lens, and salinities within the RW-lens vary both in space and in time. B_{mix} was found at a median depth of 2.8 m and the ECPT measurements showed that below B_{mix} the salinity stayed virtually constant with depth until at least 25 m BGL.

The limited size of RW-lenses is primarily caused by the permanent regionally head driven upward groundwater flow from the upper aquifer into the HCL, which prevents rainwater from reaching depths below the bottom of the HCL. Unlike RW-lenses in seepage areas, the vertical downward flow of rainwater in the infiltration areas is only limited (in absence of aquitards) by the buoyancy force of the surrounding saline groundwater and its density importantly determines lens thickness according to the Badon Ghyben Herzberg principle (Drabbe and Badon Ghijben, 1889; Herzberg, 1901). These systems build up much thicker lenses (BGH-lenses), varying from 5 to 15 m thick lenses in sandy creek ridges to 100 m thick lenses in the dunes. This difference in lens developing mechanisms explains the sudden increase in measured lens thickness (obtained by HEM) when moving from a seepage to an infiltration situation (see Fig. 5.15). Measurements (CVES, ECPT, TEC-probe, heads) at a 300 m long agricultural field located at the transition from a former salt marsh to a 0.5 m higher lying tidal creek paleo-channel, demonstrate that large variations in lens thickness and in lens developing mechanism occur at a very local (field) scale. At the former salt

marsh, measured freshwater heads were permanently higher in the sandy aquifer at 4 m depth than at 1.5 m depth in the aquitard, resulting in a continuous upward groundwater flow. This seepage limited the penetration depths of rainwater and consequently led to thin RW-lenses ($1.5 < B_{mix} < 3$ m). At only a short distance (~50 m), slightly higher freshwater heads (0.1 - 0.2 m) in the aquitard at 1.5 m than in the upper aquifer at 4 m depth produced much thicker lenses ($4 < B_{mix} < 10$ m).

Mechanisms of mixing between infiltrating rainwater and saline seepage and controlling factors

As it was established that lenses in seepage areas are limited to the extent of the upper aquitard (HCL) due to permanent upward seepage, we subsequently examined the mixing mechanisms and flow processes within the aquitard and the factors controlling lens size and mixing zone properties. For this purpose, 77 RW-lens cases, which differed in characteristics such as seepage flux and salinity, recharge, aquitard properties, dispersivity, drainage characteristics, were simulated and their time-varying vertical head and flux distributions in the aquitard were analyzed in detail. We introduced the vertical flow stagnation point (FLSP) to indicate the point below which the flow switches from having a vertical downward to a vertical upward component. The FLSP in between the drain tiles fluctuates with water table fluctuations, whereby a rising water table resulted in a deeper FLSP. Flow is downward for a large part of the RW-lens when the water table is high, but when the water table falls below the drain tile all flow in the RW-lens is upward. The FLSP responds rapidly to water table fluctuations, constantly changing flow directions for a large part of the RW-lens. The results of all 77 simulated cases showed a strong correlation ($R^2 = 0.91$) between D_{mix} and the yearly averaged position of the FSLP. Furthermore, the maximum depth of FSLP during a year (this is the depth below which no downward flow occurs), largely corresponded with B_{mix}. Based on these findings, we conclude that the oscillatory vertical flow regime in the aquitard driven by water table fluctuations is the main mechanism of mixing between infiltrating rainwater and upward saline seepage, and that it also determines the position and extent of the mixing zone in the aquitard. Recharge, seepage flux and drainage depth are the controlling factors.

Temporal dynamics of RW-lenses, drain water and soil water salinities

To examine the temporal dynamics of RW-lenses, a comprehensive set of data was collected at two tile-drained agricultural fields in the south-western delta of the Netherlands. The data consisted of groundwater and soil water salinities, groundwater levels, drain tile discharge and drain water salinity, precipitation and evapotranspiration. The field data showed that the thickness of the RW-lens (from B_{mix} to water table) varied up to 1.2 m with water table variations in response to individual recharge events. The position of D_{mix} showed a much smaller change (< 0.25 m), and fluctuated at a much longer, seasonal time scale. The base of the RW-lens (B_{mix}) stayed virtually at the same position. Numerical simulations showed that the small variations in the position of the mixing zone can be explained by the slow transient oscillatory flow regime in the permanently saturated part of the RW-lens which also controls the mixing between infiltrated rainwater and seepage water, as discussed above. Average absolute vertical flow velocities around D_{mix} were in the order of 1 mm d^{-1}. These small velocities and the fact that the flow alternates in vertical direction result in little vertical displacement, which explains why the seasonal variation of D_{mix} is very small indeed. The seasonal variation of groundwater salinity at an arbitrary point within the RW-lens is the result of the small

seasonal displacement of the position of the mixing zone.

The flow and mixing processes are much faster near the water table, which fluctuates on a daily basis in response to recharge and evapotranspiration, and conditions alternate between saturated to unsaturated. When the water table falls, most of the water with variable dissolved salt concentrations is retained as soil water, which will mix and become diluted with only a small amount of infiltrated rainwater when the soil saturates again. The salinity of the mixture will thus be close to that of the soil water before saturation, which explains the observed absence of very fresh groundwater. Although the mixing processes are fast, the temporary storage of salt in soil water has an important damping effect on groundwater salinity variations when the RW-lens grows due to the recharge by rainwater.

Soil water salinity showed a seasonal variation with lower salinities during winter and higher salinities during summer. Salt migrates upwards into the root zone by capillary rise of the groundwater at the water table. As the water table falls during the summer, the water rising through the capillaries originates from deeper parts of the RW-lens and is therefore more saline. Salinities of soil water can become significantly higher than in the groundwater due to the unsynchronized effects of capillary rise of saline water during dry periods and the flow of infiltrated rainwater during wet periods being restricted to cracks in the soil.

Preferential flow through cracks is thought to play an important role in the rapid response of the drain tile discharge to individual rain events. Groundwater of variable salinity, originating from different parts of the RW-lens, as well as infiltrated rainwater, contributes to the drain tile discharge in proportions that vary on a timescale of hours to days, and this causes the dynamic behaviour of drain water salinity.

RW-lenses in deep polders

The RW-lenses in deep polders are much different from those examined in the sub-recent transgression areas (chapter 5 and 6, and discussed above). In chapter 2, we showed for the Noordplas Polder that outside the paleochannel belts and boils, thus in the majority of the polder, RW-lenses develop down to at least 5 m BGL (Fig. 2.10). The reason that these lenses reach these relatively large depths, despite the large hydraulic heads in the aquifer below (exceeding phreatic water levels with > 1 m), is the vertical head distribution in the HCL which results from the lithological composition of the HCL. As Fig. 2.4 shows, the water table and the hydraulic head at 5 m BGL are virtually the same while the head difference between 5 m (in the HCL) and 7 m BGL (in the aquifer) is > 1 m. This large jump in vertical head is caused by the large hydraulic resistance of the lower part of the HCL which is comprised of compacted peat and clay with low hydraulic conductivity. This hydraulic head jump is so dominant that it fixes the FLSP at this depth, resulting in RW-lenses reaching this depth. Explorative numerical calculations (not shown) showed that seepage flux didn't have any impact on the position of the FLSP and therefore on lens thickness. Also, water table fluctuations by recharge variations and tile-drainage didn't have any influence on the FLSP position which stayed at a fixed position throughout the year. This is in large contrast with the RW-lenses in the sub-recent transgression areas. In these systems, head differences between the aquifer and the water table are much smaller and the aquitard is thinner and more permeable. Consequently, recharge variations, tile-drainage and seepage determine the vertical head (and flux) distribution in the HCL of the sub-recent transgression areas rather than lithological heterogeneities, and therefore, the FLSP and lens thickness.

7.3 Vulnerability to climate change and sea level rise

Anticipated future climate change (changing rainfall and evapotranspiration patterns) and sea-level rise (AR4: IPCC, 2007) will exacerbate the pressures on coastal groundwater systems world wide and need to be considered in devising coastal water management strategies. It is generally understood that sea-level rise is expected to result in the inland migration of the freshwater - saltwater interface (Oude Essink, 1996; Werner and Simmons, 2007), obviously leading to a loss of fresh groundwater resources. Much work has been done to assess the effects of sea level rise and changing recharge patterns on sea water intrusion in regional coastal aquifers, e.g. in Egypt (Sherif and Singh, 1999), the Netherlands (Oude Essink, 2001; 2010), Florida (Dausman and Langevin, 2004) and Morocco (Carneiro *et al*., 2010). An extensive review of seawater intrusion processes in coastal aquifers including effects of climate change and sea-level rise is given by Werner *et al*. (2013). Within the Interreg IV-B CLIWAT-project, to which this current study contributed to, the climate change impact on the hydrological cycle was studied, as well as adaptive water management in the coastal North Sea region. The scientific results are given in Hinsby *et al*. (2011).

The Dutch delta is already being threatened by a relatively high sea level, as nearly one third of the Netherlands is below mean sea level. For predicting effects of climate change and sea level rise to the Dutch delta, the Royal Netherlands Meteorological Institute KNMI formulated so-called KNMI06 climate scenarios (Van den Hurk *et al*., 2006). These KNMI06 climate scenarios result from the Regional Climate Models and were based on the Global Climate Models in the IPCC's Fourth Assessment report (AR4: IPCC, 2007). The so-called W+ climate scenario for the year 2100 is most used in climate change effect studies and is the driest of four KNMI06 climate scenarios. Compared to the present situation, it is characterized by greater precipitation in winter (28%), and less precipitation (-38%) and higher evaporation in summer (30%) in the year 2100 A.D. Additionally, the W+ climate scenario predicts a future sea level rise of 0.40 - 0.85 m for 2100 A.D for the Dutch coast. Effects of the W+ scenario for the Dutch coastal groundwater system were calculated for the northern Netherlands and Waddenzee area (Faneca Sànchez *et al*., 2012; Pauw *et al*., 2012), the western Netherlands (Oude Essink *et al*., 2010) and the south-western delta (Van Baaren *et al*., 2013). These studies showed that a rise in sea level will result in an increase of hydraulic heads in the upper aquifer, subsequently increasing seepage fluxes and salt loads into the polders. However, the effect of sea level rise decreases rapidly with distance and effects are limited to areas within 5 to 10 km from the coast (Oude Essink *et al*., 2010; Faneca Sànchez *et al*. 2012). Besides effects of future climate change and sea level rise, also effects of autonomous salinization were assessed. Autonomous salinization is the continuous process of deeper and more saline groundwater flowing to the surface resulting in increasing salt concentration of the seepage water and thus increasing salt loads into the polder. Thus, this autonomous process leads to increasing salinization without the change of groundwater flow patterns and is an on-going process since the reclamation of the polders, which started many hundreds of years ago (1000 A.D. - 1968 A.D.). Oude Essink *et al*. (2010) concluded that for most deep polders the majority of the increased salt loads in the deep polders is due to autonomous salinization and, in some parts of the polders, autonomous salt loading will even be doubled. Along the southwest coast of the Netherlands, sea level rise will have much more impact on salt loads by the year 2100 A.D. than in the western Netherlands (Van Baaren *et al*., 2013; Oude Essink *et al*., 2010). This is primarily caused by the fact that

the islands of the south-western delta are entirely surrounded by the sea and that the polder areas are directly situated along the coast, whereas the deep polders in the western Netherlands are at least 7.5 km from the coast line.

The above mentioned climate change effect studies for the Dutch delta described regional effects and disregarded local processes. The research presented in this thesis showed that important salinization processes by saline seepage act on a (very) local scale, such as salt loading via boils and the salinization of RW-lenses at agricultural fields, and therefore effects of future changes may be different from effects assessed by the regional studies. The vulnerability to climate change and sea level rise of the Dutch saline seepage systems examined in the current study is considered in the next paragraphs.

Climate change in Dutch deep polders

The regional studies showed that saline seepage in the Dutch deep polders will not be affected significantly by a sea level rise because the distance to the coast is too far. Besides this, current head differences between the aquifer heads and phreatic water levels are large in the deep polders (in the order of 1 – 2.5 m) and therefore a slight increase in aquifer head (e.g. 0.1 – 0.25 m), for any reason, will only marginally increase seepage flux. Given the dominance of boils in the salinization of deep polders and the associated saltwater upconing mechanisms established in chapter 2, 3 and 4, we think that the present salt loads of deep polders calculated with regional groundwater models are underestimated (e.g. Oude Essink *et al*., 2010), whereas the calculated autonomous salinization may be exaggerated. The saltwater upconing simulations showed that the largest increase in boil water salinity occurs in the first 5 to 20 years after boil creation and will be close to their maximum salinity within 100 years. This is much faster than the increase in seepage salinity by the slow autonomous upward flow of deeper and more saline groundwater calculated by the regional groundwater models. By not taking into account boils and the associated saltwater upconing mechanisms, the autonomous effects and therefore also the effects of climate change and sea level rise for deep polders cannot be estimated accurately enough. On the other hand, we expect that the number of boils will increase, subsequently leading to an increase of salt loads, and this can be seen as an autonomous process as well. Although autonomous salinization is the dominant on-going process below the Dutch deep polders, freshening of shallow aquifers and seepage water is locally occurring close to the dune area and at the edges of deep polders (e.g. Stuyfzand, 1993; Oude Essink, 1996; Delsman *et al*., 2013b).

Although climate change and sea level rise will not significantly increase salt loads into deep polders, they may affect polder water salinity in two ways, as demonstrated in chapter 3. Firstly, changing precipitation and evaporation patterns will have an impact on the dilution of saline seepage and thereby change surface water salinity. The probabilistic water and salt balance model was used to assess the effect of the W+ climate scenario on the surface water salt concentration. The results showed that surface water Cl concentrations will be slightly higher in summer and much higher in the months after the summer period (October and November) compared to the present situation (Fig. 3.7). It should be noted that, due to climate change, extreme droughts are expected to occur more often, probably leading to much larger effects on surface water salinity than illustrated by the W+ climate scenario. Secondly, it is expected that sea-level rise and changes in precipitation surplus will also reduce fresh water availability for admission into deep polders for surface water level control, salinity control and irrigation (Delta Program, 2013). Admission water originates from one of the major Dutch rivers (Rhine or Meuse) and the inlet-points may become salinized

and unsuitable if future sea-level rise and decrease of river discharge cause sea water intrusion further upstream on the river. The model results showed that a 50% reduction of the quantity of water admitted to the Noordplas Polder will have a large impact on surface water salinity (Fig. 3.7). During dry periods in summer, when there will be almost no dilution of the saline seepage water, the average chloride concentration would increases from 650 to 840 mg L^{-1}. This is also the period when demands for fresh irrigation water are highest.

Climate change vulnerability of RW-lenses

Due to their limited size and vicinity to the land surface, RW-lenses are vulnerable to climate change (changing recharge patterns) and to a rising sea level (enhancing seepage). For the south-western delta an increase of seepage due to sea level rise is expected to be significant for an area within 2 to 5 km from the coast (Oude Essink *et al*., 2010; Van Baaren *et al*., 2012a). Changing recharge patterns will affect the entire south-western delta. In chapter 5, we showed that the primary factors controlling RW-lens thickness and mixing zone salinities are recharge, seepage flux and drain tile depth. The effect of an increase of the seepage flux due to sea level rise on the position of the centre of the mixing zone, D_{mix}, can be assessed from Fig. 5.12a.

Additional model calculations were done with the 2D and 3D RW-lens models presented in chapter 5 to assess climate change and sea level rise effects to RW-lenses. The results were presented at the Delta change conference in Rotterdam (De Louw *et al*., 2010a) and at the Salt Water Intrusion Meeting-2010 in the Azores (De Louw *et al*., 2010b). The model results showed that the W+ climate scenario (wetter winters and drier summers) had a minor effect on the water table during the winter due to the rapid removal of recharge through drain tiles. However, during the much drier summer the water table dropped significantly (10 to 30 cm) compared to the present situation. Consequently, RW-lenses shrink during the drier summers but the projected increase in winter precipitation will not compensate for the lens shrinkage because the tile-drainage system efficiently discharges the higher recharge. Thus, the distribution of precipitation and evapotranspiration throughout the year, and in particular changing recharge patterns during the summer, determine the vulnerability of RW-lenses to climate change rather than the yearly average recharge. In contrast, recharge patterns throughout the year are less important for the much thicker BGH-lenses below paleochannel creek ridges and dunes which respond to long term average recharge fluxes.

7.4 Implications for sustainable freshwater supply and strategies

In the future, it is expected that freshwater demands in the Dutch delta will increase due to economic and population growths while the freshwater availability will decrease (Delta Program, 2013). The decrease of freshwater availability, especially during the summer period, is mainly due to (1) lower river base flows (Rhine, Meuse), (2) changing precipitation (-) and evaporation patterns (+), (3) sea level rise enhancing saline seepage and seawater intrusion. One of the strategies defined in the Delta Program is to encourage the self-sufficiency of areas to become less dependent on regional freshwater supply and to mitigate or to adapt to the adverse climate effects. Regional and local authorities and the direct freshwater users (mainly agriculture and horticulture) will become more and more responsible to ensure a sustainable freshwater supply for the future. Therefore, solutions should be

found in the local water system to improve benefits from the precipitation surplus and available fresh groundwater and surface water resources. This requires knowledge of the spatially and temporally varying processes of local fresh-salt water systems.

In recent years, various initiatives have been started in the south-western delta to increase the self-sufficiency of freshwater supply, such as the Water Farm (Van Baaren *et al*., 2012b) and GO-FRESH (http://publicwiki.deltares.nl/display/ZOETZOUT/Projecten). The Water Farm is a cooperation of farmers, local authorities, water board and residents that aims to manage the water inflows, -storage, -use and -outflows of an area such that no freshwater from outside the area is needed. GO-FRESH is an initiative of a consortium of researchers, farmers and water managers to increase the freshwater availability for agriculture with local measures. Currently (2013), we are testing innovative tile-drainage configurations to promote prolonged retention and storage of infiltrated freshwater in RW-lenses below agricultural fields. The tile-drainage systems are designed and implemented based on the gained knowledge of RW-lenses presented in chapter 5 and 6. Another GO-FRESH measure is the growth of BGH-lenses (temporary freshwater storage) in sandy paleo-creek ridges by artificial recharge of collected freshwater. This kind of aquifer storage and recovery systems (ASR) as a tool for self-sufficient fresh water supply are subjects of two PhD-researches of Koen Zuurbier (VU University, KWR) and Pieter Pauw (Wageningen University, Deltares).

The traditional way deep polders in the western Netherlands are connected to regional water systems via the inlet of freshwater into the polder and brackish water pumped out of the polder, needs to be changed to ensure a sustainable freshwater supply in the future. An important task for Water Boards will be to reduce salt loads from seepage. The research presented in this thesis established that the focus must be on the contribution of boils. The next section (section 7.5) reviews possible measures and their effectiveness to reduce salt loads and salt concentrations in deep polders.

The aim of the Delta Program is to guarantee that the Netherlands remains safe against flooding and that freshwater supply is adequate, now and in the future. To ensure this, on a national as well as regional scale, changes in the freshwater and saltwater system are required. Examples of such changes are moving inlet points upstream along the rivers for the regional freshwater supply, changing water levels and flow routes in polders, lakes or estuary basins, and changing dynamics and salinities (from salt to fresh or vice versa) of estuary basins and lakes. Obviously, regional up to national models are needed to assess regional effects of these changes. However, their impact on local systems requires knowledge of processes and assessment tools on a local scale. This thesis demonstrates that local processes, such as boil seepage, may have large consequences for water quality on a regional scale. Rapid assessment tools (RAT) may be useful for water managers to quickly assess effects and financial implications of changes in the water system and the implementation of measures, such as the €ureyeopener (Stuyt *et al*., 2012). Although a RAT needs to be a simple tool, it is important that the dominant processes are incorporated. The gained knowledge of local processes described in this thesis can be used and embedded in such a RAT. Another example of a RAT is the probabilistic water and salt balance model presented in chapter 3, when it will be equipped with a graphical user interface.

7.5 Adaptation and mitigation measures for deep polders

In attempts to abate surface water salinization and compensate the expected future increase of surface water salinity in deep polders, it is worth to focus attention on boils because of their dominant role in the salt load and their local nature. For example, in chapter 3, we demonstrated for the Noordplas Polder that reducing the preferential discharge via boils by 30% will result in a significantly lower surface water Cl concentration during dry periods in summer when demands are highest, i.e. from 650 to 415 mg L^{-1} (Fig. 3.7). The effectiveness and feasibility of several measures abating salinization in deep polders are discussed below. Because seepage water also contains high nutrient concentrations leading to the eutrophication of surface waters (chapter 2; ICW, 1976 and 1982; De Louw *et al*., 2000; Griffioen *et al*. 2002), measures to reduce salt loads will also help to solve the eutrophication problem of deep polders.

Boil sealing

Based on the findings that boils are dominant in the salinization and have a localized nature, we examined the possibility of sealing the boils as a measure to abate salinization in collaboration with the Rijnland District Water Control Board. This was done at three different locations which differed in hydrogeological settings and boil characteristics (Fig. 7.3). At all locations, there was a small area of 20 to 100 m^2 with multiple boils which varied in discharge and salinity. At site A (Haarlemmermeer Polder, Fig. 4.2a) the boils developed through a 6 m thick aquitard (Fig. 7.3a) and the outflow vents of the boils occurred at the surface (Fig. 4.1d). The boils at site B (Noordplas Polder, Fig. 4.2a) developed in a 7 m thick aquitard with a sandy paleochannel belt (Fig. 7.3b) and their outflow vents occurred underwater in a ditch (Fig. 4.1e). At site C there was no aquitard and the boils developed in the sandy sediments with their outflow vents in the ditch (Fig. 7.3c). According to the farmer's observations, the position and activity of the boils at site C changed regularly due to varying weather conditions (changes in atmospheric pressure). Boil activity was the highest during periods of low atmospheric pressure. The phenomenon that the discharge of springs and open wells vary with atmospheric pressure is well known and described in the literature (e.g. Rush and Johnson, 2002).

In attempts to seal the boils expanding and persisting, fluids (SAX-14 - a sodium aluminate solution) with an adjustable reaction time were injected in the aquifer near the source vent. The injected fluids subsequently flowed towards the source vent due to the flow created by the boil. A description of the monitoring activities to measure effects of the sealing attempts is given in chapter 4 (see Fig. 4.2). In addition, subsurface temperatures were measured at different depths using temperature probes (T-probes) to detect (changes in) preferential boil flow through the aquitard. At each site, a T-probe was installed in one of the boils and at different distances from the boil (Fig. 7.3a). T-probes contained ten sensors at 0.35 m depth intervals, and were inserted to a depth of 3.5 m. Soil temperature was measured and logged every hour for the period July 2008 until September 2011. The monitoring data provided useful information on the local boil systems. Some of the measurements were described in chapter 4 and an extensive description of the boil sealing experiments and measurement is given in De Louw *et al*. (2012a). The most important findings regarding the effectiveness of sealing boils are summarized below.

It was not possible to seal any boils at site C. This was probably due to the fact that there was no aquitard in which the boils could develop into discrete conduits like at site A and B. Instead, the boils acted like quick-sand pipes that regularly changed their position. The underwater position

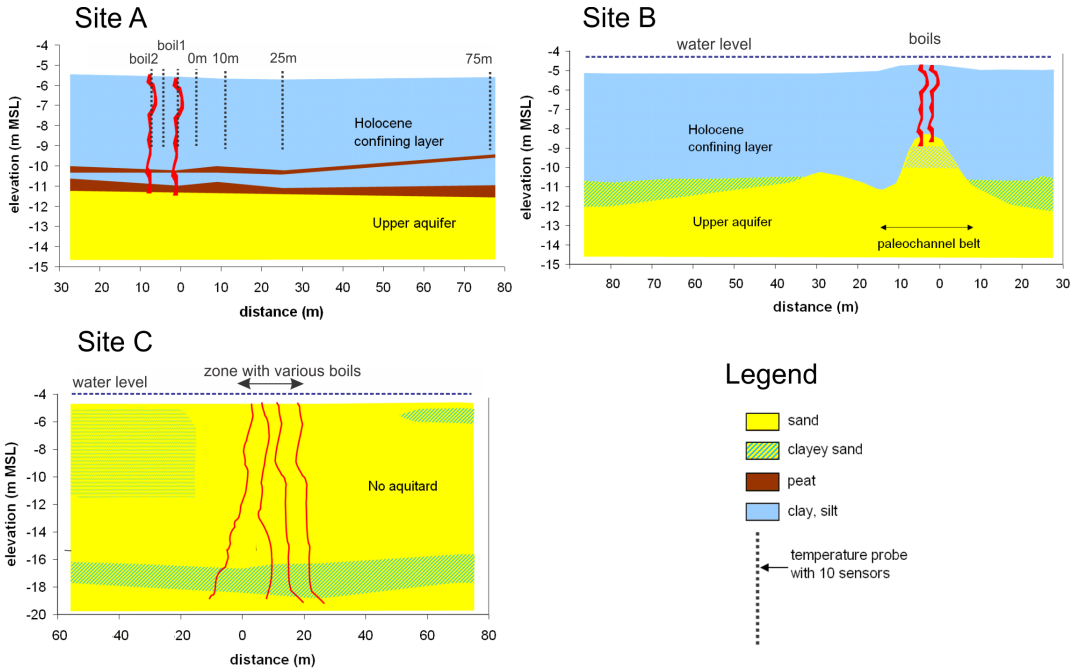

Fig. 7.3. The hydrogeological schematization of the three boil locations. The location of the temperature probes for site B and C are similar to those of site A

of the boil outflow vents at site B made it practically difficult to seal them. The difficulties were (i) finding the optimal location for injection, (ii) the adjustment of injection strategy, since the result of sealing was not directly visible, and (iii) monitoring the development of new boils. Injection of the fluids was done at ten different locations in the ditch within the boil area. Despite these practical difficulties, the total discharge of the boil area was reduced with ~50% by the sealing attempt. A reduction of boil flow was also visible in the temperature measurements (Fig. 7.4). The temperature in the boil was relatively constant (~11 ^{0}C) with depth and time due to the rapid upward flow of groundwater from deeper strata with a yearly average temperature of ~11 ^{0}C (Bense and Kooi, 2004) whereas at 5 m and 75 m from the boil, the penetration of seasonal atmospheric temperature fluctuations into the soil is clearly visible (Fig. 7.4). The notable small increase in temperature fluctuations at the boil of site B after the sealing attempt indicates only partial sealing. Note the sharp temperature increase during the boil sealing attempt due to heat producing chemical reactions of the injected expanding fluids.

At site A, two sealing attempts were carried out (Fig. 7.4). The outflow vents of the boils at the surface were visible which made the boil sealing more practicable. The temperature fluctuation slightly increased after the first attempt and significantly increased after the second attempt (Fig. 7.4). The total discharge of the boil cluster was reduced by the boil sealing attempt form 17 to 7 m^3 d^{-1} (Fig. 4.4a). Some important observations were made during the second boil sealing experiment at site A. First, the sudden cessation of groundwater discharge caused by sealing the vent of boil 1 caused a rapid increase in aquifer hydraulic head of 0.12 m at 2 m distance. Second, the discharge of boil 2 doubled as a result of the sealing attempt of boil 1. Third, by sealing off boils 1 and 2, a new boil developed at the surface at 4 m distance from boil 2 with a discharge of about 5 m^3

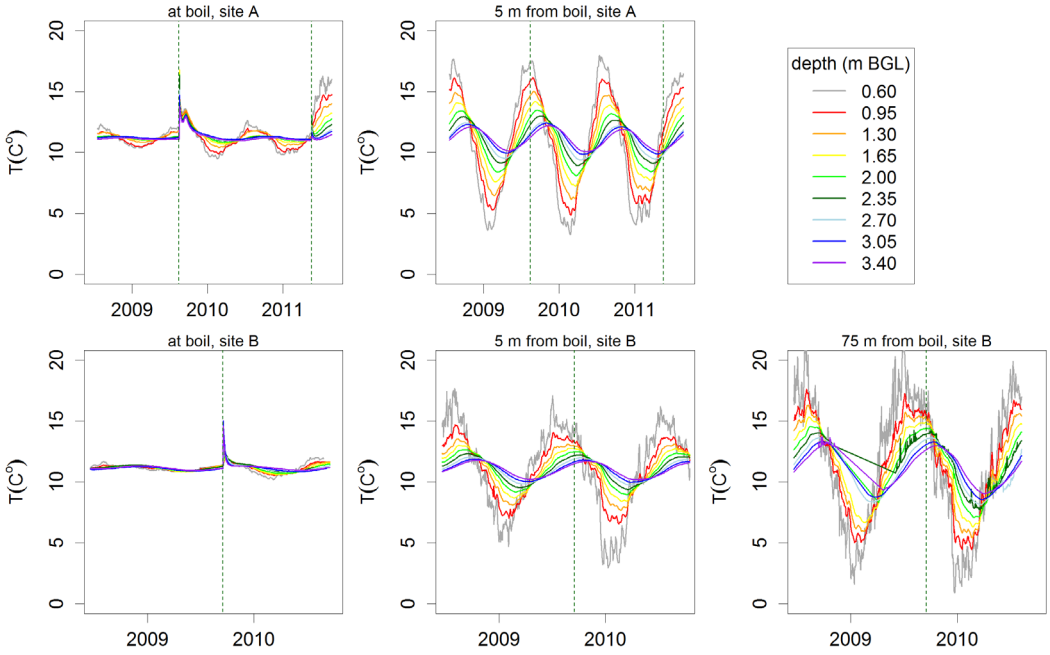

Fig. 7.4. Measured time series of temperature at different depths for locations at (or very near) the boil and at 5 m and 75 m from the boil (site A and B). The boil sealing attempts are indicated by the green dotted line.

d^{-1} and a Cl concentration of about 2 g L^{-1} (Fig. 4.4a-b). The development of new boils when boils 1 and 2 were (partly) blocked during the sealing experiment implies that existing cracks within the aquitard probably were reactivated. The regeneration of existing cracks is more likely to occur than the development of new cracks because of the only small increased aquifer hydraulic head (~0.12m). Based on these observations and because of the nature of boil development, we think that boil areas develop as described in the following way. When the water pressure in the aquifer exceeds the weight and cohesive forces of the overlying confining layer, heaving and cracking of the soil occurs over an area of 20 to 100 m^2 (chapter 4). Water starts flowing through cracks connected to the aquifer leading to the development of boils. This explains the observations that most boils occur in clusters within a small area. Sealing of the boil probably not occurred at the boil's source vent but somewhere in the confining layer resulting in the activation of existing cracks.

Regarding the practical difficulties of boil sealing, the occurrence of clustered boils in an unstable cracked zone and the development of new boils, we conclude that boil sealing is not a feasible measure to abate salinization in deep polders. Boil sealing may be more successful for boils which do not arise from heaving and cracking of the confining layer but from the removal of constructions (e.g. sheet piles, piezometers, wells) out of the confining layer leaving a direct open connection to the aquifer.

Note that reducing boil fluxes will lead to an increase in hydraulic heads resulting in an increase of diffuse and paleochannel seepage fluxes. However, since these forms of seepage are associated with a lower salinity, the overall net effect with respect to surface water salinization will be positive.

Increasing surface water levels

A well known measure to reduce seepage fluxes is decreasing the head difference over the HCL by increasing

water levels (e.g. Oude Essink *et al*., 2010; Van der Eertwegh *et al*., 2006). However, this measure is only effective in reducing salt loads when it is implemented in areas where paleochannel seepage and boils occur since these forms of seepage are the only significant contributors to the salinization of a deep polder. The widespread occurrence of boils and paleochannel belts (see Fig. 2.6 and 7.2) makes implementation practically difficult. Regarding the large head differences over the HCL in deep polders (1.0 to 2.5 m), surface water levels must be raised quite a lot in order to significantly reduce the seepage flux and salt loads. Raising surface water levels conflicts with the demands of agriculture, but implementation or adjustments of tile-drainage systems may compensate the adverse effects.

Inundating (parts of) deep polders, i.e. transforming them back into lakes, would significantly reduce seepage loads or even terminate the seepage at the location of implementation. However, side-effects of this measure should be considered since it is expected that aquifer heads, and therefore seepage, will increase in the adjacent polders. For many years there was discussion about inundating a part of the Groot-Mijdrecht Polder, the polder with the highest salt load of the Netherlands, in order to stop the saline seepage. Because this high-impact measure would involve the displacement of 12 farming houses including their associated agricultural business, it encountered big opposition. Recently, it was decided that the polder will not be inundated.

Groundwater extraction

Another way to reduce head differences over the HCL in order to reduce seepage fluxes is extracting groundwater from the upper aquifer. However, large amounts of groundwater must be extracted to sufficiently reduce the heads in the upper aquifer for large areas. For example, model calculations of De Louw *et al*. (2007) showed that seepage is reduced by ~1/10 of the extracted amount of groundwater. Besides this, the extracted groundwater will be saline due to saltwater upconing and subsequently needs to be removed from the polder. Using pipelines is an expensive solution for the removal and model calculations showed that the re-infiltration of the extracted groundwater in deeper strata will increase the seepage significantly in adjacent polders (De Louw *et al*., 2007). Another possibility is the production of fresh drinking water from the extracted saline groundwater by reverse osmosis (Olsthoorn, 2008) from which the benefits and hurdles are given in Stuyfzand and Raat (2010). The possibilities of the use of saline groundwater as a drinking water source are further examined within the PhD-research of Frank Smits (Delft University of Technology, Waternet).

Collecting saline seepage water

The water and salt balance of the Noordplas Polder presented in chapter 3 showed that > 75% of the inflow is freshwater. Unfortunately, the mixing with a relative small proportion of saline groundwater makes the surface water brackish and unsuitable for irrigation during the dry periods. Therefore, collecting saline seepage water and isolate it before it mixes with freshwater could increase the freshwater availability. There are two challenges associated with this measure: (1) the method of collecting saline seepage water, and (2) the elimination of the collected saline water out of the polder water system.

Ad 1. The spatial distribution of paleochannel and boil seepage makes the collection of saline seepage water difficult. However, one could focus on areas where large saline boils are clustered. Since most infiltrated rainwater is discharged via tile-drainage, freshwater could be collected relatively easily by connecting the drain-tiles. This would be easier than collecting the saline seepage water below the ditch. Boil water can be collected and isolated from ditch water using PVC-pipes installed around the outflow vent.

Ad 2. A probably larger and more expensive challenge is the separate discharge of the collected saline seepage and freshwater out of the polder and subsequently to the sea. Pipelines could be used or ditches could be divided into a fresh and a saline discharge part, however, both are expensive and practically difficult. Another possibility is to desalinize (reverse osmosis) the collected saline water at the source or at the location of usage. However, the method demands a lot of energy and is therefore costly and the removal of the rest-product 'the brine' is another difficulty. Saline water reverse osmosis systems are considered as a promising solution when operated with renewable energy (Stuyfzand and Raat, 2010). Re-infiltration of the collected saline seepage water into deeper strata, i.e. below the upper aquifer, is another possibility to remove saline water from the polder water system. Possible adverse effects of this method are: the increase of seepage due to an increase of heads (also for adjacent polders), the acceleration of the autonomous salinization, and chemical reactions between the infiltrated water and the resident groundwater leading to an undesirable change of groundwater quality (e.g. the release of heavy metals or arsenic). However, it is worth examining the pros and cons of re-infiltrating small amounts of saline water to reduce salt loads.

Operational saltwater management

As pointed out above, the effectiveness and feasibility of the mentioned technical measures are rather limited. Alternatively, we think that operational saltwater management could be an effective, cheap and easy to implement measure. Operational saltwater management means the dynamic and integrated control of pumping out polder water, the admission of 'boezem' water and the temporary storage of seepage water in ditches, based on weather forecasts and the real-time monitoring of salt concentrations at strategic locations. The goal of this measure is to reduce salt concentrations of the surface water system. As shown in chapter 3, the salt concentration of the pumping water is highly dynamic with time and responds to individual rain events. Major peaks of salt loads coincide with relatively low chloride concentrations as they occur during peak flows (Fig. 3.3). Heavy rainfall events probably mobilize the temporary stored seepage water in the HCL and in the surface water system. This characteristic can be used to improve the saltwater management of the polder as pointed out below.

The current strategy of pumping and admission is based on a long tradition and seems inefficient regarding the control of surface water salt concentration. During the summer 'boezem' water is admitted in order to maintain surface water levels at a fixed level and to reduce salt concentrations in the entire polder, However, most of the ditches are not reached by the admitted fresh water, and on its way through the polder, the fresh water gets salinized by the boils. Subsequently, the excess water is pumped out of the polder to maintain a fixed surface water level. The temporary cessation of the pumping during dry periods avoid salt loading of the regional surface water system. In this way, saline seepage water is temporarily stored in the polder water system and this could be limited to saline ditches with many saline boils. The temporary isolation of salt areas (with boils) from fresh areas (without boils) in the polder can easily be controlled by small automatic weirs and this will keep the freshwater fresh. Subsequently, the stored saline seepage water can be pumped out of the polder during rain events when salt concentrations are low. The findings of this thesis may be helpful to design such an operational saltwater management system. Essential knowledge about groundwater surface water interactions in deep polders and the dynamic routes of saline and fresh surface water flow, in relation to salinization processes in times of droughts, is provided by the PhD-research of Joost Delsman (Deltares, VU University Amsterdam).

Prevention of the development of new boils

Given the difficulty to significantly reduce salt loads into Dutch deep polders taking into account the dominance of boils, one should at least try to avoid the development of new boils. Every new boil will potentially increase the salt load and this process seems irreversible. Therefore, all activities that potentially increase the risk of boil development should be avoided or carried out with care and accompanied with counter measures. Examples of risky activities are the removal of soil for any reason, the installation of any structure into the HCL and the increase of the aquifer head by the infiltration of groundwater in the aquifer (e.g. aquifer thermal energy storage systems) or the cessation of groundwater abstractions. Risks of boil development should always be taken into account in plans for new land reclamation.

7.6 Adaptation and mitigation measures for RW-lenses

As pointed out in section 7.3, RW-lenses are very vulnerable to climate change (changing recharge) and sea level rise (enhancing seepage) due to their limited size and vicinity to the surface. The expected shrinking of RW-lenses and increase in RW-lens salinity will probably increase root zone salinities affecting agricultural crops. The numerical simulations and field observations presented in chapter 5 and 6 showed that, besides recharge and seepage, tile-drainage is an important factor controlling the RW-lens dimensions and characteristics. Therefore, the adjustment of tile-drainage systems could be an effective measure to increase the freshwater availability and to mitigate the adverse effects of climate change and sea level rise.

As follow up of this study, different tile-drainage systems are currently being tested at study site B (Fig. 6.2) with the aim to increase the storage of infiltrated freshwater in RW-lenses (GO-FRESH initiative, see section 7.4). One of the tested systems involves the installation of drain tiles at a depth of 1.2 m BGL, which is 0.5 m deeper than the current drainage depth, and the horizontal drain separation is reduced from 10 to 5 m. The new tile-drainage system allows the discharge of deeper and more saline groundwater from the mixing zone during rain events while the RW-lens is growing by the recharge of infiltrated rainwater until a new equilibrium is reached.

7.7 Measuring and monitoring saline seepage

In this study, we applied many different types of field measurements at different spatial and time scales to map and quantify saline seepage processes. Measuring and monitoring saline seepage is the first step in abating salinization since defining adaptation and mitigation measures is only meaningful when the spatial variability and temporal dynamics of saline seepage are known. A short review of field methods to measure saline seepage processes is given, based on our experiences.

Mapping boils

In chapter 2 and Fig. 7.4, we demonstrated that groundwater discharged via boils has a virtually constant temperature of ~11 ^{0}C during the year which makes it easy to trace boil seepage using temperature measurements. The use of temperature measurements to trace preferential saline seepage via boils and assess flow velocities was presented at the Salt Water Intrusion Meeting-2010 in the Azores (De Louw *et al*., 2010c) of which a summary is given below. Temperature was measured

using the following methods:

1) soil temperature measurements in the ditch using the temperature and soil electrical conductivity (TEC)-probe;
2) combined surface water temperature and EC survey (using coupled EC and temperature sensor);
3) lateral temperature variations using a DTS (Distributed Temperature Sensing) fibre optic cable;
4) airborne thermal infra-red measurements;
5) time series of soil-temperature depth profiles.

Fig. 2.7 clearly demonstrates the position of the boil traced by temperature-depth profiles measurements with the TEC-probe (method 1). This method is suitable for exactly locating boils when outflow vents are under water. Method 2 was applied in the Haarlemmermeer Polder where the temperature and EC was measured automatically at 10 seconds interval using a CTD-diver (Schlumberger Water Service®) while navigating over the canals (Goudriaan *et al.*, 2011). A drop in temperature (survey was carried out in summer) in combination with an increase in EC indicated the location of a saline boil. In this way, a large area could be surveyed (> 135 km of water ways) and 195 boils were mapped as well as their salinity. This method was subsequently applied in other deep polders within the management area of the Rijnland District Water Control Board (Fig. 7.2; Rijnland, 2013). A 500 m long DTS fibre optic cable (method 3) with a spatial resolution of 1 m was used to monitor the daily temperature variation at the ditch bottom during the boil sealing attempts at site B and C. The measurements were carried out for a period of 3 to 5 days with a frequency of 1 hour to trace the location of the boils and to monitor whether new boils developed during the sealing attempts (De Louw *et al.*, 2012a; Vandenbohede, *et al.*, 2013). The use of DTS measurements to estimate boil discharges is part of the PhD-research of Koen Hilgersom (Delft University of Technology). For a small pilot area in the Noordplas Polder, a remote controlled mini helicopter with onboard thermal infra-red camera was used to measure temperature differences in ditches (method 4). Although some boils could be detected with this method, it proved to be a big disadvantage that thermal infra-red only detects temperature differences at the top of surface water. Since boils discharge groundwater through the bottom of ditches, the associated temperature anomalies may not be detectable at the surface due to the mixing with the ambient water. Time series of soil-temperature depth profiles (method 5) were measured in order to monitor changes in preferential flow as demonstrated in Fig. 7.4. In general, measurements of subsurface temperatures using temperature probes provide valuable insight into groundwater flow patterns and vertical flow velocities can be assessed from measured temperature envelopes (e.g. Stallman, 1965; Vandenbohede and Lebbe, 2010).

Monitoring water and salt fluxes in deep polders

Our results presented in chapter 3, have confirmed the need for frequent measurements of polder water discharge and discharge-weighted concentrations at the outlet of the polder, in order to obtain reliable model simulations of water and salt fluxes and to assign them to the different sources. The model results showed that model input and output uncertainty can be reduced by improving the quality of field measurements. Monitoring activities should therefore be concentrated on those parameters which have the strongest impact on the modeled water and salt fluxes. The most sensitive parameters are boil flux, boil water salinity and the admission of 'boezem' water, all of which show significant interdependencies (Fig. 3.6). This implies that focusing monitoring efforts on increasing the accuracy

of a single parameter will automatically lead to a greater accuracy of correlated parameters. The estimation of the total boil flux, which is one of the most uncertain and most important parameters, can therefore be improved by collecting accurate temporal data about the admission of 'boezem' water or boil water salinity.

Mapping rainwater lenses

In chapter 5, we described the results of different geophysical and hydrological measurements to map the characteristics and spatial variability of rainwater lenses. The groundwater salinity change with depth and the dimensions of rainwater lenses can be accurately determined using a TEC-probe and ECPT. Since conductivity contrasts of fresh and saline groundwater dominate the measured soil-EC depth profiles rather than differences in lithology, no correction for formation is essential for deriving dimensions of rainwater lenses. However, when absolute salinity values are of interest, the geophysical measurements must be combined with salinity values obtained from groundwater sampling. The TEC-probe can be applied manually until a depth of about 4 m BGL and is therefore very suitable for measurements in agricultural fields and in ditches. ECPTs are pushed mechanically into the subsurface reaching much larger depths (> 25 m) than with the TEC-probe and are needed when rainwater lenses are thicker than 4 m. Surface geophysics can be used to delineate rainwater lenses for larger areas. Cross sections of groundwater salinity can be acquired using CVES and are therefore suitable to map the spatial variation of rainwater lens thickness within an agricultural field. However, the exact depth of the rainwater lens's base and the mixing zone dimensions cannot be accurately obtained with CVES without the combination of TEC-probe or ECPT measurements. Helicopter-borne EM was applied successfully to map rainwater lens thickness for a large area. 21 ECPTs were used to improve the resistivity-depth inversion models of the HEM-data but only little adjustment was needed, making this technique very promising for data-poor coastal areas throughout the world. The ECPT salinity depth profiles were surprisingly well reproduced by the HEM-measurements, which made it possible not only to map the lens thickness but also the salinity change of the transition zone.

Multi-screen groundwater sampling was applied to monitor the RW-lens dynamics. The use of surface geophysics to monitor temporal variations of shallow subsurface resistivities is difficult due to the impact of unsaturated zone conditions, temperature effects and non-unique interpretation of the measurement data (Goes *et al*., 2009).

7.8 Suggestions for further research

Surface water eutrophication by nutrient-rich seepage

In this study we focused on salinization due to saline seepage. The chemical data presented in chapter 2 (Table 2.1) and studies of e.g. Griffioen *et al*. (2002) and ICW (1976, 1982) showed that, besides salt, seepage water contains high concentrations of phosphate and ammonium. De Louw *et al*., 2000 estimated for the Noordplas Polder that ~50% of the nitrogen load and > 70% of the phosphate load is caused by groundwater seepage leading to the eutrophication of surface waters. However, it is unknown how the different seepage types contribute, and in particular boils, to the nutrient loads and what the temporal variations are. Phosphor and nitrogen are involved in redox-processes when flowing through the HCL and discharging into ditches, which complexes the assessment of their time-varying contribution.

The probabilistic water and salt balance model presented in chapter 3 can be used to

simulate daily varying nutrient loads incorporating uncertainties of input parameters. The first step is the conditioning of the model with high-frequency discharge-weighted Cl concentrations and discharge measurements of the pumping water in order to quantify the water fluxes and conservative solute transport, as demonstrated in chapter 3. The second step is adding the main chemical processes to the model concept. High-frequency discharge-weighted measurements of nutrient concentrations are required to condition the model and to derive behavioural parameter sets for simulation of the daily varying nutrient loads and concentrations. Subsequently, the nutrient loads can be assigned to the different sources.

Delsman *et al* (2013a) recently described an improved GLUE-based end member mixing approach (G-EMMA) to identity various sources and quantify their contribution to surface water chemical loading, adequately dealing with their large spatial variation. G-EMMA was successfully applied in a sub-catchment of the Haarlemmermeer Polder.

Chemical consequences of mixing between rainwater and saline seepage in RW-lenses

The mixing between infiltrating rainwater and upward saline seepage in RW-lenses occurs at shallow depth. The chemical compositions of the two water types differ significantly. Infiltrating rainwater is oxic and may contain nutrients and contaminants from fertilizers whereas saline seepage is anoxic, contains the nutrients phosphate and ammonium and many other solutes in high concentrations comparable to those found in seawater. These two water types mix in a dynamic environment in the vicinity of the surface and the resulting chemical processes and consequences are unknown. The mixing may adversely impact the shallow groundwater quality or the loading of nutrients from seepage via tile-drainage systems into surface water systems. This subject is part of the PhD-research of Sara Eeman (Wageningen University).

Interactions between RW-lens and soil water salinity

The research presented in chapter 5 and 6 focused on the characteristics and temporal behaviour of thin RW-lenses which are of great importance from an agricultural perspective due to their limited size and vicinity to the land surface. Salt present in the RW-lens migrates upwards to the root zone by capillary rise during the summer period, possibly affecting crop growth. RW-lens characteristics and dynamics are important boundary conditions for the soil water system. Root zone salinity is the crucial parameter to assess when salt damage to crops is of interest. Although field data of soil water salinities were collected (chapter 6), the interactions between RW-lens dynamics and soil water salinity are still not fully understood. These aspects need to be studied in more detail with additional field data combined with variably saturated solute transport modeling. Furthermore, cracks may significantly affect soil water salinities (and drain water salinities), as discussed in chapter 6, but their exact role is still unclear. Dual porosity or dual permeability models may be helpful to analyze the influence of this kind of macro-pore flow through the unsaturated zone.

Hydraulic resistance of the Holocene confining layer (HCL)

The hydraulic resistance of the HCL is an important parameter which determines diffuse and paleochannel seepage fluxes in Dutch polders. However, as discussed in chapter 2 and 3, the hydraulic resistance of the HCL is uncertain due to its vertical heterogeneity and spatial variability and the large uncertainties of the hydraulic conductivity of the sediments. Moreover, the presence of boils may reduce the lumped hydraulic resistance for a certain area significantly. This is for example important when using pumping test data to derive hydraulic resistances. It can be argued that outside the boils and paleochannel belts, the HCL

is almost impermeable for flow in areas where compacted basal peat is present in the HCL, and that all seepage occurs through boils and paleochannel belts. Regarding the uncertainties and importance, it is worth focusing research on the hydraulic resistance of the HCL at different spatial scales, including the effects of boils. The research may consist of a combination of collecting additional field data (local pumping test, hydraulic conductivity measurements, tracer tests to estimate flow velocities) at different spatial scales combined with detailed (stochastic) groundwater modeling of flow through the HCL.

Implementation of boils in regional groundwater model studies

The dominant contribution of boils to the salinization of deep polders is clearly demonstrated in chapter 2 and 3. Boils should therefore always be taken into account in salinization assessment studies. A major challenge would be the incorporation of boils in regional groundwater models, since there are large differences in scales between boils and regional models. The analysis presented in chapter 4 showed that saltwater upconing by preferential discharge via boils operates at very local scales whereas typical model cell sizes used in regional groundwater models are much larger, varying in sizes from 25x25 m to 250x250 m (e.g. Oude Essink *et al*., 2010; NHI-2.2., 2011). Therefore, saltwater upconing mechanisms via boils and consequently boil water salinities and salt loads cannot be assessed correctly with the conventional regional groundwater models. More research is needed on how these small scale phenomena can be incorporated in large scale groundwater models.

Prevention of boil development

As discussed in section 7.5, it is extremely difficult to significantly reduce salt loads via boils and therefore the future development of new boils should be avoided as much as possible. To provide water managers with practical information on how to avoid the development of new boils, more knowledge is needed of the geo-mechanical aspects of boil development in general and in relation to any intervention in the HCL (e.g. infrastructural works).

Operational saltwater management

Operational saltwater management in deep polders, as described in section 7.5, could be an effective measure to reduce salt concentrations of the water pumped out of deep polders and subsequently of the regional water system. An operational saltwater management system consists of (i) a real-time monitoring network, (ii) a data assimilating model that simulates and forecasts salt concentrations and discharge, (iii) operation decision rules to control surface water levels, pumping, storage, and admission of water, and (iv) automatically controlled water works (e.g. weirs, pumps, inlets). An optimal design of such an operational saltwater management system requires more knowledge of these aspects individually as well as their integration.

Airborne electromagnetic measurements

In chapter 5 we demonstrated that the salinity distribution of groundwater in aquifers and rainwater lens characteristics can be mapped successfully for large areas using helicopter electromagnetic measurements within reliable ranges. A solid estimate of the salinity distribution in the subsoil is the first step in studying freshwater–saltwater processes. Impacts of future changes on the salinity distribution (e.g. for freshwater supply) can only be assessed accurately when the present salinity distribution is known. An airborne electromagnetic survey is an appropriate way to obtain the necessary data for a reliable salinity distribution of the subsoil (Faneca Sànchez *et al*., 2012). When an airborne electromagnetic survey is combined with variable density numer-

ical modeling, the inversion models of airborne data can be improved significantly. How to optimize this should be subject to further research. It is also worth investigating how airborne electromagnetic measurements can be used in data-poor areas providing groundwater models with the required hydrogeological and salinity information.

Quantifying local flow systems with temperature measurements
Temperature measurements were very useful to trace preferential seepage through the HCL (chapter 2, section 7.5 & 7.7). Measured time series of soil-temperature depth profiles (Fig. 7.4) were used to assess vertical flow velocities through the HCL (De Louw *et al*., 2010c). Detailed monitoring of soil-temperature depth profiles (Fig. 7.4) in and around ditches or other watercourses is a promising and cheap method to study and quantify local groundwater flow patterns and the dynamic interactions between surface water, local groundwater and seepage.

Acknowledgement

This study was part of various research projects. The research in the Noordplas Polder was done in collaboration with the Rijnland District Water Control Board, Westelijke Tuinbouw Organisatie and Dienst Landelijk Gebied. The detailed measurements of the local boil systems in the Haarlemmermeerpolder and the Noordplas Polder were part of a field study to examine the possibilities of sealing boils in order to reduce salt loads, carried out in collaboration with the Rijnland District Water Control Board. The research in the south-western delta was part of CLIWAT, the INTERREG IV-B project (www.cliwat.eu), the Dutch Knowledge for Climate Program "Climate Proof Freshwater Supply" (http://knowledgeforclimate.climateresearchnetherlands.nl) and the Project 'Salinization of phreatic groundwater in the Province of Zeeland', in collaboration with the Province of Zeeland, the Scheldestromen Water Board, Dienst Landelijk Gebied and the Zuidelijke Land en Tuinbouw Organisatie.

The analysis of the data was done in collaboration with Deltares (Utrecht, the Netherlands), TNO Geological Survey of the Netherlands (Utrecht, the Netherlands), VU University Amsterdam (Amsterdam, the Netherlands), Wageningen University (Wageningen, the Netherlands), the Rijnland District Water Control Board (Leiden, the Netherlands), Ghent University (Ghent, Belgium), Bundesanstalt für Geowissenschaften und Rohstoffe (BGR) (Hanover, Germany) and Flinders University – National Centre for Groundwater Research and Training (Adelaide, Australia).

References

Acharya, S., Jawitz, J.W., Mylavarapu, R.S., 2012. Analytical expressions for drainable and fillable porosity of phreatic aquifers under vertical fluxes from evapotranspiration and recharge. Water Resources Research 48, W11526, doi:10.1029/2012WR012043.

Antonellini, M., Mollema, P., Giambastiani, B., Bishop, K., Caruso, L., Minchio, A., Pellegrini, L., Sabia, M., Ulazzi, E., Gabbianelli, G., 2008. Salt water intrusion in the coastal aquifer of the southern Po Plain, Italy. Hydrogeology Journal 16, 1541-1556.

Antonellini, M., Mollema, P.N.: Impact of groundwater salinity on vegetation species richness in the coastal pine forests and wetlands of Ravenna, Italy. Ecological Engineering, 36(9), 1201-1211, 2009.

Archie, G.E., 1942. The electrical resistivity log as an aid in determining some reservoir characteristics. Petroleum Transactions of AIME 146, 54-62.

Bakker, M., 2000. The size of the freshwater zone below an elongated island with infiltration. Water Resources Research 36(1), 109-117.

Barlow, P., Reichard, E., 2010. Saltwater intrusion in coastal regions of North America. Hydrogeology Journal 18(1), 247-260.

Bear, J., Cheng, A.H.D., Sorek, S., Ouazar, D., Herrera, I., (Ed.), 1999. Seawater intrusion in coastal aquifers–concepts, methods, and practices. Dordrecht, The Netherlands: Kluwer Academic Publishers.

Bear, J., Zhou, Q., Bensaba, J., 2001. Three dimensional simulation of seawater intrusion in heterogeneous aquifers, with application to the coastal aquifer of Israel. Proc. of first international conference on saltwater intrusion and coastal aquifers: monitoring, modeling, and management. Essaouira, Morocco, 13pp.

Becker, M.W., Georgian, T., Ambrose, H., Siniscalchi, J., Fredrick, K., 2004. Estimating flow and flux of groundwater discharge using water temperature and velocity. Journal of Hydrology 296, 221-233.

Benke, K.K., Lowell, K.E., Hamilton, A.J., 2008. Parameter uncertainty, sensitivity analysis and prediction error in a water-balance hydrological model. Mathematical and Computer Modelling 47 (11-12), 1134-1149.

Bense, V.F., Kooi, H., 2004. Temporal and spatial variation of shallow subsurface temperature as a record of lateral variations in groundwater flow. Journal of Geophysical Research 109, B04103.

Berendsen, H.J.A., 1998. Birds-eye view of the Rhine-Meuse delta (The Netherlands). Journal of Coastal Research 14(3), 740-752.

Berendsen, H.J.A., Stouthamer, E., 2000. Late Weichselian and Holocene palaeogeography of the Rhine-Meuse delta, the Netherlands. Palaeogeography, Palaeoclimatology, Palaeoecology 161(3-4), 311-335.

Beven, K., 2006. A manifesto for the equifinality thesis. Journal of Hydrology 320 (1-2), 18-36.

Beven, K., 1993. Prophecy, reality and uncertainty in distributed hydrological modeling. Advances in Water Resources 16 (1), 41-51.

Beven, K.J., Binley, A.M., 1992. The future of distributed models: model calibration and predictive uncertainty. Hydrological Processes 6, 279–298.

Blasone, R.S., Madsen, H., Rosbjerg, D., 2008a. Uncertainty assessment of integrated distributed hydrological models using GLUE with Markov chain Monte Carlo sampling. Journal of Hydrology 353 (1-2), 18-32.

Blasone, R.S., Vrugt, J.A., Madsen, H., Rosbjerg, D., Robinson, B.A., Zyvoloski, G.A., 2008b. Generalized likelihood uncertainty estimation (GLUE) using adaptive Markov Chain Monte Carlo sampling. Advances in Water Resources 31 (4), 630-648.

BMNED, 2011. Geotechnical research for CLIWAT pilot area B (climate change and water). Report 0100685/071032292, rev. B (in Dutch).

Bobba, A. G., 2002. Numerical modelling of salt-water intrusion due to human activities and sea-level change in Godavari Delta, India. Hydrological Sciences (47), 67–80.

Boekelman, R.H., 2001. Development of freshwater lenses. Proc. 16th Salt Water Intrusion Meeting, Miedzyzdroje, Wolin Island, Poland, 5-9.

Bower, J.W., Motz, L.H., Durden, D.W., 1999. Analytical solution for determining the critical condition of saltwater upconing in a leaky artesian aquifer. Journal of Hydrology 221, 43–53.

Carneiro, J.F., Boughriba, M., Correia, A., Zarhloule, Y., Rimi, A., El Houado, B., 2010. Evaluation of climate change effects in a coastal aquifer in Morocco using a density-dependent numerical model. Environ. Earth Sci. 61, 241–252.

Cartwright, K., 1974. Tracing shallow groundwater systems by soil temperature. Water Resources Research 10 (4), 847-855.

Chidley, T.R.E., Lloyd, J.W., 1975. A mathematical model study of freshwater lenses. Groundwater 15(3), 215-222.

Cirkel, D.G., Witte, J.P.M., Van der Zee, S.E.A.T.M., 2010. Estimating seepage intensities from groundwater level time series by inverse modelling: A sensitivity analysis on wet meadow scenarios. Journal of Hydrology 385, 132-142.

Collins, W.H., Easley, D.H., 1999. Freshwater lens formation in an unconfined barrier island aquifer. J. Am. Water Resour. Ass. 35, 1-22.

Custodio, E., 2010. Coastal aquifers of Europe: an overview. Hydrogeology Journal 18 (1), 269-280.

Custodio, E., Bruggeman, G.A., 1987. Groundwater problems in coastal areas, studies and reports in hydrology. UNESCO, International Hydrological Programme, Paris.

Dagan, G., Bear, J., 1968. Solving the problem of local interface upconing in a coastal aquifer by the method of small perturbations. Journal of

Hydraulic Research 6(1), 15–44.
Dausman, A., Langevin, C.D., 2005. Movement of the saltwater interface in the surficial aquifer system in response to hydrologic stresses and water management practices, Broward County, Florida. U.S. Geological Survey Scientific Investigations Report 2004–5256, 73pp.
De Louw, P.G.B., Griffioen J., Van Eertwegh, G.A.P.H., 2000. High nutrient and chloride loads to surface water in polder areas due to groundwater seepage. In: Sililo, O. (Ed.), Past Achievements and Future Challenges. A.A. Balkema, Cape Town, South Africa, 418-486.
De Louw, P.G.B., Bakkum, R., Folkerts, H., Van Hardeveld, H., 2004. The effect of water management on the chloride and nutrient surface water loads in Polder de Noordplas. Water- en solute balances and effects of different water management practices. TNO report NITG 04-241 (in Dutch).
De Louw, P.G.B., Stuurman, R.J., 2005. Strange time series 4 (rare reeks 4): The non-fluctuating hydraulic head. Stromingen 11(2), 49-52 (in Dutch).
De Louw, P.G.B., Oude Essink, G.H.P., Maljaars, P. 2007. Background study: seepage reduction techniques, TNO report 2007-U-R0357/B, 82pp (in Dutch).
De Louw, P.G.B. (Ed.), 2007. Salinization in the Netherlands. NHV-special 7, ISBN 90-803565-7-3, Netherlands Hydrological Society, Utrecht, 94pp (in Dutch).
De Louw, P.G.B., Oude Essink, G.H.P., Stuyfzand, P.J., Van der Zee, S.E.A.T.M., 2010. Upward groundwater flow in boils as the dominant mechanism of salinization in deep polders, The Netherlands. Journal of Hydrology 394, 494-506.
De Louw, P.G.B., Voortman, B.R., Van Baaren, S.E., Eeman, S., Vermue, E., Oude Essink, G.P.H., 2010a. Climate effects on shallow rainwater lenses on top of saline groundwater. Proc. of the Deltas in times of climate change conf., Rotterdam, the Netherlands, 79-80.
De Louw, P.G.B., Voortman, B.R., Oude Essink, G.P.H., 2010b. Spatial variation of shallow rainwater lenses on top of saline groundwater: merging model and monitoring results. Proc. of the 21th Salt Water Intrusion Meeting, Azores, Portugal, 355-358.
De Louw, P.G.B., Vandenbohede, A., Oude Essink, G.H.P., Doornenbal, P., 2010c. Tracing preferential saline seepage and assessing its flow velocities using temperature measurements. Proc. of the 21th Salt Water Intrusion Meeting, Azores, Portugal, 65-68.
De Louw, P.G.B., Van de Velde, Y., Van der Zee, S.E.A.T.M., 2011a. Quantifying water and salt fluxes in a lowland polder catchment dominated by boil seepage: a probabilistic end-member mixing approach. Hydrology and Earth System Sciences 15, 2101-2117.
De Louw, P.G.B., Eeman, S., Siemon, B., Voortman, B.R., Gunnink, J., Van Baaren, S.E., Oude Essink, G.H.P., 2011b. Shallow rainwater lenses in deltaic areas with saline seepage. Hydrology and Earth System Sciences 15, 3659-3678.
De Louw, P.G.B., Doornenbal, P., Hendriks, D.M.D., 2012a. Field research about sealing boils. Deltares-report. 1201949-000, 52pp (in Dutch).
De Louw, P.G.B., Eeman, S., Van Baaren, S.E., Oude Essink, G.H.P., 2012b. Constantly alternating upward and downward head-driven flow as mixing mechanism between rainwater and saline seepage. Proc. 22th Salt Water Intrusion Meeting, Armação dos Búzios, Rio de Janeiro, Brazil, 227.
De Louw, P.G.B., Vandenbohede, A., Werner, A.D., Oude Essink, G.H.P., 2013a. Natural saltwater upconing by preferential groundwater discharge through boils, Journal of Hydrology 490, 74-87.
De Louw, P.G.B., Eeman, S., Oude Essink, G.H.P., Vermue, E., Post, V.E.A., 2013b. Rainwater lens dynamics and mixing between infiltrating rainwater and upward saline groundwater seepage beneath a tile-drained agricultural field. Journal of Hydrology 501, 133-145.
Dellwig, O., Watermann, F., Brumsack, H.J., Gerdes, G., Krumbein, W.E., 2001. Sulphur and iron geochemistry of Holocene coastal peats (NW Germany): a tool for palaeoenvironmental reconstruction. Palaeogeography, Palaeoclimatology, Palaeoecology 167, 359-379.
Delsman, J.R., Oude Essink, G.H.P. Beven, K.J., Stuyfzand, P.J., 2013a. Uncertainty estimation of end-member mixing using generalized likelihood uncertainty estimation (GLUE), applied in a lowland catchment. Water Resources Research 49(8), 4792-4806.
Delsman, J.R., Hu-a-ng, K., Vos, P.C., de Louw, P.G.B., Oude Essink, G.H.P., Bierkens, M.F.P., 2013b. Palaeo-modeling of coastal salt water intrusion during the Holocene: an application to the Netherlands (submitted).
Delta Program, 2012. Werk aan de Delta. Deltaprogramma 2012. Maatregelen van nu, voorbereiding voor morgen. Ministerie van Infrastructuur en Milieu, Ministerie van Economische Zaken, Landbouw en Innovatie. Den Haag. 80pp (www.deltacommissaris.nl) (in Dutch).
Diersch, H.J.G., Prochnow, D., Thiele, M., 1984. Finite-element analysis of dispersion-affected saltwater upconing below a pumping well. Applied Mathematical Modelling 8, 305-312.
Drabbe, J., Badon Ghijben, W., 1889. Nota in verband met de voorgenomen putboring nabij Amsterdam. Tijdschr. Van Koninklijk Instituut Van Ingenieurs 5, 8–22 (in Dutch).
Eeman, S., Leijnse, A., Raats, P.A.C., Van der Zee, S.E.A.T.M., 2011. Analysis of the thickness of a freshwater lens and of the transition zone between this lens and upwelling saline water. Advances in Water Resources 34(2), 191-302.
Eeman, S., Van der Zee, S.E.A.T.M., Leijnse, A., De Louw, P.G.B., Maas, C., 2012. Response to recharge variation of thin rainwater lenses and their mixing zone with underlying saline

groundwater. Hydrology and Earth System Sciences 16, 3535-3549.
Faneca Sànchez, M., Gunnink, J. L., van Baaren, E. S., Oude Essink, G. H. P., Siemon, B., Auken, E., Elderhorst, W., De Louw, P.G.B., 2012. Modelling climate change effects on a Dutch coastal groundwater system using airborne electromagnetic measurements. Hydrology and Earth System Sciences 16, 4499-4516.
Feddes, R.A., 1987. Crop factors in relation to Makkink reference crop-evapotranspiration. Evaporation and Weather. CHO-TNO, the Netherlands. Proc. and information 39, 33-45.
Fetter, C.W., 1972. Position of the saline water interface beneath oceanic islands. Water Resources Research 8, 1307-1314.
Fetter, C.W., 1994. Applied hydrogeology. 3rd edition. Prentice Hall, New Jersey 07548, ISB 0-02-336490-4, 691pp.
Flowers T.J., 2004. Improving crop salt tolerance. Journal of Experimental Botany 55, 307-319.
Freer, J., Beven, K., Ambroise, B., 1996. Bayesian estimation of uncertainty in runoff prediction and the value of data: An application of the GLUE approach. Water Resources Research 32 (7), 2161-2173.
Friedman, P.S., 2005. Soil properties influencing apparent electrical conductivity: a review. Computers and Electronics in Agriculture 46, 45-70.
Geotomographie, 2004. SensInv2-D – Manual, available at: www.geotomographie.de.
Giambastiani, B.M.S., Antonellini, M., Oude Essink, G.H.P., Stuurman, R.J., 2007. Saltwater intrusion and water management in the unconfined coastal aquifer of Ravenna (Italy): a numerical model. Journal of Hydrology 340 (1-2), 91-104.
Goes, B.J.M., Oude Essink, G.H.P., Vernes, R.W., Sergi, F., 2009. Estimating the depth of fresh and brackish groundwater in a predominantly saline region using geophysical and hydrological methods, Zeeland, the Netherlands. Near Surface Geophysics 7, 401-412.
Goudriaan, R., De Louw, P.G.B., Kramer, M., 2011. Mapping saline boils in the Haarlemmermeer Polder. H_2O 3, 29-32 (in Dutch).
Green, T.R., Taniguchi, M., Kooi, H., Gurdak, J.J., Allen, D.M., Hiscock, K.M., Treidel, H. Aureli, A., 2011. Beneath the surface of global change: Impacts of climate change on groundwater, Journal of Hydrology 405, 532–560.
Griffioen, J., De Louw, P.G.B., Boogaard, H.L., Hendriks, R.F.A., 2002. The background surface water loads of N, P and Cl due to groundwater seepage and mineralization of peat in central-west Netherlands. TNO report NITG 02-166-A (in Dutch).
Haasnoot, M., Vermulst, J.A.P.H., Middelkoop, H., 1999. Impacts of climate change and land subsidence on the water systems in the Netherlands: terrestrial areas. RIZA report 99.049 (Lelystad), 114pp.
Harbaugh, A.W., Banta, E.R., Hill, M.C., and McDonald, M.G., 2000. MODFLOW-2000, the U.S. Geological Survey modular ground-water model – User guide to modularization concepts and the groundwater flow process: U.S. Geological Survey Open-File Report 00-92, 121pp.
Henry, H.R., 1964. Effects of dispersion on salt encroachment in coastal aquifers. Water-Supply Paper 1613-C. US Geological Survey.
Herzberg, A., 1901. Die Wasserversorgung einiger Nordseebäder. J. Gasbeleucht. Wasserversorgung 44, 815-819 (in German).
Hijma, M.P., Cohen, K.M., Hoffmann, G., Van der Spek, A.J.F., Stouthamer, E., 2009. From river valley to estuary: the evolution of the Rhine mouth in the early to middle Holocene (western Netherlands, Rhine-Meuse delta). Netherlands Journal of Geosciences - Geologie en Mijnbouw 88-1, 13-53.
Hinsby, K. Auken, E., Oude Essink, G.H.P., De Louw, P.G.B, Jørgensen, F., Siemon, B., Sonnenborg, T.O., Vandenbohede, A., Wiederhold, H., Guadagnini, A., Carrera. J. (Eds.), 2011. Assessing the impact of climate change for adaptive water management in coastal regions. Special issue Hydrology and Earth System Sciences 2011.
Holzer, T.L., Clark, M.M., 1993. Sand boils without earthquakes. Geology 21, 873-876.
Hooghoudt, S.B., 1940. General consideration of the problem of field drainage by parallel drains, ditches, watercourses, and channels. Publ. No.7 in the series Contribution to the knowledge of some physical parameters of the soil (titles translated from Dutch). Bodemkundig Instituut, Groningen, The Netherlands.
Hooper, R.P., Christophersen, N., Peters, N.E., 1990. Modelling stream water chemistry as a mixture of soil water end-members - An application to the Panola Mountain catchment, Georgia, U.S.A. Journal of Hydrology 116 (1-4), 321-343.
ICW (Dutch Institute for Land and Water Management Research), 1976. Hydrology and water quality of central-west Netherlands. Institute of Land and Water Management Resources, Wageningen. Regional Studies 9. (in Dutch).
ICW (Dutch Institute for Land and Water Management Research), 1982. Ground- and surface water quantity and quality of Northern-Holland. Institute of Land and Water Management Resources, Wageningen. Regional Studies 16. (in Dutch).
IPCC (Intergovernmental Panel on Climate Change), 2007. Climate Change 2007: The Physical Science basis: Contribution of Working Group I to the Fourth Assessment Report of the Intergovernmental Panel on Climate Change, edited by S. Solomon *et al.*, Cambridge Univ. Press, New York.
Jakovovic, D., Werner, A.D., Simmons, C.T., 2011. Numerical modelling of saltwater upconing: Comparison with experimental laboratory observations. Journal of Hydrology 402, 261–273.
Johannsen, K., Kinzelbach, W., Oswald, S.E., Wittum, G., 2002. The saltpool benchmark problem–

numerical simulation of saltwater upconing in a porous medium. Advances in Water Resources 25, 335–348.

Jolly, I.D., McEwan, K.L., Holland, K.L., 2008. A review of groundwater–surface water interactions in arid/semi-arid wetlands and the consequences of salinity for wetland ecology. Ecohydrology 1, 43-58.

Kalbus, E., Schmidt, C., Molson, J.W., Reinstorf, F., Schirmer, M., 2009. Influence of aquifer and streambed heterogeneity on the distribution of groundwater discharge. Hydrology and Earth System Sciences 13, 69-77.

Katerji, N., Van Hoorn, J.W., Hamdy, A., Mastrorilli, M., 2003. Salinity effect on crop development and yield, analysis of salt tolerance according to several classification methods. Agricultural Water Management 62(1), 37-66.

Keary, P., Brooks, M., 1991. An Introduction to Geophysical Exploration. 2nd edition. Blackwell Science.

Keery, J., Binley, A., Crook, N., Smith, J.W.N., 2007. Temporal and spatial variability of groundwater-surface water fluxes: Development and application of an analytical method using temperature time series. Journal of Hydrology 336, 1-16.

Kim, K.Y., Seong, H., Kim, T., Park, K.H., Woo, N.C., Park, Y.S., Koh, G.W., Park, W.B., 2006. Tidal effects on variations of fresh–saltwater interface and groundwater flow in a multilayered coastal aquifer on a volcanic island (Jeju Island, Korea). Journal of Hydrology 330, 525– 542.

Kishel, H.F., Gerla, P.J., 2002. Characteristics of preferential flow and groundwater discharge to Shingobee Lake, Minnesota, USA. Hydrological Processes 16 (10), 1921-1934.

Kolb, C.R., 1976. Geologic control of sand boils along Mississippi River levees. In Coates, D.R., Ed., Geomorphology and Engineering: Stroudsburg, Pennsylvania, Halstead Press, 99-114.

Kuczera, G., Parent, E., 1998. Monte Carlo assessment of parameter uncertainty in conceptual catchment models: The Metropolis algorithm. Journal of Hydrology 211 (1-4), 69-85.

Kwarteng, A.Y., Viswanathan, M.N., Al-Senafy, M.N., Rashid, T., 2000. Formation of fresh groundwater lenses in northern Kuwait. Journal of Arid Environments 46, 137–155.

Langevin C.D., Shoemaker W.B., Guo Weixing W.: MODFLOW-2000, The US Geological survey Modular Ground-Water Model–Documentation of the SEAWAT-2000 Version with the Variable-Density Flow Process (VDF) and the Integrated MT3DMS Transport Process (IMT): US Geological Survey Open-file report 03-426, 2003.

Langevin, C.D., 2008. Modeling axisymmetric flow and transport. Ground Water 46(4), 579-590.

Langevin, C.D., Thorne, D.T., Dausman, A.M., Sukop, M.C., Guo, W., 2007. SEAWAT Version 4: A computer program for simulation of multi-species solute and heat transport: U.S. Geological Survey Techniques and Methods. Book 6, Chapter A22, 39pp.

LaSage, D.M., Sexton, J.L., Mukherjee, A., Fryar, A.E., Greb, S.F., 2008. Groundwater discharge along a channelized coastal plain stream. Journal of Hydrology 360, 252-264.

Lebbe, L., 1999. Parameter identification in fresh-saltwater flow based on borehole resistivities and freshwater head data. Adv. Water Resour 22(8), 791-806.

Li, S., Zhang, Y., Jiao, X., Han, C., Zhu, H., 2004. Earthquake-induced liquefaction and pore water pressure based on cusp catastrophe model. Yingyong Lixue Xuebao/Chinese Journal of Applied Mechanics 21 (4), 151-155.

Li, Y., Craven, J., Schweig, E.S., Obermeier, S.F., 1996. Sand boils induced by the 1993 Mississippi River flood: Could they one day be misinterpreted as earthquake-induced liquefaction? Geology 24, 171-174.

Ma, T.S., Sophocleous, M., Yu, Y.S., Buddemeier, R.W., 1997. Modeling saltwater upconing in a freshwater aquifer in south-central Kansas. Journal of Hydrology 201, 120-137.

Maas, K., 2007. Influence of climate change and sea level rise on a Ghyben Herzberg lens. Journal of Hydrology 347(2), 223-228.

Makkink, G.F., 1957. Testing the Penman formula by means of lysimeters. Journal of the Institution of Water Engineers 11, 277-288.

McNeill, J.D., 1980. Electromagnetic Terrain Conductivity at Low Induction Numbers. Geonics Ltd. Technical Note TN-6, Geonics Ltd., Mississauga, Ontario, Canada.

Meinardi, C.R., 1983. Fresh and brackish groundwater under coastal areas and islands. GeoJournal 7.5, 413-425.

Meisler, H., Leahy, P.P., Knobel, L.L., 1984. Effect of eustatic sea-level changes on saltwater-freshwater relations in the Northern Atlantic coastal plain. U.S. Geological Survey Water-Supply Paper 2255.

Molenat, J., Gascuel-Odoux, C., Ruiz, L., and Gruau, G., 2008. Role of water table dynamics on stream nitrate export and concentration in agricultural headwater catchment (France), Journal of Hydroloy 348, 363–378.

Mulder, E.F.J., Geluk, M.C., Ritsema, I., Westerhof, W.E., Wong, T.E., 2003. The subsoil of the Netherlands. Geology of the Netherlands, part 7. Geological Survey of The Netherlands.

Muleta, M.K. and Nicklow, J.W., 2005. Sensitivity and uncertainty analysis coupled with automatic calibration for a distributed watershed model. Journal of Hydrology 306, 127–145.

Murdoch, L.C., Kelly, S.E., 2003. Factors affecting the performance of conventional seepage meters. Water Resources Research, 39 (6), pp. SWC21-SWC210.

Nadia Carluer, N., De Marsily, G., 2004. Assessment and modelling of the influence of man-made networks on the hydrology of a small watershed: implications for fast flow components, water quality and landscape management. Journal of Hydrology 285, 76-95.

Nash, J.E., Sutcliffe, J.V., 1970. River flow forecasting through conceptual models. Part I: a discussion of principles. Journal of Hydrology 10, 282-290.

Navoy, A. S., 1991. Aquifer-estuary interaction and vulnerability of groundwater supplies to sea level rise-driven saltwater intrusion. PhD thesis. Pennsylvania State University, U.S.A.

NHI 2.1 (2011). National Hydrological Instrument. Hoogewoud, J.C., Veldhuizen, A.A., Prinsen, G. Changes NHI 2.1. Deltares report 1203516-000-BGS-0013 (www.nhi.nu) (in Dutch).

NHI 2.2 (2011). National Hydrological Instrument. Hoogewoud, J.C., Veldhuizen, A.A., Prinsen, G., Hunink, J. Description of changes in NHI 2.2. Deltares report 1204179-000-BGS-003 (www.nhi.nu) (in Dutch).

Obermeijer, S.F., 1995. Using liquefaction-induced features for paleoseismic analysis. In Obermeijer, S.F., Jibson, R.W. (Eds.). Using ground failure features for paleoseismic analysis. U.S. Geological Survey Open-File Report 94-683, 1-98.

Ojha, C.S.P., Singh, V.P., Adrian, D.D., 2003. Determination of critical heads in soil piping. Journal of Hydraulic Engineering ASCE 129 (7), 511-518.

Olsthoorn, T.N., 2008. Brackish groundwater as a new resource for drinking water; specific consequences of density dependent flow, and positive environmental consequences. In: C. Langevin, L. Lebbe, M. Bakker & C. Voss (eds), Program and proceedings of 20th Salt Water Intrusion Meeting (June 23–27 2008 Naples USA), Univ Florida, IFAS Research, pp 174–177.

Oude Essink, G.H.P. 2001. Saltwater intrusion in a three-dimensional groundwater system in the Netherlands: a numerical Study. Transport in porous media 43(1), 137-158.

Oude Essink, G.H.P., 1996. Impact of sea level rise on groundwater flow regimes. A sensitivity analysis for the Netherlands. PhD thesis, Delft University of Technology, Delft Studies in integrated water management: no. 7 (ISBN 90-407-1330- 8), 428pp.

Oude Essink, G.H.P., 2001. Saltwater intrusion in 3D large-scale aquifers: a Dutch case. Phys. & Chem. of the Earth 26(4), 337-344.

Oude Essink, G.H.P., 2008. Impacts of climate change on the coastal groundwater systems in The Netherlands. In: C. Langevin, L. Lebbe, M. Bakker & C. Voss (eds), Program and proceedings of 20th Salt Water Intrusion Meeting (June 23–27 2008 Naples USA), Univ Florida, IFAS Research, pp 178–181.

Oude Essink, G.H.P., Van Baaren, E.S., De Louw, P.G.B., 2010. Effects of climate change on coastal groundwater systems: A modeling study in The Netherlands. Water Resources Research 46, W00F04, doi:10.1029/2009WR008719.

Ozkan, S., 2003. Analytical study on flood induced seepage under river levees. PhD thesis, Louisiana State University, Louisiana, USA.

Pappenberger, F., Beven, K., Horritt, M., Blazkova, S., 2005. Uncertainty in the calibration of effective roughness parameters in HEC-RAS using inundation and downstream level observations. Journal of Hydrology 302, 46-69.

Pauw, P.S., De Louw, P.G.B., Oude Essink, G.H.P. 2012. Groundwater salinization in the Wadden Sea area of the Netherlands: quantifying the effects of climate change, sea level rise and anthropogenic interferences. Netherlands Journal of Geosciences 91-3, 373-383.

Pollock, D.W., 1994. User's Guide for MODPATH/MODPATH-PLOT, Version 3: A particle tracking post-processing package for MODFLOW, the U.S. Geological Survey finite-difference groundwater flow model: U.S. Geological Survey Open-File Report 94-464, 234pp.

Pomper, A.B., Wesseling, J. 1978. Chloride content of surface water as a result of geologic processes and groundwater flow in a coastal area in The Netherlands. Seminar on Selected Water Problems in Islands and Coastal Areas with Special Regard to Desalinization and Groundwater, Valetta, Malta.

Post, V.E.A., 2004. Groundwater Salinization Processes in the Coastal Area of The Netherlands due to Transgressions during the Holocene. PhD thesis, Free University Amsterdam, 138pp.

Post, V.E.A., Abarca, E., 2010. Saltwater and freshwater interactions in coastal aquifers. Hydrogeology Journal 18(1), 1-4.

Post, V.E.A., Kooi, H., 2003. Rates of salinization by free convection in high-permeability sediments: Insights from numerical modeling and application to the Dutch coastal area. Hydrogeology Journal 11 (5), 549-559.

Post, V.E.A., Kooi, H., Simmons, C.T., 2007. Using hydraulic head measurements in variable-density ground water flow analyses. Ground Water 45(6), 664-671.

Post, V.E.A., Van der Plicht, H., Meijer, H.A.J., 2003. The origin of brackish and saline groundwater in the coastal area of the Netherlands. Geologie en Mijnbouw/Netherlands Journal of Geosciences 82(2), 133-147.

Poulter, B., Goodall, J.L., Halpin, P.N., 2008. Applications of network analysis for adaptive management of artificial drainage systems in landscapes vulnerable to sea level rise. Journal of Hydrology 357(3–4), 207-217.

Ranjan, P., Kazama, S., Sawamoto, M., 2006. Effects of climate change on coastal fresh groundwater resources. Global Environmental Change 16, 388–399.

REGIS II, 2005. Hydrogeological model of The Netherlands. Report: Vernes, R.W., Van Doorn, Th.H.M. From Guide layer to Hydrogeological Unit. Explanation of the construction of the data set. TNO report NITG 05-038-B. (in Dutch). Website: www.dinoloket.nl.

Reilly, T.E., Goodman, A.S., 1987. Analysis of saltwater upconing beneath a pumping well. Journal of Hydrology 89, 169-204.

Rijnland (1967). Research on surface water salinity in Noordplas Polder. Rijnland District Water Control Board. (in Dutch).

Rijnland (1975). Research on surface water salinization in Noordplas Polder. Rijnland District Water Control Board. (in Dutch).
Rijnland (1981). Research surface on water salinity in Haarlemmermeer polder. Rijnland District Water Control Board. (in Dutch).
Rijnland, 2013. Boils inventory. Report Rijnland District Water Control Board (in Dutch).
Rinaldo, A., Botter, G., Bertuzzo, E., Uccelli, A., Settin, T., Marani, M., 2006. Transport at basin scales: 1. Theoretical framework. Hydrology and Earth System Sciences 10 (1), 19-29.
Ritsema, C.J., Groenenberg, J.E., 1993. Pyrite oxidation, carbonate weathering, and gypsum formation in a drained potential acid sulfate soil. Soil Science Society of America Journal 57, 968-976.
Roest, C.W.J., Van Bakel, P.J.T., Smit, A.A.M.F.R., 2003. Actualisering van de zouttolerantie van land- en tuinbouwgewassen ten behoeve van de berekening van de zoutschade in Nederland met het RIZA-instrumentarium, Alterra (in Dutch).
Rotzoll, K., Oki, D.S., El-Kadi, A.I., 2010. Changes of freshwater-lens thickness in basaltic island aquifers overlain by thick coastal sediments. Hydrogeology Journal 18, 1425–1436.
Roux, H., Dartus, D., 2006. Use of parameter optimization to estimate a flood wave: Potential applications to remote sensing of rivers. Journal of Hydrology 328 (1-2), 258-266.
Rozema, J., Flowers, T., 2008. Crops for a salinized world. Science 322, 1578-1582.
Rush, J.D., Johnson, G.S., 2002. Response of well-water elevations and spring discharge to changes in barometric pressure, Eastern Snake River Plain Aquifer, Hagerman, Idaho. Idaho Water Resources Institute, 23pp.
Sakr, S. A., 1999. Validity of a sharp-interface model in a confined coastal aquifer. Hydrogeology Journal 7(2), 155-160.
Schot, P.P., Dekker, S. C., Poot, A., 2004. The dynamic form of rainwater lenses in drained fens. Journal of Hydrology 293, 74-84.
Schultz, E., 1992. Water management of the drained lakes in the Netherlands, PhD thesis, 507pp., Delft Univ. of Technol., Netherlands (in Dutch).
Seed, H.B., Idriss, I.M., 1967. Analysis of liquefaction: Niigata earthquake. America Society of Civil Engineering, Journal of Soil Mechanics and Foundations Division 93, 83-108.
Sellmeijer, J.B., Koenders, M.A., 1991. A mathematical model for piping. Applied Mathematical Modeling 15 (6), 646-651.
Sherif, M.M., Singh, V.P., 1999. Effect of climate change on sea water intrusion in coastal aquifers. Hydrological Processes (13), 1277-1287.
Siemon, B., Christiansen, A.V., Auken, E., 2009. A review of helicopter-borne electromagnetic methods for groundwater exploration. Near Surface Geophysics 7, 629-646.
Siemon, B., Ullmann, A., Mitreiter, I., Ibs-von Seht, M., Voß, W., Pielawa, J., 2011. Airborne geophysical investigation of CLIWAT pilot areas, survey area Schouwen, The Netherlands, BGR Archives-No. 0129932, Hanover.
Sikkema, P. C., van Dam, J.C., 1982. Analytical formulae for the shape of the interface in a semi-confined aquifer. Journal of Hydrology 56, 201-220.
Simmons, C.T., 2005. Variable density groundwater flow: From current challenges to future possibilities. Hydrogeology Journal 13, 116-119.
Soulsby, C., Petry, J., Brewer, M.J., Dunn, S.M., Ott, B., Malcolm, I.A., 2003. Identifying and assessing uncertainty in hydrological pathways: A novel approach to end member mixing in a Scottish agricultural catchment. Journal of Hydrology 274 (1-4), 109-128.
Spear, R.C., Hornberger, G.M., 1980. Eutrophication in Peel Inlet, II. Identifcation of critical uncertainties via generalized sensitivity analysis. Water Resources Research 14, 43-49.
Stafleu, J., Maljers, D.M., Gunnink, J.L., Menkovic, A., Busschers, F.S., 2011. 3D modelling of the shallow subsurface of Zeeland, the Netherlands. Netherlands Journal of Geosciences 90-4, 293-310.
Stafleu, J., Maljers, D.M., Busschers, F.S., Gunnink, J.L., Schokker, J., Dambrink, R.M., Hummelman, H.J., Schijf, M.L., 2013. GeoTop modeling. TNO-report 2012-R10991, 216pp.
Steppuhn, H. Van Genuchten, M.T., Grieve, C.M., 2005. Root-zone salinity. I. Selecting a product-yield index and response function for crop tolerance. Crop science 45(1), 209-220.
Stoeckl, L., Houben, G., 2012. Flow dynamics and age stratification of freshwater lenses: Experiments and modeling. Journal of Hydrology 458-459, 9-15.
Stolte, J., 1997. Manual for soil physical measurements, version 3. Wageningen, DLO Winand Staring Centre for Integrated Land, Soil and Water Research, Technical Document 37, 77pp.
Stuurman, R.J., Oude Essink, G.P.H., Broers, H.P., Van der Grift, B., 2006. Monitoring zoutwaterintrusie naar aanleiding van de Kaderrichtlijn Water "verzilting door zoutwaterintrusie en chloridevervuiling", TNO report 2006-U-R0080/A, Utrecht, 84pp (in Dutch).
Stuyfzand, P.J., 1989. A new hydrochemical classification of water types. IAHS Publ. 182, 89-98.
Stuyfzand, P.J., 1993. Hydrochemistry and Hydrology of the Coastal Dune Area of the Western Netherlands. PhD thesis, Free University Amsterdam, ISBN 90-74741-01-0, 366 pp.
Stuyfzand, P.J., Stuurman R.J., 1994. Recognition and genesis of various brackish to hypersaline groundwaters in The Netherlands. In: G. Barrocu (Ed.), Proc. 13th Salt Water Intrusion Meeting, University of Cagliari, Sardinia, 125-136.
Stuyfzand, P.J., Stuurman R.J., 2008. Origin, distribution and chemical mass balances for brackish and saline groundwaters in The Netherlands. In: G. Barrocu (Ed.), Proc. 1st SWIM-SWICA Joint Saltwater Intrusion Conference, Cagliari-Baia de Chia, Sardinia, 151-164.
Stuyfzand, P.J., 2007. Oorzaken van verzilting,

hun herkenning en de risicofactoren voor de drinkwatervoorziening, 1-25. In De Louw, P.G.B. (Ed.), 2007. Salinization in the Netherlands. NHV-special 7, ISBN 90-803565-7-3, Netherlands Hydrological Society, Utrecht, 94pp (in Dutch).

Stuyfzand, P.J., Raat, K.J., 2010. Benefits and hurdles of using brackish groundwater as a drinking water source in the Netherlands. Hydrogeology Journal 18, 117–130.

Stuyt, L., Hoogvliet, M. Van Bakel, J. Veraart, J. Paulissen, M. Delsman, J., Oude Essink, G.H.P., 2013. Kansrijkheid van anders omgaan met zout. Een druppel op de gloeiende plaat, of niet? Memo van Alterra, Deltares en Bakelse Stroom voor deelprogramma zoetwater (in Dutch).

Sulzbacher, H., Wiederhold, H., Siemon, B., Grinat, M., Igel, J., Burschil, T., Günther, T., Hinsby, K., 2012. Numerical modelling of climate change impacts on freshwater lenses on the North Sea Island of Borkum using hydrological and geophysical methods. Hydrology and Earth System Science 16, 3621-3643.

Surridge, B.W.J., Baird, A.J., Heathwaite, A.L., 2005. Evaluating the quality of hydraulic conductivity estimates from piezometer slug tests in peat. Hydrological Processes 19, 1227-1244.

TACFD (Technical Advisory Committee on Flood Defenses), 1999. Technical Report on Sand Boils (piping). Road and Hydraulics Division of the Directorate-General for Public Works and Water Management, The Netherlands.

Taniguchi, M., Turner, J.V., Smith, A.J., 2003. Evaluations of groundwater discharge rates from subsurface temperature in Cockburn Sound, Western Australia. Biogeochemistry 66, 111-124.

Taylor, R.G. Scanlon, B., Döll, P., Rodell, M., van Beek, R. Wada, Y., Longuevergne, L., Leblanc, L., Famiglietti, J.S., Edmunds, M., Konikow, L., Green, T.R., Chen, J., Taniguchi, M., Bierkens, M.F.P., MacDonald, A., Fan, Y., Maxwell, R.M., Yechieli, Y., Gurdak, J.J., Allen, D.M., Shamsudduha, M., Hiscock, K., Yeh, P.J.-F., Holman, I., Treidel, H., 2012. Ground water and climate change, Nature Climate Change, DOI: 10.1038/NCLIMATE1744.

Tellam, J.H., Lloyd, J.W., Walters, M., 1986. The morphology of a saline groundwater body: its investigation, description and possible explanation. Journal of Hydrology 83, 1-21.

Tesoriero, A.J., Duff, J.H., Wolock, D.M., Spahr, N.E., Almendinger, J.E., 2009. Identifying pathways and processes affecting nitrate and orthophosphate inputs to streams in agricultural watersheds. Journal of Environmental Quality 38 (5), 1892-1900.

Tiemeyer, B., Lennartz, B., Kahle, P., 2008. Analysing nitrate losses from an artificially drained lowland catchment (North-Eastern Germany) with a mixing model. Agriculture, Ecosystems and Environment 123 (1-3), 125-136.

Tiemeyer, B., Moussa, R., Lennartz, B., Voltz, M., 2007. MHYDAS-DRAIN: A spatially distributed model for small, artificially drained lowland catchments. Ecological Modelling 209 (1), 2-20.

Turnbull, W.J., Mansur, C.I., 1961. Investigation of underseepage-Mississippi River levees. Transactions of the ASCE 126 (1), 1429-1485.

Underwood, M.R., Peterson, F.L., Voss, C.I., 1992. Groundwater lens dynamics of atoll islands. Water Resource Research 28(11), 2889–2902.

Vaeret, L., Leijnse, A., Cuamba, F., Haldorsen, S., 2011. Holocene dynamics of the salt-fresh groundwater interface under a sand island, Inhaca, Mozambique. Quaternary Int. 257, 74–82.

Van Baaren, E.S., Oude Essink, G.H.P., Janssen, G.M.C.M., De Louw, P.G.B., Heerdink, R., Goes, B., 2013. Freshening/salinization of phreatic groundwater in the province of Zeeland: Results of 3D-density dependent groundwater model. Deltares Report (in Dutch).

Van Baaren, E.S., De Louw, P.G.B., Oude Essink, G.H.P., Pauw, P.S., Harezlak, V., 2012a. Climate proof areas: innovative solutions for improving the freshwater availability. Proc. 22th Salt Water Intrusion Meeting, Armação dos Búzios, Rio de Janeiro, Brazil, 121.

Van Baaren, E.S., Ottow, B.T., Pauw, P.S., Van Ek, R., De Louw, P.G.B., 2012b. The Water Farm. Proc. 22th Salt Water Intrusion Meeting, Armação dos Búzios, Rio de Janeiro, Brazil, 161.

Van Bakel, P.J.T, Stuyt, L.C.P.M., 2011. Actualisering van de kennis van de zouttolerantie van landbouwgewassen. Op basis van literatuuronderzoek, expertkennis en praktische ervaringen. Alterra-report 2201, ISSN 1566-7197. Wageningen (in Dutch).

Van Dam, J.C., Sikkema, P.C., 1982. Approximate solution of the problem of the shape of the interface in a semi-confined aquifer. Journal of Hydrology 56, 221-237.

Van de Plassche, O., 1982. Sea-level change and water-level movements in the Netherlands during the Holocene, Mededelingen Rijks Geologische Dienst 36, 1-93.

Van de Ven, G.P. (Ed), 2003. Man-made lowlands, history of water management and land reclamation in The Netherlands. Uitgeverij Matrijs, Utrecht. 293pp.

Van den Hurk, B., Klein Tank, A., Lenderink, G., Ulden, A. van, Oldenborgh, G.J. van, Katsman, C, Brink, H. van den, Keller, F., Bessembinder, J., Burgers, G., Komen, G., Hazeleger, W., Drijfhout, S., 2006. KNMI Climate Change Scenarios 2006 for the Netherlands. KNMI, De Bilt, Scientific Report WR 2006-01.

Van der Eertwegh, G.A.P.H., Nieber, J.L., De Louw, P.G.B., Van Hardeveld, H.A., Bakkum, R., 2006. Impacts of drainage activities for clay soils on hydrology and solute loads to surface water. Irrigation and drainage 55, 235-245.

Van der Meij, J. L. and Minnema, B., 1999. Modelling of the effect of a sea-level rise and land subsidence on the evolution of the groundwater density in the subsoil of the northern part of the Netherlands, Journal of Hydrology 226(3–4), 152–166.

Van der Valk, L., 1996. Geology and sedimentology of Late Atlantic sandy, wave-dominated

deposits near The Hague (Zuid-Holland, The Netherlands): a reconstruction of an early prograding coastal sequence. Mededelingen Rijks Geologische Dienst 57, 201–228.
Van der Veer, P., 1977. Analytical solution for steady interface flow in a coastal aquifer involving a phreatic surface with precipitation. Journal of Hydrology 34, 1-11.
Van der Velde, Y., de Rooij, G. H., and Torfs, P. J. J. F., 2009. Catchment-scale non-linear 10 groundwater-surface water interactions in densely drained lowland catchments, Hydrology and Earth System Science 13, 1867–1885.
Van der Velde, Y., Rozemeijer, J. C., De Rooij, G. H., Van Geer, F. C., and Broers, H. P., 2010. Fieldscale measurements for separation of catchment discharge into flow route contributions. Vadose Zone J. 9, 25–35.
Van Huissteden, J., R. Petrescu, A.M., D. Hendriks, D.M., Rebel, K.T., 2010. Sensitivity analysis of a wetland methane emission model based on temperate and arctic wetland sites. Biogeosciences 6 (12), 3035-3051.
Van Meir, N., 2001. Density-dependent Groundwater Flow: Design of a Parameter Identification Test and 3D-simulation of Sea-level Rise. PhD thesis, Ghent University, Belgium, 319pp.
Van Puijenbroek, P.J.T.M., Janse, J.H., Knoop, J.M., 2004. Integrated modelling for nutrient loading and ecology of lakes in The Netherlands. Ecological Modelling 174 (1-2), 127-141.
Van Rees Vellinga, E., Toussaint, C.G., Wit, K.E., 1981. Water Quality and hydrology in a coastal region of The Netherlands. Journal of Hydrology 50, 105-127.
Van Schaik, N.L.M.B., 2009. Spatial variability of infiltration patterns related to site characteristics in a semi-arid watershed. Catena 78 (1), 36-47.
Van Wirdum, G., 1991. Vegetation and hydrology of floating rich fens. PhD thesis, University of Amsterdam.
Vandenbohede, A., and Lebbe, L., 2007. Effects of tides on a sloping shore: Groundwater dynamics and propagation of the tidal wave. Hydrogeology Journal 15(4), 645-658.
Vandenbohede A., Luyten, K., Lebbe, L., 2008. Impacts of global change on heterogeneous coastal aquifers: case study in Belgium. J Coast Res 24(2B), 160–170.
Vandenbohede, A., Courtens, C., Lebbe, L., De Breuck, W., 2010. Fresh-salt water distribution in the central Belgian coastal plain: an update. Geologica Belgica 11(3), 163-172.
Vandenbohede, A., De Louw, P.G.B., Doornenbal, P., 2013. Characterizing preferential groundwater discharge through boils using temperature. Submitted to Journal of Hydrology.
Velstra, J., Groen, J., De Jong, K., 2011. Observations of salinity patterns in shallow groundwater and drainage water from agricultural land in the Northern part of the Netherlands. Irrigation and drainage 60, 51–58.
Vink, T., 1954. De Rivierstreek. (Met steun van De Nederlandse Organisatie voor Zuiver-Wetenschappelijk Onderzoek.) Uitgever N.V. Bosch & Keuning, Baarn. 840pp. (in Dutch).
Volker, A., 1961. Source of brackish groundwater in Pleistocene formations beneath the Dutch polderland. Economic Geology 56, 1045-1057.
Vos, P., Zeiler, F., 2008. Holocene transgressions of southwestern Netherlands, interaction between natural and antrophogenic processes. Grondboor & Hamer 3-4 (in Dutch).
Vos, P.C., Bazelmans, J., Weerts, H.J.T., Van der Meulen, M.J., 2011. Atlas van Nederland in het Holoceen. Amsterdam, 93 pp.
Voss C.I., Provost A.M., 2008. SUTRA, a model for saturated–unsaturated variable density groundwater flow with solute or energy transport, manual. US Geological Survey, Reston, Virginia, USA.
Weert, F. Van der Gun, J, Reckman, J., 2009. Global Overview of Saline Groundwater occurrence and Genesis. Report no. GP 2009-1.
Weerts, J.T., 1996. Complex Confining Layers. Architecture and Hydraulic Properties of Holocene and Late Weichselian deposits in the Fluvial Rhine-Meuse Delta, The Netherlands. PhD thesis, University of Utrecht.
Werner, A.D., Simmons, C.T., 2007. Impact of sea-level rise on sea water intrusion in coastal aquifers. Groundwater 47 (2), 197–204.
Werner, A.D., Bakker, M., Post, V.E.A., Vandenbohede, A., Lu, C., Ataie-Ashtiani, B., Simmons, C.T., Barry, D.A., 2013. Seawater intrusion processes, investigation and management: Recent advances and future challenges. Advances in Water Resources 51, 3-26.
Werner, A.D., Jakovovic, D., Barry, D.A., Simmons, C.T., Zhang, H., 2012. Discussion on "Experimental observations of saltwater up-coning" by Werner, A.D, Jakovovic, D., Simmons, C.T., 2009. Journal of Hydrology 458-459, 118-120.
Werner, A.D., Jakovovic, D., Simmons, C.T., 2009. Experimental observations of saltwater up-coning. Journal of Hydrology 373, 230-241.
Wesseling, J., 1980. Saline seepage in The Netherlands: occurrence and magnitude. Research on possible changes in the distribution of saline seepage in The Netherlands 26, 17–33. Committee for Hydrological Research (CHO-TNO), Proc. and Informations.
Wit, K.E., 1974. Hydrological investigations in central-west Netherlands. Institute of Land and Water Management Resources, Wageningen. Nota 792 (in Dutch).
Wriedt, G., Spindler, J., Neef, T., Meißner, R., Rode, M., 2007. Groundwater dynamics and channel activity as major controls of in-stream nitrate concentrations in a lowland catchment system. Journal of Hydroloy 343, 154–168.
Zaadnoordijk, W.J., Velstra, J., Vergroesen, A.J.J., Mankor, J., 2009. Groot Mijdrecht: inzicht in functioneren wellen. Stromingen 15(2), 31-40.
Zhang, H., Hocking, G.C., Seymour, B., 1997. Critical and supercritical withdrawal from a two-layer

fluid through a line sink in a partially bounded aquifer. Journal of Aust Math Soc Ser B Appl Math 39, 271–279.
Zhou, Q., Bear, J., Bensabat, J., 2005. Saltwater upconing and decay beneath a well pumping above an interface zone. Transport in Porous Media 61, 337–363.

Summary and conclusions

Motivation

More than 50% of world's population lives in coastal areas and is largely dependent on fresh groundwater resources for domestic, agricultural and industrial purposes. However, in many coastal areas, groundwater is brackish to saline which may pose problems for the sustainable exploitation of fresh groundwater. In low-lying coastal areas that lie below mean sea level, saline groundwater may reach the surface by upward groundwater flow. This process is referred to as 'saline seepage' and is the main subject of this PhD-thesis. Saline seepage leads to the salinization of surface waters, shallow groundwater and soil water in the root zone. Climate change and future rise in sea level are expected to increase saline seepage and reduce the availability of both fresh surface water and groundwater. Predicting effects of future changes, defining effective water management strategies for a climate proof sustainable freshwater supply and successful implementation of any measure are only meaningful when all relevant processes involving saline seepage are fully understood. This thesis describes the spatial variability and temporal dynamics of salinization processes involving saline seepage in deltaic areas. The research focused on the preferential saline seepage through boils leading to surface water salinization (Part I) and the interaction between thin rainwater lenses and saline seepage leading to the salinization of shallow groundwater and the root zone (Part II). These two processes were identified as important contributors to the salinization of the Dutch delta which was the study area of this PhD-research.

Research

The spatial variability and temporal dynamics of salinization processes involving saline seepage were analyzed and quantified based on field campaigns supported by numerical and analytical methods. The field campaigns involved field techniques applied at scales varying from local point scale to measurements at polder catchment and island scale. Saline seepage processes in deep polders and in particular preferential discharge through boils (Part I) were examined in two deep polders (reclaimed lakes) in the western part of The Netherlands: the Noordplas Polder and the Haarlemmermeer Polder. Two boils were examined in detail and in the Noordplas Polder an extensive monitoring campaign was conducted to identify the dominant salt sources and to quantify their temporal varying contribution to surface water salinization. The characteristics and dynamics of thin rainwater lenses and the interactions with saline seepage (Part II) were examined in the southwestern delta of The Netherlands by using different types of field measurements applied at different scales. By combining the applied techniques, we could extrapolate measurements at point scale (groundwater sampling, temperature and electrical soil conductivity (TEC)-probe measurements, electrical cone penetration tests (ECPT)) to field scale (continuous vertical electrical soundings (CVES), electromagnetic survey with EM31), and even to regional scale using helicopter-borne electromagnetic measurements (HEM). Based on these measurements we selected two tile-drained agricultural fields to study the rainwater lens dynamics. To this end, we

collected for a period of 2 years monthly ground and soil water salinity in combination with daily observations of water table elevation, drain tile discharge and drain water salinity. Numerical modeling was applied to analyze the processes controlling the size and characteristics of rainwater lenses in saline seepage areas and their dynamic behaviour.

Results and conclusions

Part I: Preferential saline seepage through boils

Based on field observations and measurements, we distinguished three types of seepage in a deep polder which differ in flux and salt concentration: (i) diffuse, background seepage through the low permeability sediments (clay, peat) of the Holocene confining layer (HCL), (ii) preferential seepage through permeable, sandy paleochannel belts in the HCL, and (iii) intense preferential seepage via boils. Boils are small conduits in the upper aquitard (HCL) connecting the aquifer with the surface through which water preferentially discharges at high velocities in the order of 10^2 to 10^4 m d^{-1}. The largest seepage fluxes and highest chloride concentrations are found in boils producing an average chloride concentration of 1100 mg L^{-1} for the Noordplas Polder with a recorded maximum of 2850 mg L^{-1}. Permeable, sandy, paleochannel belts cut through the less permeable, lower part of the HCL resulting in higher seepage fluxes through paleochannel belts and a much higher average chloride concentration (~600 mg L^{-1}) than found for the diffuse seepage (average Cl concentration ~100 mg L^{-1}). The differences in salinity for the seepage forms are explained by the combination of the typical aquifer salinity distribution found below deep polders (5 to 10 m freshwater gradually increasing in salinity with depth) and upconing mechanisms. Concentrated forms of seepage at higher rates tend to discharge groundwater from deeper strata with more salty groundwater than diffuse forms of seepage at low rates which discharge only fresh groundwater from the aquifer top.

To quantify the water and salt fluxes in a deep polder on a daily time scale, and taking into account the uncertainty of parameters, a probabilistic (GLUE) dynamic water and salt balance model on a daily time scale has been set up and successfully applied to the Noordplas Polder. To incorporate the uncertainty of model input parameters, their values were sampled randomly from uniform parameter distributions within ranges which were defined based on measurements. The model was conditioned on measurements of daily to weekly polder water discharge, salt concentrations and salt loads leaving the Noordplas Polder, and of groundwater levels to produce a set of input parameter combinations which simulate the system equally well. With this set of behavioural parameters, we quantified the contribution and uncertainty of different sources to the water and salt balance of the deep polder and effects of different scenarios. The results showed that the far most dominant salinization source in the Noordplas Polder is boil seepage with an average contribution of 66% (± 7.2%) to the total salt loads from only 15% (± 4.7%) of the total water flux. Standard deviations are given between brackets. Regarding the omnipresence of saline boils in Dutch deep polders and the typical salinity distributions found below most deep polders (i.e. fresh above salt groundwater) we presume that boils are the most likely dominant salinization source in most Dutch deep polders.

The large contribution of boils to the total salt loads arises from the much higher salinity of groundwater discharging via boils than via other forms of seepage. Based

on field measurements in the Noordplas Polder and the Haarlemmermeer Polder and numerical modeling we conclude that saltwater upconing is the key mechanism leading to elevated salinities of boil water. The numerical simulations showed that boil water is a mixture of groundwater from different depths with different salinities. Mixing is enhanced near the boil where streamlines from different depths and with different salinities converge. The contribution of different aquifer depths to boil discharge showed an inverse relationship with the aquifer salinity distribution. That is, the boil extracted per meter aquifer more low-salinity groundwater from above the centre of the transition zone (shallow contribution) than high-salinity groundwater from below the centre of the transition zone (deep contribution). This is due to the buoyancy force established by density differences which gives an extra upward lift to fresh groundwater with lower density compared to saline groundwater below the transition zone. The key factors controlling saltwater upconing mechanisms and boil salinity in Dutch polders are: (i) boil discharge rate, (ii) aquifer's horizontal hydraulic conductivity, and (iii) the aquifer salinity (= density) distribution characterized by the position of the centre of the transition zone and the density contrast within the upper aquifer. When boils are clustered, natural saltwater upconing is a function of the total discharge of a boil cluster, whereas the boil-to-boil salinity variations within a cluster are determined by the discharge of individual boils and their position relative to neighbouring boils. Regional lateral flow significantly modifies flow patterns by dividing the groundwater flow system into a local boil system overlying the regional flow system. Despite this, regional flow has only a minor effect on the relative contributions of saline and fresh groundwater to boil discharge and thus on boil salinity.

Part II: Thin rainwater lenses in areas with saline seepage

Point measurements (TEC, ECPT) below 30 agricultural fields with saline seepage showed a gradual mixing zone between infiltrated rainwater and upward seeping saline groundwater. The centre of this mixing zone (D_{mix}) was found at a median depth of 1.7 m below ground level and almost all mapped lenses lacked truly fresh groundwater. For the purpose of this study the thin rainwater lens in saline seepage areas was defined as the entire groundwater body from the base of the mixing zone (B_{mix}, which is the depth at which the salinity equals the salinity of regional groundwater) to the water table. With this definition, the rainwater lens (further referred to as RW-lens) is not purely a freshwater lens, and salinities within the RW-lens vary both in space and in time. B_{mix} was found at a median depth of 2.8 m and the ECPT measurements showed that below B_{mix} the salinity stayed virtually constant with depth until a depth of at least 25 m below ground level.

The limited size of RW-lenses is primarily caused by the permanent regionally head driven upward groundwater flow from the upper aquifer into the HCL which prevents rainwater from reaching depths below the bottom of the HCL. Unlike RW-lenses in seepage areas, the vertical downward flow of rainwater in the infiltration areas is only limited (in absence of aquitards) by the buoyancy force of the surrounding saline groundwater and its density importantly determines lens thickness according to the Badon Ghyben Herzberg principle. These systems build up much thicker lenses (BGH-lenses), varying from 5-15 m thick lenses in sandy creek ridges to 100 m thick lenses in the dunes. As it was established that lenses in seepage areas are limited to the extent of the upper aquitard (HCL) due to permanent upward seepage, we subsequently examined the mixing mechanisms and flow processes within the aquitard and the factors controlling lens size and mixing zone properties with numerical modeling.

We introduced the vertical flow stagnation point (FLSP) to indicate the point below which the flow switches from having a vertical downward to a vertical upward component. The FLSP in between the drain tiles fluctuates with water table fluctuations, whereby a rising water table results in a deeper FLSP. Flow is downward for a large part of the RW-lens when the water table is high, but when the water table falls below the drain tile all flow in the RW-lens is upward. Based on these findings, we concluded that the transient oscillatory vertical flow regime in the aquitard driven by water table fluctuations is the main mechanism of mixing between infiltrating rainwater and upward saline seepage and determines the position and extent of the mixing zone in the aquitard. Recharge, seepage flux and drainage depth are the controlling factors.

The time varying field data showed that the thickness of the RW-lens (from B_{mix} to water table) varied up to 1.2 m with water table elevation in response to individual recharge events. The position of D_{mix} showed a much smaller change (< 0.25 m), and fluctuated at a much longer, seasonal time scale. The base of the RW-lens (B_{mix}) stayed virtually at the same position. Numerical simulations showed that the small variations in the position of the mixing zone can be explained by the slow transient oscillatory flow regime in the permanent saturated part of the RW-lens, which also controls the mixing between infiltrated rainwater and seepage water. The flow and mixing processes are much faster near the water table, which fluctuates on a daily basis in response to recharge and evapotranspiration, and conditions alternate between saturated to unsaturated. When the water table falls, most of the water with variable dissolved salt concentrations is retained as soil water, which will mix and become diluted with only a small amount of infiltrated rainwater when the soil saturates again. The salinity of the mixture will thus be close to that of the soil water before saturation, which explains the observed absence of very fresh groundwater. Although the mixing processes are fast, the temporary storage of salt in soil water has an important damping effect on groundwater salinity variations when the RW-lens grows due to the recharge by rainwater. Soil water salinity showed a seasonal variation with lower salinities during winter and higher salinities during summer. Salt migrates upwards into the root zone by capillary rise of the groundwater at the water table. As the water table falls during the summer, the water rising through the capillaries originates from deeper parts of the RW-lens and is therefore more saline. Salinities of soil water can become significantly higher than in the groundwater due to the unsynchronized effects of capillary rise of saline water during dry periods and the flow of infiltrated rainwater during wet periods being restricted to cracks in the soil. Preferential flow through cracks is thought to play an important role in the rapid response of the drain tile discharge to individual rain events. Groundwater of variable salinity, originating from different parts of the RW-lens, as well as infiltrated rainwater, contributes to the drain tile discharge in proportions that vary on a timescale of hours to days, and this causes the dynamic behaviour of drain water salinity.

Implications for sustainable freshwater supply in the Dutch delta

The research presented here contributes to the objectives of the sub-program 'Freshwater supply' of the Dutch Delta Program by providing new quantitative understanding of the salinization mechanisms of saline seepage in the Dutch coastal groundwater systems. This provides a scientific basis for formulating monitoring strategies, effective measures and solutions, as well as long-term strategies for a sustain-

able and economically-effective supply of freshwater.

The research demonstrates that local saline seepage processes have major implications for the salinization of regional water systems. Since the localized boils are dominant in the salinization of deep polders, effective measures to abate salinization should be focused on boils. Field experiments showed that sealing boils is difficult because of the development of new boils. Increasing surface water levels (> 0.5m) could be effective when applied in ditches with many large boils. However, reducing salt loads in deep polders remains a difficult task. Therefore, the most important message is to prevent the development of new boils due to activities in the polders like digging and the construction of infrastructural works. With the knowledge that salt loads will not decrease in the future, it is important to find solutions for a more sustainable freshwater supply. There are many possibilities but all solutions require a made-to-measure approach and knowledge of all aspects of the water system. Aquifer storage of freshwater in wet times and recovery in dry periods may be a feasible measure at a local scale. Operational salt water management is a potential effective solution at a larger (polder) scale. Operational saltwater management means the dynamic and integrated control of pumping out polder water, the admission of fresh water and the temporary storage of saline seepage water in ditches, based on weather forecasts and the real-time monitoring of salt concentrations at strategic locations. The temporary isolation of salt areas (with boils) from fresh areas (without boils) in the polder can easily be controlled by small automatic weirs. Subsequently, the stored saline seepage water can be discharged during rain events when salt concentrations are low.

The thickness of rainwater lenses in saline seepage areas and the dynamic behaviour of salinities within the lens and the soil moisture in the unsaturated zone above them are of great importance from an agricultural perspective. However, the small dimensions and dynamic behaviour of the rainwater lenses, especially the rapid removal of recharge through drain tiles and the loss of freshwater by evapotranspiration, make them very vulnerable to climate change. Rainwater lenses may be expected to shrink due to evapotranspiration during drier summers, which are expected to become more frequent under future climate change but the projected increase in winter precipitation may not compensate for the lens shrinkage because the tile-drainage system efficiently discharges the recharge. Alternative tile-drainage configurations that promote prolonged retention and storage of infiltrated freshwater in rainwater lenses could be a way to mitigate the potential adverse effects of future climate change. The optimal design of such configurations is subject of current research in the southwestern delta (Go-Fresh project). Another high potential local solution to increase the freshwater supply is the temporary subsurface storage of freshwater in sandy paleochannel ridges.

Finally, the knowledge and experiences obtained in the Dutch delta with finding solutions for a sustainable and economically-effective freshwater supply in a changing climate can be applied in other deltas worldwide where the freshwater supply is under pressure.

Samenvatting en conclusies

Motivatie

Meer dan 50% van de wereldbevolking woont in kustgebieden en is afhankelijk van zoete grondwatervoorraden voor drinkwater, landbouw en industriële doeleinden. Echter, in veel kustgebieden is het grondwater brak of zout wat de duurzame exploitatie van zoet grondwater bemoeilijkt of zelfs onmogelijk maakt. In de laaggelegen kustgebieden onder zeeniveau kan het brak-zoute grondwater het oppervlak bereiken door opwaartse stroming. Dit proces wordt aangeduid als zoute kwel en is het hoofdonderwerp van dit proefschrift. Zoute kwel leidt tot verzilting van het oppervlaktewater, het ondiep grondwater en het bodemwater in de wortelzone. Het ligt in de verwachting dat door de voorspelde klimaatverandering en toekomstige stijging van de zeespiegel, de zoute kwel zal toenemen en de beschikbaarheid van zoet grond- en oppervlaktewater zal afnemen. Het voorspellen van effecten van toekomstige veranderingen, het definiëren van een effectieve watermanagementstrategie voor een klimaat-robuuste, duurzame zoetwatervoorziening en de inzet van succesvolle maatregelen, zijn alleen mogelijk als alle relevante processen van zoute kwel worden begrepen. Dit proefschrift beschrijft de ruimtelijke variabiliteit en temporele dynamiek van verziltingsprocessen door zoute kwel in deltagebieden. De nadruk van het onderzoek lag op preferente zoute kwel via wellen en de interactie tussen dunne regenwaterlenzen en zoute kwel. Deze twee processen zijn aangemerkt als zeer belangrijke verziltingsprocessen in de Nederlandse delta, het studiegebied van dit PhD-onderzoek. De preferente zoute kwel leidt tot verzilting van het oppervlaktewater en speelt vooral in diepe polders (Deel I). De interactie tussen dunne regenwaterlenzen en zoute kwel leidt tot de verzilting van het ondiepe grondwater en de wortelzone en speelt vooral in de zuidwestelijke delta en het noordelijke kustgebied (Deel II).

Onderzoek

De ruimtelijke variabiliteit en temporele dynamiek van verziltingsprocessen door zoute kwel zijn onderzocht en gekwantificeerd door veldonderzoek te combineren met numerieke en analytische berekeningen. Uiteenlopende veldtechnieken zijn toegepast op verschillende schaalniveaus, variërend van lokale puntmetingen tot metingen op polderschaal en eilandniveau. Het onderzoek naar (preferente) zoute kwel processen in diepe polders (Deel I) is uitgevoerd in twee West-Nederlandse droogmakerijen: Polder de Noordplas en de Haarlemmermeerpolder. Twee wellen zijn in detail onderzocht en een uitgebreid monitoring campagne is uitgevoerd in Polder de Noordplas om de belangrijkste zoutbronnen in beeld te brengen en hun in de tijd variërende bijdrage aan de verzilting van het oppervlaktewater te kwantificeren. Het onderzoek naar de karakteristieken en het temporele gedrag van dunne regenwaterlenzen en hun interacties met zoute kwel (Deel II) is uitgevoerd in de zuidwestelijke delta (provincie Zeeland). Door de combinatie van verschillende meettechnieken konden karakteristieken van regenwaterlenzen verkregen uit puntmetingen (prikstok TEC-probe, elektrische sonderingen ECPT, bemonstering en analyse van grond- en bodemwater), worden geëxtrapoleerd naar het niveau van landbouwpercelen gebruikmakend van CVES (continue verticale elektrische sonderingen) en elek-

tromagnetische metingen (EM31). Het was zelfs mogelijk om de karakteristieken van regenlenzen voor een groot deel van het eiland Schouwen-Duivenland te karteren door gebruik te maken van elektromagnetische metingen vanuit een helikopter (HEM). Vervolgens zijn op basis van deze metingen twee typische landbouwpercelen geselecteerd om de dynamiek van de lenzen te onderzoeken. Hiertoe is voor een periode van 2 jaar, elke maand het zoutgehalte van het bodem- en grondwater op verschillende dieptes gemeten, in combinatie met hoogfrequente metingen (ieder uur) van de grondwaterstand, neerslag, drainwaterafvoer en het zoutgehalte van het drainwater. Numerieke modellen zijn gebruikt om de processen te analyseren die de karakteristieken van de regenwaterlenzen en hun dynamisch gedrag bepalen.

Resultaten en conclusies

Deel I: preferente zoute kwel via wellen

Op basis van veldwaarnemingen en –metingen, zijn drie typen kwel in een diepe polder onderscheiden die variëren in zowel flux als zoutgehalte (Fig. 1): (i) diffuse achtergrondkwel door de slecht doorlatende sedimenten (klei, veen) van de Holocene deklaag, (ii) zandbanenkwel door goed doorlatende zandbanen in de Holocene deklaag, en (iii) intense preferente kwel via wellen. Wellen zijn dunne open kanalen in de Holocene deklaag die het eerste watervoerende pakket met het oppervlak verbinden en waardoor kwelwater preferent met hoge snelheid (10^2 tot 10^4 m d^{-1}) naar het oppervlak stroomt. De grootste kwelfluxen en zoutgehaltes in de polder zijn gemeten in wellen. De

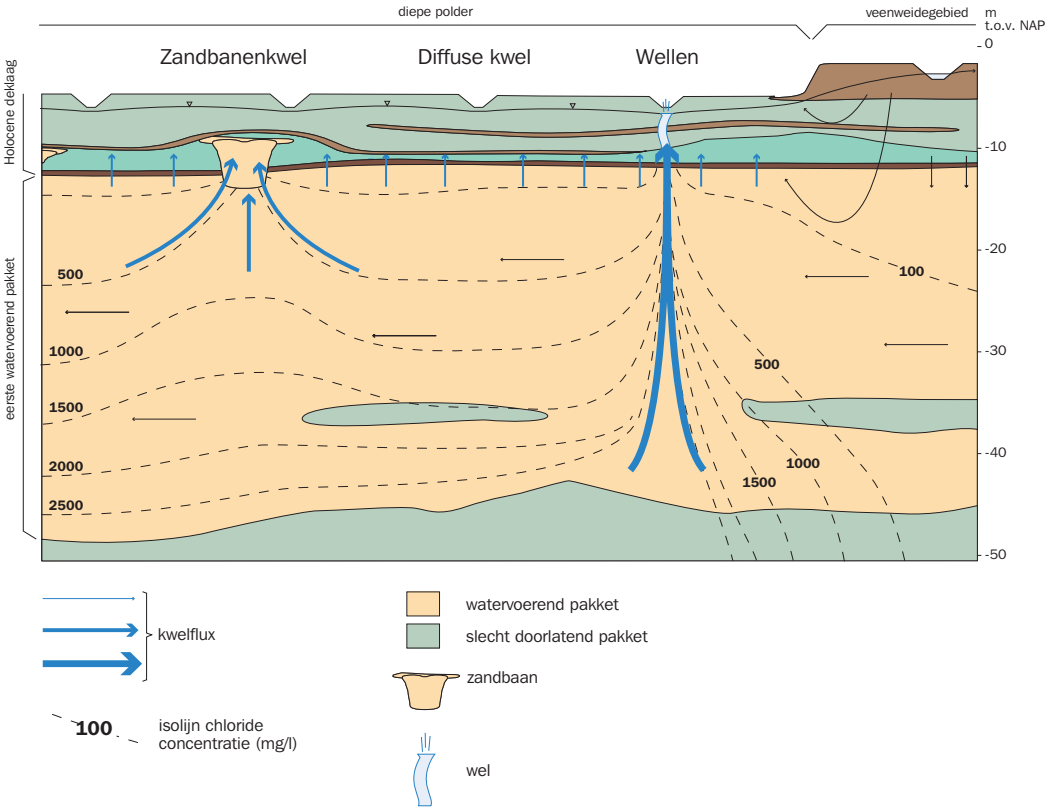

Fig. 1. Drie typen kwel in een diepe polder met verschillende fluxen en zoutgehaltes

gemiddelde gemeten Cl-concentraties in wellen voor Polder de Noordplas en de Haarlemmermeerpolder waren respectievelijk 1100 mg L^{-1} en 1500 mg L^{-1} met een maximum van meer dan 5000 mg L^{-1} in de Haarlemmermeerpolder. De meeste zandbanen doorsnijden het onderste en minst doorlatende deel van de Holocene deklaag waardoor grotere kwelfluxen met hogere Cl-concentraties (~600 mg L^{-1}) zijn gevonden voor zandbanenkwel dan voor diffuse kwel (~100 mg L^{-1}). De verschillen in zoutgehaltes van de drie typen kwel worden veroorzaakt door een combinatie van (1) het typische zoutprofiel dat onder de Holocene deklaag in de diepe polders van West-Nederland wordt aangetroffen (namelijk 5 – 15 m zoet water dat geleidelijk toeneemt in zoutgehalte met de diepte) en (2) het 'upconing' (opkegel) mechanisme. Geconcentreerde vormen van kwel met hoge snelheden trekken grondwater van diepere lagen en daardoor met hogere zoutgehaltes aan dan diffuse kwel met lage snelheden (Fig. 1). Diffuse kwelsystemen voeren voornamelijk zoet grondwater afkomstig van het bovenste deel van het eerste watervoerende pakket af.

Om de water- en zoutfluxen in een diepe polder op dagelijkse basis te kunnen kwantificeren, daarbij rekening houdend met de onzekerheid van parameters, is een probabilistisch (GLUE) dynamisch water -en zoutbalans model op dagelijkse basis opgesteld en succesvol toegepast voor Polder de Noordplas. De onzekerheid van de inputparameters is meegenomen door hun waarden random te samplen uit uniforme parameterverdelingen die zijn gebaseerd op metingen. Vervolgens is het model gekalibreerd op dagelijkse tot wekelijkse metingen van de hoeveelheid uitgemalen polderwater, het zoutgehalte en zoutvrachten, en grondwaterstanden in de polder. Dit leverde een set combinaties van inputparameters op die het totale systeem even goed konden simuleren. Met deze set aan 'behavioural' parametercombinaties zijn de bijdragen en bijbehorende onzekerheid van alle bronnen aan de water- en zoutbalans van de diepe polder gekwantificeerd, evenals het effect van verschillende toekomstscenario's. De resultaten tonen onomstotelijk aan dat wellen verreweg de meeste dominante verziltingsbron in Polder de Noordplas zijn, met een bijdrage van gemiddeld 66% (± 7.2%) aan de totale zoutvracht van de polder en met slechts een 15% (± 4.7%) bijdrage aan de totale waterflux. Gezien het algemeen voorkomen van zoute wellen in de Nederlandse diepe polders en de typische zoutverdeling in de ondergrond (zoet boven zout grondwater), kunnen we stellen dat wellen de meest waarschijnlijke dominante verziltingsbron in de meeste Nederlandse diepe polders zijn.

De hoge bijdrage van wellen aan de zoutbelasting komt door het veel hogere zoutgehalte van grondwater dat via wellen aan de oppervlakte komt dan via zandbanen en diffuse kwel. Veldmetingen in Polder de Noordplas en Haarlemmermeerpolder en numerieke simulaties tonen aan dat zoutwater 'upconing' het proces is dat leidt tot de hoge zoutgehaltes van welwater. De simulaties laten zien dat het welwater bestaat uit een mix van grondwater afkomstig van verschillende dieptes met verschillende zoutgehaltes. In een situatie zonder regionale stroming draagt het gehele eerste watervoerende pakket bij aan de afvoer van een wel. Het mixen vindt voornamelijk plaats dicht bij de wel waar stroombanen van grondwater met verschillende zoutgehaltes convergeren. De bijdrage van verschillende dieptes aan de afvoer van welwater laat een inverse relatie zien met de zoutverdeling in het eerste watervoerende pakket. Dit betekent dat de wel per meter watervoerend pakket meer ondiep grondwater met een laag zoutgehalte onttrekt dan diep grondwater met een hoog zoutgehalte. Dit is te wijden aan het 'buoyancy'-effect (opwaartse kracht) veroorzaakt door dichtheidsverschillen van grondwater (door verschillen in zoutgehalte) die een extra opwaartse kracht geven aan het zoetere, lichtere grondwater. De belangrijkste factoren die het 'upconing'

mechanisme van wellen en daardoor het zoutgehalte van wellen bepalen, zijn: (i) de afvoer van een wel, (ii) horizontale doorlatendheid van het watervoerend pakket, en (iii) de zoutverdeling (= dichtheidsverdeling) van het grondwater in het watervoerend pakket. Bepalend bij de zoutverdeling zijn de diepte van de overgangszone en het dichtheidsverschil tussen het grondwater boven en onder de overgangszone, terwijl de dikte van de overgangszone nauwelijks een rol speelt. Het 'upconing' mechanisme van geclusterde wellen, dat wil zeggen meerdere uitstroomopeningen binnen een gebiedje van 20-100 m^2, is een functie van de totale afvoer van een welcluster. De variatie in zoutgehalte tussen de wellen binnen een cluster wordt bepaald door de afvoer van een individuele wel en zijn positie ten opzichte van andere wellen in het cluster. Regionale laterale grondwaterstroming beïnvloedt zeer sterk het stromingspatroon rondom de wel waarbij het watervoerend pakket wordt onderverdeeld in een lokaal welsysteem bovenop het regionale grondwatersysteem. Ondanks dit grote effect op de grondwaterstroming heeft regionale stroming slechts een klein effect op de relatieve bijdragen van zoet en zout grondwater aan de welafvoer en dus op het zoutgehalte van de wel.

Deel II: Dunne regenwaterlenzen in zoute kwelgebieden

Puntmetingen (TEC, ECPT) op 30 landbouwpercelen met zoute kwel laten een geleidelijke overgangszone (mix-zone) zien tussen geïnfiltreerd regenwater en opwaarts stromend zout kwelwater (Fig. 2). Het midden van deze mix-zone (D_{mix}) zit op een zeer geringe diepte, gemiddeld 1.7 m beneden maaiveld, en in bijna alle onderzochte regenwaterlenzen werd geen zoet grondwater aangetroffen (zoet = Cl < 300 mg L^{-1}). Op basis van deze metingen is de dunne regenwaterlens in gebieden met zoute kwel (verder aangeduid als RW-lens) gedefinieerd als het volledige grondwaterlichaam van grondwaterstand tot aan de basis van de mix-zone (B_{mix}). B_{mix} is de diepte waar beneden geen menging met regenwater plaatsvindt en waar het zoutgehalte dus gelijk is aan het zoutgehalte van het regionale grondwater (Fig. 2). Met deze definitie is de RW-lens dus geen pure zoetwaterlens en variëren zoutgehaltes

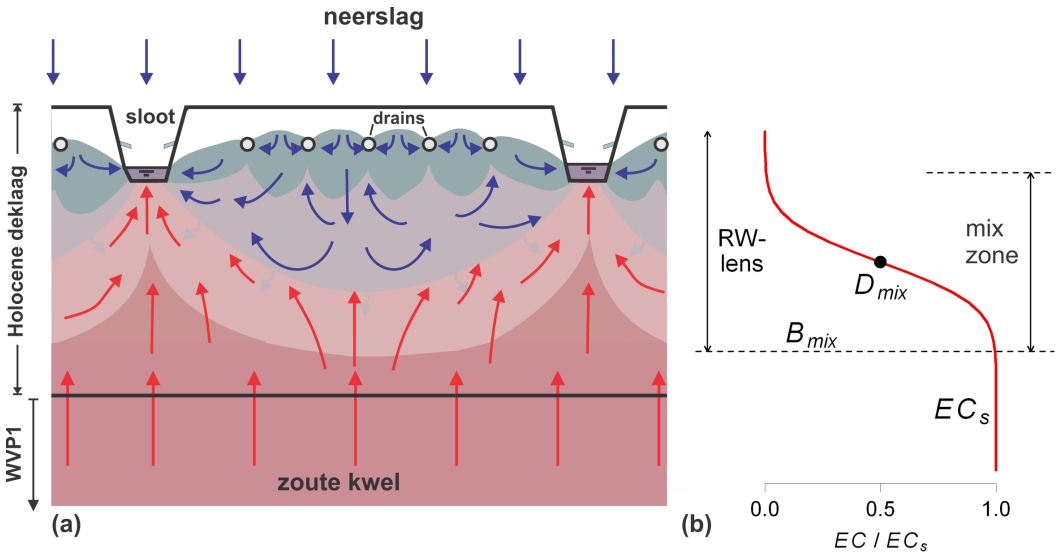

Fig. 2. (a) Schematische weergave van een regenwaterlens in een zout kwelgebied (RW-lens). (b) Profiel van het zoutgehalte van het grondwater met de diepte. D_{mix} is het midden van de mix-zone waar het zoutgehalte (EC) de helft van het zoutgehalte van het kwelwater (EC_s) is. B_{mix} is de basis van de mix-zone waar het zoutgehalte gelijk is aan dat van het zoute kwelwater (EC_s).

binnen de RW-lens zowel in ruimte, diepte als in tijd. B_{mix} werd op een gemiddelde diepte van 2.8 m beneden maaiveld aangetroffen. ECPT-metingen laten zien dat beneden B_{mix} het zoutgehalte constant met de diepte blijft tot minimaal een diepte van 25 m (= diepte van de ECPT-metingen).

De geringe dikte van de RW-lens wordt primair veroorzaakt door de permanent opwaartse grondwaterstroming van het eerste watervoerende pakket (WVP1) naar de slechtdoorlatende Holocene deklaag (Fig. 2). Dit voorkomt dat geïnfiltreerd regenwater het eerste watervoerende pakket bereikt. In tegenstelling tot deze RW-lenzen in zoute kwelgebieden, wordt de neerwaartse stroming van regenwater in infiltratiegebieden (bij afwezigheid van slechtdoorlatende kleilagen) alleen maar beperkt door de 'buoyancy' kracht van het onderliggende zoute grondwater. De dichtheid van dit zoute grondwater bepaalt in belangrijke mate de dikte van de lens volgens het Badon Ghyben Herzberg principe. Deze systemen produceren daardoor veel dikkere zoetwaterlenzen (BGH-lenzen), variërend van 5-15 m dikke lenzen in zandige kreekruggen tot 100 m dikke lenzen in de duinen. Na vaststelling dat RW-lenzen in kwelgebieden zich uitsluitend in de slechtdoorlatende Holocene deklaag ontwikkelen, zijn de stromingsprocessen in de deklaag nader onderzocht met numerieke modellen. Om deze processen beter te kunnen duiden en begrijpen, is het verticale stromingsstagnatiepunt (FLSP, 'vertical flow stagnation point') geïntroduceerd wat het punt aangeeft waar beneden de stroming verandert van een neerwaartse naar een opwaartse component. De FLSP tussen 2 drainagebuizen fluctueert met de grondwaterstand waarbij een stijgende grondwaterstand resulteert in een diepere FLSP. De stroming is neerwaarts in een groot deel van de RW-lens met een hoge grondwaterstand terwijl alle stroming in een RW-lens omhoog is gericht zodra de grondwaterstand beneden drainageniveau zakt. De numerieke resultaten tonen aan dat dit oscillerende, door grondwaterstandsfluctuaties gedreven verticale stromingsregiem, het mix-mechanisme tussen regenwater en zoute kwel is en de diepte en dikte van de mix-zone bepaalt. Grondwateraanvulling, kwelflux en drainage diepte zijn de belangrijkste factoren die op dit mechanisme invloed hebben.

De veldmetingen laten zien dat de dikte van de RW-lens (van B_{mix} tot grondwaterspiegel) varieert met ongeveer 1.2 m op jaarbasis en reageert op individuele regenbuien. De positie van D_{mix} verandert veel minder in de tijd (< 0.25 m), en fluctueert op een veel langere, seizoenale tijdschaal. De basis van de RW-lens (B_{mix}) blijft vrijwel op dezelfde positie. Numerieke simulaties laten zien dat deze kleine verplaatsing van de mix-zone kan worden toegeschreven aan het trage oscillerende stromingsregiem in het permanent verzadigde deel van de RW-lens. Stromings- en mix-processen zijn veel sneller in de zone waarin de grondwaterspiegel fluctueert door de dagelijkse variatie van neerslag, verdamping en drainage, en waar verzadigde en onverzadigde condities elkaar continu afwisselen. Wanneer de grondwaterspiegel daalt, blijft het meeste water van de RW-lens met opgelost zout achter als bodemwater. Als de bodem dan weer verzadigd raakt, mixt het achtergebleven bodemwater met slechts een klein deel geïnfiltreerd regenwater. Het zoutgehalte van het grondwater na mixen zal dus erg lijken op het zoutgehalte van het bodemwater voor verzadiging en dit verklaart de afwezigheid van zoet grondwater in bijna alle onderzochte RW-lenzen. Hoewel de mix-processen snel zijn, heeft de tijdelijke berging van zout in het bodemwater dus een belangrijk dempend effect op variaties in zoutgehaltes van het grondwater wanneer de lens groeit door infiltrerend regenwater. Het zoutgehalte van het bodemwater vertoont een seizoensvariatie met lagere zoutgehaltes tijdens de winter en hoge zoutgehaltes tijdens de zomer. Zout migreert omhoog richting de wortelzone door capillaire opstijging van het bovenste grondwater.

Wanneer gedurende het zomerhalfjaar de grondwaterstand daalt, zal het water dat via de capillaire poriën opstijgt van steeds grotere diepte komen en dus zouter zijn. Metingen tonen aan dat het zoutgehalte van het bodemwater zelfs veel hoger kan worden dan dat van het grondwater. Dit wordt veroorzaakt door het niet-synchrone effect van capillaire opstijging van zout water tijdens droge perioden en infiltratie van regenwater door scheuren (macro-poriën). Preferente stroming via scheuren speelt ook een belangrijke rol bij de snelle reactie van de drainage-afvoer op individuele regenbuien. Geïnfiltreerd regenwater en grondwater van verschillende dieptes in de RW-lens met verschillende zoutgehaltes dragen bij aan de drainage-afvoer in verhoudingen die variëren op een tijdschaal van uren tot dagen, en dit veroorzaakt het sterk dynamische karakter van het zoutgehalte van drainagewater.

Implicaties voor de zoetwatervoorziening in de Nederlandse delta

Dit onderzoek draagt bij aan de doelstellingen van het Deelprogramma Zoetwater van het Deltaprogramma door het aanleveren van nieuwe en kwantitatieve kennis van verziltingsprocessen door zoute kwel in de Nederlandse delta. Deze kennis biedt een wetenschappelijke basis voor het formuleren van monitoringstrategieën, effectieve maatregelen en oplossingen en lange termijn strategieën voor een duurzame en economisch haalbare zoetwatervoorziening.

Het onderzoek laat zien dat lokale zoute kwelprocessen grote implicaties hebben voor de verzilting van regionale watersystemen. De zeer lokaal voorkomende wellen zijn dominant in de verzilting van veel diepe polders en effectieve maatregelen tegen verzilting moeten dan ook gericht zijn op het aanpakken van de bijdrage van wellen. Veldproeven hebben aangetoond dat het dichten van natuurlijke wellen (ontstaan door opbarsting van de deklaag) erg lastig is door de grote kans op het ontstaan van nieuwe wellen in bestaande scheuren. Peilopzet kan effectief zijn bij een flinke peilverhoging (> 0.5 m) in sloten waar grote wellen voorkomen. Echter, het verminderen van de zoutbelasting in diepe polders door zoute kwel blijft een lastige opgave. De belangrijkste boodschap is dan ook dat zoveel mogelijk moet worden voorkomen dat er nieuwe wellen ontstaan door activiteiten zoals graven in de deklaag en aanleg van infrastructurele werken. Met het gegeven dat de zoutbelasting niet minder zal worden in de toekomst, is het zinvol om naar oplossingen te zoeken voor een optimalere vorm van zoetwatervoorziening. Er zijn veel mogelijkheden maar alle oplossingen vergen maatwerk en kennis van het watersysteem in al zijn aspecten. Voor kapitaalkrachtige gewassen kan worden gezocht naar mogelijkheden voor ondergrondse opslag van zoetwater in natte tijden voor gebruik in droge tijden. Operationeel zoutwaterbeheer (sturen op zout) is een kansrijke oplossing op grotere schaal. Met operationeel zoutwaterbeheer wordt bedoeld het dynamische operationele beheer van uitmalen, inlaten van zoet water, en tijdelijk bergen van zout kwelwater op basis van weersvoorspellingen en real-time zoutmonitoring op strategische locaties in de polder. Het tijdelijk isoleren van peilvakken met veel zoute wellen in droge tijden kan eenvoudig plaatsvinden met behulp van automatische stuwtjes. Afvoer van het tijdelijk geborgen zoute water vindt vervolgens plaats tijdens regenbuien wanneer zoutconcentraties laag zijn.

De dunne regenwaterlenzen in zoute kwelgebieden, zoals in de zuidwestelijke delta en het noordelijke kustgebied, zijn erg kwetsbaar voor klimaatverandering. De verwachte drogere zomers zullen leiden tot nog dunnere lenzen en een toename van zoutconcentraties in zowel de regenwaterlens als in de onverzadigde bodem erboven. In gebieden zonder

zoetwateraanvoer vanuit het hoofdwatersysteem, zoals in grote delen van de zuidwestelijke delta, is de landbouw in kwelgebieden voor de zoetwatervoorziening aangewezen op deze dunne neerslaglenzen. De lensdikte en dynamische gedrag van zoutgehaltes in het bodem- en grondwater zijn daarom van groot belang voor de landbouw. Naast de kwelflux en meteorologische omstandigheden (neerslag en verdamping), wordt de dikte van regenwaterlenzen en de dynamiek daarvan sterk bepaald door buisdrainage. Hoewel aan de eerste twee natuurlijke factoren weinig valt te doen, is het goed mogelijk om nieuwe drainagesystemen te ontwikkelen die de regenwaterlens laten groeien en daardoor de zoutgehaltes in de wortelzone beperken. Ook is ondergrondse opslag van zoet water in nabijgelegen kreekruggen een kansrijke oplossing om de zelfvoorzienendheid van agrariërs voor hun zoetwaterbehoefte in droge tijden te vergroten. Deze typen lokale oplossingen worden momenteel uitgebreid getest in de zuidwestelijke delta binnen het Kennis voor Klimaat-project 'Go-Fresh'.

Ten slotte, de kennis en ervaring die in de Nederlandse delta worden opgedaan met het vinden van oplossingen voor een duurzame en economisch haalbare zoetwatervoorziening in een veranderd klimaat, kunnen worden toegepast in andere delta's en kustgebieden in de wereld waar de zoetwatervoorziening onder druk staat.

Dankwoord

Ik heb lang zitten dubben hoe ik nu eens een origineel dankwoord zou kunnen schrijven. Origineel zou een enkel, groot BEDANKT zijn geweest, maar dat vond ik toch iets te kort. Heel even overwogen om het op rijm te doen, mijn verdediging is immers op 6 december, de verjaardag van Sinterklaas. Uiteindelijk is het dan toch een standaard en lange opsomming geworden van bedankjes en een terugblik op een mooie en leerzame periode in mijn leven.

Laat ik in ieder geval beginnen met een groot BEDANKT aan iedereen die op de een of andere manier heeft bijgedragen aan mijn proefschrift. Zo vergeet ik niemand en kan ik nu rustig een paar personen in het bijzonder gaan noemen.

Ik begin dan ook met Roelof (Stuurman) en Kenneth (Rijsdijk), jullie zijn mijn paranimfen en niet zonder een reden. Jullie zijn allebei gedreven onderzoekers die mij hebben geïnspireerd in het doen van onderzoek en waar ik veel van heb geleerd. Roelof, bij jou kwam ik in 1995 terecht als dienstweigeraar en kon meteen aan de slag in het prachtige Merkske stroomgebied, een mooi meanderend beekje op de grens van Nederland en België. Veldwerk vormde de basis van deze ecohydrologische studie, en na gedane zaken eindigden we vaak in Hoogstraten aan een Vlaamse maaltijd met een pot bier. Vanaf het begin heb je mij aangespoord om te promoveren, iets waar jij zelf niet aan toe bent gekomen, maar wel belangrijk vond. Daarmee ben je eigenlijk de aanjager van mijn promotieonderzoek. En kijk nu, het is gelukt! Ik kijk uit naar de hervatting van onze samenwerking en het liefst in complexe, grondwatergevoede (kust)wetlands elders op de wereld, want daar gaat ons hart echt sneller van slaan, toch?

Kenneth, jij vroeg in 2007 of ik mee wilde naar Mauritius om een stukje moeras droog te leggen om in den droge dodo-botten te kunnen opgraven. Hoewel ik in dat jaar ook aan mijn promotieonderzoek begon en het allemaal wel erg veel zou kunnen worden, twijfelde ik toch geen moment en zei meteen ja. Een jongensdroom! En die dodo heeft me veel gegeven. Naast het werken in een fantastisch, multidisciplinair team en media-avonturen als de Beagle en Klokhuis, was het ook vooral de wetenschappelijke uitwerking van interessante onderzoeksvragen waar ik de vruchten van heb geplukt en profijt van heb gehad tijdens mijn eigen promotieonderzoek. Water bleek namelijk niet alleen belangrijk bij de opgraving maar speelde ook een sleutelrol bij het ontstaan van het dodo-massagraf 4200 jaar geleden. Een wereldwijde extreme klimaatverandering leidde tot verdroging en verzilting van de enige zoetwateroase in de omgeving waar de dieren massaal naar toe trokken om te drinken en stierven door te zout of te weinig water. Nog even gedacht om het studiegebied van mijn promotieonderzoek uit te breiden naar Mauritius, maar dat was toch iets te ver van de kern, hoewel dit echt een heel interessant kust-grondwatersysteem is waar verzilting een duidelijke en belangrijke rol speelt.

Pieter (Stuyfzand), tijdens de NHV-verziltingsdag die we samen hebben georganiseerd in 2004, gaf je al aan dat ik bij jou op zoute kwel zou kunnen promoveren. Het duurde nog een paar jaar voordat de mogelijkheid daar was en toen zijn we samen dit bijzondere traject gestart. Bedankt hiervoor en de steun en hulp tijdens het onderzoek. Sjoerd (van der Zee), jij hebt me de eerste kneepjes van het wetenschappelijk schrijven bijgeleerd. Fijn dat je het mogelijk maakte dat Sara en ik samen aan de regenwaterlenzen konden werken. Je was altijd erg enthousiast over de veldresultaten en bent gaande weg ook steeds meer de waarde van veldonderzoek gaan inzien.

Gu (Oude Essink), toen jij bij TNO kwam, gingen we al vrij snel samen met verzilting aan de slag in Friesland (bodemdaling en zoute kwel). De combi maakt ons een sterk team, jij het numerieke werk, en ik het veldonderzoek. Ik zal nooit je eerste veldwerk ooit vergeten. Blauwbekkend stonden we in horizontale witte strepen tijdens één van de strengste sneeuwstormen van deze eeuw, bijna vastgevroren aan de prikstok. Logisch dat je niet meteen de lol van het veldwerk inzag maar gedurende de jaren wel de meerwaarde. Met jouw achtergrond en onze op stoom gekomen samenwerking was het logisch dat jij co-promotor werd. Ik weet dat je uiteindelijk graag meer tijd had willen besteden aan mijn onderzoek maar tegelijkertijd werd verzilting een hype in Nederland wat veel Deltares-werk opleverde en je tijd opslokte. Ik ben je dankbaar voor je energie, het fungeren als klankbord zowel inhoudelijk als wanneer ik het even niet zag zitten, het creëren van de randvoorwaarden voor mijn promotieonderzoek (inclusief de Australië trip), en de introductie in de SWIM-wereld (leuke congressen). Ik hoop dat we samen blijven optrekken in nog mooiere zoet-zout projecten.

Sara (Eeman), ik ben erg blij dat we samen het veldwerk in Zeeland konden oppakken en aan de Zeeuwse lenzen konden werken. Bedankt voor de fijne samenwerking. Esther (Vermue), jouw bodemvochtmetingen geven een grote meerwaarde aan het regenwaterlenzenonderzoek in Zeeland want voor de boeren draait het uiteindelijk toch om het zout in de wortelzone.

Geert (van Wirdum), de prikstok die jij hebt ontworpen voor diepteprofielen van temperatuur en elektrische geleidbaarheid hebben me veel mooie data opgeleverd. Hoewel jij hem voor hoogvenen gebruikte en daar gemakkelijk tot 10 meter diep ging, duwde ik hem in de stugge klei tot maximaal 4 meter diep. Maar het werkte, met de nodige reparaties.

Mike (van der Werf), jij bent vaak meegegaan naar Zeeland waar we een bijzonder meetnet hadden geïnstalleerd. De computer die de data logde had jij boven op een 5 meter hoge hooistapel in de schuur van de boer geplaatst, alleen te bereiken via een gammele steile ladder. Dat jij gewend bent om de Eiger Nordwand te beklimmen was duidelijk maar ik had toch echt wel een beetje hoogtevrees. Niet alles is gelukt wat we in gedachte hadden (bijvoorbeeld de 200 continue zoutmetingen van het grondwater op verschillende dieptes en locaties) maar uiteindelijk heeft het meetnet voldoende mooie data opgeleverd.

Andre (Cinjé) en Pieter (Doornenbal) bedankt voor jullie hulp in het veld. En nu komt een (waarschijnlijk niet complete) lijst van studenten die mij hebben geholpen met het verzamelen van een grote hoeveelheid veldgegevens of die me numeriek hebben ondersteund: Jackie (Leng), Bram (de Vries), Julia (Claas), Bernard (Voortman), Tim (Favier), Ruben (Goudriaan), Piet (Maljaars), Runa (Wils), Marian (Koskamp), Tommasso (Letterio), Francesco (Sergi), Sjors (Stevens), Bas (de Veen), Corné (Prevo), Valentina (Marconi).

Pieter (Pauw) en Joost (Delsman), collega's zoute onderzoekers, jullie zijn later met jullie promotieonderzoek begonnen dan ik en hadden me zelfs bijna ingehaald, maar gelukkig net niet. Leuk dat ik daarom nog wat kan bijdragen aan jullie mooie onderzoek.

Alexander (Vandenbohede), leuk dat we samen aan twee wellen-papers hebben kunnen werken, zoutwater 'upconing' door wellen (hoofdstuk 4) en eentje over het karakteriseren van wellen met temperatuur. Het gebruik van temperatuurmetingen om

grondwaterstroming te karakteriseren is een nog redelijk onontgonnen terrein met veel potentie. Zullen we hiermee verder gaan?

Ype (van der Velde), wat gaaf dat we aan elkaars proefschrift hebben kunnen bijdragen in de vorm van twee publicaties. Ik hoop dat het lukt om in de toekomst te blijven samenwerken want jouw ideeën en manier van onderzoeken inspireren.

Ik heb ook veel hulp gehad van Deltares en TNO collega's, bedankt Esther (van Baaren) en Marta (Faneca Sànchez) voor het meewerken aan onderdelen van mijn proefschrift en het verziltingsonderzoek mee op de kaart zetten, Remco (van Ek) voor de gemeende interesse en inbedding van mijn onderzoek in het Deltares onderzoeksprogramma, Marijn (Kuijper) voor de reflectie van mijn ideeën en mentale steun, Dimmie (Hendriks) voor het op de rails zetten van een planning toen ik even door de bomen het bos niet meer zag, Jarno (Verkaik) voor de nodige Seawat-hulp, Wiebe (Borren) voor de introductie in de wereld van optimaliseren, Peter (Vermeulen) voor de niet-stationaire stroombanen, Gerrit (Hendriks) voor de hulp met GIS en de vogels, Jelle (Buma) voor de vriendschap, Gijs (Janssen) voor het overnemen van het NHV secretaris-stokje, Jacco (Hoogewoud) voor de altijd kritische blik, Ronald (Vernes) en Denise (Maljers) voor de geologische kennis en data, John (Lambert) voor de bio-sealing, Han (Bruinenberg) en Roel (Savert) voor de mooie illustraties en Roel voor de professionele opmaak van mijn proefschrift, Hans Peter (Broers) voor de discussies over stroombanen en reistijden, Jasper (Griffioen) voor de al meer dan 15 jaar lange samenwerking op het gebied van zoute, nutriëntrijke kwel, en er valt nog veel meer te doen.

Ik ben veel dank verschuldigd aan TNO en Deltares die het mogelijk hebben gemaakt dat ik parttime aan een promotieonderzoek heb kunnen werken. Daar hebben veel personen aan bijgedragen maar in het bijzonder wil ik Bennie (Minnema) noemen. Bedankt dat je me niet hebt laten kiezen tussen de dodo en mijn promotieonderzoek en dat je in zag dat parttime promotieonderzoek doen niet betekent dat je in 4 jaar klaar bent. Je ondersteunde mijn reis naar Australië maar vond dat ik me beter in een klooster kon terugtrekken voor de eindsprint van mijn promotie. Ik denk dat je hier geen gelijk in had, een retraite in een klooster zou ook vast bijzonder zijn geweest maar Australië was in alle opzichten goed.

Jan (Gunnink) en Aleid (Bosch), super dat ik mijn onderzoek aan het Interreg IV-B CLIWAT-project kon koppelen. I want to thank the Cliwat-project group and especially Bernard (Siemon) for the helicopter EM data of Schouwen-Duivenland which are awesome and really improved the knowledge of rainwater lenses in coastal areas, and Klaus Hinsby for undertaking the lead in producing scientific output of the Cliwat-project in the form of a HESS-special.

I want to thank all members of the reading committee (Mark Bierkens, Koos Groen, Luc Lebbe, Theo Olsthoorn, Cliff Voss) for taking the time to read my PhD-thesis and for their nice and inspiring words.

Mijn onderzoek in de diepe polders heb ik samen met het Hoogheemraadschap van Rijnland mogen doen en daarvoor mijn grote dank. Gé (van der Eertwegh), toen jij nog bij het waterschap werkte, initieerde je het Noordplas-onderzoek (vorige eeuw, 1998) met een zeer gedurfd, uitgebreid en kostbaar meetnet. Het was duidelijk dat je uit de onderzoekswereld kwam. En mede door dat meetnet heeft het onderzoek veel nieuwe

kennis opgeleverd over zoute kwel in diepe polders. Ook Dienst Landelijk Gebied (Harm Janssen) en de WLTO hebben in belangrijke mate aan het Noordplas-onderzoek bijgedragen. Frank (van Schaik) jij was en bent de constante factor bij Rijnland, vanaf het begin erbij en nog steeds van de partij als het gaat om meten aan water. Dat deden we ook in detail bij het project 'veldonderzoek naar wellen dichten' dat mede door Birgitta (van der Wateren) en Jos (van Rooden) mogelijk is gemaakt en daarvoor dank. Verder wil ik Dolf (Kern), Mark (Kramer), Henk (Folkerts), Ronald (Bakkum), Wulf (Vaarkamp), Henk (van Hardeveld) en Tine (Bardoel) bedanken voor de bijdragen aan de projecten in de diepe polders die allemaal op de een of andere manier in dit proefschrift zijn verwerkt.

Mijn andere studiegebied was Zeeland, en daar hebben we in samenwerking met de provincie Zeeland, Waterschap Scheldestromen, Dienst Landelijk gebied en de ZLTO uitgebreid onderzoek gedaan naar de verzilting van het freatische grondwater. Iedereen die aan dit project heeft meegewerkt bedankt want uiteindelijk heb ik bijna de helft van mijn proefschrift aan dit onderzoek te danken. Lein (Kaland) van de provincie Zeeland was de projectleider en zorgde ervoor dat we al het onderzoek konden doen dat nodig was. Dat betekende naast de numerieke uitdagingen, heel veel meten. Carla (Michielsen), jij was erg belangrijk om het onderzoek relevant te laten zijn voor de landbouwsector en je bracht de onderzoekers dichter bij de boeren en andersom. Rinus (Meeuwse), je bent altijd kritisch en scherp en dat is goed. Ik ben blij dat we onze kennis kunnen blijven inzetten en uitbreiden in nieuwe Zeeuwse projecten.

Bijzonder vond ik de samenwerking met de boeren. Door nieuwsgierigheid gedreven, werkten jullie mee aan het onderzoek en maaiden, ploegden en oogstten om mijn meetapparatuur heen. Veel dank daarvoor. Rien (van den Hoek), op jouw perceel (hoofdstuk 5 en 6) ben ik veel meer te weten gekomen over de karakteristieken en dynamiek van dunne regenwaterlenzen. En het onderzoek gaat door, we onderzoeken samen of we met een nieuwe vorm van drainage de regenwaterlenzen kunnen vergroten. Jan (van de Velde), jouw perceel (hoofdstuk 5 en 6) ligt op de overgang van een kreekrug (infiltratiegebied) met een meer dan 8 m dikte zoetwaterlens naar een superzout kwelgebied met bijna zeewater op één meter diepte. Perfecte locatie om deze twee totaal verschillende systemen op korte afstand van elkaar te onderzoeken. Jan (Dorrepaal), al sinds 1999 kom ik op jouw perceel (hoofdstuk 2, 4 en 7) om je wellen te bekijken en te bemeten. Je hebt ze liever niet maar ik was er stiekem toch blij mee. We hebben veel verschillende metingen kunnen doen, variërend van prikstokmetingen, glasvezelkabelmetingen tot en met thermisch infrarood-metingen vanuit een minihelikopter. Kees (Avis), jouw waarnemingen van wellen die door weersveranderingen verdwijnen en actief worden heb ik in mijn proefschrift verwerkt (hoofdstuk 7). Leuk dat we samen de zoute wellen problematiek via het NCRV programma 'Altijd Wat' voor een groter publiek voor het voetlicht hebben kunnen brengen. Timo (Steenwijk), jouw wellen zijn het mooist (hoofdstuk 4 en 7). De waterdruk onder de deklaag is in deze hoek van de Haarlemmermeer zo groot dat de wellen midden op je land zijn ontstaan. Erg lastig voor jou maar handig voor mij omdat ik ze zo goed kon bemeten. Ik had ze graag voor je gedicht maar dat is helaas niet helemaal gelukt, maar ook dat heeft de wetenschap weer verder gebracht.

Vincent (Post), je hebt me heel erg geholpen in de eindfase van mijn onderzoek, en misschien had ik je daarom wel helemaal bovenaan moeten zetten, maar dit past chronologisch beter. Elke keer als ik het even niet zag zitten, was jij er weer om me er bovenop te praten. Je hebt daar talent voor. Maar misschien nog wel belangrijker, de leuke dingen, zoals de regenwaterlenzen paper waar we samen aan hebben gewerkt liep vooral door

jou als een trein, en natuurlijk het kanoën in de zee voor jullie huis, de coastal walk en fish and chips in Marino. En niet te vergeten de gezellige avondjes met jullie (Fran en jij) hebben zonder twijfel bijgedragen aan een onvergetelijke tijd in Adelaide. We hopen jullie snel weer te zien.

My stay at the National Centre for Groundwater Research and Training, Flinders University (Adelaide) was great. At NCGRT I found the right atmosphere to work on the last part of my PhD-thesis. Thank you Adrian (Werner) and Vincent (Post) for making my stay at the NCGRT possible and for your contributions to the papers. Thanks Dana (Jacovovic) and Carlos (Miraldo) for sharing your office with me, your help, the nice talks, and the lovely tea, Megan (Sebben) for letting me work on your nice project at the Picanninie Ponds wetlands, and Okke (Batelaan), Leanne (Morgan), Saskia (Noorduijn), Daan (Herckenrath) for the nice chats, squash, bbq, beers that made my stay a very pleasant one. Special thanks for Renee (Spinks) for helping us to start up in Australia, no worries…

Naast het promoveren was er gelukkig veel tijd voor ontspanning. Tijdens de gezellige avondjes en kampeerweekendjes met jullie kwam altijd wel de status van mijn onderzoek voorbij. Bedankt voor de vriendschap, het meeleven en het aanhoren van mijn verhalen, Monique, Chris, Katja, Ivo, Ernst, Melanie, William, Saskia, Jelle, Daphne, Saskia, Jan. Ook belangrijk waren de maandagavonden en zaterdagmiddagen wanneer ik mijn hoofd leeg schopte en kopte en dat deed (en doe) ik samen met jullie, Hercules 9.

In de groene oase van Pierre en Riet zijn we altijd heel erg welkom en kunnen we lekker bijtanken in de Limburgse natuur of juist overspoeld worden door de gezellige drukte met Johan, Kim, Julie en Maartje.

Pap en mam, bedankt voor jullie steun en voor het zijn van een super opa en oma voor de kids. Pap, jij hebt zelfs direct meegeholpen met mijn promotieonderzoek door bij Deltares draadjes aan sensoren te solderen, epoxy te gieten en mee te helpen met de installatie van de temperatuursensoren in het veld. En erg leuk dat je samen met Koen ons in Australië kwam op zoeken. Koen, het samen struinen door de natuur geeft me altijd veel inspiratie en nu krijg ik er echt weer meer tijd voor. Su, super bedankt voor de mooie kaft die je aan mijn proefschrift hebt gegeven.

En dan het thuisfront. Corine, Jens, Nina en Mick, jullie zijn het allerbelangrijkste in mijn leven. Redelijk geruisloos heb ik aan mijn promotieonderzoek kunnen werken en mijn doel om jullie hier zo min mogelijk mee te belasten is gelukt. Pas in het laatste jaar begonnen jullie wat te merken van mijn grote werkstuk toen ik ook wat vaker in onze vrije tijd aan de slag moest. Wat gaaf dat we juist tijdens die eindfase een tijdje in Australië hebben gewoond. De afwisseling van keihard werken en Australische avonturen beleven was perfect. Corine, jij maakte dat mogelijk door al mijn 'normale' taken over te nemen. Super. Maar nog belangrijker, jij hielp me snel weer uit de eindfase-dips zodat ik weer verder kon. Zo was er naast het harde werken toch nog veel ruimte over om de wildernis in te trekken, lekker in de zee te zwemmen, koala's te kijken en gezellig te bbq-en. Ja, genieten kunnen we wel! Australië was een mooie gezamenlijke afsluiting van een bijzondere en leerzame periode in mijn leven.

Zo, dat was dat. En nu komt er weer ruimte voor andere mooie dingen.

Curriculum vitea

Perry de Louw was born on 8 October 1970 in Nuenen. He attended high school (VWO) at the Eckart-college in Eindhoven from 1983-1989. In 1989 he moved to Utrecht to study physical geography at the University of Utrecht. Perry graduated in 1995 after finishing his M.Sc. thesis on hydrological triggering of shallow landslides in Costa Rica. After his M.Sc. studies Perry did an internship at a sugar cane company in the northern desert of Peru focussing on optimising groundwater extractions schemes.

He started his professional career in 1995 at TNO as a hydrogeologist and worked on various projects dealing with groundwater-surface water interaction, ecohydrological systems, integrated water resource management, and coastal groundwater systems. He acted as secretary of the Netherlands Hydrological Society (NHV) from 2002-2008. Since 2007 he has participated in an international scientific team that excavate one of the richest (mid-Holocene) fossil sites ever found on a volcanic island (Mauritius) and which contains a large quantity of dodo bones. Here he coordinated the geohydrological research and part of the excavations which involved realizing a small polder in the marsh to enable dry excavations. In 2007 Perry commenced working on part-time basis on this PhD-thesis, while continuing working on both TNO (until 2008) and Deltares (since 2008) applied research projects. In 2012 Perry moved for half a year with his family to Adelaide, Australia where he worked for five months as a guest researcher at the National Centre for Groundwater Research and Training, Flinders University. Here he worked on two publications of his PhD-thesis. Currently, Perry is involved in various applied research projects at Deltares focussing on sustainable freshwater supply and other subjects directly related to his PhD-research.

Peer reviewed publications (2009-2013)

This thesis (chapter 2-5)

De Louw, P.G.B., Oude Essink, G.H.P., Stuyfzand, P.J., Van der Zee, S.E.A.T.M., 2010. Upward groundwater flow in boils as the dominant mechanism of salinization in deep polders, The Netherlands. Journal of Hydrology 394, 494-506.

De Louw, P.G.B., Van de Velde, Y., Van der Zee, S.E.A.T.M., 2011. Quantifying water and salt fluxes in a lowland polder catchment dominated by boil seepage: a probabilistic end-member mixing approach. Hydrology and Earth System Sciences 15, 2101-2117.

De Louw, P.G.B., Vandenbohede, A., Werner, A.D., Oude Essink, G.H.P., 2013. Natural saltwater upconing by preferential groundwater discharge through boils, Journal of Hydrology 490, 74-87.

De Louw, P.G.B., Eeman, S., Siemon, B., Voortman, B.R., Gunnink, J., Van Baaren, S.E., Oude Essink, G.H.P., 2011. Shallow rainwater lenses in deltaic areas with saline seepage. Hydrology and Earth System Sciences 15, 3659-3678.

De Louw, P.G.B., Eeman, S., Oude Essink, G.H.P., Vermue, E., Post, V.E.A., 2013. Rainwater lens dynamics and mixing between infiltrating rainwater and upward saline groundwater seepage beneath a tile-drained agricultural field. Journal of Hydrology 501, 133-145.

Related to this thesis

Delsman, J.R., Hu-a-ng, K., Vos, P.C., de Louw, P.G.B., Oude Essink, G.H.P.,

Bierkens, M.F.P., 2013. Palaeo-modeling of coastal salt water intrusion during the Holocene: an application to the Netherlands. Hydrology and Earth System Sciences (in review).

Eeman, S., Van der Zee, S.E.A.T.M., Leijnse, A., De Louw, P.G.B., Maas, C., 2012. Response to recharge variation of thin rainwater lenses and their mixing zone with underlying saline groundwater. Hydrology and Earth System Sciences 16, 3535-3549.

Faneca Sànchez, M., Gunnink, J. L., van Baaren, E. S., Oude Essink, G. H. P., Siemon, B., Auken, E., Elderhorst, W., De Louw, P.G.B., 2012. Modeling climate change effects on a Dutch coastal groundwater system using airborne electromagnetic measurements. Hydrology and Earth System Sciences 16, 4499-4516.

Oude Essink, G.H.P., Van Baaren, E.S., De Louw, P.G.B., 2010. Effects of climate change on coastal groundwater systems: A modeling study in The Netherlands. Water Resources Research 46, W00F04, doi:10.1029/2009WR008719.

Pauw, P.S., De Louw, P.G.B., Oude Essink, G.H.P., 2012. Groundwater salinization in the Wadden Sea area of the Netherlands: quantifying the effects of climate change, sea level rise and anthropogenic interferences. Netherlands Journal of Geosciences 91-3, 373-383.

Vandenbohede, A., De Louw, P.G.B., Doornenbal, P., 2013. Characterizing preferential groundwater discharge through boils using temperature. Journal of Hydrology (in review).

Other

De Boer, E.J., Vélez, M.I., Tjallingii, R., Rijsdijk, K.F., Vlug, A., Prendergast, A.L., De Louw, P.G.B., Florens, F.B.V., Baider, C., Hooghiemstra, H., 2013. Decadal- to millennial-scale climate variability in the SW Indian Ocean from a 8000-yr long multiproxy record in the Mauritian lowlands. Quaternary Science Reviews (in revisions).

Claessens, L.P.A.M., Van Heteren, A. H., De Louw, P.G.B., Meijer, H.J.M., Janoo, A., De Vos, J. Rijsdijk, K.F., 2013. Structure of a Holocene dodo assemblage and effects of anthropogenic ecosystem disturbance. Nature (in review).

Meijer, H.J.M., Gill, A., De Louw, P.G.B., Van Den Hoek Ostende, L.W., Hume, J.P., Rijsdijk, K.F., 2012. Dodo remains from an in situ context from Mare aux Songes, Mauritius. Naturwissenschaften 99(3), 177-184.

Rijsdijk, K.F., Hume, J.P., Bunnik, F., Florens, F.B.V., Baider, C., Shapiro, B., Van der Plicht, J., Janoo, A., Griffiths, O., Van den Hoek Ostende, L.W., Cremer, H., Vernimmen, T., De Louw, P.G.B., Bholah, A., Saumtally, S., Porch, N., Haile, J., Buckley, M., Collins, M., Gittenberger, E., 2009. Mid-Holocene vertebrate bone Concentration-Lagerstätte on oceanic island Mauritius provides a window into the ecosystem of the dodo (Raphus cucullatus). Quaternary Science Reviews 28 (1-2), 14-24.

Rijsdijk, K.F., Zinke, J., De Louw, P.G.B., Hume, J.P., Van der Plicht, J., Hooghiemstra, H., Meijer, H.J.M, Vonhof, H.B., Porch, N., Florens, F.B.V., Baider, C., Van Geel, B., Brinkkemper, J., Vernimmen, T., Janoo, A., 2011. Mid-Holocene (4200 kyr BP) mass mortalities in Mauritius (Mascarenes): Insular vertebrates resilient to climatic extremes but vulnerable to human impact. Holocene 21(8), 1179-1194.

Van der Velde, Y., Rozemeijer, J.C., De Rooij, G.H., Van Geer, F.C., Torfs, P.J.J.F., De Louw, P.G.B., 2011. Improving catchment discharge predictions by inferring flow route contributions from a nested-scale monitoring and model setup. Hydrology and Earth System Sciences, 15 (3), 913-930.